ECOHYDROLOGIC EVALUATION OF WETLANDS ON PHOSPHATIC CLAY SETTLING AREAS

By

DANIEL LIMEHOUSE MCLAUGHLIN

A DISSERTATION PRESENTED TO THE GRADUATE SCHOOL
OF THE UNIVERSITY OF FLORIDA IN PARTIAL FULFILLMENT
OF THE REQUIREMENTS FOR THE DEGREE OF
DOCTOR OF PHILOSOPHY

UNIVERSITY OF FLORIDA

2009

To my parents

ACKNOWLEDGMENTS

I thank my supervisory committee members, Drs. Matt Cohen, Wiley Kitchens, and Mike Annable for their strong support and extend a special gratitude to my chair, Dr. Mark T. Brown for his guidance throughout this project and my graduate studies at the University of Florida. I would like to also thank the mining company representatives who provided site information and access and conveyed their significant reclamation experience with Clay Settling Areas; in particular I would like to mention Rosemarie Garcia and Keith Hancock at Mosaic, John Wester at PCS, Gary Blitch at CF Industries, and Tim King at the Tenoroc Fish Management Area. I would like to thank FIPR, who funded this research and provided strong foundation of decades of phosphate mining reclamation research to build upon. I am extremely appreciative for all the long hours in the field provided by Wes Ingwersen, Sean King, Carrie Boyd, Julie McLaughlin, Elliot Campbell, and Tyler Hollingsworth who endured hot and not so favorable conditions in support of this work.

I thank my entire family and especially my parents for all their continued support throughout my life. And finally, I am grateful to the newest member of my family, my fiancée Laurie, for her level-headedness, motivation, and love.

TABLE OF CONTENTS

page

LIST OF TABLES

LIST OF FIGURES

Abstract of Dissertation Presented to the Graduate School
of the University of Florida in Partial Fulfillment of the
Requirements for the Degree of Doctor of Philosophy

ECOHYDROLOGIC EVALUATION OF WETLANDS ON PHOSPHATIC CLAY SETTLING AREAS

By

Daniel Limehouse McLaughlin

May 2009

Chair: Mark T. Brown
Major: Environmental Engineering Sciences

Clay Settling Areas (CSAs) are prominent features of the post phosphate mining landscape that currently comprise 40,500 hectares in central Florida. Wetland creation on CSAs seems feasible since surface water features naturally form due to the isolated watersheds and low-permeability clays that are characteristic of these systems. Hydrologic evaluations of a series of CSAs using surface water, groundwater, and climatic data were performed to calculate water budgets of potential wetland areas. Water budget calculations resulted in significant residual losses that suggested underestimation of summer evapotranspiration (ET) when using traditional climatic-based models. Analysis of the diurnal surface water fluctuations supported these findings and resulted in ET rates as much as two times typical summer values in the region, demonstrating the highly productive nature of these systems. Surface water and groundwater analysis concluded that groundwater flow may be limited, though the potential for seepage into the surface water features was observed. The hydrologic evaluations were used to create temporal models to aid in active wetland restoration of CSAs by providing hydroperiod and water depth predictions.

To relate hydrology with the biota, transects were established down a hydrologic gradient from upland into the surface water features, where a series of soil moisture probes were installed

at different depths along the transects. Root biomass allocation with depth and transpiration of *Salix caroliniana* were also measured along these transects to observe effects of the hydrologic regime on plant behavior. Soil moisture data demonstrated the large capillary forces of the clayey soils, with saturation levels occurring over a meter above the water table. Root biomass allocation was to depths over one meter and into the water table with little preclusion from the clays. The results from the transpiration studies supported the evidence of high evapotranspiration rates of these systems, and found that this was in large part due to the transpiration of *Salix caroliniana*. These results revealed attributes of *Salix caroliniana* that, along with maintained saturation levels through most of the soil profile, explain its success on CSAs and demonstrate the presence of broad transitional zones appropriate for wetland restoration.

CHAPTER 1
INTRODUCTION

Statement of the Problem

Currently about 20 km^2 in Florida are mined for phosphate each year, the majority in central Florida and a smaller portion in north Florida (FIPR, 2009). Prominent features in the post mining landscape are Clay Settling Areas (CSAs), which are used to dewater clay slurry, one of the major by-products of the beneficiation process. CSAs are diked areas that are typically constructed on mined land, 10-15 meters above ground, and often about 2-3 km^2 in area. As of 2004, Florida had 470 km^2 of CSAs (Garlanger *et al.*, 2005), approximately 40% of the post mining landscape. The general topography of CSAs following reclamation consists of a fairly flat terrain, which slopes downward towards the locations where dewatering took place through outfall structures. Isolated, small depressional areas may also develop due to the topography that existed prior to filling with clays, such as mine cuts and spoil piles, and differential settling of the clays. These types of depressions, along with the lower elevations surrounding the dewatering structures, tend to accumulate surface water and thus are potential sites for wetland development and restoration.

This research focused on evaluating surface and groundwater hydrology of CSAs to provide a better understanding of CSA hydrologic regimes and how they may affect wetland restoration within these systems. While it is seems reasonable that functional wetlands can be established on CSAs, there is little known about the long-term hydrologic regimes of these areas and the major determinants affecting these regimes. Since water depth and hydroperiod are critical variables affecting structure and processes in wetlands, it is imperative to understand CSA hydrology when attempting to best manage these systems to promote development of viable wetlands (Odum *et al.*, 1990). The lack of a significant surface outflow on most older

CSAs, along with the low infiltration rates of the clays may cause the surface water hydrology to be driven primarily by evapotranspiration (ET), rain, and overland flow and with little groundwater connection (Reigner and Winkler, 2001). While some work has investigated ET (Odum *et. al*., 1991), infiltration (Reigner and Winkler, 2001), and overland flow (Riekerk *et al*., 1990; Reigner and Winkler, 2001; Lewelling and Wylie, 1993) on CSAs, better quantification of these hydrologic flows and an understanding of how they may vary among CSAs are needed when trying to predict hydrologic regime and develop restoration plans for wetlands on CSAs. Furthermore, the magnitude of ET and infiltration rates on the large footprint that CSAs encompass of the post-mining landscape is of primary concern to the regional hydrology, particularly since there is current concern that phosphate mining is limiting flows to downstream water bodies such as the Peace River.

In addition to the effect surface water hydrology has on wetland development, the groundwater dynamics and associated soil water availability determine the extent to which the wetland environment extends beyond typically inundated regions. There has been some research performed on groundwater regimes within a CSA (Murphy *et al*., 2008; Riekerk *et al*., 1990; Lewelling and Wylie, 1993), but the role that the clayey soils of CSAs play in surface water, groundwater, and soil moisture interactions is not well understood. Furthermore, the clayey soils may partially control the interactions between vegetation and soil water, particularly rooting and transpiration rates. A better knowledge of these interactions and how they are affected by the clayey soils is needed when creating or enhancing wetlands in intermittent or rarely flooded areas.

Phosphate Mining and CSAs

Phosphate is one of the three primary plant nutrients found in chemical fertilizers which are essential in modern agriculture. Florida is one of the main regions in the world where

phosphate mining occurs; contributing over 75% to the domestic supply and approximately 25% of the world's supply (FIPR, 2008). The central Florida phosphate district's deposits are mined from the Bone Valley Member of the Peace River Formation, and the phosphate deposits in the north Florida phosphate district occur in the Statenville Formation (FIPR, 2008). Both formations are part of the Miocene-age Hawthorn Group (FIPR, 2008). The phosphate deposits are open-pit mined, where 5 to 10 m of overburden containing sand and clay is removed and deposited to the side as spoil piles and the matrix containing the phosphate deposits is mined and sent to a beneficiation plant. The beneficiation process employs physical means to separate the phosphate rock from sand tailings and clay with each component making up approximately a third of the total matrix. The clay slurry that results from this process is only 2-5% solids and is transported to CSAs where the suspended clays dewater and settle (FIPR, 2008). Phosphatic clay consists of the following clay minerals, listed in descending order of abundance: smectite, palygorskite, illite, and kaolinite (Beriswill, 1989). The most abundant mineral, smectite, has the greatest shrink-swell capacities, reducing the stability of the clay substrate (Beriswill, 1989). The surfaces of CSAs become 50-60% solids within three to five years (FIPR, 2009), but remain at an unconsolidated consistency below the surface which limits weight bearing strength and residential development (Lamont *et al.*, 1975).

CSAs are typically constructed on previously mined areas, up to 20 m above grade, and with embankments built using overburden material. When CSAs are constructed on mined land, the pre-fill topography underlying the CSA is a function of the mining process and is an undulating surface of mine cuts and overburden spoil piles. The clay slurry is stage filled on this land surface, with intermittent no-fill periods to maximize clay storage. The clays are highly plastic, phosphatic clays which consolidate at a very slow rate and as a function of clay depth

(Reigner and Winkler, 2001). The variability in clay fill thickness resulting from the pre-filled topography, causes differentially settling and a depression-rich topography. CSA post-reclamation topographies generally consist of multiple and isolated depressional features with a minimal to obsolete drainage pattern (Lewelling and Wylie, 1993).

Sand tailings and overburden material are often deposited on CSA surfaces to cap the clays and promote further consolidation and compaction, resulting in increased heterogeneity of the soils and topography. One mining company, CFI Industries, differs from the traditional filling process by mixing the sand and clay remaining from beneficiation before filling CSAs with both. The co-deposited clay and sands of these types of CSAs create even more heterogeneity in the soils since sand-clay ratios vary with depth and increase with distance from where they were deposited (Garlanger, 1982).

As a result of the large amount of area in Florida that is and will be CSAs, reclamation is of primary concern. The clays typically require at least a ten year time period of consolidation before reclamation attempts are made (Odum *et al.*, 1983). Reclamation consists of flattening the outside slopes of the dikes, minor interior grading and shaping, and revegetation. A large amount of reclamation projects have been directed towards developing lands for agriculture and grazing. Up to 1988, the majority of reclamation had converted CSAs to pasture (Rushton, 1988), though research in the creation of valuable wildlife habitat has been performed (Schnoes and Humphrey, 1980; Odum *et al.*, 1991; Rushton, 1988).

Due to the water-holding potential of the clays and the depressional topography that results from consolidation and differential settling, it seems reasonable that creation of isolated wetlands would be a feasible reclamation alternative to provide not only suitable wildlife habitat but also other wetland functions. Some research has focused on wetland development on CSAs,

through the process of natural succession alone and with vegetation enhancement using wetland species (Odum *et al*., 1991; Rushton, 1988; Boyd, 2007; Ingwersen, 2006). Rushton (1988) found that natural succession typically followed the course of initial cover of *Typha spp*. followed by *Ludwigia peruviana*, *Baccharis halimifolia*, *Salix caroliniana* and *Myrica cerifera* (in upland transition), with *Salix caroliniana* as the dominant canopy species. It was concluded that without a seed source in close proximity that these areas tended to remain in such arrested successional states dominated by herbaceous and shrub species with a pure canopy of *Salix caroliniana*. Rushton (1988) did, however, encounter CSAs closer to a floodplain seed source which had hardwood species such as *Acer rubrum* and *Quercus laurifolia* colonize.

Odum *et al*. (1991) and Rushton (1988) demonstrated the short-term success of planting a number species typical of forested wetlands such as *Taxodium distichum* and *Fraxinus pennsylvanica*, and Ingwersen (2006) documented survival of these species 20 years after planting. Boyd (2007) conducted five field trials where a suite of herbaceous, shrub, and tree species were introduced to 3 CSAs and found varying success among different species and across different hydrologic regimes. One of the main conclusions of all these studies was that active restoration via vegetation enhancement may prove to be successful, but that hydrology appears to be the primary factor in controlling the survival of planted tree, shrub, and herbaceous species; calling for a better understanding of CSA hydrology and site-specific factors that determine hydrologic regimes.

Hydrologic Flows of CSA Surface Water Features

To understand surface hydrology of a water feature, water budgets that accurately account all inflows and outflows to the system must be performed. These inflows and outflows include rainfall, surface water inflow and outflow, infiltration and exfiltration, ET, and overland flow (runoff) from the surrounding watershed. Figure 1-1 shows all major hydrologic inputs and

outputs to isolated surface water features of a CSA, with S representing storage of surface water within the two shown features. The dikes and substrate directly below the clay fill and above the undisturbed, or virgin, soil consist of overburden left from the mining process. The water table of the groundwater system within the CSA, defined as local groundwater, is also shown in Figure 1-1 along with the regional water table underlying the CSA. The local groundwater within the CSA is confined by the clay fill and shown perched above the regional water table (Figure 1-1).

A systems diagram also depicting the major water inputs and outputs of an isolated surface water feature within a CSA is given in Figure 1-2 using the diagramming language developed by H.T. Odum (Odum, 1994). The boundary of the diagrammed system in Figure 1-2 is the extent of the clay fill (shown with red in Figure 1-1) and thus the dikes as lateral boundaries, and where the clay fill overlies the overburden and/or virgin soil as the vertical boundary. Inputs to an isolated surface water feature include direct rainfall and runoff from the watershed surrounding the feature (Figures 1-1 and 1-2). Outputs of the surface water include surface water outflow, ET, and infiltration (Figures 1-1 and 1-2). While not shown in Figure 1-1, some CSAs have active outfalls which allow surface water outflow. Figure 1-2 shows a switch controlling outflow, which represents the presence/absence of an active outfall structure creating outflow as a function of surface water stage. ET is shown in Figure 1-2 as the cumulative loss from evaporation directly from the surface water and transpiration from vegetation.

Two infiltration terms are shown in Figures 1-1 and 1-2, with Infiltration^1 representing loss of surface water to the local groundwater of the CSA and laterally through the dike; and Infiltration^2 represents flow of local groundwater towards the regional water table. Dike seepage is defined here strictly as loss of surface water laterally through the dike, thus a component of surface water infiltration (Figure 1-2), and does not include flow of local groundwater through

the dike. The latter can be viewed as local groundwater flow towards the regional water table (Figures 1-1 and 1-2). The loss of local groundwater of a CSA affects the quantity of local groundwater within a CSA which in turn inversely affects infiltration of surface water (Figure 1-2). While the above discussion and figure assume loss of surface water to the local groundwater system, observation and evaluation of the reverse, groundwater flow towards the surface water features (exfiltration), is not limited by such an assumption.

Local CSA Groundwater

Groundwater flow to (exfiltration) or from (infiltration) surface water features can potentially be a major water pathway of some wetland systems. The magnitude of this flow is largely determined by the hydraulic conductivity of the soil that underlies the system and the elevation of the surrounding water table relative to that of the surface water. It seems reasonable to assume that this pathway may be negligible to wetlands established on CSAs as a result of the clayey soils. In fact, most hydrologic studies of CSAs have assumed it to be zero (Reigner and Winkler, 2001). Carrier *et al.* (1983) reported very low conductivities from laboratory testing of phosphatic clays that were approximately 0.0035 m/day. Lewelling and Wylie (1993) measured lateral saturated hydraulic conductivities of CSA soils using slug tests within multiple wells on three CSAs and found much higher values ranging from 0.01 to 3.4 m/day. The highest conductivities measured by Lewilling and Wylie (1993) were at wells installed on a sand-clay mix CSA, whereas the other two CSAs had pure clay fill and conductivities near or less than 1 m/day measured.

With low hydraulic conductivities, local groundwater to and from surface water features may be limited. Clayey soils with low conductivities have been found to result in negligible vertical and lateral distribution of groundwater, where ET is the predominant flow and the water table elevations strongly reflect the surface relief (Levine and Salvucci, 1999; Rosenberry and

Winter, 1997). Lewelling and Wylie (1993) found that water tables surrounding surface water features of the three CSAs did not fluctuate in response to surface water fluctuations and concluded that there was little connection between the local groundwater and surface water of the systems. In their study of four CSAs, Reigner and Winkler (2001) measured groundwater levels at topographic high areas surrounding surface water features and observed groundwater elevations that were substantially above the elevations of the surface water features and water tables that reflected surface elevations. From these observations, the authors also concluded that the surface water and local groundwater systems were fairly disconnected. It is possible, however, that the presence of sand tailings, overburden caps, or a sand-clay mix may increase conductivities, movement of groundwater, and connection between local groundwater and surface water systems of CSAs. In fact, Murphy *et al*. (2008) observed lateral transport of groundwater across a CSA with sand tailings deposited and significant inflows to an isolated surface water feature within the CSA.

Loss of local groundwater to the regional water table is a possible flow affecting local groundwater storage within a CSA. Using the hydraulic conductivities measured by Carrier *et al*. (1983) and an estimated clay thickness of 6 m and head difference of 9 m between a CSA water table and the intermediate aquifer below the clay surface, Reigner and Winkler (2001) estimated vertical loss to be approximately 0.5 cm/year. It should be noted, that this estimate used the lower conductivities reported by Carrier *et al*. (1983) and the higher values from Lewelling and Wylie (1993) would result in increased infiltration. Water balances and model simulations for four CSAs performed by Reigner and Winkler (2001) resulted in negligible vertical losses of local groundwater.

Lewelling and Wylie (1993) studied the potentiometric elevations of local groundwater within three CSAs and the intermediate aquifer that underlie the CSAs and found different results due to different fill material of the three sites. The potentiometric surface of the intermediate aquifer system underlying the Mobil CSA was 5 to 8 m lower than the water table elevation within the CSA, suggesting little hydraulic connectiveness between the two aquifer systems. The Mobil CSA was an older CSA that had the clay fill extending all the way to the limestone of the intermediate aquifer system. The Agrico and CFI CSAs, however, had potentiometric surfaces of the intermediate aquifer within .35 m and 0.1 m of the water tables, respectively, demonstrating better connection between CSA local groundwater and regional groundwater systems. The clays of Agrico did not extend to the intermediate aquifer but rather had an underlying layer of overburden which was approximately 13 m thick. Also, the Agrico CSA had rows of overburden spoil piles that were left from mining and which clay was deposited on. The clay thickness over these piles, however, was as shallow as 0.35 m in some places. In systems similar to Agrico, which have spoil piles that extend up near the land surface, water may short circuit down and infiltrate through the overburden piles and to the regional groundwater system. The CFI CSA had a sand-clay mix deposited which resulted in higher infiltration rates which was observed further by Lewelling and Wylie (1993) with more rapid response of groundwater levels following rain events compared to the other two CSAs.

There has been some debate that cracks in the clays could result in increased vertical flow of water out of CSAs (Reigner and Winkler, 2001). Cracks can develop during drying of the clays due their high shrink-swell potential (Beriswill, 1989) and may not recover when re-wetted (Reigner and Winkler, 2001). These cracks, however, may not create a direct pathway out of the systems as a result of them not extending the entire depth of the CSAs (Reigner and Winkler,

2001). The cracks typically develop to maximum depths equaling the water table depths within the CSAs because of at and beyond depths of the water table, soil moisture will compensate for changes in volume rather than forming cracks. The cracks can, however, deliver flow to clay covered overburden piles, causing the hydraulic conductivity of the overburden sands to limit flow rather than the much more impermeable clays, possibly supporting the connectiveness observed at Agrico CSA by Lewelling and Wylie (1993). It follows that cracks could also develop within surface water features during prolonged dry periods and these cracks may not heal following inundation. If such surface water features are overlying overburden piles, then the submerged cracks may provide pathways for vertical infiltration of both surface water and local groundwater to the regional groundwater system. So while it is often assumed that there is little connection between surface water and groundwater systems of CSAs, infiltration of surface water is negligible, and that there is also minimal connection between local CSA and regional groundwater systems, such assumptions should be evaluated and validated on a site-specific basis.

Dike Seepage

Lateral flow, or dike seepage, of surface water in contact with the dikes is another possible water loss of surface water features on CSAs. As a result of CSAs typically being elevated above the surrounding landscape, it seems plausible that the head difference may cause significant outflow through the dikes. However, similar to vertical flow out of the systems, this lateral flow may be limited by the permeability of the clays along the edge of the berm. Though the dikes are typically constructed using overburden material, CSAs are typically bowl-like resulting in layers of clay that overly the full height of the interior sides of the dikes (Lewelling and Wylie, 1993). Also, because clays settle out slowly, the clays are typically the thickest at the

lowest portion of the CSAs where surface water accumulates and where dike seepage could be the most probable (Reigner and Winkler, 2001).

Reigner and Winkler (2001) placed paired groundwater wells across the dike at five locations of a CSA to evaluate dike seepage. They measured an average head difference of 0.61 m from the interior surface water and across the berm. Though hydraulic conductivities of the berm were not measured, Reigner and Winkler (2001) calculated dike seepage for two different flow paths, either through clay or saturated overburden, while using assumed values for saturated lateral hydraulic conductivities of clays and overburden. In the case that dike seepage occurred through a layer of clay, calculated dike seepage rates ranged from 0.0004 to 0.004 cm/year, with the range a function of the range of conductivities used in calculation. If the majority of the flow, however, was through the saturated overburden, then calculated dike seepage ranged from 2.3 to 48 cm/year depending on the permeability of the saturated overburden (0.3 to 6 m/day). In their study, however, Reigner and Winkler (2001) documented that the groundwater profiles across the five dike locations were below the overburden of the dike and across the clay overlying the dikes, indicating the impermeability of the clays was limiting lateral outflow. Similar to their analysis of the vertical flow out of the system, the authors assumed zero lateral outflow and confirmed this with water balances and model simulations.

Riekerk *et al*. (1990) used heat- pulse flow meters in groundwater wells installed in the perimeter dikes of two elevated CSAs and determined that there was lateral flow out of the systems ranging from 10 to 20 cm/year. Murphy *et al*. (2008) measured natural solute and stable isotope signatures of waters within and outside a CSA to evaluate the hydraulic connectivity to the surrounding landscape. The authors determined that shallow CSA water was present in significant concentrations in waters surrounding the CSA indicating outflow of surface water

from the CSA, though the actual pathway could not be identified with the methodology. So again, dike seepage may also vary among CSAs depending on water levels and dike construction.

Runoff

The watershed that contributes runoff, or overland flow, to the surface water features of a CSA are limited to the area of the CSA and bounded by the perimeter dikes. Reigner and Winkler (2001) calculated curve numbers for four CSAs based on published values and the sites' soil, land use, topography, and vegetation type and reported values ranging from 82.1 to 96.3. When performing event storm simulations with five different simulation models and data on rainfall and discharge out of the CSAs, the curve numbers dropped significantly, ranging from 54 to 76.5. These values are low for the impermeable clays characteristic of these systems but as Reigner and Winkler (2001) explain, these lower curve numbers may indicate low antecedent moisture conditions and during such conditions, storage in cracks could be quite large, thereby decreasing runoff from the watershed. It should be noted that Reigner and Winkler (2001) determined runoff as total discharge from an entire CSA and defined surface water features within a CSA as intermittent storages, and runoff to these features was not evaluated.

In their study of three CSAs, Lewelling and Wylie (1993) also measured runoff as total discharge from the sites and observed mixed results. The older CSA, Mobil, experienced rapid responses at the CSA outfall to rainfall as a result of its smaller drainage area, steeper slope, and less undulating topography. The Agrico mine experienced much more delayed and smaller responses near the outfall end because of the presence of more interior depressional features increasing storage. Rapid runoff to these depressional features was observed, however. The third CSA, CFI, only had one period of measurable flow at the outflow structure and, therefore, rainfall/runoff relationships were not evaluated. Riekerk *et al.* (1990) also measured rather low

runoff to rainfall ratios for one CSA studied by measuring and defining runoff as discharge from the site. Similar to Lewelling and Wylie (1993) and Reigner and Winkler (2001), the authors attributed these low ratios to surface water storage features within the studied basin.

When evaluating surface water runoff and precipitation relationships, attention must be placed for what location these relationships are being analyzed. The studies discussed above were primarily interested in total surface water flow out of the entire CSA system. These flows to rainfall ratios were found to be small in most situations due to storage areas within the basins. These storage areas could be intermittent storage areas if they are simply cracks, but isolated wetlands if they are larger and actual surface water features. In closer examination of runoff flows to these depressional features, it may be found that they experience runoff to rainfall ratios more characteristic of clay soils. The impermeable clays may contribute runoff fairly quickly after storm events to wetlands established on CSAs with similar curve numbers that were originally calculated by Reigner and Winkler (2001) using published values. More research is needed on rainfall and runoff relationships of depressional features within CSAs rather than solely examining total discharge from an entire CSA.

Surface Water Outflow

Soon after reclamation, the outfalls used for dewatering CSAs during stage filling typically continue to create surface water outflow. However, with continued consolidation, the land surfaces below the outfall inverts often settle to elevations which cause surface waters to become disconnected from the outfalls, limiting surface water outflow to periods with high stage. In fact, it has been frequently observed that CSA discharge structures are elevated over a meter above average surface water levels with no qualitative signs of recent outflow (Reigner and Winkler, 2001). Reigner and Winkler (2001) observed that water storage on the CSAs was greater than anticipated due to underestimates of clay consolidation, and that continued discharge

from CSAs after reclamation, which is designed for to maintain downstream baseflow, was less than expected. CSA outfall structures are designed with concern of the impermeable clays causing more discharge than compared to pre-mined conditions. Underestimation of consolidation and the subsequent increase in storage, however, decrease long-term discharge to less than pre-mined conditions, creating concerns of maintaining baseflows that are sufficient to sustain downstream receiving waters (Reigner and Winkler, 2001).

Riekerk *et al.* (1990) monitored four CSAs over a four and a half year period and observed consistent surface outflow from only one of the sites. Two other sites did experience one short period of outflow but following an extreme rain event, and outflow never occurred from the fourth CSA. Lewelling and Wylie (1993) also monitored outflow at three CSAs during a two year study and found only one, Mobil CSA, where outflow occurred more than once. Though the Mobil CSA experienced a high outflow following substantial storms, it took just that to have any outflow occur, and outflow was only experienced 6% of the duration of the study. In a two year study of four CSAs, Reigner and Winkler (2001) measured total discharge of 7, 33, 68, and 106 cm from the four sites over the two year period, demonstrating how the activity of outfalls and surface water outflow contributions to water budgets vary among CSAs.

Evapotranspiration

The lack of surface water outflow from most CSAs and the low infiltration rates of the clay soils likely causes ET to be the most important water loss of surface water features within CSAs (Reigner and Winkler, 2001). Therefore, it is imperative to accurately account for ET when attempting to understand surface water hydrology of CSAs. Numerous methods are used to estimate ET including climatic-based empirical models, analysis of continuous water level data, energy balance methods, lysimeters, water balances, and transpiration measurements (Drexler *et al.*, 2004).

There are a suite of empirical equations available to estimate potential ET (PET) using climatic data and which often produce inconsistent results. PET is defined as the amount of water that could evaporate and transpire from a particular landscape with no limitations from soil water availability. Lu *et al.* (2005) conducted a study to compare six commonly used empirical models and their applicableness in the Southeastern U.S. The authors compared three temperature based methods (Thornwaite, Hargreaves-Samani, and Hamon) and three radiation based methods (Makkink, Turc, and Priestly-Taylor). Climatic data for PET estimation was collected for 36 forested watersheds in the Southeast. The PET estimations from the various models were significantly different across the watersheds, with greater differences found between the temperature based methods. The results from the different methods were also compared to reported actual ET (AET) for each watershed. It was assumed by the authors that PET exceeds AET as a result of water restrictions and, therefore, PET calculated by the various methods was compared to AET by examining the linear correlation between the two. Compared to the reported AET values, Priestly-Taylor, Turc, and Hamon produced the best estimations and are given by the authors as recommended models to calculate PET in the Southeast. It should be noted that the reported AET values were calculated using watershed-scale long-term water balances of each watershed. This method assumes change in water storage to be negligible over a long period of time and, thus, AET was simply the difference between precipitation and runoff, likely creating some error.

Jacobs *et al.* (2002) performed a detailed study of ET at Paynes Prairie, a large freshwater marsh system in Gainesville, FL. Different from the work by Lu *et al.* (2005), Jacobs *et al.* (2002) considered the effect of soil water availability and separated ET into two stages, wet stage when water availability was not restricting and dry stage when it was. The authors used an

energy-balance method, the eddy covariance method, to quantify AET, and this method is much more accurate than the method used to obtain the reported values used by Lu *et al*. (2005), though only feasible to perform on a smaller scale. During the study period, Jacobs *et al*. (2002) found average AET values of 0.41 and 0.44 cm/day for May and June, respectively. Similar to Lu *et al*. (2005), Jacobs *et al*. (2002) compared measured AET values to estimations by several empirical methods which included Penman, Penman-Monteith, and Priestly-Taylor. The Penman-Monteith method accounts for effects from vegetation type on ET in addition to climatic drivers by including community specific canopy resistance terms (Drexler *et al*., 2004). It was expected that the models should be in agreement with the AET values during wet conditions but should overestimate, by only providing values for PET, during periods with limited soil water availability. The authors found that the Penman-Monteith method produced the best results during the wet conditions, but that the other two methods overestimated ET by more than 20%. And as expected, all three methods overestimated ET during the drier stages.

Mao *et al*. (2002) performed a study of ET from three wetland environments of the Upper St. Johns River Basin, Florida. They used lysimeters in a *Cladium jamaicense* dominated marsh, *Typha latifolia* dominated marsh, and in an open water system to determine AET rates. Similar to the other two studies, Mao *et al*. (2002) compared measured AET values to values calculated by empirical models which included Penman-Monteith, Priestly-Taylor, and Reference-ET empirical methods. The reference crop method is simply an extension of the Penman-Monteith method, where parameters for canopy surface resistance and albedo are based on an extensive surface of well watered and uniform grass, and multiplicative coefficients for different crops (crop coefficients) are applied (Drexler *et al*., 2004). The study was performed for three years and resulted in yearly average AET rates of 0.32, 0.33, and 0.35 cm/day for the open water,

Typha latifolia, and *Cladium jamaicense* systems, respectively. When comparing daily AET to the three estimates of PET, it was found that all three methods needed manipulation of coefficients within the empirical equations to produce consistency between AET and PET. The required adjustments varied seasonally demonstrating limitations to solely applying climatic-based empirical equations with no seasonal considerations.

Lysimeters and energy-balance methods can provide accurate estimates of wetland ET but are only applicable at a small scale and are equipment and labor intensive (Drexler *et al*., 2004). Climatic-based empirical models can be applied for ET estimates at a larger scale, but result in inconsistent results (Mao *et al*., 2002; Jacobs *et al*., 2002; Lu *et al*., 2005) and do not account for water stress (Jacobs *et al*., 2002) and seasonal effects from variable growth characteristics of different species (Mao *et al*., 2002). Analysis of continuous surface water data using the White (1932) method offers a fairly non-intensive method of directly measuring ET and for an entire surface water feature. The White method requires two assumptions: 1) ET ceases at night which allows calculation of hourly groundwater flow during the night and 2) the calculated hourly groundwater flow from the night is constant and can be applied throughout the day (Hill and Neary, 2007; Mitsch and Gosselink, 1993).

The White method has often been applied to water table fluctuations where knowledge of the specific yield of the soils is required, while a specific yield of one is typically used when the method is applied to surface water fluctuations (Hill and Neary, 2007; Mitsch and Gosselink, 1993). At rather shallow surface water levels and non-cylindrical bathymetries, however, the specific yield of the surrounding soils may result in overestimation of ET (Hill and Neary, 2007). With shallow surface water levels, a unit area drop in water level over one day may occur both within the ponded free water and within the soil at the edges of the feature. The drop that occurs

in the surrounding soils results in a composite specific yield that is less than one, and applying a specific yield equal to one in such cases overestimates ET rates. Hill and Neary (2007) found limited effects from this phenomenon with surface water levels above 15 cm.

In situ measurements of transpiration are becoming more popular to document different transpiration rates of species and to determine transpiration rates at the stand level while using biometric data for a stand and various methods to scale up transpiration measurements. Measurement of sap flow rates within a stem and/or trunk can be used to quantify water use by plants. Often two approaches, stem heat balance (SHB) and trunk segment heat balance methods (THB), are used (Smith and Allen, 1996) which have proven to give accurate results when compared to gravimetric measurements of water use (Akilan *et al*., 1994; Baker and Bavel, 1997; Weibel and Boersma, 1995; Steinberg *et al*., 1989, Guitierrez *et al.,* 1993; Heilman and Ham, 1990). Both methods supply heat to a trunk or stem segment and utilize the heat as a tracer for sap movement within a plant, but differ in the method of applying and measuring the heat.

The THB method uses electrode probes placed within the sapwood tissue to provide heat between two also internally placed thermocouples which measure temperature change across the instrumented segment of trunk (Cermak *et al.,* 2004). In contrast, the SHB externally heats and measures temperature change along a stem segment to determine transpiration rates (Smith and Allen, 1996). The SHB method is typically applied to tree branches and trunks of smaller trees (Steinberg *et al.,* 1990), and is often preferred to the THB when measuring flow rates in smaller stem diameters of angiosperms (< 120 mm), due its ability to determine flow rates using bulk heat transfer and independent of internal wood variation (Hall *et al.,* 1998; Herzog *et al*., 1996). Furthermore, known sapwood area is required to determine flow rates in the THB method since the measured rates are in terms of sap velocity whereas the SHB method provides cumulative

stem flow rates independent of variation in xylem anatomy (Hall *et al.*, 1998). One other approach to determine transpiration rates utilizes ventilated chambers to enclose portions of vegetation and measure water vapor and/or CO_2 fluxes to determine transpiration rates, and has been tested alongside sap flow measurements with consistent results (Cienciala and Lindroth, 1995a).

While simply measuring transpiration of a select number of individuals provides transpiration rates of those individuals, application of a scaling-up method is required to determine stand level transpiration of a certain species or community from measured rates. Various scaling methods are available which all use biometric measurements of both the instrumented individuals and the entire population on a given area (Cermak *et al.*, 2004). This biometric data can include leaf area, basal area, and sapwood area. To accurately determine stand level transpiration for a population, all individuals within the stand must have equivalent water availability and individuals to be instrumented must be randomly selected and cover the distributions of size and age of the entire population within the stand (Cermak *et al.*, 2004).

The above discussion simply refers to the various methods of measuring ET and transpiration and was provided to shed some light on the numerous options that could be applied when evaluating CSA ET. There has been some work, however, on ET from CSAs. Munroe (1991) used ventilated enclosure chambers to quantify the amount of moisture released by photosynthesizing vegetation typical of CSAs. *Typha latifolia*, *Salix caroliniana*, and *Ludwigia peruviana* were all studied and are all early successional plants which dominate CSAs. The study concluded that all three species had transpiration rates that were greater than rates associated with open water in Florida and as high as or higher than PET rates predicted with various temperature-based methods. This matched their hypothesis that the adaptive features of

early successional, eutrophic vegetation that colonize CSAs include high rates of transpiration. Other studies of *Salix spp.* transpiration have also documented the potential for high water use by this early-successional genus (Cienciala and Lindroth, 1995b; Cleverly *et al.*, 1997; Wickburg, 2006) and measured rates of *Salix spp.* stand level transpiration higher than typically reported total ET (Conger, 2003; Hall *et al.*, 1998, Gripp *et al.*, 1989).

ET is likely the major water loss of CSAs which are dominated by early-successional species, particularly *Salix caroliniana*; and the dominance of these species along with adequate water availability and the high residual nutrients of the clays (Brown *et al.*, 2008) may result in ET rates which exceed values typical of the region. This stresses the caution of solely using climatic-based methods to determine CSA ET. Rather, a suite of methods should be applied to evaluate transpiration and total ET of these systems to accurately account for this major water loss pathway.

Ecohydrology

Ecohydrology is an emerging science which seeks to understand the dynamics of and interactions between climate, soil, and vegetation and thus the dual regulation of the biotic and abiotic components of an ecosystem (Rodriquez-Iturbe, 2000). Currently, the predominant focus of research in this field is on plant behavioral traits, particularly rooting depths and transpiration rates, and how these simultaneously both affect and are selected for by the vadose zone hydrology in water-limited environments (Laio *et al.*, 2001a; Rodriquez-Iturbe, 2000; Guswa *et al.*, 2002; Wilcox and Thurow, 2006). At the heart of these interactions is soil moisture regime which integrates the actions of climate, vegetation, and soil, and is both of function and a determinant of vegetation water use (Rodriquez-Iturbe *et al.*, 2001; Guswa et al., 2002). The ecohydrologic approach may be a valuable strategy to aid in ecosystem restoration by providing an understanding of the interactions between biotic and abiotic components (Zalewski, 2000).

While this approach has typically been applied to arid regions and sustainability of water resources (Zalewski, 2000), it may also prove useful in restoration of wetlands in humid climates. Such an application of the science would require a switch in focus from vadose zone hydrology, drought, and water stress to soil saturation levels, water table depths, and capillary fringe heights that are required for wetland environments which are rarely inundated. Additionally, these parameters partially determine the resistance of wetland vegetation within typically inundated regions to prolonged dry conditions. Furthermore, the clayey soils of CSAs may uniquely affect the relationships between hydrology and vegetation while the potentially high transpiration rates of CSA vegetation likely play a major role in CSA hydrology; stressing the need for an ecohydrologic approach when evaluating wetlands on CSAs.

Soil texture controls rooting depths and various hydrologic components which induce effects on vegetation and that include overland flow, infiltration, soil moisture dynamics, capillary forces, and soil water availability (Laio *et al*., 2001b). The effect of texture on rooting depths has been evaluated extensively in arid climates, where rooting depth often decreases with increasing clay content (Schenk and Jackson, 2002; Laio *et al*., 2001a). It has also been shown, however, that rooting depth typically increases in humid climates and in arid climates alongside riparian environments where water tables are shallower and which can be relied upon for a constant source of water versus exploitation of periodic rains by shallower root systems (Snyder and Williams 2000). Little is known about rooting depths of vegetation within CSAs, a setting which combines clayey conditions with a wet environment, with the exception of the hypothesis that roots likely follow developing cracks (Reigner and Winkler, 2001).

Soil texture also strongly determines the role between soil water and soil water availability. Soil water potential, the potential energy of water measured in pressure relative to pure free

water, is used to quantify the availability of soil water for plant uptake. Unsaturated conditions create a negative soil water potential which is a function of gravitational, matric, and osmotic pressures. Soil water potential near zero pressure reflects saturated conditions and pressures of or less than -1.5 MPa are typically reported as negative pressures that induce permanent wilting of vegetation (Dingman, 2002). Soil moisture alone cannot be used to evaluate soil saturation and water stress, as the relationship between the soil water potentials of these conditions and soil moisture is determined by and different per soil texture (Dingman, 2002). For example, a typical sandy soil will reach saturation at a volumetric water content (VWC) of approximately 40% and permanent wilting point at slightly less than 10%, compared to typical clayey soil which reaches these values at approximate VWCs of 50% and 30%, respectively (Dingman, 2002). So while clayey soils have a higher water holding capacity and saturation occurs at higher soil moisture value, transpiration ceases and stress is induced at greater water contents in clay than in sandy soils. This highlights the need to couple soil moisture measurements with moisture release curves which relate soil moisture as VWC to soil water potential.

The water-holding potential of clays has been found to create water stress to vegetation more frequently than do coarser soils (Laio *et al*., 2001a). This phenomenon, however, has been predominately observed in arid climates where the sensitivity of water stress to soil texture may be more significant. Through model simulation, Laio *et al*. (2001a) demonstrated that under wetter conditions, water stress is less sensitive to soil texture. Furthermore, Laio *et al*. (2001a) concluded that less stress occurs to vegetation in finer soils compared to coarser soils when under wetter conditions, and this switch of the effects of soil texture has been referred to as the inverse texture effect. Furthermore, clay content significantly increases capillary fringe heights that extend above the water table (Dingman, 2002), which may maintain near saturation levels in

shallow soil profiles when the water table is near the soil surface. The potential capillary fringe heights in the absence of water removal can be quantified while developing a moisture release curve and is approximately the absolute value of soil water potential where soil moisture values begin to significantly decrease with decreasing water pressure (Dingman, 2002). Transpiration rates and the location of water uptake, dictated by rooting depths, control where and the extent to which these capillary forces are interrupted and competed with, all affecting soil moisture spatial and temporal dynamics which in turn have a feedback on plant behavior.

The effect of water limitations on reducing AET to below PET has already been mentioned, and what soil moisture value may induce such stressed conditions is a site-specific value that cannot be solely examined with moisture release curves. The latter stems from the large variability in soil water pressures that induce stomatal closure well before permanent wilting point is reached (Laio et al., 2001a). While -1.5 MPa is often assumed induce permanent wilting of temperate crops, it has been shown that this value does vary for different species (Laio et al., 2001a)). More importantly, the negative pressure which creates the onset of stomatal closure and reduction of transpiration before permanent wilting occurs varies quite substantially among species (Laio et al., 2001a). Jacobs *et al.* (2002) found that AET significantly departed from PET at a VWC of 0.09 in their wetland system of study. This VWC value is extremely low and was experienced when the water table dropped below 1 m. The soils at this site, however, were sands with an organic surface layer. The clayey soils of CSAs likely cause ET to be affected at much higher soil moisture values but at greater depths to water tables, with the latter also greatly depending on rooting depths.

Figure 1-3 shows a systems diagram of the effects of clay and rooting depths on hydrologic flows within CSAs. The hydraulic conductivity of the soil is shown as a function of the ratio of

sand to clay, with the higher amount of sand relative to that of clay increasing conductivity. While Figure 1-3 shows this simply as a relationship between sand and clay, other soils such as overburden deposits also increase hydraulic conductivity. Runoff amounts to a surface water feature decrease with increasing conductivity, shown as an inverse relationship between runoff and conductivity (Figure 1-3). With less runoff, there is more water to infiltrate and be stored in the vadose zone as soil moisture. The soil moisture infiltrates towards the local groundwater, and this flow is a direct function of the conductivity. With more clay and a lower hydraulic conductivity, the potential for capillary forces to create flow from the water table towards the vadose zone is increased. The magnitude of the capillary fringe is therefore shown in Figure 1-3 as an inverse relationship with hydraulic conductivity. With minimal rooting depth, vegetation uses soil moisture within the vadose zone for water requirements and transpiration, depleting soil moisture storage. As rooting depth increases, vegetation can potentially rely on the local groundwater for a more constant water source.

Plan of Study

To better understand CSA hydrology and its potential role in the creation or enhancement of wetlands within CSAs, this study collected and used continuous hydrologic and climatic data from eight CSAs in north and central Florida, along with topographic data, to evaluate hydrologic regimes of CSAs and the major determinants of these regimes. The hydrologic evaluations were used to answer the following questions: Do hydrologic regimes vary between CSAs, and are there regimes typical of CSAs that are conducive to wetland development? Can water budgets be performed which accurately account for all inflows and outflows and that allow prediction of hydrologic regime to couple with restoration plans? How do site specific factors such as sand tailings, overburden deposits, and topography affect the hydrologic regimes among CSAs and thus wetland restoration attempts?

Water budgets of surface water features within the eight monitored CSAs were performed to account for all inputs and outputs using field collected data. Inputs include direct rainfall and runoff from the surrounding watershed. Therefore, collected rainfall and surface water well data were used in storm event analysis to evaluate the effect of rainfall intensities and antecedent conditions on stage responses. Outputs of the surface water include surface water outflow, ET, and infiltration. While not all of the monitored sites had active outfalls, several did, and thus, outflow channels were instrumented with wells to provide data for determining discharge rates. ET is likely the most important water loss pathway on CSAs and, therefore, a major goal of this research was to develop accurate estimates of ET rates. Different methods for estimating ET were explored including the use of various climatic-based empirical models, continuous water level data, and transpiration measurements. Infiltration of surface water is extremely variable on CSAs, leading to much speculation of the magnitude and spatial variability of this flow. Surface water infiltration ($I_{infiltration}^{1}$) is shown in Figure 1-2 as loss of surface water to the local groundwater of the system and as lateral seepage of surface water out of the dikes, and is defined here as the cumulative effect of these rates. Water exchange between the local groundwater and surface water was evaluated using groundwater wells installed in the upland areas of the sites and measured hydraulic conductivities. Networks of groundwater wells were installed on the dikes to provide data to estimate dike seepage. Total infiltration losses of surface water were estimated using continuous surface water data. An analysis of the loss of local groundwater ($Infiltration^{2}$) within the sites to the regional groundwater (Figures 1-1 and 1-2) was not included in this study.

Water balances of the inflows and outflows of the instrumented surface water features were performed using changes in storage to evaluate the accuracy of the various hydrologic flow

estimates and to document differences among CSAs in terms of input and output contributions to surface water budgets. Temporal models for the instrumented surface water features were developed from the water budgets while using the best estimates for infiltration, runoff, and ET. These models were used to predict the temporal characteristics of the hydrology of CSAs in terms of stage and to further evaluate the hydrologic flow estimates through simulation.

Since the extent of a wetland environment is not limited to the inundated regions and is a function of soil moisture regime just upland of the flooded regions, it is critical to understand how CSA soils affect soil moisture regime and more importantly, soil water availability, when restoring wetlands on rarely flooded areas. An ecohydrologic study was included to evaluate interactions between soils, hydrology, and dominant wetland vegetation of CSAs. Particular focus was placed on how the clayey soils affect the interactions between local groundwater and soil moisture regimes, soil moisture values and soil water availability, and soil water availability and rooting depths and transpiration rates.

Three sites were instrumented to continuously measure soil moisture with depth and groundwater levels along a hydrologic gradient to observe the relationship between water table fluctuations and soil moisture regimes. Soils were also sampled along the gradient to develop moisture release curves and determine the relationship between soil moisture values and soil water potential. The moisture release curves also allowed determination of capillary fringe heights and soil moisture values that represented saturation values and permanent wilting points. At two of the sites, root biomass allocation with depth and transpiration rates of *Salix caroliniana* were measured and related to the measured soil moisture regimes and associated soil water availabilities.

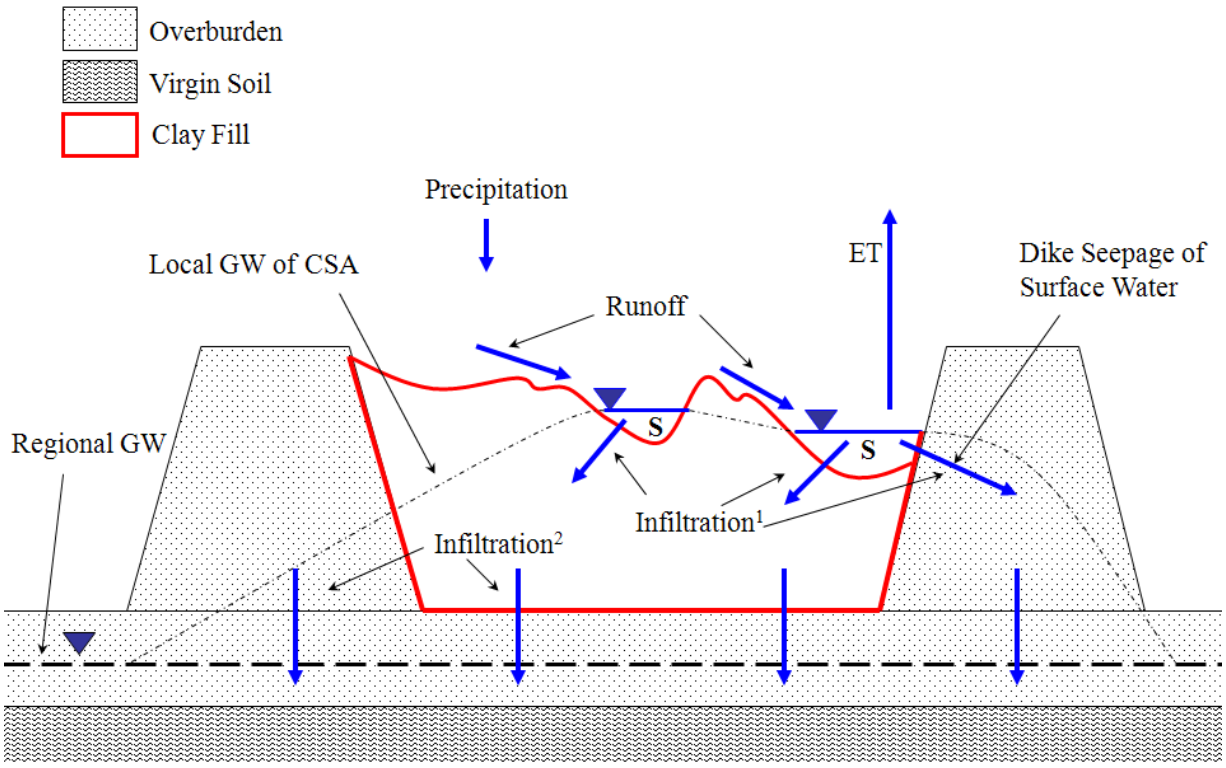

Figure 1-1. Hydrologic flows of isolated surface water features on a CSA

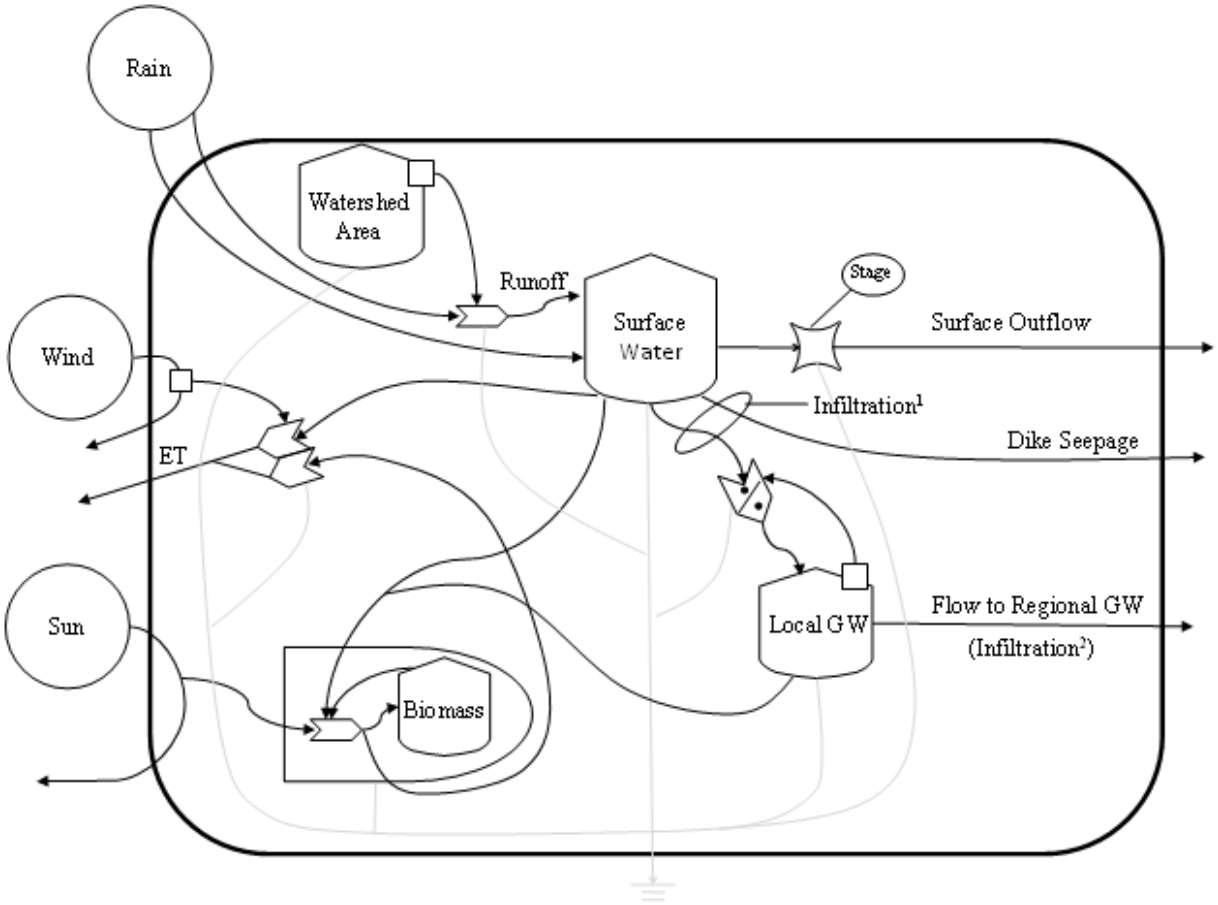

Figure 1-2. Systems diagram of hydrologic flows of a surface water feature within a CSA.

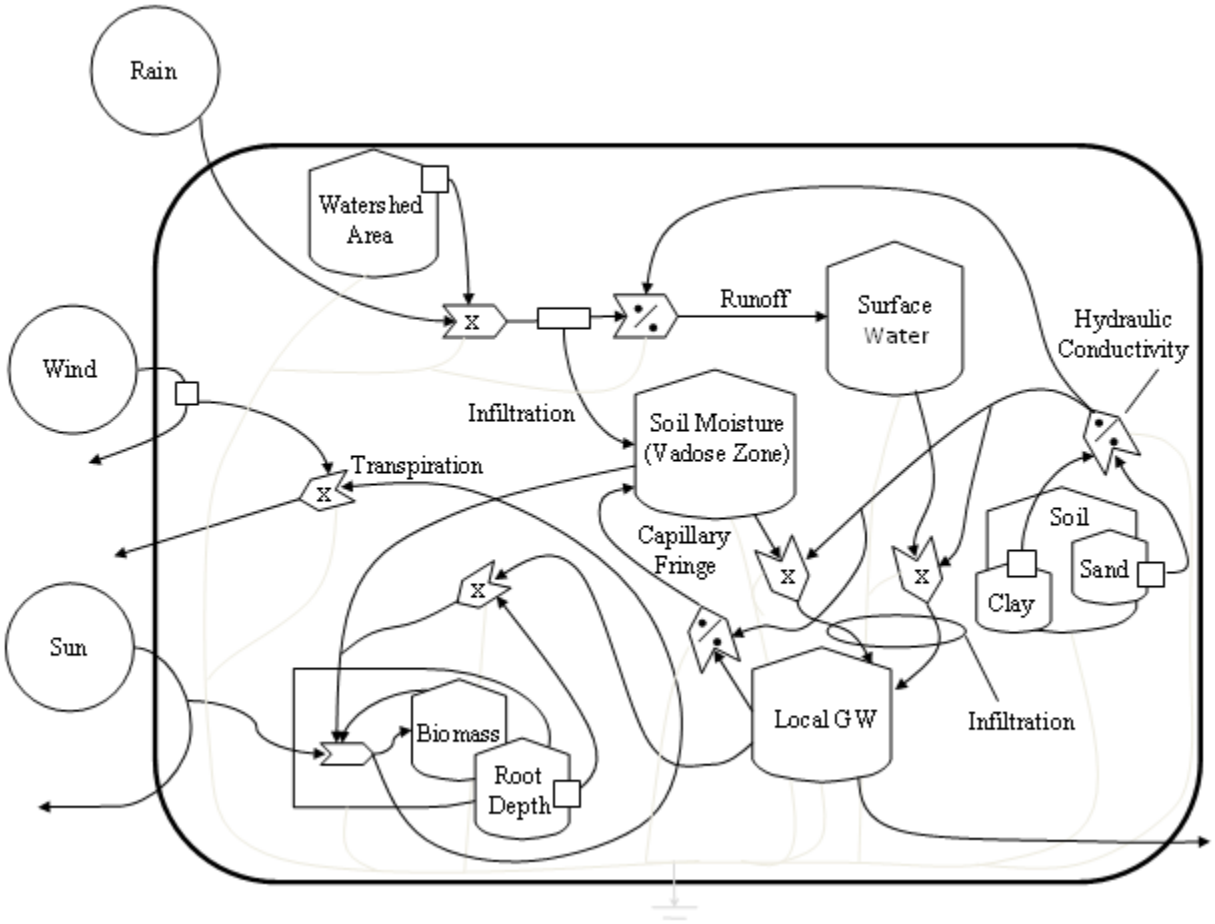

Figure 1-3. Systems diagram of effects from hydraulic conductivity and rooting depths on hydrologic flows of a CSA.

CHAPTER 2
METHODS

Eight CSAs were monitored to evaluate hydrologic regimes of CSAs, the major determinants affecting these regimes, and ecohydrologic relationships between CSA biota and soils. This chapter discusses the various methods employed during these evaluations. Descriptions of the eight monitored sites and the hydrologic instrumentation protocol are presented first, followed by a description of how surface water regimes were assessed and compared. The water budget section explains methods used to determine the various hydrologic flows of the instrumented surface water features including ET, overland flow or runoff, surface water outflow, and dike seepage. The water budget section also presents the methods used in calculating water balances for the surface water features, assessing groundwater flows, and analyzing daily declines. The latter was a detailed evaluation of the daily decline rates observed during daytime and nighttime hours to better separate ET and groundwater flows. The temporal hydrologic models section discusses how the results from the water balances were utilized in development of models to predict surface water stage. The ecohydrology section presents the methods employed to create moisture release curves, continuously measure soil moisture regimes with depth, and determine root biomass allocation and transpiration rates of *Salix caroliniana* individuals.

Site Descriptions

Hydrologic monitoring from fall of 2004 through summer of 2008 of eight CSAs, which ranged in size and age, was conducted to evaluate all inputs and losses to the surface water systems. The nature of fill also differed among the eight sites, with four sites having pure clay, three sites having sand tailings deposited over pure clay on portions of the sites, and one site with sand-clay mix co-deposited (Table 2-1). Some sites had multiple small depressional features

whereas others had larger contiguous wetland areas, but the vegetation within the wetland features of all sites was similar (Table 2-1). The two PCS sites are in Hamilton County in northern Florida, and all other sites are in Hardee and Polk Counties in central Florida.

Instrumentation for Hydrologic Monitoring

The collected hydrologic data included precipitation from HOBO® data-logging tipping bucket gauges (factory calibrated; accuracy = 1.0 %) (Onset Computer Corporation, Bourne, MA) and continuous water levels from surface water and groundwater wells. Solinst® mini LT 15' continuous logging pressure transducers (accuracy = 0.5 cm, resolution = 0.1 cm) were deployed in the wells to collect continuous water level data (Solinst Canada Ltd., Ontario, Canada). Locations of all wells on the eight sites are shown in Figures 2-1, 2-3, 2-5, 2-7, 2-9, 2-11, 2-13, and 2-15 along with the digital elevation models (DEMs) of the sites. Well locations, inundated areas with maximum water levels, and the contributing watersheds of the instrumented surface water features within the eight CSAs are shown in Figures 2-2, 2-4, 2-6, 2-8, 2-10, 2-12, 2-14, and 2-16 The inundated areas are shown using the maximum water level recorded at each surface water feature during the period of study to provide spatial reference of the zones of maximum flooding that occurred during data collection. The pressure transducers measured total pressure, in equivalent height of water, and therefore needed to be corrected for barometric pressure. Solinst® Barologgers (accuracy = 0.5 cm, resolution = 0.15 cm) were installed at each site to provide barometric pressure data and were programmed to record simultaneously with the pressure transducers. The pressure transducers were originally programmed to record every hour, but were then set to record on 15 minute intervals to provide more data.

Surface water wells were installed in the deepest part of the main surface water feature of each site. Wells were constructed of 5.08 cm diameter Schedule 40 polyvinyl chloride (PVC) pipe that was slotted and screened along the entire length. The space between the hand-augered

hole and the well screen was packed with coarse silica sand up to 20 cm below ground surface. Initially when installed in inundated conditions, the surface water wells were sealed with surrounding clay and if found dry at a later date, hydraulic cement was used to cap and seal the well. The wells were screened below ground to allow for belowground water table recordings in the event the water feature became dry. Direct measurements at the wells during site visits were conducted to calibrate the continuous data. Three sites had multiple surface water features instrumented (Figures 2-3, 2-7, and 2-15). The original surface water well at CFI SP-1 was moved to a new location during summer 2007 since it was found that the new location was actually at a lower elevation (Figure 2-11). The well was moved to provide water level fluctuations at the deepest part of the feature, and all water levels from the original well position were adjusted to reflect surface water levels at the new well position.

One monitoring groundwater well was installed via hand-augering at each site in an area just upland of and adjacent to the main surface water feature. These wells were slotted and screened from the bottom of the borehole to 0.5 m below the ground. The space between the borehole and the well was packed with coarse silica sand along the screened section of pipe, which was followed with clay and then hydraulic cement to cap and seal the well. Another groundwater well was installed at a later date further from the feature and at a higher elevation than the first groundwater well to observe how groundwater dynamics may change with distance from surface water. These wells were 10.16 cm in diameter and installed using a gas-powered auger. Three sites had an additional groundwater well later installed in an intermediate elevation between the other two groundwater wells. The ground elevations of all wells were used to represent groundwater and surface water levels relative to one benchmark, the ground surface of the surface water well.

At three sites that had surface water in contact with surrounding dikes, wells were installed on the tops and downward slopes of the dikes (Figures 2-1, 2-3, and 2-7). Only discrete groundwater levels were recorded at the dike wells and with a float measuring tape on site visits to provide data for dike seepage estimation. The dike wells were 10.16 cm in diameter and installed with a gas-powered auger.

HOBO® weather stations (Onset Computer Corporation, Bourne, MA) were installed on three of the eight hydrology sites, one in north Florida at PCS SA 10 and two in central Florida at Mosaic K5 and CFI SP-1. The weather stations installed in open areas of each site contained relative humidity, temperature, and PAR sensors along with an anemometer to measure average wind speed, wind gusts, and wind direction. All sensors were factory calibrated and were programmed to record at one hour intervals.

Light detection and ranging (LiDAR) technology was employed, along with subsequent analysis to correct for vegetation structure, to gather the most recent and accurate topographic information for the eight CSAs. The technology is not capable of penetrating water and only gives water surface elevation and, therefore, no topographic information was obtained for areas flooded during the collection period. LiDAR topography maps were generated as DEMs for the sites by the National Center for Airborne Laser Mapping (NCALM) at the University of Florida, Gainesville, Florida (Figures 2-1, 2-3, 2-5, 2-7, 2-9, 2-11, 2-13, and 2-15). These maps were estimated to be accurate to 15 cm vertically and 12 cm horizontally, with a cell resolution of 1 m^2. To supplement and check LiDAR data, surveying was performed using a Topcon RL 20 laser level (Topcon Positioning Systems, Livermore, CA USA). Surveying data was used preferentially to LiDAR data when possible such as to develop transect profiles and to determine relative elevation differences between locations of reasonable proximity.

Evaluation of Flooding Regimes

Surface water depth fluctuations and frequency and duration of dry periods were compared among CSAs. Multiple surface water features, referred to as surface water-1 (SW-1) through surface water-3 (SW-3), instrumented within individual sites allowed these comparisons within a single CSA. In these cases, water levels measured at the multiple features were presented as water elevations relative to the elevation of the ground surface at the SW-1 well, so to compare all water elevations relative to one benchmark. Comparisons of water level signatures and the relative water elevations of the multiple surface water features were performed to observe if and when features on one CSA were isolated from one another. The surface water elevations of features which were connected to an outfall system were evaluated in reference to the invert elevations of the outfall to determine depths at which surface water outflow occurred.

Surface water data from 2005 to 2007 collected at a marsh system and a forested wetland within the Green Swamp system in central Florida was provided by Southwest Florida Water Management District. The Green Swamp marsh system is a 0.69 ha marsh dominated by *Panicum hemitomon* and *Pontedaria cordata* located at 28^0 23’40’’N and 81^0 58’15’’W. The forested system is a 0.73 ha cypress dome dominated by *Taxodium ascendens* located at 28^0 21’43’’N and 81^0 56’47’’W. The hydrologic regimes of these isolated wetland systems were compared to those of the surface water features within the monitored CSAs to evaluate differences in terms of water depths and fluctuations.

Water Budgets

Water budgets of surface water features within the CSAs were performed to account for surface water inputs, outputs, and storage all in terms of depth.

ET Estimation

ET was estimated using seven empirically based models and climatic data from the weather stations. Data from the closest CSA with a weather station were used for sites where a weather station was not installed. Data gaps due to equipment failure were supplemented with data from the nearest weather stations that are part of the Florida Automated Weather Network program operated by the University of Florida's Institute of Food and Agricultural Sciences. Data from the Ona and Frostproof IFAS weather stations were used when needed for the central Florida sites and from the Live Oak station for the north Florida sites. The weather data used in the various models included daily photosynthetic active radiation (PAR), minimum, maximum and average daily temperature and relative humidity, and average daily wind speed. Total solar radiation (W/m^2) was estimated from PAR ($\mu mol/m^2/sec$) using a conversion factor of 0.435 (Meek *et al.*, 1984). The seven empirical models used to estimate potential ET (PET) included Priestly-Taylor, Penman, Penman-Monteith, Hargreaves-Samani, Hamon, Makkink, and Turc whose equations follow:

Priestly-Taylor Method:

$$\lambda PET=\alpha*(R_n-G)*\Delta/(\Delta+\gamma) \quad (2\text{-}1)$$

Penman Method:

$$PET= [\Delta*(Rn-G) + \gamma*K_E*\rho_w*\lambda*u_2*(e_s-e_a)]/ \rho_w* \lambda*(\Delta+ \gamma) \quad (2\text{-}2)$$

Penman-Monteith Method (modified by the FAO for expansive short grass and commonly referred to as the Reference Crop Method (Drexler *et al.*, 2004)):

$$PET=[0.408*\Delta*(R_n-G) + \gamma*(900/(T+273))*u_2*(e_s-e_a)]/(\Delta+ \gamma*(1+0.34u_2)) \quad (2\text{-}3)$$

Hargreaves-Samani Method:

$$\lambda PET=0.0023*R_a*TD^{0.5}*(T+17.8) \quad (2\text{-}4)$$

Hamon Method:

$$PET=0.1651*L_d*RHOSAT*KPEC \quad (2\text{-}5)$$

Makkink Method:

$$PET=0.61*(\Delta/(\Delta+ \gamma))*(R_s/58.5)-0.12 \quad (2\text{-}6)$$

Turc Method:
RH<50%
$PET=0.013*(T/(T+15))*(R_s+50)*(1+(50-RH)/70)$

RH>50%
$PET=0.013*(T/(T+15))*(R_s+50)$ (2-7)

where PET is the daily potential ET (mm/day); λ is the latent heat of vaporization (MJ/kg); α=1.26 for wet or humid conditions; R_n is the net radiation ($MJ/m^2/day$) and is calculated as the difference between net shortwave radiation and net longwave radiation where shortwave radiation is total radiation minus albedo of water (0.05) and longwave is a function of total incoming radiation, clear sky radiation, temperature, and relative humidity (equations not shown); G is the heat flux density to the ground which is assumed to be negligible when calculating daily PET; Δ is the slope of the saturation vapor pressure temperature curve ($kPa/^oC$); γ is the psychrometric constant ($kPa/^oC$); K_E is a coefficient reflecting efficiency of vertical transport of water vapor and is calculated as a function of wetland area(equation not shown); ρ_w is the density of water (kg/m^3); T is average daily air temperature (^oC); u_2 is the wind speed at 2m height (m/s); (e_s-e_a) is the saturation vapor pressure deficit (kPa); R_a is the extraterrestrial solar radiation ($MJ/m^2/day$); TD is the daily difference between the maximum and minimum air temperature (^oC); L_d is the daytime length in multiples of 12 hours; RHOSAT is the saturated vapor density (g/m^3); KPEC is a calibration coefficient=1.2; R_s is the daily solar radiation ($MJ/m^2/day$); and RH is the relative humidity (%).

The Penman method is typically applied to open water systems (Dingman, 2002) and wetland systems (Mitsch and Gosselink, 2000) and, therefore, Penman-estimated ET rates were initially selected for use in the runoff analysis, water balance analysis, and temporal hydrologic modeling. The sensitivity, however, of using other methods for estimating ET during such analyses was considered.

Runoff Analysis

An evaluation of runoff inputs, or overland flow, to isolated surface water features was conducted to observe differences among features in terms of responses to rain events. Runoff analysis was performed for measured rain events during periods when no surface outflow occurred to avoid inclusion of outflow estimation error in the analysis. Stage response (m) for each rain event was measured as the stage increase from midnight of the day it rained to midnight of the day after it rained (Figure 2-17). Event response was defined as the amount of input resulting from direct rainfall and runoff, and therefore represents the hypothetical increase of surface water from direct rainfall and runoff in the absence of ET (Figure 2-17). Event response was calculated as stage response plus the Penman-estimated ET for day it rained. Accounting for ET while determining event response avoided underestimation of total input resulting from a rain event. A runoff analysis that only used changes in water levels from midnight to midnight would fail to account for any runoff or rainfall inputs that were removed via ET and thus not observed with daily stage increase. Regressions of event response versus magnitude of rain were performed to determine if total inputs from a rain event could be adequately predicted from rainfall and independent of watershed size and antecedent conditions. Runoff depths were calculated by subtracting the rainfall amount from the event response and represent total input as depth from overland flow.

Delineation of watersheds is required to determine the contributing area to a surface water feature, which is needed to determine runoff coefficients using the following equation (Mitsch and Gosselink, 1993):

$$\text{Runoff Volume} = C * A_{up} * P \quad (2\text{-}8)$$

where runoff volume (m^3) is the volume of overland flow from the contributing area, A_{up} (m^2), to the surface water feature resulting from rain, P (m). The runoff coefficient, C, therefore

represents the percentage of total rain falling on the contributing area that is delivered to the surface water feature through overland flow (Mitsch and Gosselink, 1993). Dividing Equation 2-8 by the area of the receiving surface water feature, A_w, and rearranging to solve for the runoff coefficient results in the following equation:

$$C = (A_{wet}/A_{up})*(\text{runoff depth}/P) \quad (2\text{-}9)$$

where runoff depth (m) represents the volume of overland flow per receiving area and calculated as previously discussed, and the inverse of A_w/A_{up} is defined as the upland to wetland area ratio. Upland to wetland ratios were determined by delineating watersheds within a CSA. Each CSA was considered to be the main watershed and subwatersheds were delineated within this main watershed using a multiple watershed approach to determine the contributing areas of each surface water feature (Brown *et al*., 2008). Since upland and wetland areas varied with fluctuations in surface water stage, ratios of upland to wetland area were calculated for different surface water levels at 10 cm increments using the DEMs, and the ratios for each water feature were modeled as a function of surface water stage.

Typical runoff analysis routes the volume of water from a rain event through a stream network to an outlet in order to quantify storm event flows at that point (Garbrecht and Martz, 2000). The goal here, however, was not to route water to outlets but to determine runoff volumes received by the isolated depressions within a CSA and thus required a multiple watershed approach. Defining the watershed as the entire CSA would distribute all overland flow within the CSA to only the lowest isolated features, whereas the overland flow may be distributed to and stored in isolated depressions at higher elevations throughout the CSA (Figure 2-18). Multiple watershed delineation of the CSAs was performed using the DEMs and the Spatial Analyst tool in ArcGIS® 9.2 (Brown *et al*., 2008). The amount of watersheds delineated

using the ArcGIS® procedure was based on the z-limit feature within the Spatial Analyst tool (Figure 2-19). The z-limit is a measure of the difference between the lowest point within a watershed and the lowest point on the watershed boundary, thus representing the depth of a watershed. The z-limit allows watershed delineation at multiple scales of analysis. A z-limit of zero generates over a thousand subwatersheds for a CSA, a z-limit of 20 cm delineates hundreds of subwatersheds, and when a large enough z-limit is used then the entire CSA is delineated as one watershed (Figure 2-19). The multiple delineated watersheds for the CSAs included in the runoff analysis are shown in Figures 2-20 through 2-26 (Brown *et al*., 2008). Two sites, PCS SA 10 and Mosaic K5, have the monitored watershed with a dividing line shown to represent separation of watersheds when surface water features become disconnected with shallow surface water levels (Figures 2-21 and 2-26).

Two sites, PCS SA 10 and Mosaic H1, had three functions determined relating upland to wetland area ratios to stage using three different scales of watershed delineation to evaluate effects of scale on runoff coefficients. The largest scale delineated the entire CSA as one watershed contributing to the surface water feature. The smallest scale of analysis produced the highest number of individual watersheds within the CSA and therefore the smallest size watershed contributing to the surface water feature. Upland to wetland ratio-stage functions were determined for all other water features with the smallest scale of analysis while adding contributing areas in the case water features merged with stage increase (Brown *et al.*, 2008). The latter was necessary since some surface water features were separate at low water levels, but became connected at higher water levels (Figures 2-21 and 2-26). These water features, therefore, essentially became one larger water feature at higher water levels with their watersheds being combined.

The upland to wetland area ratio for an individual rain event was calculated with the stage prior to the rain event and the determined upland to wetland area ratio-stage function. The ratio, along with the rain and calculated runoff depth, were used to calculate a runoff coefficient, C, for the event using Equation 2-9. Runoff coefficients were calculated for each rain event with no surface water outflow for water features on all but one site, Tenoroc 4, and at the three scales of watershed delineation for a feature at PCS SA 10 and Mosaic H1. For these two features, the coefficients were averaged over all events and compared among the different scales of watershed analysis. Average coefficients for all water features using the smallest scale of delineation were compared to observe differences both among and within the sites.

As a constant runoff coefficient for a feature may not be applicable to all events or conditions, models for predicting the coefficient based on magnitude of rain event and antecedent conditions were explored. Antecedent conditions were represented with two different indices. The antecedent rain index following Woods and Rowe (1996) was related to the 14 day history of rainfall prior to the event being modeled with the following equation which weights recent rainfall more heavily:

$$\text{Antecedent rain index} = I_1/1 + I_2/2 + I_3/3 + \ldots\ldots + I_{13}/13 + I_{14}/14 \qquad (2\text{-}10)$$

where I_n is the rainfall(m) that occurred n days previous to the event being modeled. Another index, the antecedent ET index, representing the amount of ET that occurred previous to the event and was calculated by summing the ET (m/day) of the previous 14 days (Dingman, 2002). Multiple variable regression to determine predictive models for runoff coefficients was performed in Microsoft Excel® using the calculated runoff coefficients as the dependent variable and rainfall amount, antecedent rain indices, and antecedent ET indices as independent variables.

The multiple regression models were compared to the simpler models that predicted total input solely from rainfall depths. All measured positive event responses were summed over the period of analysis and compared to the estimates from the various runoff models to compare the models' efficiency in predicting runoff.

Surface Water Outflow

Five monitored sites had outfall structures that were periodically active during the monitoring period. Two sites, PCS SA10 and PCS SA 01, had v-notched weirs as the outfall structures. The weir inverts were surveyed to determine the elevation difference between the inverts and the ground surfaces at the surface water wells of the nearby water features. The surface water wells were installed at a distance away from the weirs where there was no effect from the hydraulic slope induced from flow over the weir. The distance was at least the recommended value of twice the vertical dimension of the weir opening (Dingman, 2002). Surface water data and the surveyed elevations were used to determine when the outfall structures were active.

Three sites, Tenoroc 4, Mosaic HP-10, and Mosaic K5, had channel systems which were connected to multiple depressional features across the CSAs and that produced surface water outflow at certain stages. The effluent end of the channels at Teneroc 4 and Mosaic K5 were instrumented with wells to provide data for outflow calculations. Two wells were installed with logging pressure transducers in the center of each channel and at least 50 m apart. The upstream and downstream wells were surveyed to determine relative elevation differences between the two. The channel cross section at the upstream well was surveyed to determine cross-sectional flow area and wetted perimeter as a function of surface water level at the upstream well. The elevation differences and continuous water level data from the set of wells were used to calculate

daily hydraulic slope (m/m). The hydraulic slopes were used to determine surface water outflow (m/day) using the Manning's equation:

$$Q_o/A_w = 1.0*R^{2/3}*S^{1/2}*A_x/n \quad (2\text{-}11)$$

where Q_o/A_w is the surface water outflow (m/day), R is the wetted perimeter, S is the hydraulic slope (m/m), A_x is the cross-sectional flow area, and n is a Manning's roughness coefficient. A_w, the wetland area, was calculated using surface water data and upland to wetland ratio-stage functions. The roughness coefficient was field calibrated with velocity measurements using an Acoustic Doppler Velocity (ADV) meter and the velocity-area flow calculation technique, where velocities were measured at 6/10 depth and at 50 cm increments across the width of the channel (Dingman, 2002).

Water Balances

Water balances for the monitored surface water features were calculated using stage, rainfall, predicted runoff depths, Penman-estimated ET, and surface water outflow data and the basic water balance equation:

$$\Delta S/\Delta t = P - Q_o/A_w + R + G_i/A_w - G_o/A_w - ET \quad (2\text{-}12)$$

where S is stage (m), t is time (days), P is precipitation (m/day), Q_o/A_w is surface water outflow (m/day), R is runoff depth (m/day) into the wetland from the surrounding watershed calculated as previously discussed, G_i/A_w and G_o/A_w are groundwater inflow and outflow (m/day), and ET is Penman-estimated ET (m/day). The balance between groundwater inflow and outflow to the surface feature was treated as a residual value (m/day), and water balances were performed with data from periods when no so surface water outflow occurred simplifying Equation 2-12:

$$\Delta S/\Delta t = P + R - ET - Residual \quad (2\text{-}13)$$

In the cases where channels were instrumented to provide more accurate outflow estimates, the surface water outflow term, Q_o/A_w, was included in Equation 2-13.

The resulting residual values represented infiltration/exfiltration plus any propagated errors from the calculation of the other flows. It was assumed that most of the error was associated with ET and, therefore, positive residual values represented a combination of underestimation of ET and/or infiltration. Total runoff depths as percentage of rain and the resulting residuals were compared among features to identify differences among and within the sites.

Dike Seepage

Dike wells were installed on the dikes of PCS SA 10, PCS SA 01, and Mosaic H1 to determine lateral dike seepage of surface water from features with surface water in contact with the dikes. Slug tests were performed in the dike wells on three different occasions by removing a volume of water and using pressure transducers to collect data on the time of recovery to the initial static water level. The Hvorslev (1951) method was used to calculate lateral saturated hydraulic conductivities of the groundwater features and dikes using the following equation:

$$K_s = r2*\ln(L/R)/(2*L*T_0) \quad (2\text{-}14)$$

where K_s is saturated hydraulic conductivity (cm/s), r is the radius of the well casing (cm), R is the radius of the well screen (cm), L is the length of the well screen below the initial water level (cm), and T_0 is the time it takes for the water level to rise 63 % of the initial displacement (s).

Discretely collected groundwater levels in each of the dike wells and survey data of the dike profiles were used to develop groundwater profiles across the dikes. The hydraulic conductivities, groundwater profiles, and surface water levels were used to calculate dike seepage with a derivation of the Darcy equation for bank loss:

$$q_b = [k_s*D*L_b(dh/dx)]/A_w \quad (2\text{-}15)$$

where q_b is dike seepage (m/day), k_s is lateral saturated hydraulic conductivities (m/day), D is the depth of surface water within the dike (m), L_b is the length of dike (m), dh/dx is the slope of the hydraulic gradient across the dike (m/m), and A_w is the area (m^2) of the surface water feature in

contact with the dike. Dike length was defined as the length of dike in contact with surface water and was measured using ArcGIS®. Wetland area was determined with the upland to wetland ratio-stage function and stage. Dike seepage was estimated at different water depths in contact with the dikes to observe sensitivity of that parameter. Performing this analysis only on sites that have surface water in contact with the dikes followed the definition of dike seepage as lateral seepage of surface water (Figure 1-2).

Local Groundwater Analysis

An evaluation of hydraulic gradients between the surface water features and water tables of the surrounding uplands was performed to assess local groundwater flow direction. Continuous water level data from the groundwater and surface water wells, along with topographic data either from surveying or LiDAR, were used to determine the groundwater elevations relative to surface water elevations. The elevation differences between the recorded groundwater levels and surface water levels were evaluated to determine hydraulic gradients and thus direction of potential groundwater flow. As the potential for groundwater flow is created by the hydraulic gradient but limited by the saturated lateral hydraulic conductivity, slug tests were performed in the groundwater wells to obtain estimates of hydraulic conductivities. The same method of determining saturated hydraulic conductivities used in dike seepage was employed and on three different occasions. Conductivities and elevation differences between groundwater and surface water were compared to determine differences among sites in terms of potential groundwater flows.

Daily Decline Analysis

Analysis was performed to evaluate daily decline of surface water levels in detail. Time periods where no rainfall or surface water outflow occurred were identified for each site. Linear regression was performed with surface water levels (15 minute to 1 hour increments) during

these times to calculate average surface water loss in terms of depth per day. The daily (24 hrs) decline rates were compared to the associated daily ET rates calculated with the Penman method to observe how well the methods predicted loss and if significant differences occurred, suggesting infiltration and/or exfiltration. Daily decline rates were averaged over the growing and non-growing seasons to compare with estimates and reported measurements of seasonal ET. Growing season was defined as the beginning of May through October. Additionally, the decline rates were compared among water features to observe differences in rates of surface water loss.

At selected surface water features, the original Solinst® pressure transducers were replaced by newer Solinst® transducers, including barologgers®, which were more accurate (0.25 cm) with a higher resolution (0.005 cm). The resolution of the data collected by the new transducers allowed analysis of diurnal fluctuations in surface water and separation of nighttime and daytime declines. With accurate measurement of changes in surface water during nighttime hours when ET is negligible, groundwater flows can be determined and used to back calculate out ET using the surface water change during the entire 24 hour period. The White (1932) method was utilized to calculate groundwater flow and ET rates (cm/day) using the equation:

$$ET = S_y*(24h \pm s) \quad (2\text{-}16)$$

where ET is ET (cm/day), S_y is the specific yield (dimensionless) and equal to 1.0 for surface water, h is the net groundwater inflow rate (cm/hr) calculated during nighttime hours, and s is the net fall (+) or net rise (-) of surface water over 24 hours. The analysis of surface water levels with the White method was performed with surface water levels deeper than 15 cm to avoid overestimation calculated rates as was found to by Hill and Neary (2007) to occur at shallower water depths.

Daily ET rates and groundwater flow as infiltration rates were calculated for days with no rainfall or surface water outflow. A negative infiltration rate was defined as groundwater inflow to a surface water feature and thus exfiltration. Monthly averages of the calculated daily rates were determined and compared among sites and to monthly average daily Penman-estimated ET rates. Total daily declines (decline over 24 hrs) measured with the new pressure transducers were determined with linear regression, and the resulting slopes were also included in the comparison among calculated ET rates with Equation 2-16 and Penman-estimated ET.

Temporal Hydrologic Modeling

Hydrologic models were developed that predicted daily stage (m) for the instrumented surface water features using rainfall, Penman-estimated ET rates, the developed runoff models, and Equation 2-13 with the exclusion of the residual term. Daily ET was estimated with the daily climatic data and Penman method. Infiltration rates equivalent to the residuals from the water balances were included and the models' predictive abilities were evaluated by comparing to actual surface water data. Seasonal, multiplicative coefficients applied to Penman-estimated ET rates were explored and infiltration rates were adjusted in an iterative approach to produce the best fits. Seasonal coefficients refer to coefficients multiplied by Penman-estimated ET rates in the non-growing (November to April) and growing seasons (May to October). The seasonal ET coefficients are analogous to the crop coefficients used in the Canopy Cover Coefficient method which is typically performed in conjunction with the FAO adjusted Penman-Monteith method with grass as the reference crop (Drexler *et al*., 2004). The quality of fit between the modeled stage and actual stage was quantified using a square of the correlation coefficient, R^2, value for nonlinear regressions with the equation:

$$R^2 = 1.0\text{-}SS_{reg}/SS_{tot} \quad (2\text{-}17)$$

where SS_{reg} is the sum of the squares of the differences between predicted stage and actual stage and SS_{tot} is the sum of the squares of the differences between predicted stage and average actual stage.

Ecohydrology

Experimental Design

An ecohydrologic evaluation of *Salix caroliniana* and CSA soils and hydrology was performed on Mosaic K5, CFI SP-1, and Williams during the summer of 2007. *Salix caroliniana* was chosen to evaluate ecohydrologic relationships on CSAs as it is the dominant canopy species on CSAs (Rushton, 1988) and thus potentially plays a significant role in the hydrodynamics of CSAs. Furthermore, since one of the study objectives was to evaluate the potential spatial extent of the wetland environment in terms of soil moisture regimes and available soil water, the species was an optimal choice to couple soil water regimes to rooting depths and transpiration rates since it is an obligate wetland species (DEP, 1994) and of wetland woody species, *Salix* spp. is one of most sensitive to drought (Wickberg, 2006; Pockman and Sperry, 2000).

The study was conducted along established transects from an upland area into a surface water feature. Groundwater wells provided water table depths along the transect, and surface water wells within the water feature provided water levels at the lowest point of the transects. The design for the layout of the ecohydrology study for Mosaic K5 is shown in Figure 2-27 with an elevation profile and a plan view showing well positions. The elevations were surveyed as relative to the ground surface at the surface water well. Four ecohydrology (E.H.) stations were established across the transect at Mosaic K5 and in different zones of dominant vegetation (Figure 2-27). The dominant species for each zone are listed in Figure 2-27 and in descending order of dominance. The highest area, referred to as the upland zone, had an E.H. station established at the zero distance. The transitional zone station was established in an area 50 cm

lower than and 41 m from the station at the upland zone. The E.H. station within the saturated zone was established 100 m from the upland station at an elevation 25 cm lower than the transition zone station. The station at the inundated zone was established 200 m away from and at an elevation 1.45 m lower than the upland zone station. Each of these stations, except for the station within the saturated zone, had a well installed which continually recorded levels with a Solinst® pressure transducer. At each E.H. station, except for the inundated zone station, soil moisture probes were installed and soils were sampled to perform moisture release curve analysis in the laboratory. At each E.H. station, transpiration data was collected and root biomass was sampled from *Salix caroliniana* individuals.

A similar design and data collection scheme was implemented at CFI SP-1. The site was never inundated during the study and, therefore, only three E.H. stations were established which all had adjacent groundwater wells (Figure 2-28). The upland zone station was established in sand-dominated soils and at an elevation 2 m higher than the saturated zone station. The transitional zone station was established 30 cm higher and 30 m away from the saturated zone station. A similar setup to CFI SP-1 was employed at Williams Co., which also did not experience inundation during the study period and only had three stations established. While the same data was collected at Mosaic K5 and CFI SP-1, transpiration studies or root sampling were not conducted at Williams Co., where only sampling for moisture release curve analysis and installation of soil moisture probes were performed.

Moisture Release Curves

Soils were sampled at each E.H. station to determine moisture release curves that were characteristic of the soils and relate volumetric water content (VWC) to water potential. The samples were transported back to the laboratory where they were allowed to soak in water for 3 days. Hysteretic behavior between moisture release curves of wetting and drying soils has often

been observed (Dingman, 2002). Wetting the samples first resulted in moisture release curves representing drying soils. The samples were removed from the water and allowed to dry in constant conditions with no sun or direct heat. At 1-3 day increments during the drying period, subsamples (approximately 100 cm^3) were removed and placed into sealed bags where they were allowed to equilibrate for four days. Decagon Devices EC-5® dieletric soil moisture probes were inserted into the sub samples to obtain average VWC (m^3/m^3) (accuracy = 3 % VWC, resolution = 0.1 % VWC; independent of soil texture and salinity) for each subsample (Decagon Devices, Pullman, WA, USA).

Immediately after removing the soil moisture probes, subsamples were analyzed for water potential. A UMS T5® tensiometer (range = 0 to -850 hPa) was inserted in the wetter samples to record negative water potential (-hPa) (UMS, Munich, Germany). A UMS Infield 7® was used to obtain direct readings from the tensiometer. The tensiometer was checked daily by wetting the ceramic tip to obtain a measurement of 0.0 hPa (± 3 hPa). The instrument's range limited its application to only wetter samples in order to avoid cavitation. The drier samples were analyzed with a Decagon Devices WP4T® to obtain water potential (-MPa) with accuracy of 0.1 MPa from -0.0 to -10 MPa and 1.0 % from -10 to -300 MPa (Decagon Devices, Pullman, WA, USA). The instrument utilizes the chilled mirror dew point technique and a dew point potentiometer to measure water potential (Scanlon *et al*., 2002). The WP4T® was calibrated daily using the supplied 0.5 molal KCl calibration standard. The accuracy of the instrument limits confident results to a minimum water potential of -0.2 MPa, corresponding to 2000 hPa. Therefore, samples having water potential values out of the ranges of both instruments and in between -850 and -2000 hPA was possible.

Subsamples were weighed immediately after measurement of the water potential to determine weight wet and then dried in 70 ^{o}C oven until constant weight was reached. Gravimetric water content (GWC) was then determined with the following equation:

$$GWC = (\text{wet weight (g)} - \text{dry weight (g)})/\text{dry weight (g)} \quad (2\text{-}18)$$

Some of the drier samples prevented measurement of VWC with the soil moisture probes since upon drying the samples became crumbled and inhibited good contact with the probe. Typically, the GWC is used along with the bulk density of the soil to calculate VWC, which is the product of the two. Clays with high porosities, however, do not have constant bulk densities due to their shrink-swell properties causing measurement of weights and volumes in the field to be difficult (Hochman *et al*., 2001). Rather, the bulk densities are a function of the GWC, and often empirical relationships are developed to relate the two from which GWC can then be used to calculate VWC. Bulk densities and GWCs over a range of moisture contents, however, were not determined.

Measured VWC and GWC were empirically related using samples which had both VWC and GWC measured to indirectly determine the empirical relationship between bulk density and GWC. GWC was determined for the wetter samples which had VWC measured with the probes to provide a sufficient data set to relate measured VWC with GWC. A typical equation that relates GWC and bulk density for shrink-swell clays follows (Hochman *et al*., 2001):

$$\text{Bulk Density (g/cm}^3\text{)} = (1\text{-}e)/(1/ad + GWC) \quad (2\text{-}19)$$

where e is the air-filled porosity, ad is absolute density of solid matter in the soil (typically taken as 2.65 g/cm^3), and GWC is (g/g). Equation 2-19 was used with the measured GWCs of the samples with coupled measurements of VWC and GWC to determine a calculated VWC. Since the air-filled porosity was not measured, the parameter was adjusted to fit a one to one

relationship between the VWCs measured with the EC-5 probe and the VWCs calculated with the GWCs and Equation 2-19. Bulk densities were determined for the samples without a measured VWC using the measured GWCs and Equation 2-19 with adjusted air-filled porosity. The resulting bulk densities and GWCs were used to calculate a VWC for the samples which prohibited a VWC measurement.

The upland station at CFI SP-1 had sand-dominated soils which allowed the typical calculation of VWC with GWC and bulk density for the cases where measurement of VWC was not possible. The bulk density of non-clay soils does not vary over moisture contents and therefore one bulk density was measured and applied. Bulk density was determined by sampling a known volume of soil in the field with a bucket auger. The sample was brought back to the lab where it was dried and weighed to determine bulk density with dry weight and known volume.

All water potentials were converted to negative water pressure (-cm H_20) and were related to the measured and/or calculated VWCs, with the measured values preferentially used. When water potentials are plotted versus VWCs, the resulting relationship is referred to as a moisture release curve (Dingman, 2002). A moisture release curve was developed for soils sampled at each E.H. station and analyzed for critical values including saturation level, permanent wilting point (PWP), and capillary fringe height. Saturation level corresponded to the VWC that was related to a water potential near zero (Dingman, 2002). A VWC that induced PWP, assuming permanent wilting occurs at -15,000 cm H_20, was identified for each station (Dingman, 2002). The height of the capillary fringe was determined by observing the inflection point of each moisture release curve. Capillary fringe heights were assumed to be equivalent to

the absolute value of the water potential where VWCs begin to significantly change with decreasing water potential (Dingman, 2002).

Soil Moisture Analysis

Decagon Devices EC-5® dielectric soil moisture probes were installed at prescribed depths at each E.H. station, excluding the inundation zone at Mosaic K5. A 7.62 cm diameter corer was used to create a hole slightly over 1 m deep that was adjacent to the groundwater well and in an area within 5 cm of the surface elevation of the groundwater well. The soil moisture probes were installed at 10, 25, 40, 70, and 100 cm depths below the ground surface at the upland and transitional stations. Depths of 10, 20, 35, and 50 cm were used at the saturated stations. The probes, which consist of two prongs, were installed in the sidewall of the cored hole and perpendicular to the ground surface to avoid effects from infiltrating water pooling on the probes. The probes were inserted into the sidewall so that they were completely covered. The removed soil was backfilled and packed in best attempts to mimic the initial bulk density of the cored hole. The soil moisture probes were connected to a Decagon Devices Em5b® logger which was placed in a water resistant container. The logger was set to record soil moisture as VWC every hour. Soil moisture levels were related to water potential using the moisture release curves and compared to accompanying groundwater levels to evaluate interactions between the water table and soil moisture regimes.

Root Biomass Analysis

The coring method (Snowdon *et al*., 2002) was used around *Salix caroliniana* trees to sample root biomass with depth at increments of 15 cm and to a total depth of 1.5 m using a 7.62 cm diameter corer Sampling was performed near each E.H. station, including at the inundated station of Mosaic K5. Root biomass was sampled from three trees at each location and with three cores per tree. Trees were sampled at locations within 5 cm of the surface elevation of

their respective soil moisture station. Sampled trees were limited to diameters at breast height (dbh) ranging from 7 to 10 cm to minimize the effect of different tree age on root biomass allocation. Samples were taken to a lab where they were washed, sieved with 2 mm mesh, and dried in 70 ^{o}C oven until constant weight was achieved. Root biomass data were expressed as average dry biomass per sampled volume per depth and related to soil moisture data to observe how root allocation responded to soil moisture dynamics.

Transpiration Analysis

Stems of four *Salix caroliniana* trees surrounding each ecohydrology station were instrumented with Dynamax Sapflow® flexible gauges, along with a Dynamax Flow 4 DL® sapflow logger, to obtain stem flow rates as mass of water per hour using the stem heat balance (SHB) technique (Dynamax, Houston, TX, USA). Sapflow® technology has been tested and proven to give accurate measurements (< 10 % error) of water flow within stems when comparing to gravimetric methods (Akilan *et al*., 1994; Baker and Bavel, 1997; Weibel and Boersma, 1995; Steinberg *et al*., 1989, Guitierrez *et al.*, 1993; Heilman and Ham, 1990) and has been applied to measuring transpiration of *Salix* spp. (Cleverly *et al*., 1997; Hall *et al*., 1998; Conger, 2003; Nagler *et al*., 2003).

The SHB technique applies a small, constant and known amount of heat to a stem with a flexible heater. Foam rubber insulation around the heater and foam insulation collars around the stem above and below the sensor limit direct insolation and naturally induced temperature gradients from affecting the heat balance measurements (Steinberg *et al*., 1989). The method assumes steady-state and no in change heat storage within the stem, and as such, the continuous input of heat must be balanced by outflow of heat from the system. Change in heat storage within a stem over a day has been found to have negligible effects on measured sap flow from smaller stems and when flow rates are averaged as opposed to recording instantaneous rates

(Weibel and Boersma, 1995). The flux of heat out of the system is partitioned as radial conductive flux into the insulation and to the ambient (Q_r), vertical conduction up and down the stem tissue (qu and qd), and convective flux carried by the sap stream (Q_{flow}) (Figure 2-29). The heat flux transported by the sap stream, Q_{flow}, is directly proportional to the flow rate of water, F, in the stem section (Baker and Bavel, 1997). A thermopile adjacent to the heater allows measurement of radial flux, and thermocouples below and above the heater measure temperature gradients and stem conduction above and below the heater as well as temperature gradients across heater. The SHB instrumentation, how the various fluxes are measured, and the calculation of sap flow in mass flux of water are described with Figure 2-29 and the following equations following Baker and Bavel (1997) and Dynamax (2005):

$$F = (P_{in} - Q_v - Q_r)/(C_p * dT) \quad (2\text{-}20)$$

where F is flow rate (gH_20/s), P_{in} is power input (W), Q_v is vertical heat flux (W), Q_r is radial heat flux (W), Cp is heat capacity of water (1142.78 J/g/K), and dT (K) is temperature change from below the heater to above the heater. The temperature difference, dT, is calculated as the average temperature difference across the sensor measured with thermocouples A-Ha and B-Hb. The power input, P_{in}, is calculated following Ohms law with:

$$P_{in} = V^2/R \quad (2\text{-}21)$$

where V is the input voltage (V) and R (Ω) is the resistance. The vertical stem heat flux, Q_v, is calculated by applying Fourier's Law for one-dimensional heat flow with:

$$Q_v = qu + qd = K_{st} * A * dT_u/dX + K_{st} * A * dT_d/dX \quad (2\text{-}22)$$

where qu is the vertical stem flux above and away from the sensor, qd is the vertical stem flux below and away from the sensor, K_{st} is the thermal conductivity of the stem (W/m/K) taken as 0.42 W/m/K for woody stems (Steinberg *et al.*, 1989), A is cross sectional area of the stem (m^2),

dT_u/dX and dT_d/dX are the measured temperature gradients above (measured with thermocouple A-B) and below the heater (measured with thermocouple Ha-Hb), respectively, and dX is the spacing (m) between each of the two thermocouple junctions A-B and Ha-Hb. The radial heat flux, Q_r, is computed as:

$$Q_r = K_{sh} * (C\text{-}Hc) \quad (2\text{-}23)$$

where K_{sh} is the sheath conductance (W/V_o) which is a constant factor that relates the radial heat flux to the thermopile output, (C-Hc), with V_o representing the voltage output from the thermopile. K_{sh} is unique to every stem gauge and instrumented diameter and therefore has to be determined for each gauge and each installation. The K_{sh} is determined during periods of no flow where F is equal to zero and all other values are measured and known. Zero flow, or when transpiration is not occurring, is typically measured during rain events or nighttime when relative humidity approaches 100 % (Cienciala and Lindroth, 1995a).

Four slightly flexible sapflow gauges were used, two that were installed on stems with diameters ranging from 24 to 32 cm and two installed on stems with diameters of 45 to 65 cm (Dynagage® Models SGB 25 mm and SGB 50 mm). Straight stems with sufficient length were selected and were sanded to remove all bark and to give a smooth surface to provide the best contact between the stem and gauge. A silicon grease-based electrical insulating compound was applied to the stem surface to ensure good thermal contact between the stem and gauge and to avoid condensation (Smith and Allen, 1996). A thin sheet of food plastic wrap was wrapped around the stem after applying the silicone compound to further minimize condensation on the stems (Dynamax, 2005). Plumbers putty was applied around the top and bottom of the sensor body to provide a water-proof seal between the exposed stem and sensor body so to avoid water intrusion during rain events.

All instructions and materials provided by Dynamax (2005) to avoid natural temperature gradients and direct insolation were applied which included foam insulated collars above and below the sensor body and two reflective heat shields around each installation. The sensors were installed at least 1 m above the soil surface to further minimize natural temperature gradients (Hall *et al.*, 1998). Additionally, foil wrap was wrapped around the sensor and around the stem from the sensor to the base of the tree and extending 1 m above the sensor and its collars (Guitierrez *et al.*, 1993). Provided extension cables were used to connect the gauges to the Flow 4 logger, and electrical tape was used on the connections to avoid electrical shorting.

The Dynamax Flow 4 DL® sapflow logger and provided software required input of each instrumented stem area for all four gauges and the heater resistance, R (Ω), unique to each sensor which was used in Equation 2-21. The required voltage to each sensor has to be enough to ensure a measurable dT (> 1.0 ^{o}C) during high flow but low enough not to damage the stem (Smith and Allen, 1996). A voltage input of 5.0 V to each sensor was set with the sapflow logger as recommended by Dynamax (2005) when using the SGB 25 and SGB 50 gauges on trees capable of high transpiration rates. Voltage was supplied to the sapflow logger, which allocated it to the four sensors, with two DC marine batteries in parallel with a solar panel to maintain full charge of the batteries.

A default value for Ksh of 0.8 was first manually entered into the Flow 4 DL® sapflow logger until it could be calculated during a no flow event during the first instrumented night. The auto-calibration function provided in the Flow 4®software was employed every other day beginning on the first night following instrumentation to determine average Ksh values over a three hour period from 3am to 6am for each stem, which were automatically updated in the logger.

Topographic relief between sampled trees and their respective station was limited to 10 cm. A station was instrumented for at least 14 days before the sapflow system was moved to another station. Diameter, leaf area index, and canopy size of instrumented stems were measured and recorded. Each canopy was treated as an ellipse, and the longest diameter of healthy leaves and the diameter perpendicular to that diameter were measured. Leaf area index was measured with a Sunfleck® Ceptometer (Decagon Devices, Pullman, WA, USA) that measures and calculates LAI using radiation (PAR) transmittance (Chen *et al*., 1997). LAI and canopy size were used to determine total leaf area of each instrumented stem.

The Flow 4® logger was programmed to record average hourly stem flow rates which were converted to daily flow rates. The daily stem flow rates were divided by the cross-sectional area of the instrumented stems to obtain stem flow per stem cross-sectional area (g $H_2O/cm^2/day$). These rates were then divided by the daily ET rates as estimated with the Penman method using on-site climatic data. Indexing with the daily Penman-estimated ET allowed comparison among sensors, stations, and sites while excluding climatic effects. The indexed daily stem flow rates from all four sensors collected over the 14 day period were averaged to calculate average daily stem flow rate (g H_2O/cm^2/Penman ET) for each station.

A 120 m^2 (6 m x 20 m) belted transect surrounding each station that encompassed all instrumented stems was established with the soil moisture station as the center and where all *Salix caroliniana* trees were measured for dbh (cm) to calculate total basal area (cm^2) per station with:

$$\text{Total Basal Area} = \Sigma(\pi*(dbh/2)^2) \quad (2\text{-}24)$$

The total basal areas of each station were used along with the daily stem flow rates to calculate daily stand level *Salix caroliniana* transpiration (cm) for each station. Three different scaling-up

methods were explored, all that were biometric-based using basal area as the parameter to relate measured stem flow rates to stand transpiration. The regression biometric scaling method as described in Martin *et al.* (2001) and Cermak *et al*. (2004) plots measured stem flow rates (g/day) versus the instrumented stem areas and fits a linear regression line through the origin. Prior to plotting, the stem flow rates (gH_20/day) were divided by the corresponding Penman-estimated ET (cm) and by the density of water (g/cm^3), and these indexed rates (cm^3/day/Penman ET (cm)) were used to develop a regression line to relate basal area with daily stem flow/Penman ET. All measured stem flow rates during the entire sampling period for each station were used to develop one regression equation for each station. The resulting regression line was used along with total stand basal area (cm^2) to calculate one ratio of stand level transpiration to Penman ET that represented each station and over the entire sampling period following:

$$Q_{stand}/\text{Penman ET} = B_{stand}*m/\text{Stand A} \quad (2\text{-}25)$$

where Q_{stand}/Penman ET is the ratio daily stand transpiration to Penman ET(cm/cm), B_{stand} is the total basal area of the stand (cm^2), m is the slope of the regression line that relates daily stem flow indexed with Penman ET ($cm^3\ H_20/cm$) to basal area (cm^2), and Stand A is the area of the stand (1.2E6 cm^2).

The simple biometric scaling method used total stand basal area and the sum of daily stem flow rates to calculate one transpiration rate per day using all four measured flow rates during a day following Cermak *et al*. (2004) and Conger (2003) and with:

$$Q_{stand} = \Sigma Q_{tree}*(B_{stand}/\Sigma B_{tree})*(1/\text{Stand A})*(1/\rho) \quad (2\text{-}26)$$

where Q_{stand} is stand transpiration (cm H_20/day), Q_{tree} is stem flow rate from each instrumented stem (g/H_20/day), B_{stand} is the total basal area of the stand (cm^2), B_{tree} is the cross-sectional area of each instrumented stem (cm^2), Stand A is the area of the stand (1.2E6 cm^2) and ρ is the

density of water (0.998 g/cm^3). Each daily transpiration rate was divided by the associated Penman-estimated ET to determine ratios of stand transpiration to estimated total ET.

The discrete biometric scaling approach, a method similar to the simple biometric scaling method, was applied that calculates a daily stand transpiration rate (cmH_20/day) for each measured stem flow with:

$$Q_{stand} = (Q_{tree}/B_{tree})*(B_{stand}/\text{Stand A})*(1/\rho) \quad (2\text{-}27)$$

Calculating a stand transpiration rate for each stem flow rate resulted in four rates for each day (one for each measured flow rate) allowing a range of stand level transpiration rates and the effects from stem flow variability to be analyzed. The transpiration rates determined with the discrete biometric method were divided by the Penman-estimated ET (cm) for the corresponding day, and the indexed rates were averaged over the sampling period to calculate average ratios of stand transpiration to Penman ET for each station along with standard deviations. Applying either the simple or discrete biometric methods allowed evaluation of variability in rates over the sampling period, whereas only the discrete method directly documented the effects from the variability in measured daily stem flow rates on calculated transpiration rates. The regression biometric method allowed neither since all measured stem flow rates were used to develop one regression equation. Results from all three scaling methods were compared and both the daily stem flow rates and stand level transpiration rates were compared between stations and among sites.

Scaling up to stand level transpiration using measured stem flow, total basal area, and either of the three biometric methods assumed that all *Salix caroliniana* trees in a belted transect had the same water availability and experienced similar stem flow rates per stem area as the instrumented stems in that belted transect. The assumption of water availability is reasonable as

the belted transects were established in fairly flat areas that immediately surrounded the soil moisture station. It was speculated that sapwood depth per radii, and thus conductive stem area per total stem area, may decrease with development of heartwood with age and size, which is the case with most tree species (Stewart, 1966; Shigo and Hillis, 1973). Since larger trees also contribute more to stand transpiration due to their larger basal area, size class distributions, in terms of dbh, of trees on the belted transects were evaluated and compared. Stem hydraulic conductivity was indirectly evaluated by determining sapwood depth per stem radii to address equitable stem flow rates per stem area across all tree sizes present on a transect. A 5 mm tree corer was used on 18 *Salix caroliniana* trees that spanned the range of trees found on the belted-transects at Mosaic K5. Cores were sampled at breast height and to a depth slightly greater than the radius of the tree. Cores were sealed in air tight bags and placed on ice during transport to the lab where they were refrigerated until processing. Initially cores were visually analyzed to observe a change of translucent wood, sapwood, to darker wood and thereby marking the transition of sapwood to heartwood (Stewart, 1966; Shigo and Hillis, 1973; Schaeffer *et al*., 2000).

Moisture content and dry wood density per core depth were determined for each tree core sample to further and more accurately determine sapwood depths. Cores with bark removed were segmented into 5 mm sections which were weighed to determine green weight of each subsample. The core subsamples were then dried in at 70 ^{o}C overnight and weighed to obtain dry weight. Moisture content of each subsample was calculating by dividing water weight by green wood weight (Barbour and Whitehead, 2003). Dry wood density of each subsample was determined by dividing the dry wood weight by the known volume of subsample (5 mm long x 5 mm diameter cylinder) (Roderick and Berry, 2001). Sudden decreases in moisture content

(Barbour and Whitehead, 2003; Holbrook and Zwieniecki, 2005) or increases in density (Lamb and Marden, 1970; Shigo and Hillis, 1973; Holbrook and Zwieniecki, 2005) with depth were used to mark the transition to heartwood. Moisture content and dry wood density were evaluated along each core to observe if tree sizes used in scaling up stem flows to stand level transpiration lost sapwood, and thus conductivity, to heartwood. If so, Equations 2-25, 2-26, and 2-27 were adjusted to decrease conductive stem area with increasing basal area using an allometric equation based on basal area.

Table 2-1. Description of sites

Proprietor	Site Designation	Site Age (yrs)[1]	Area (ha)	Description
Mosaic	K5	20	158	An older *Salix caroliniana* stand on most of the site. A number of large wetland areas.
Mosaic	H1	32	56	Multiple depressional features with *Salix caroliniana* and *Typha* spp.. Sand tailings on portions of site.
Mosaic	HP-10	??	77	Capped with sand that was later removed which exposed multiple depressional features. Dominated by younger *Salix caroliniana.*
PCS	SA 10	17	229	80 ha wetland on E side dominated by older *Salix caroliniana*
PCS	SA 01	41	43	5 ha wetland on SW side dominated by older *Salix caroliniana* . Sand tailings surround wetland.
Teneroc Fish Mngmt.	Tenoroc 4	40	110	Muliple wetlands between spoil rows with some tree plantings mixed with *Salix caroliniana*
Williams Company	Williams Co.	35	544	An older *Salix caroliniana* stand on most of the site. A number of large wetland areas.
CF Industries	CFI SP-1	25	57	Sand-clay mix. 9 ha wetland on W lobe; 8 ha wetland on East lobe. Trees planted on E lobe mixed with *Salix caroliniana.*

[1] Refers to years since filling ceased.

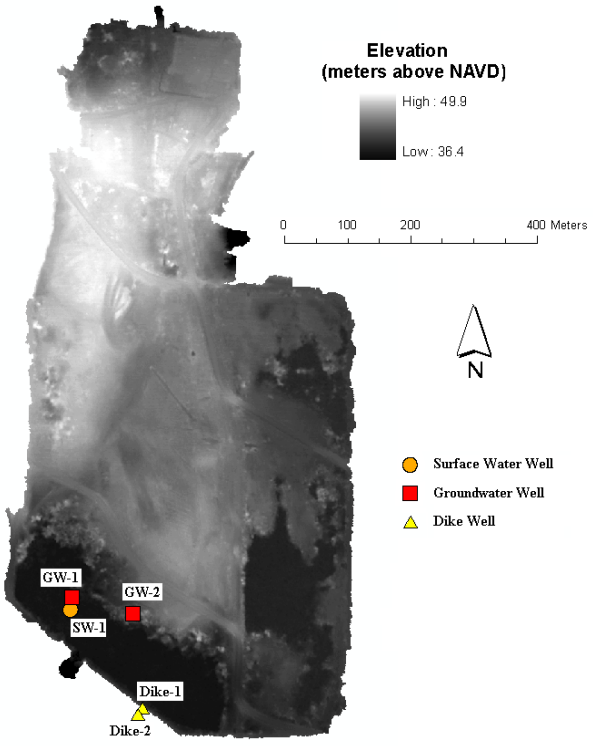

Figure 2-1. Well locations and DEM of PCS SA 01

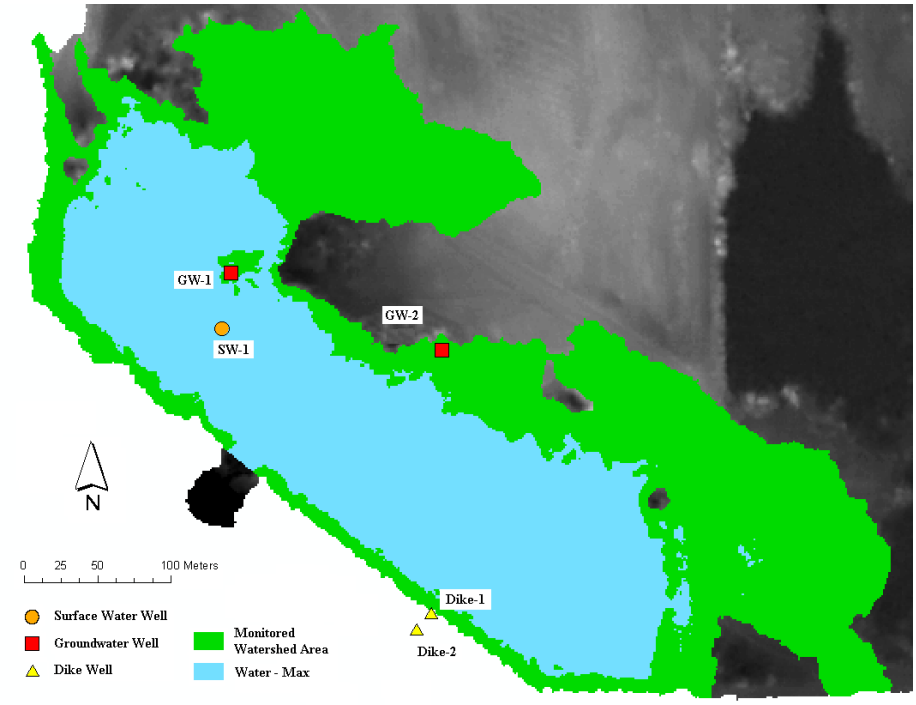

Figure 2-2. Well locations and maximum water at PCS SA 01

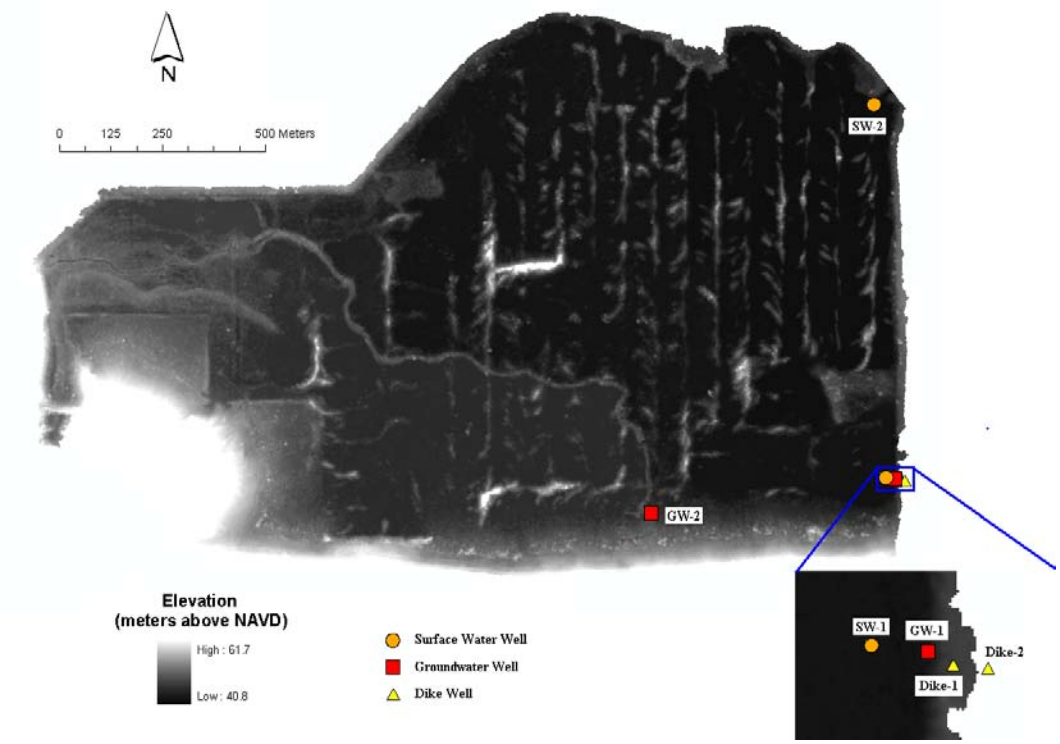

Figure 2-3. Well locations and DEM of PCS SA 10

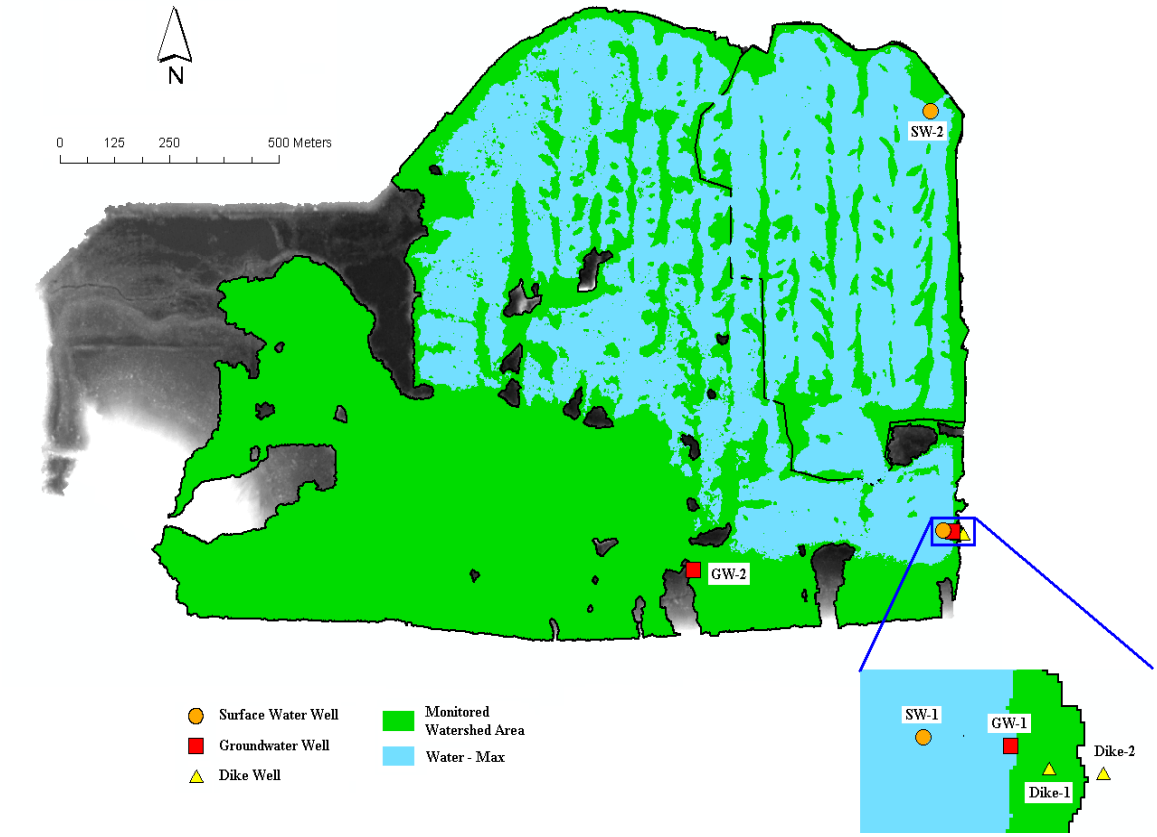

Figure 2-4. Well locations and maximum water at PCS SA 10

Figure 2-5. Well locations and DEM of Williams Co.

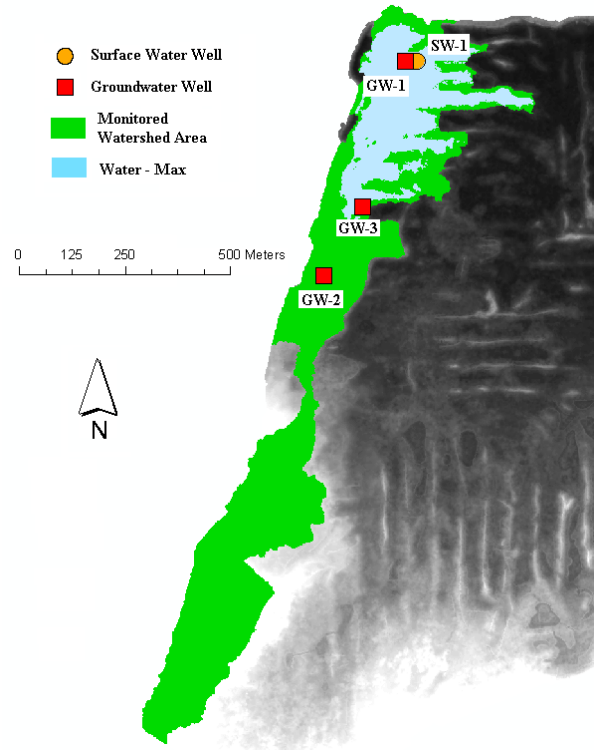

Figure 2-6. Well locations and maximum water at Williams Co.

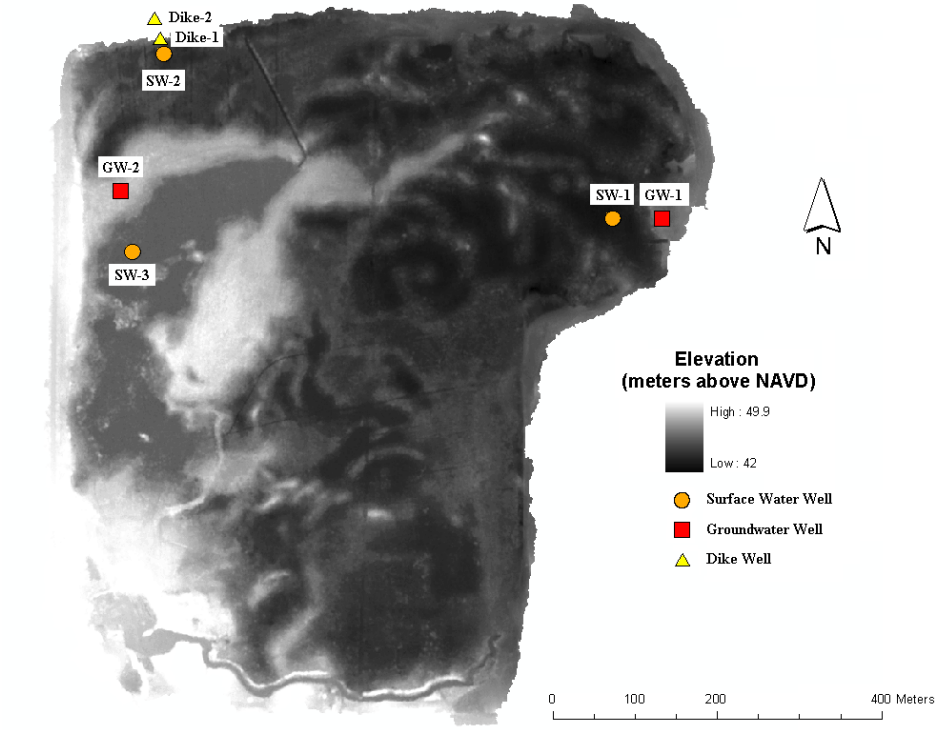

Figure 2-7. Well locations and DEM of Mosaic H1

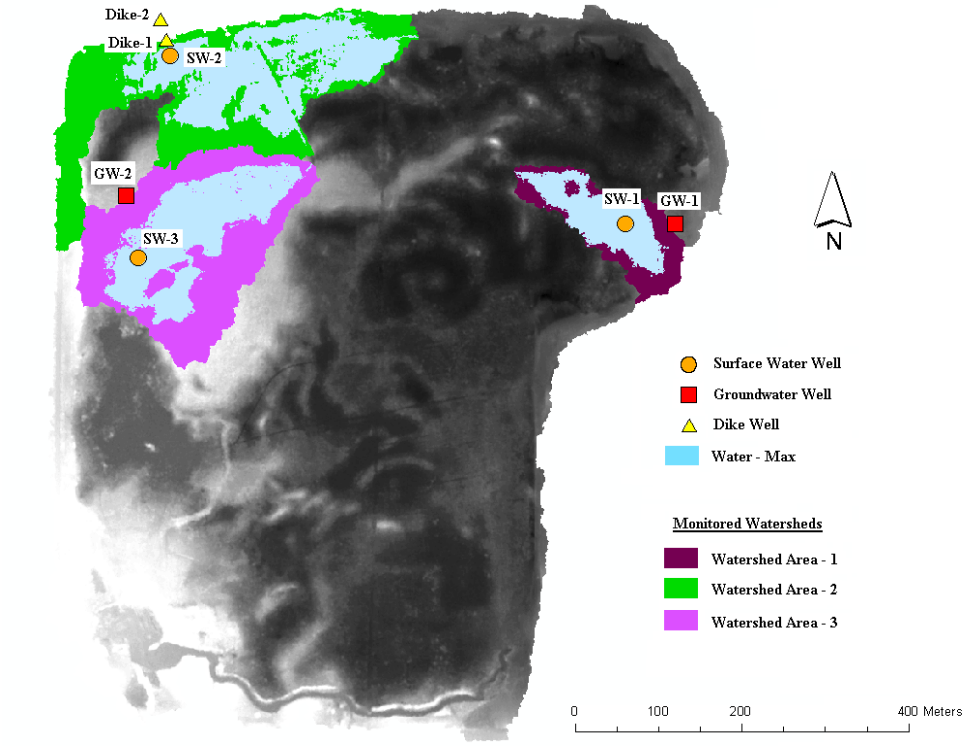

Figure 2-8. Well locations and maximum water at Mosaic H1

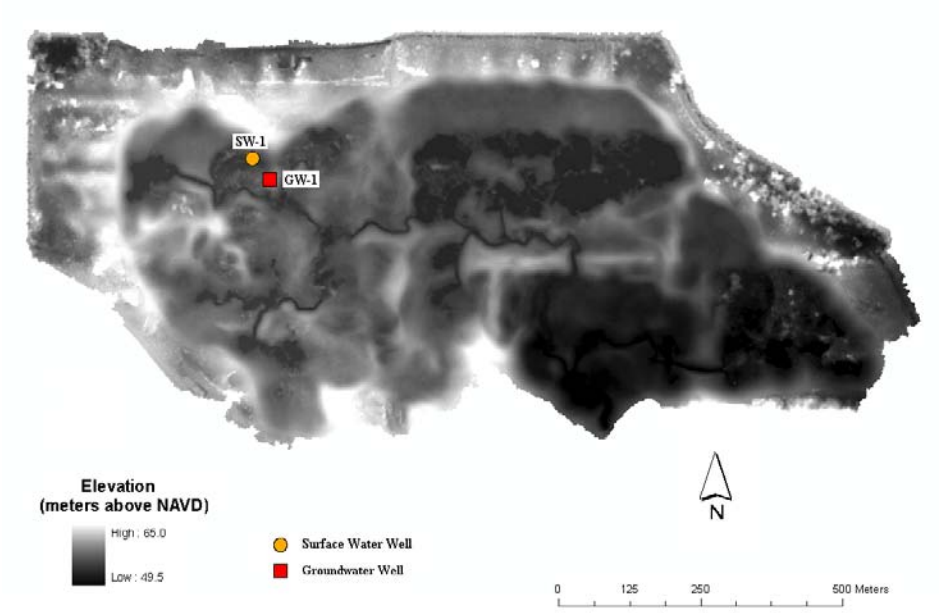

Figure 2-9. Well locations and DEM of Mosaic HP-10

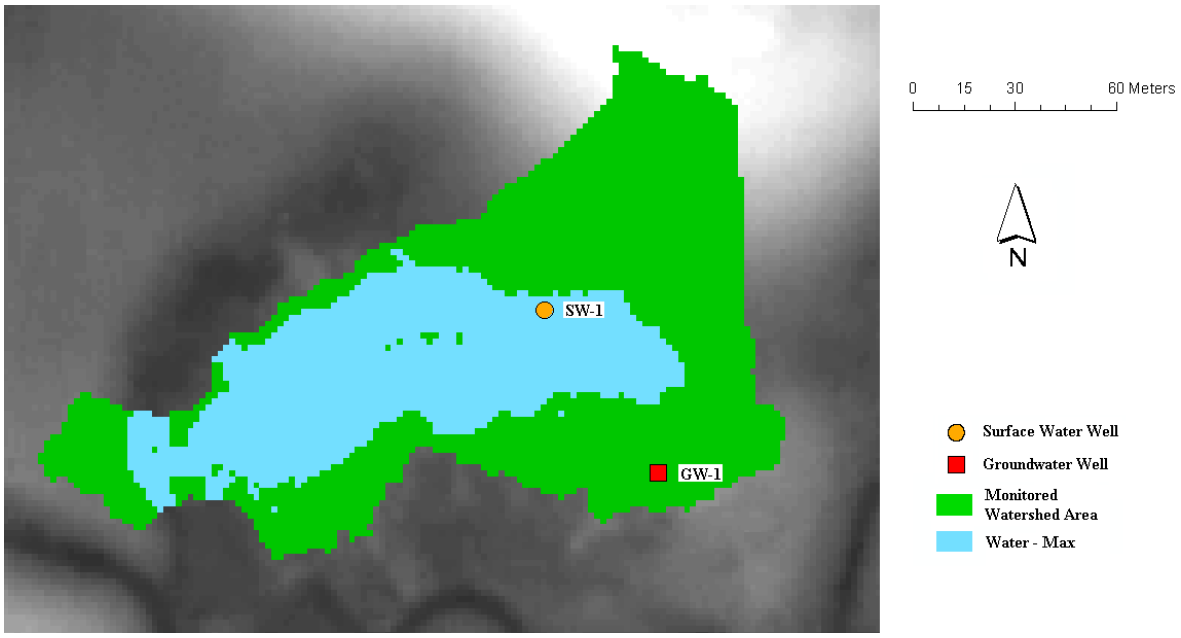

Figure 2-10. Well locations and maximum water at Mosaic HP-10

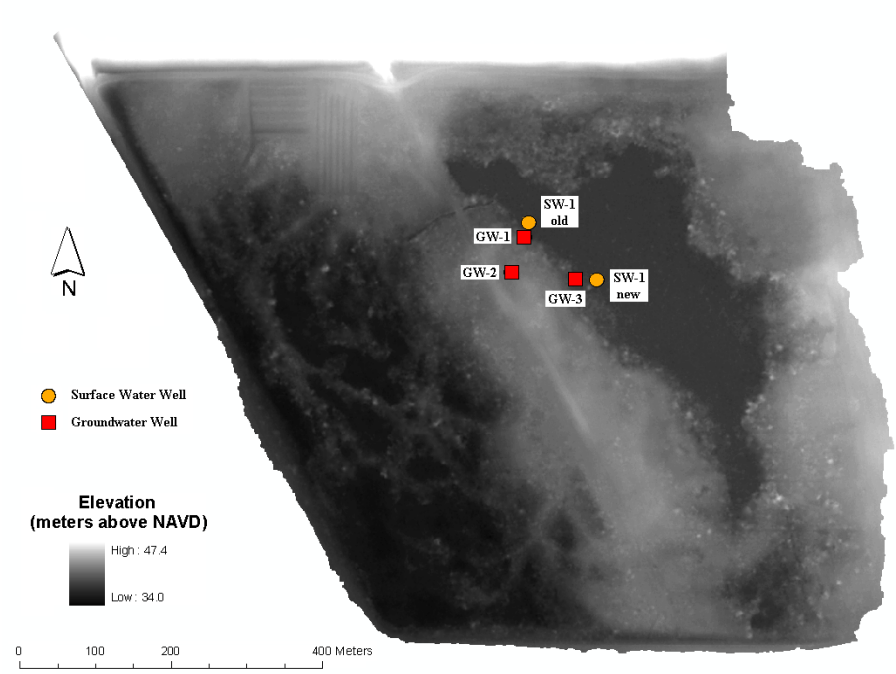

Figure 2-11. Well locations and DEM of CFI SP-1

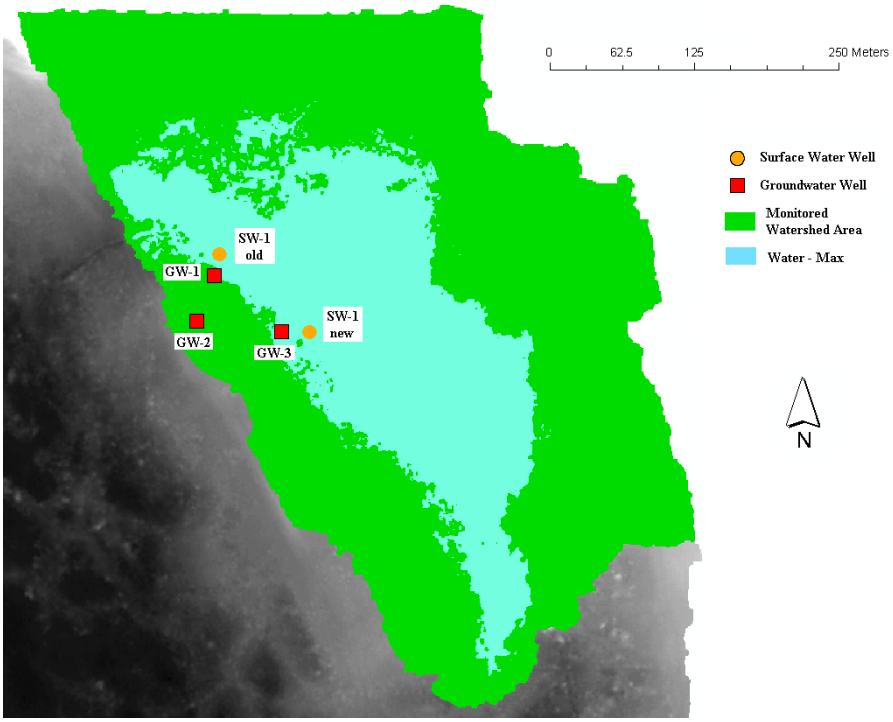

Figure 2-12. Well locations and maximum water at CFI SP-1

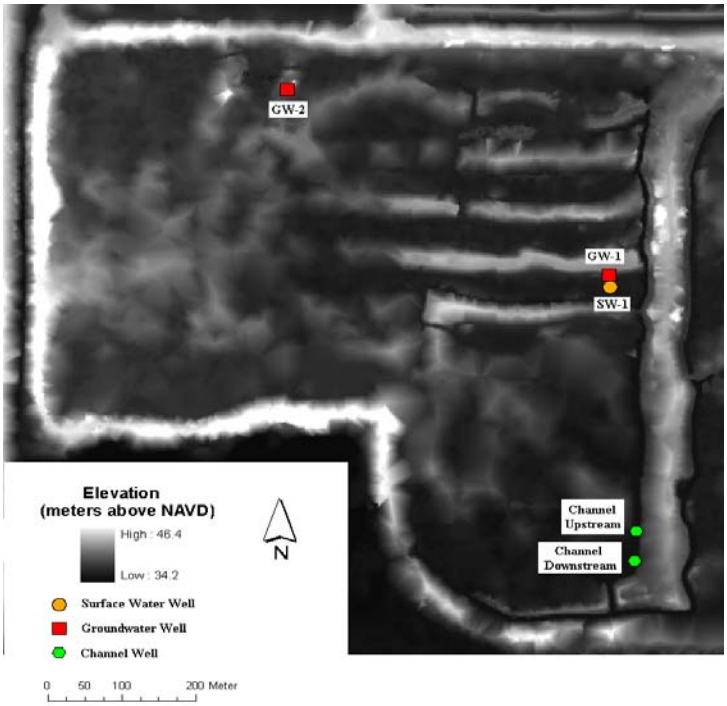

Figure 2-13. Well locations and DEM of Tenoroc 4

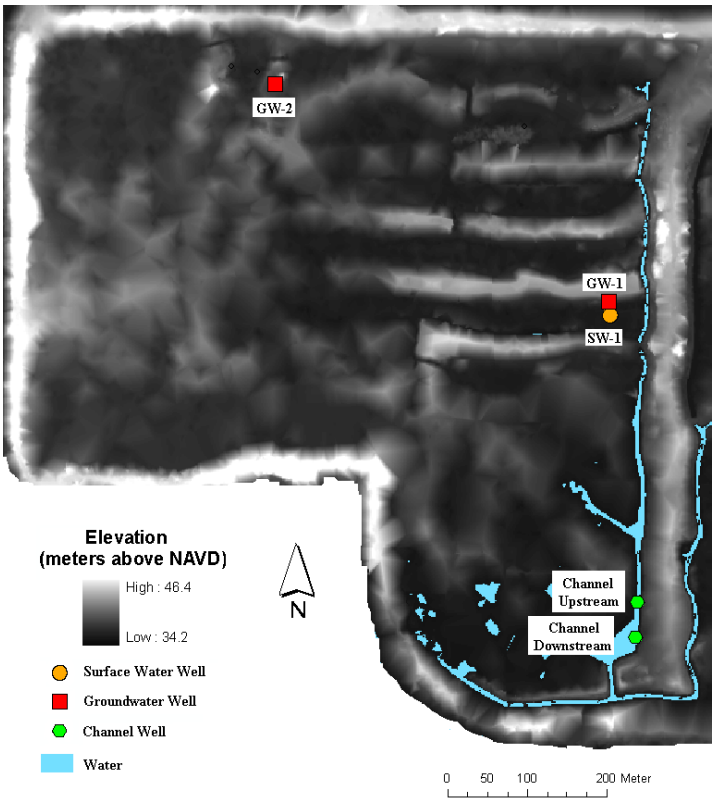

Figure 2-14. Well locations and maximum water at Tenoroc 4

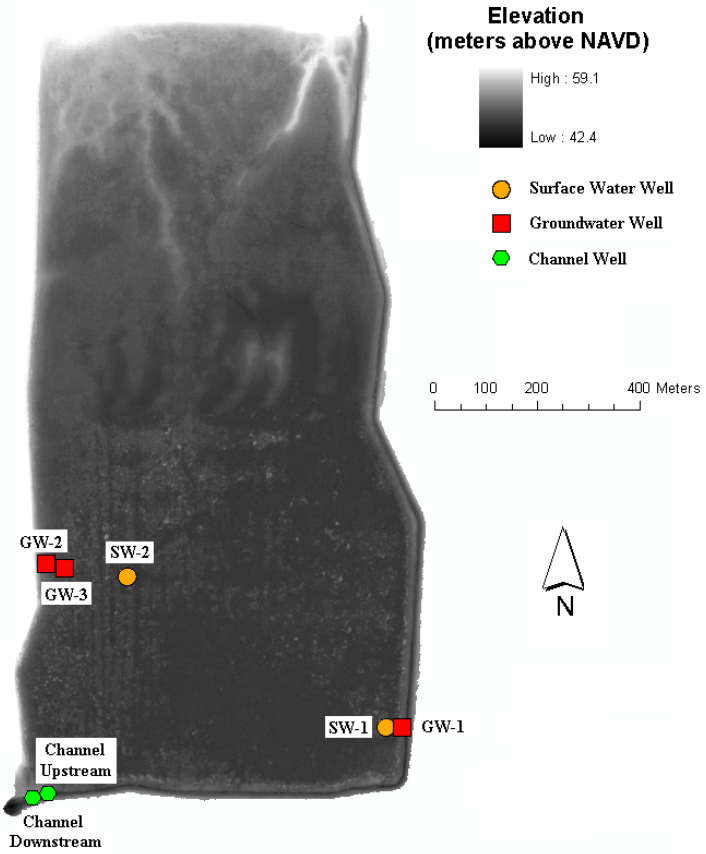

Figure 2-15. Well locations and DEM of Mosaic K5

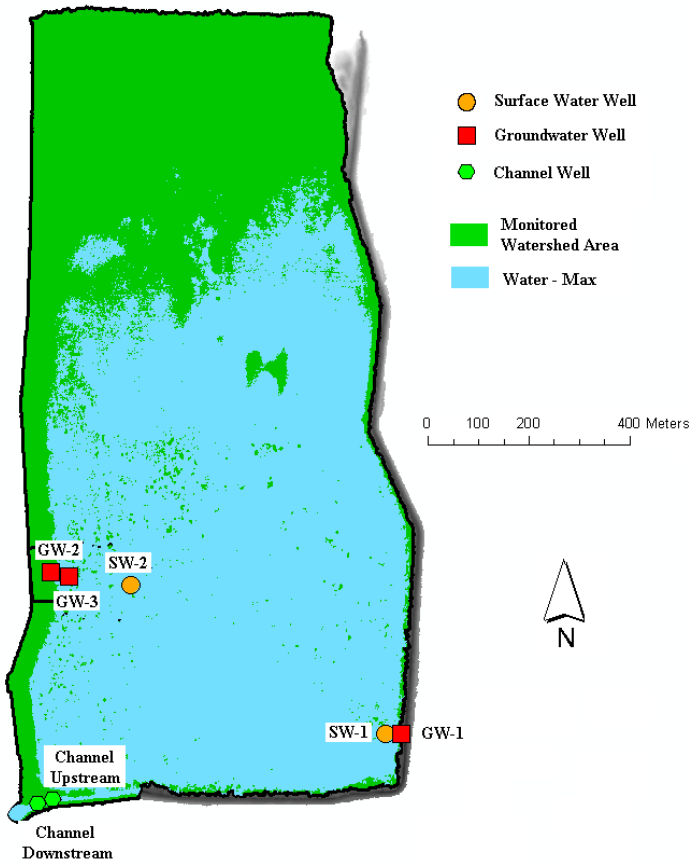

Figure 2-16. Well locations and maximum water at Mosaic K5

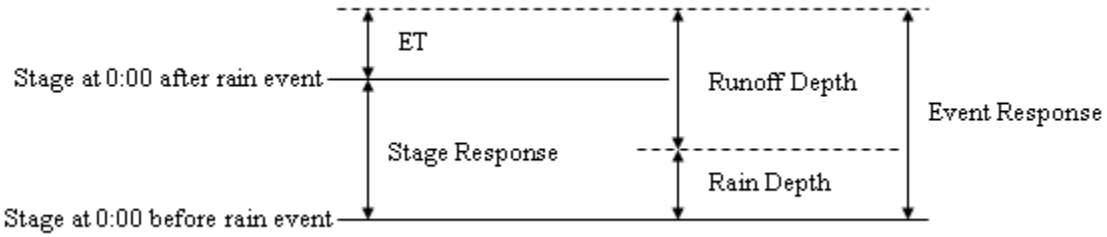

Figure 2-17. Definition of terms used in runoff analysis

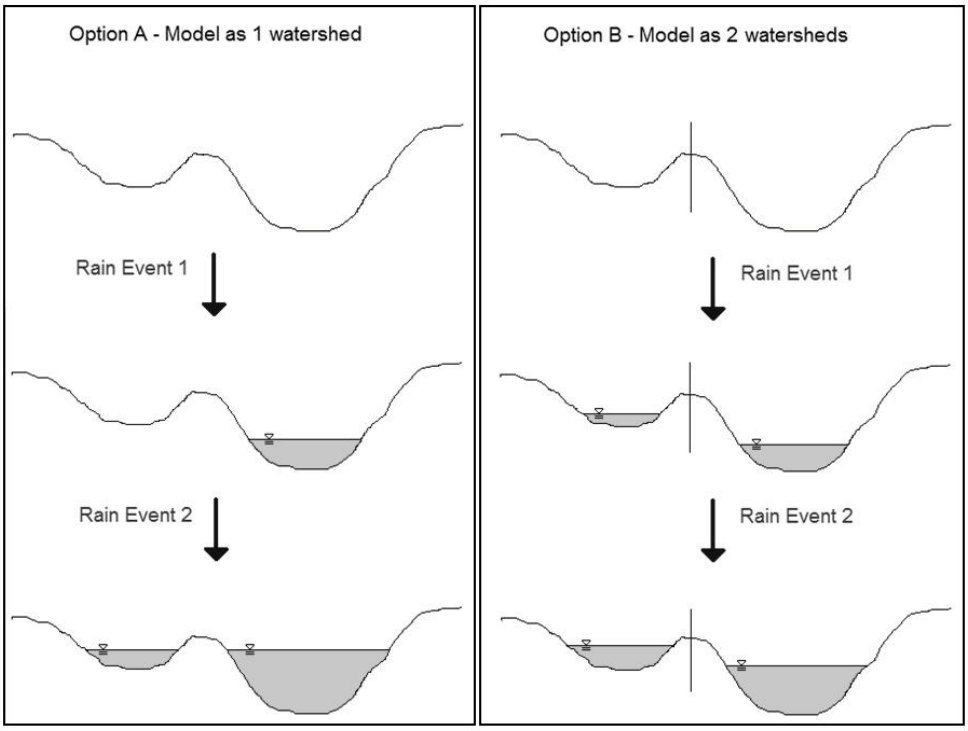

Figure 2-18. Hypothetical response to rain events at two depressional features treated as one watershed vs. separate watersheds

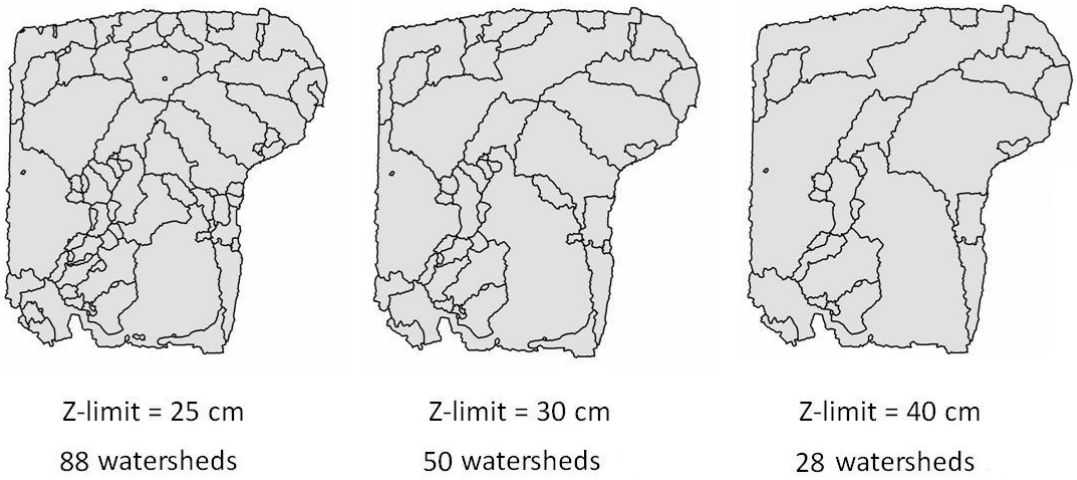

Figure 2-19. Watershed scales at Mosaic H1

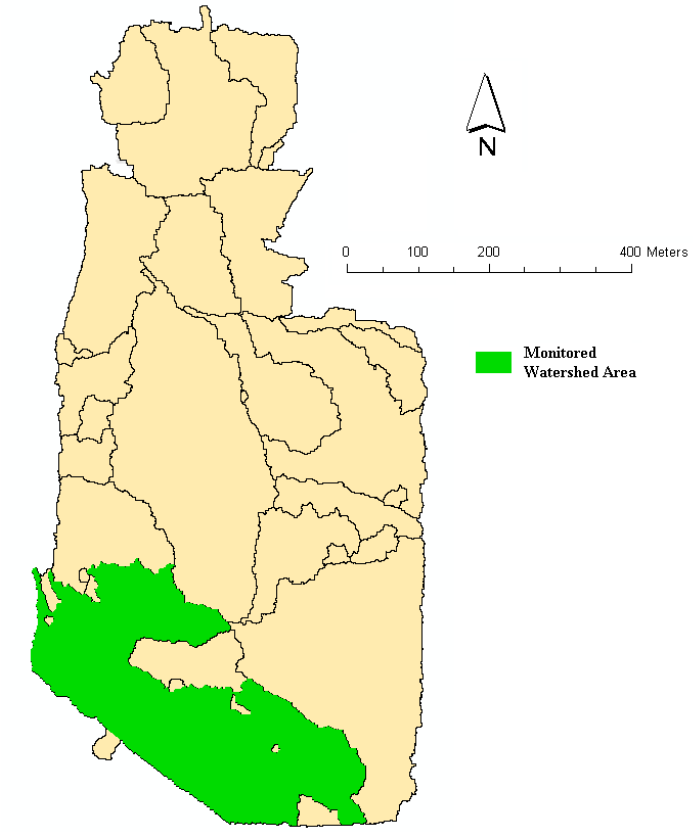

Figure 2-20. Watershed delineation for PCS SA 01

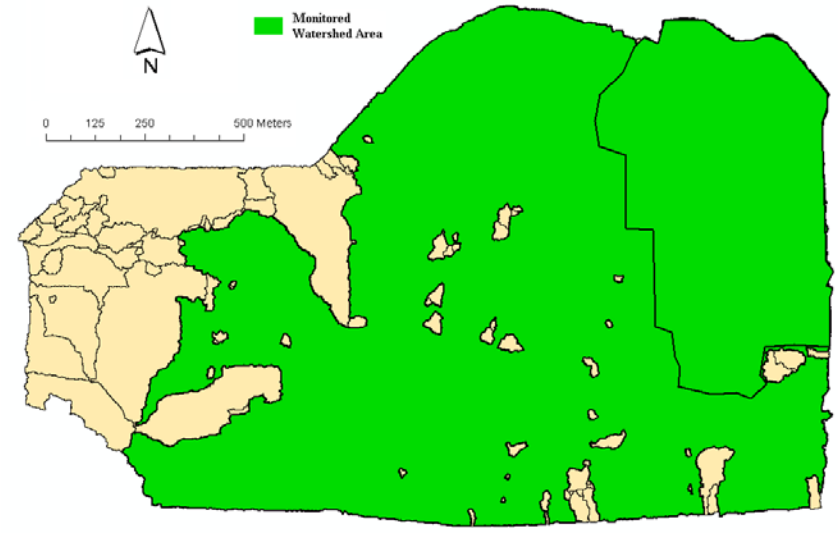

Figure 2-21. Watershed delineation for PCS SA 10

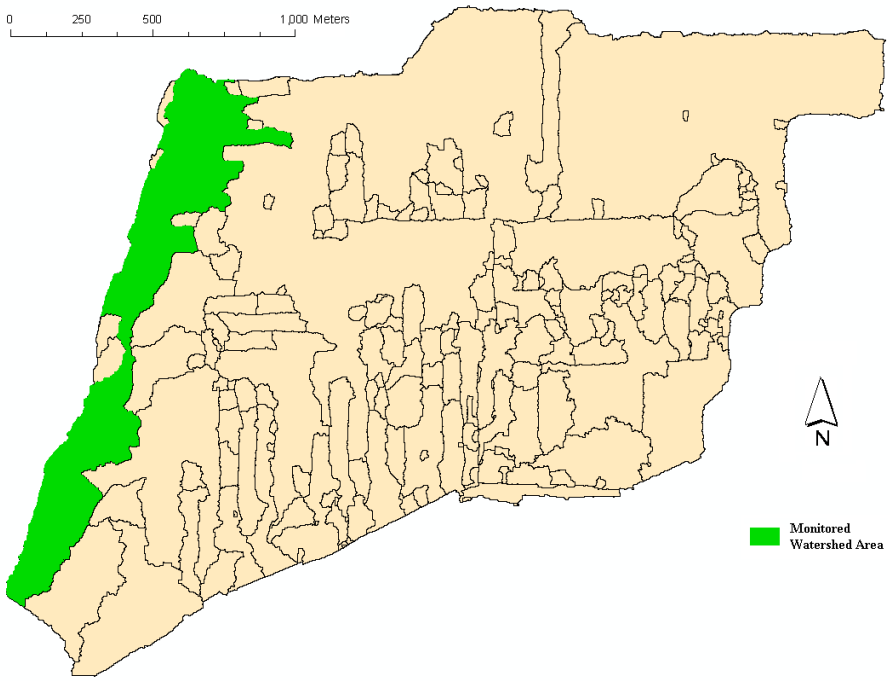

Figure 2-22. Watershed delineation for Williams Co.

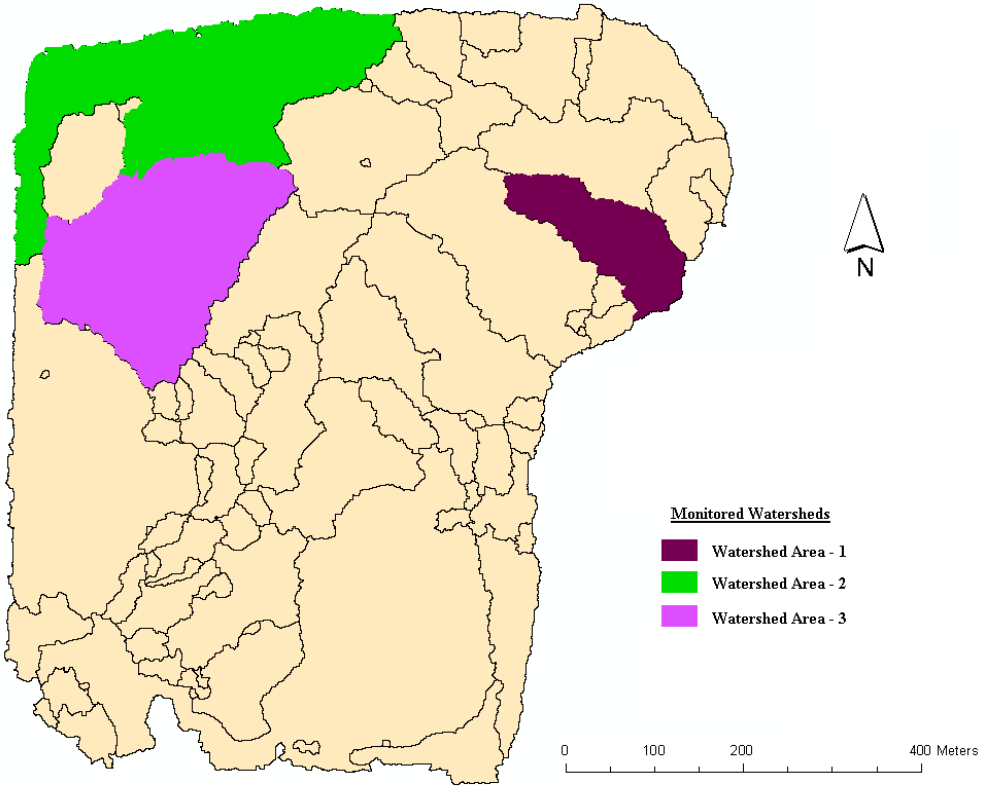

Figure 2-23. Watershed delineation for Mosaic H1

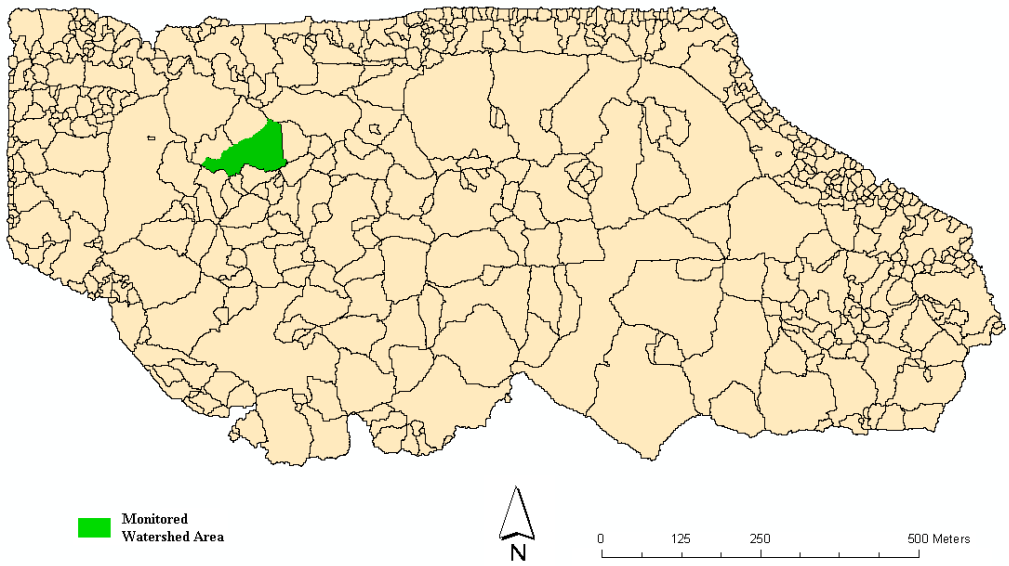

Figure 2-24. Watershed delineation for Mosaic HP-10

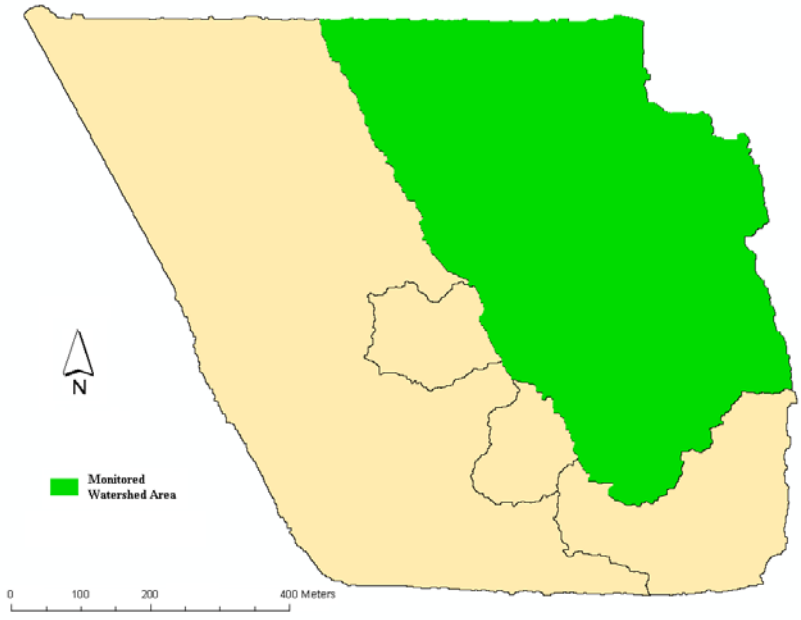

Figure 2-25. Watershed delineation for CFI SP-1

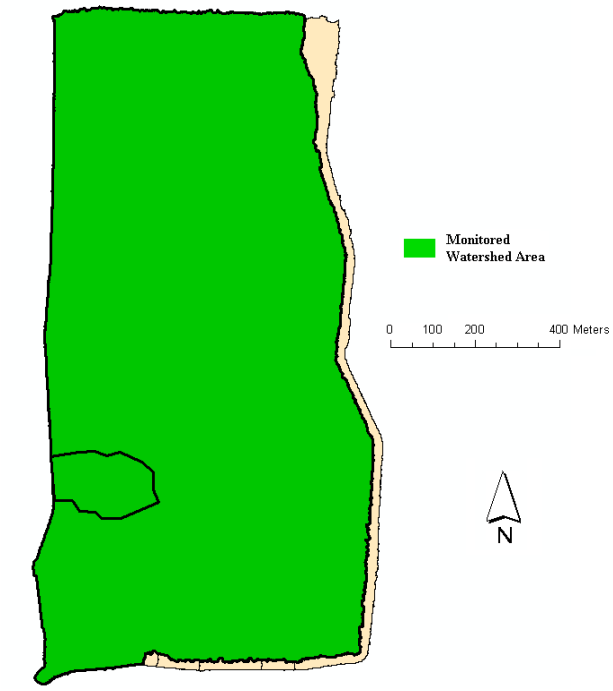

Figure 2-26. Watershed delineation for Mosaic K5

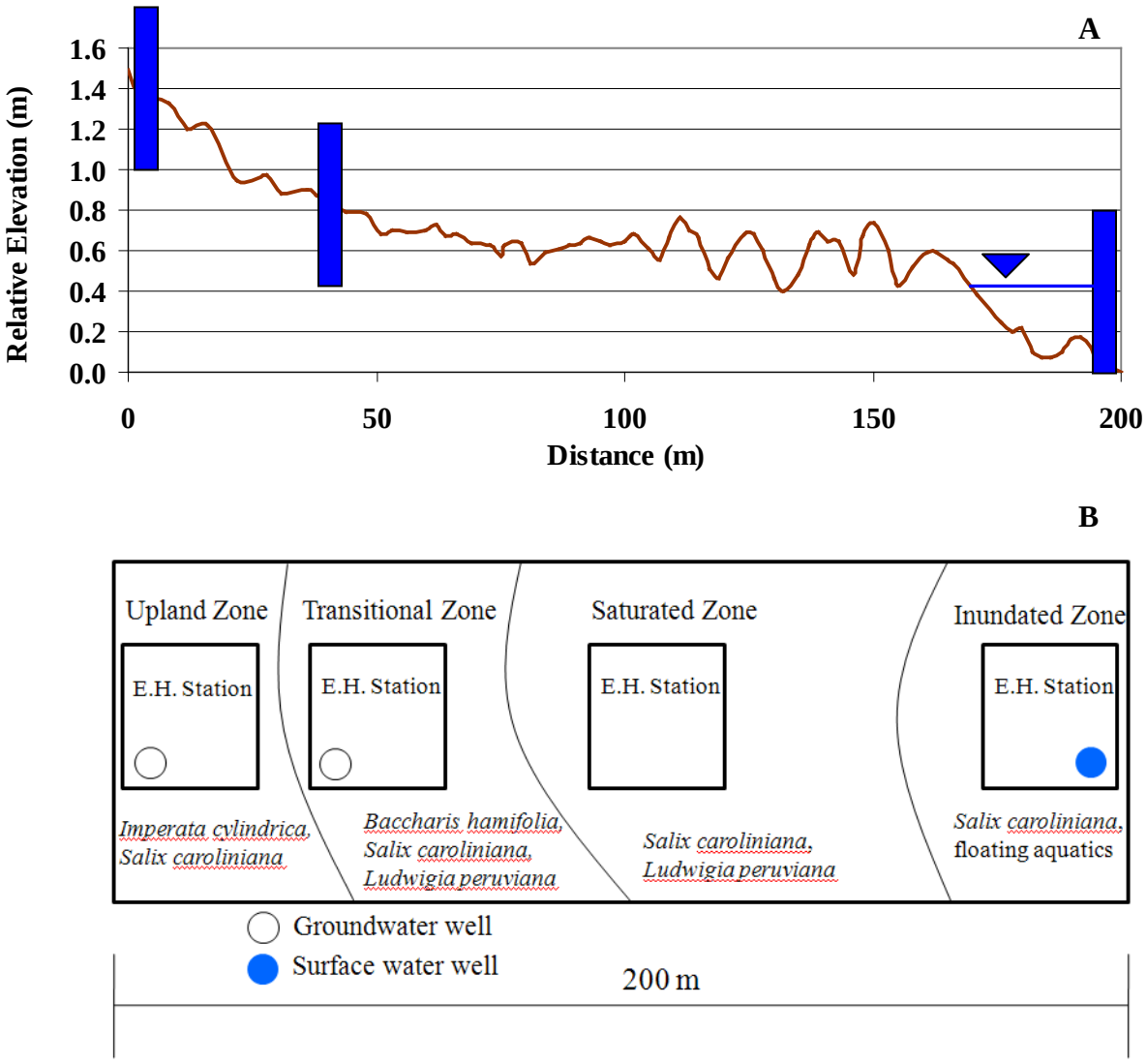

Figure 2-27. Ecohydrology design at Mosaic K5. A) Elevation profile. B) Plan view.

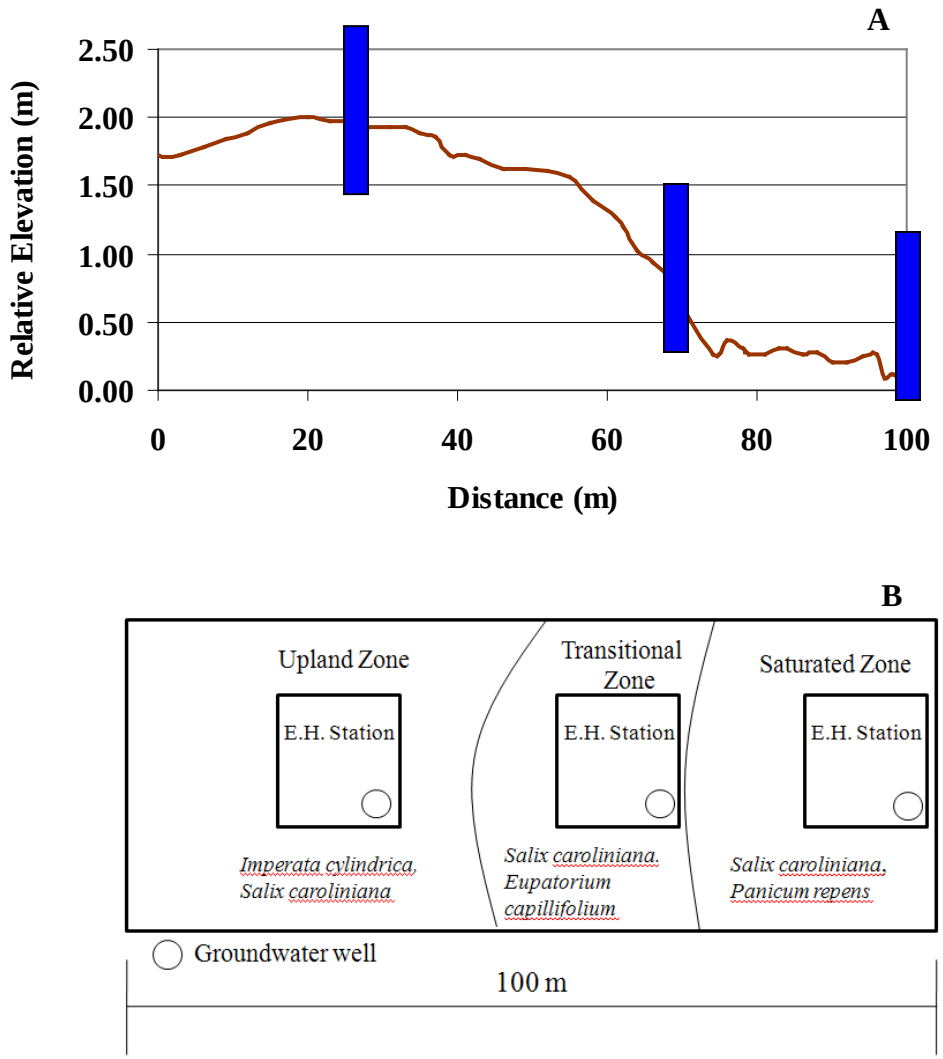

Figure 2-28. Ecohydrology design at CFI SP-1. A) Elevation profile. B) Plan view.

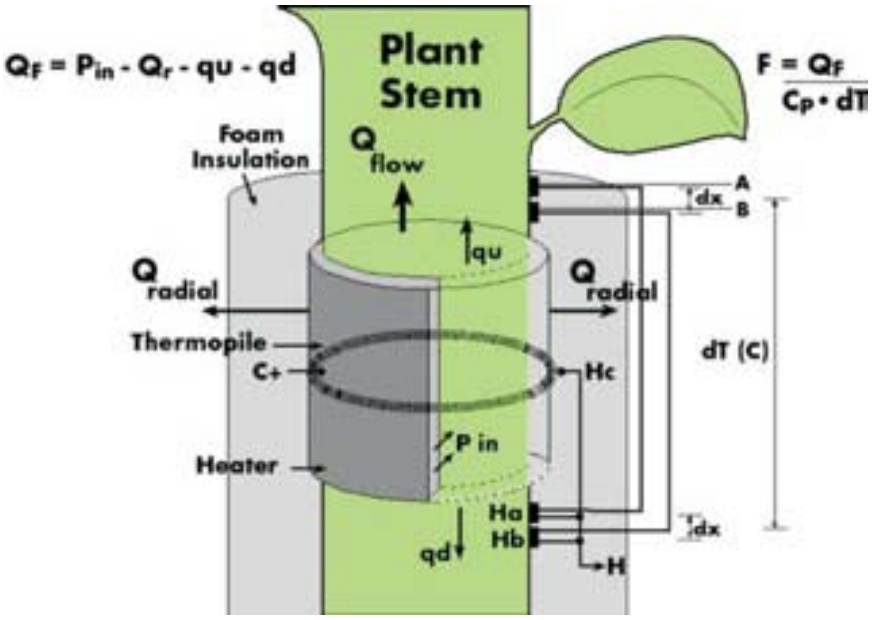

Figure 2-29. Schematic of sapflow gauges and SHB approach (Dynamax, 2005)

CHAPTER 3
RESULTS

Evaluation of Flooding Regimes

Eight CSAs were instrumented for monitoring precipitation and water levels within dominant surface water features to evaluate and compare flooding regimes of CSAs (Figures 2-1 through 2-16). Three CSAs had multiple surface water features instrumented to observe differences in hydrologic regimes of isolated features within a single CSA. These sites included Mosaic H1, PCS SA 10, and Mosaic K5 which had three, two, and two features instrumented, respectively. Precipitation data and water depths at surface water features within all eight sites are shown in Figures 3-1 through 3-16. The surface water levels of most features experienced decline starting in spring 2006 through the remainder of the record with some sites having significant dry periods due to the drought years of 2006 and 2007. PCS SA 01 experienced the reverse, however, with increasing water levels as a result of a beaver dam causing its outfall to become essentially inactive. Inserts were mortared in place in the outfall structure during May 2006 to completely block any surface water outflow from PCS SA 01 so that an accurate water balance could be performed.

Three other sites experienced surface water outflow during the period of study including PCS SA 10, Mosaic HP-10, and Mosaic K5. PCS SA 10 experienced outflow through a weir when surface water-1 (SW-1) reached 1.47 m which occurred August 2005 through April 2006 (Figure 3-3). Mosaic HP-10 experienced intermittent outflow throughout its record through a ditch network that exited the site via a buried pipe. It was determined that outflow from HP-10 occurred when surface water levels were at 0.45 m or above (Figure 3-15). There is a gap in the data for HP-10 from 2/13/08 to 3/12/08 due to equipment failure. Surface water outflow

occurred from Mosaic K5 through a vegetated swale when surface water feature-1 (SW-1) reached 0.5 m which occurred frequently throughout the period of study (Figure 3-13).

Water depths and frequency of flooding and drying substantially varied from site to site (Figure 3-17). The features at the PCS SA 10 and SA 01 remained flooded throughout the study period and had more buffered regimes with less response to rain events, slower rates of decline, and greater water depths than the other six sites (Figures 3-1, 3-3, and 3-17). Mosaic K5 SW-1 and HP-10 also experienced permanent flooding, with the exception of K5 during a brief period in June 2006, but with shallower water depths due to the elevation position of their outflow systems compared to that of PCS SA 10's outfall which was less active (Figures 3-13, 3-15, and 3-17). Mosaic H1 surface water-1 (SW-1) and Williams Co. experienced a flashier hydrologic regime with steeper declines, greater responses to rain events, and significant dry periods with depths below ground reaching over 0.5 m and 1.5 m, respectively (Figures 3-9, 3-5, and 3-17). Variation in contributing areas and upland soils likely created the differences in responses to rainfall observed at the different systems, while infiltration rates may have varied between features and potentially resulted in the different decline rates observed.

Tenoroc 4 and CFI SP-1 experienced the most extensive dry periods, which occurred for the majority of the record for Teneroc 4 and consistently since November 2006 at CFI SP-1 (Figures 3-7 and 3-11). Despite wells being installed 1.3 m below ground at SP-1 and 1.54 m below ground at Tenoroc 4, water levels still dropped below the well depths. As such, it can only be concluded that water levels fell to at least or greater than the well depths for these two systems.

Also shown in Figure 3-17 is a shaded bar representing the range of water depths that are characteristic of isolated wetlands typical of Florida (Brown and Tighe, 1991). Some surface

water features, such as those at Mosaic HP-10 and Mosaic H1, experienced water depths that predominately fell within this characteristic range during the four year period of study. The two PCS systems, however, consistently had surface water levels much greater than typical maximum depths, whereas the surface water features at Tenoroc 4 at CFI SP-1 experienced depths below ground that were often greater than below ground depths that are characteristic of isolated wetlands during dry periods.

Water levels from July 2005 to July 2007 for PCS SA 01, PCS SA 10 SW-1, Mosaic H1 SW-1, and Williams Co. were compared to daily water level data collected at a *Taxodium* spp. wetland system and a marsh system within the Green Swamp in central Florida (data provided by Southwest Florida Water Management District) (Figure 3-18). It should be noted that the Green Swamp systems and the Mosaic H1 and Williams Co. CSAs are in central Florida, whereas the two PCS sites are in north Florida which may have experienced different climatic conditions over the period. The total rain amounts, however, from July 2005 to July 2007 of the two regions were within 10 cm. While the Mosaic H1 and Williams Co. systems experienced similar trends in terms of seasonal flooding and drying as the marsh and *Taxodium* spp. systems, their increases following rain events and declines were often more pronounced illustrating their flashy hydrologic regimes. The buffered and deep systems at the two PCS sites had water depths much greater than occurred at the two Green Swamp systems. It appears that some CSAs have more buffered and deeper systems compared to natural wetland systems, while other CSA features may experience similar regimes as natural wetland systems but often with more fluctuation in water depths (Figures 3-17 and 3-18**)**.

As previously mentioned, three sites had multiple surface water features instrumented with wells (Figures 3-3, 3-9, and 3-13). The two surface water features instrumented at PCS SA 10

had similar rates of decline, responses to rain events, and depths when SW-1 was over 1.0 m in depth (Figure 3-3). At lower levels, however, the 2nd feature (SW-2) had steeper declines and increases and shallower water depths. The water level elevations at SW-2 were determined in reference to the ground surface at SW-1 well to compare surface water elevations of the two features relative to one benchmark. The relative water elevations over the period of study demonstrate that indeed the two systems became connected when SW-1 had depths of or above 1.2 m (Figure 3-19) and experienced surface water outflow when depths at SW-1 were above 1.47 m. Both features at Mosaic K5 also experienced similar fluctuations at specific depths, around 0.4 m at SW-1, and different surface water signatures at lower water levels (Figure 3-13). Evaluating the water level elevations at SW-2 relative to SW-1 revealed that the two systems became connected when SW-1 was at 0.39 m (Figure 3-20), and therefore both experienced surface water outflow through the channel system when water levels at SW-1 were 0.5 m or above. The relationships between the two surface water features at both PCS SA 10 and Mosaic K5 demonstrate that systems exist on CSAs that can be disconnected with different hydrologic regimes but which merge at higher water levels.

Three isolated surface water features were instrumented at Mosaic H1 and which had considerably different hydrologic regimes (Figure 3-9). Surface water-3 (SW-3) experienced permanent flooding, a buffered hydrologic regime, and greater water depths compared to the other two features which had flashier regimes and extensive dry periods (Figure 3-9). The differing signatures illustrate that these three systems never became connected during the period of study, and this is more evident when expressing SW-2 and SW-3 water level elevations relative to SW-1 (Figure 3-21). From the relative elevations, it appears that SW-2 and SW-3 are separate perched systems suggesting that the level pool assumption should not be applied across

an entire CSA. Furthermore, these results reveal that not only does hydrologic regime vary among CSAs but also among individual surface water features within a single CSA. Hydrologic regimes of surface water features vary among and within CSAs in terms of response to rain events and decline rates due to site-specific factors such as watershed configuration and soil type; stressing the need for a detailed evaluation of runoff, infiltration, and ET rates of surface water features within CSAs and the factors that affect these flows.

Water Budget

Water budgets of all instrumented surface features were performed to account for all hydrologic flows. These flows included ET, runoff (overland flow), surface water outflow, dike seepage, and infiltration/exfiltration. ET was estimated with various climatic-based empirical methods, and runoff was measured and modeled using surface water and precipitation data. Surface water outflow for features where it occurred was also evaluated in the water budgets. Water balances were performed using the estimated ET rates, runoff depths, and surface water outflow amounts, while assuming that groundwater inflow and outflow was zero. Residuals were calculated that balanced inflows and outflows with change in stage, and it was assumed that these residuals represented infiltration and/or underestimation of ET. The potential for groundwater inflow and outflow as addressed by determining water table elevations in surrounding uplands relative to surface water elevations and by measuring hydraulic conductivities of the upland soils. ET and infiltration were further evaluated by analyzing daily declines and utilizing the White method to calculate ET and infiltration rates with continuous surface water data. The runoff analysis, water balances and the resulting residuals, groundwater levels and hydraulic conductivities, and the calculated infiltration and ET rates were all compared among the instrumented surface water features to further identify differences in hydrologic regimes and the site-specific factors affecting these regimes.

ET Estimation

Climatic-based empirical models were used to provide initial estimates of daily ET to include in the water balances and to compare with the calculated ET rates using continuous surface water data and the White method. A suite of empirical methods were employed to determine the extent of variability in rates calculated by numerous methods. Daily ET (mm/day) was estimated with seven empirical models using hourly climatic data from the three weather stations installed in canopy free areas. Figure 3-22 shows the monthly averages of daily ET as estimated by the different methods using weather data from Williams Company during 2006. The daily ET estimates from 2/1/06 through 1/31/07 were summed to give total estimated ET (m) during the time period (Table 3-1). The Penman, Hargreaves, and Priestly Taylor methods resulted in the highest estimates. The Hamon method estimated similar rates during the summer months but much lower rates in the winter months.

Penman-estimated ET rates were initially selected for use in the runoff and water balance analyses since the Penman method is typically applied to wetland systems (Mitsch and Gosselink, 2000) and as a result of it producing one of the highest estimates of daily ET. The latter was selected for since it was thought that ET from CSAs may be high and a major contributor to the water budgets of these systems. ET was estimated with the Penman method from January 2006 through June 2008 using on-site climatic data from the weather stations at Williams Co., PCS SA 10, and CFI SP-1 and monthly averages of these estimates are shown in Figure 3-23. The daily rates were totaled to calculate yearly ET in 2006 and 2007 (Table 3-2). The two central Florida sites, Williams Co. and CFI SP-1, had similar rates and seasonal trends with slightly less yearly totals estimated at Williams Co, which is farther north. The northern site, PCS SA 10, had less total ET but with higher rates during the later summer months.

Runoff Analysis

Runoff, or overland flow, was evaluated in a three step process to quantify differences in responses to rainfall among surface water features within CSAs and to develop predictive runoff models for inclusion in the hydrologic temporal models. The response in stage as a function of rainfall depths was first evaluated to determine runoff to rainfall ratios experienced by the surface water features and if runoff could be adequately predicted solely as a function of rain depth. Upland to inundated area ratios determined with LiDAR data were used to relate contributing area to runoff depths and to calculate runoff coefficients, which were compared among surface water features. Finally, multiple regression was performed to observe the effects of antecedent conditions and rainfall depth on runoff coefficients, and thus runoff amounts, and to develop models that predict runoff coefficients with rain depth and antecedent conditions as independent variables. Runoff analysis was performed for one surface water feature at each of the eight hydrology sites except for Tenoroc 4 which had limited periods of inundation. Additionally, another surface water feature at Mosaic H1, SW-3, was included in the analysis (Figure 3-9). Time periods when surface water outflow occurred from the sites with outfalls were excluded from the analysis.

The relationships between event responses and rainfall depths were explored for all sites and linear regression resulted in the best fits for these relationships. Event response represents the stage response plus ET predicted by the Penman method during the day of the rain event, and subtracting the direct rain depth from the event response results in runoff depth (Figure 2-17). Event responses versus rain events for PCS SA 01, PCS SA 10, and Mosaic H1 SW-1 are shown in Figures 3-24, 3-25, and 3-26. A 45^{o} (1:1) line is also shown on the figures to highlight when the responses became greater than the rainfall amount. Event responses of PCS SA 01 and SA 10 followed the 1:1 line more closely than the responses at Mosaic H1 SW-1. Two regression

lines of event response versus rain depth are shown in Figures 3-24, 3-25, and 3-26. While the regression lines with a non-zero y-axis intercept produces a slightly better fit, subtracting one from the slope of the regression line with a zero y-axis intercept for event response provides a quantification of runoff depths in terms of percentages of rain amounts. These results demonstrate that PCS SA 01 and SA 10 typically experienced runoff amounts equaling 38 % and 58 % of direct rainfall, respectively, while runoff amounts equaling 173 % of the direct rainfall occurred at Mosaic H1 SW-1.

Event responses plotted against rain depth for Mosaic K5 and Mosaic H1 SW-3 are shown in Figures 3-27 and 3-28. Strong linear relationships resulted for both sites, though the relationship for Mosaic K5 may be influenced by the maximum event response (Figure 3-27). Nevertheless, it appears that Mosaic K5 experienced more runoff than the two PCS sites and less than Mosaic H-1 SW-1. SW-3 at Mosaic H1 experienced runoff depths which almost equaled direct rainfall (99.6 %) compared to runoff depths at Mosaic SW-1 that were 173% of rainfall, demonstrating the different runoff characteristics at separate features within one CSA (Figures 3-26 and 3-28).

The event responses at CFI are shown in Figure 3-29, which followed the 1:1 line extremely close and with a maximum response of 0.09 m. The regression line for responses experienced at CFI SP-1 had a slope near one demonstrating the response to a rain event was primarily due to direct rainfall with small runoff depths equaling approximately 21 % of rainfall. The event responses that occurred at Williams Co. and Mosaic HP -10 significantly departed from the 1:1 line and with maximums of 0.2 m and 0.35 m, respectively (Figures 3-30 and 3-31). Subtracting one from the slope of the regression lines reveals that runoff depths were approximately 1.5 and 3.8 times the rainfall at Williams Co. and Mosaic HP-10, respectively.

The relationships between event responses and rain experienced at these sites, however, were not as strong as found with the other sites.

The linear relationships between event response and rain depth that were found for most surface water features demonstrate runoff can be predicted adequately from rain data alone. The strong relationships also suggest that runoff was primarily influenced by event magnitude and less by antecedent conditions or upland to wetland ratios. The event response analysis did not include upland to wetland ratios and therefore did not account for contributing areas, which changed substantially with stage. The strong correlation between rain and runoff despite varying contributing areas implies that runoff may be more controlled by a perimeter effect from the upland versus the actual size of the watershed of these sites, where micro-topography and depressional storage may limit runoff. Williams Co. and Mosaic HP-10 may be the exception, however, since their linear relationships were not as strong, suggesting greater influence from contributing areas and/or antecedent conditions on runoff events at these sites.

For at least 6 of the surface water features, the results from the event response analysis suggest that runoff may be adequately predicted with rainfall data independent of antecedent conditions or upland to wetland ratios. With that said, runoff coefficients were still calculated to compare the coefficients of the instrumented surface water features and to include the effects of contributing areas. To observe the effect from scale of watershed delineation, runoff coefficients were calculated for PCS SA 10 and Mosaic H1 SW-1 at three watershed scales. Watershed delineation scale refers to the amount of watersheds delineated in a CSA, with the largest scale of analysis treating the entire CSA as one contributing watershed and the smallest scale delineating the most watersheds within a CSA that contribute to separate isolated surface features (Figure 2-19). Upland to wetland ratios were calculated as a function of stage using

LiDAR data and for each scale of watershed delineation (Figures 3-32 and 3-33). Large, medium, and small scales correspond to 1, 239, and 523 watersheds delineated within PCS SA 10 and to 1, 88, and 333 watersheds at Mosaic H1 SW-1. A power function performed better for PCS SA 10, whereas an exponential function resulted in the best fit for Mosaic H1 SW-1. The coefficients of determination (R^2) indicated a good fit for the different scales of watersheds for both sites.

Runoff coefficients were calculated using the upland to wetland area ratios as a function of stage, runoff depths (event response minus rain depth), rainfall amounts, and Equation 2-9. Runoff coefficients were calculated for each rain event and at the three scales of watershed analysis for PCS SA 10 and Mosaic H1 SW-1. Table 3-3 lists the average runoff coefficients using different scales of watershed analysis, large, medium, and small. Runoff coefficients for both sites increased with smaller scale analysis, as to be expected since contributing areas to the surface water features decreased with decreasing scale. While the runoff coefficients for PCS SA 10 increased, they remained much lower than the coefficients for Mosaic H1 SW-1, supporting similar results from the event response analysis (Figures 3-25 and 3-26).

Runoff coefficients for the remaining six features were calculated using the smallest scale of watershed analysis to determine upland to wetland ratios as functions of stage (Figures 2-20 through 2-26). Careful attention was placed when developing the ratios to account for the convergence of surface water features as was observed in the analysis of flooding regimes (Figures 3-19 and 3-20). As surface water features merge, so do their contributing areas which needs to be accounted for while calculating upland to wetland ratios, and this was done when utilizing the multiple watershed approach. Upland to wetland ratios were successfully related to stage for all eight features with coefficients of determination equaling 0.91 or greater. The

resulting average runoff coefficients (C) and upland to wetland ratios (Up/Wet) with standard deviations for all eight surface water features are shown in Table 3-4 along with the regression slopes of event response versus rain depths with y-intercept equal to zero. The standard deviations demonstrate that the runoff coefficients were dynamic and influenced by upland to wetland ratios and/or antecedent conditions, and that the upland to wetland ratios varied substantially as they were a function of stage. While Mosaic H1 SW-1 had the highest runoff coefficient, Mosaic HP-10 experienced the greatest runoff depths with an event response slope of 4.79 (Table 3-4). The greater runoff depths despite a lower runoff coefficient results from Mosaic HP-10's much higher upland to wetland ratios due to the small area of this feature compared to the surrounding contributing area.

Runoff coefficients must be coupled with contributing areas when using the coefficients to compare total runoff amounts (Table 3-4). Williams Co. had the second highest runoff coefficient but one comparable to the PCS SA 01's coefficient. The event response slope, however, for Williams Co. was much higher than that of PCS SA 01's which can be explained by a larger contributing area at Williams Co. PCS SA 01 also experienced less runoff than PCS SA 10 but had a higher runoff coefficient. Again, this can be explained by the contributing areas, which were much smaller at PCS SA 01. CFI SP-1 had both the lowest runoff coefficient and event response slope. Similar to the results in the event response analysis, Mosaic H1 SW-3 had a much lower runoff coefficient than Mosaic H1 SW-1 but with comparable contributing areas, demonstrating the different runoff responses that may be experienced by separate features on an individual CSA.

The results from the event response analysis suggest that for most of the sites runoff depth, defined as event response minus rain depth, can be predicted by estimating event response with

rain data. The alternative is to predict runoff coefficients using rain depth and antecedent conditions and then apply rain depths to the upland to wetland ratios with these coefficients to predict runoff depths using a rearrangement of Equation 2-9. Multiple variable regression was employed to predict runoff coefficients and observe if prediction of runoff could be improved with inclusion of antecedent conditions and contributing area. Multiple regression was performed with the calculated runoff coefficients as dependent variables and rainfall and the various antecedent condition indices as the predictive variables. The rainfall antecedent condition reflected the rainfall history over the preceding 14 days before the analyzed rain event and weighted recent rain more heavily using Equation 2-10. The ET index simply summed the daily Penman-estimated ET over the previous 14 days to quantify history of soil drying before the rain event.

Multiple regression models for Mosaic H1 SW-1 and Williams Company resulted in coefficients of determination equaling 0.76 and 0.81, respectively. Predicted and the calculated runoff coefficients plotted for different rain events are shown in Figure 3-34 and 3-35. The model for Mosaic H1 SW-1 was less successful at predicting runoff coefficients than the linear model at predicting event response from rain depth. The resulting model for Williams Company, however, predicted runoff coefficients better than event response was predicted with rain suggesting that antecedent conditions may have influenced runoff more at Williams Co. (Figures 3-35 and 3-30). Similarly, the multiple regression performed better for Mosaic HP-10 resulting in an R^2 of 0.81 compared to an R^2 of 0.60 when predicting event response from rain depths (Figure 3-31). While event response was predicted at PCS SA 10 using rain depth with an R^2 of 0.85, multiple regression was able to better predict runoff coefficients (R^2=0.94).

The multiple regression models developed for the remaining four sites resulted in much lower R^2's compared to the other multiple regression models and to the R^2's that were achieved when predicting event response from rain depth (Table 3-5). The R^2's listed in Table 3-5 refer to the linear models which predict event response from rain but while allowing y-axis intercepts to be non-zero. The fact that most simple models for predicting runoff from rain performed better than the multiple regression models, which included upland to wetland areas, suggests that runoff may have been primarily from a constant contributing area such as the edges of the feature which do not change significantly with stage. This is supported by the linear models which demonstrated that runoff was a fairly constant percentage of rain depth despite changing upland to wetland ratios.

To further assess the models' abilities to predict runoff amounts, positive event responses measured during periods of no outflow were summed and compared to predictions made by the various models. Since the event responses included rain events, the comparison was made between the sums of measured event responses and the sums of rain plus predicted runoff depths. Both the simple linear models and the multiple regression models for PCS SA 10, Mosaic H-1 SW-1, and Williams Co were evaluated (Table 3-6). In all three cases, the simple linear models resulted in higher total rainfall plus predicted runoff amounts, which were more comparable to the total of the measured event responses. Only the linear models' abilities were evaluated for PCS SA 01, Mosaic K5, CFI SP-1, and Mosaic H1 SW-3 since it was found that the linear models for these sites performed far better than the multiple regression models (Table 3-7). All totals are within 5 cm except for Mosaic H1 SW-3 whose measured was over predicted by 15 cm.

Surface Water Outflow

The presence and activity of outfall structures at all eight CSAs were assessed to include effects of surface water outflow on the water budgets of the instrumented surface water features. Mosaic K5 and Tenoroc 4 both had channels allowing outflow and which were instrumented in May 2006 with upstream and downstream wells, separated by at least 50m (Figures 2-15 and 2-13). Figures 3-36 and 3-37 show water levels in the upstream and downstream wells, where the downstream levels are given as water level elevations relative to levels at the upstream well. The channel at Tenoroc 4 experienced high water levels but low flow as indicated by the similar elevations experienced in the upstream and downstream wells. When comparing the channel surface water levels with the water levels in Figure 3-7, it appears that the channel acted as the main water feature of the site rather than a channel draining a feature (Figure 2-14). This channel connects to another larger channel before exiting over a weir, and the elevation of the weir and the backflow force caused from the larger channel may have limited the flow from the Tenoroc 4 channel. The channel at Mosaic K-5 experienced lower levels and more frequent drying (Figure 3-37). Furthermore, there were positive heads differences between the water elevations at the upstream and downstream wells indicating outflow from the site occurred.

A flow measurement was performed at the channel on Mosaic K5 on 9/26/2006 at the upstream well using an ADV velocity meter. The velocity-area flow calculation technique, where velocities were measured at 6/10 depth and at 50 cm increments across the width of the channel, was used to determine an average flow rate of 0.078 m3/sec. The cross sectional profile of the channel at the upstream well was obtained as relative to the ground surface of the well, which was the lowest point in the profile (Figure 3-38). The profile was treated as a triangle to determine cross sectional area and wetted perimeter using surface water levels at the upstream well at the time of velocity measurements. The measured flow and these parameters were used

along with Equation 2-11, solving for the Manning's roughness coefficient which equaled 0.256 $sec/m^{1/3}$. Other measurement attempts of velocity were unsuccessful due to dry conditions in the channel during subsequent field visits. The resulting coefficient with the one measurement is on the high end for channels, which typically range from 0.1 to 0.15 for channels with high plant growth (Dingman, 2002). The channel was dominated by dense *Typha* spp. including significant detritus likely resulting in a high roughness coefficient, though caution should be used when applying a coefficient from one set of velocity measurements.

Using the continuous well data to determine cross sectional area, wetted perimeter and the daily average head difference along with Equation 2-11 and a Manning's coefficient of 0.256 $sec/m^{1/3}$, average daily flow (m^3) was calculated for Mosaic K5 (Figure 3-39). The channel was visited on 8/17/06 when flow was occurring and it was determined that there were at least three connection points to SW-1 which facilitated flow from SW-1 to the channel. The channel does, however extend the whole length of the east side of the CSA and it could not be determined if flow from other isolated features would have been possible. Assuming that the majority of channel flow was from SW-1 and that direct rainfall to the ditch was negligible, the outflow from SW-1 was calculated in terms of depth/day. The upland to wetland ratios as function of stage were used along with the flow data to determine daily outflow (cm) from SW-1 (Figure 3-40). During the 1.68 years that were analyzed for channel flow, 64.77 cm of outflow from SW-1 was estimated resulting in 5.3 E^5 m^3 of total flow.

The weir at PCS SA 10 created outflow when SW-1 had water levels of 1.47 m or above which only occurred during the first part of the site's record, 8/5/05 to 4/27/06 (Figure 3-3). During this time, the weir experienced short-circuiting of flow through cracks in the structure, thereby restricting any calibration of the weirs. The structure was repaired during a drier time in

May 2006 to allow calibration after subsequent increases in water levels. Water levels never increased enough, however, to create outflow and therefore calibration was not performed. As a result, outflow during the period of occurrence could not be calculated or included in the water budgets. As discussed earlier, PCS SA 01 had an active outfall which was affected by an upstream beaver dam that was found in early spring 2005. Insertion of inserts in the outfall structure during May of 2006 successfully blocked outflow and allowed more accurate runoff modeling and water balances.

Williams Co. had an outfall via a pipe through its dike which was visited on numerous field visits and when the site had the highest surface water levels recorded during the study period. At these times, surface water levels never reached the pipe invert and were always at least one meter below the invert. The pipe flow and ditch network at Mosaic HP-10 was never instrumented to provide data for flow analysis. It was determined with LiDAR elevations and site visits during pipe flow events that flow occurred at the site when surface water levels were above 0.45 m which happened quite frequently (Figure 3-15). CFI SP-1 had a small channel which connected its two lobes. The instrumented feature was on the east lobe that drains to the west lobe which has an outflow off the entire CSA. Through surveying the channel elevations relative to the surface water well, it was determined that this occurred when surface water levels were approximately 0.80 m or above (Figure 3-11). Water levels reached this level only once during a three day period in April 2005. Mosaic H1 had no active outflow paths from the entire site during the period of study.

Water Balances

Rainfall, Penman-estimated ET, runoff depths, and outflow rates were used to perform water balances where the inflows and outflows were balanced with residuals to result in the observed change in stage. Residuals were assumed to represent infiltration and/or

underestimation of ET with the Penman method, and were evaluated along with the inflows and outflows to identify differences among surface water features. Water balances were performed for time periods when constant inundation occurred and for one surface water feature at all sites, except for Tenoroc 4 due to its limited periods of inundation. Additionally, another surface water feature at Mosaic H1, SW-3, was evaluated. Since the outfall at PCS SA 10 SW-1 was active only in the beginning of the record and calibration of the weir was inhibited, the balances were calculated for the period since the structure became inactive. Similarly, analysis for PCS SA 01 was done only for the period of following the installation of inserts in the weir. Two different time periods, 239 and 238 days, for Mosaic H1 SW-1 were evaluated where surface water data were positive. Four different periods of records at Mosaic K5 SW-1 were analyzed including time periods when no channel outflow occurred and one longer period, 5/18/06 to 1/18/08, which had intermittent channel outflow and that encompassed some of the shorter time periods evaluated. These four periods for Mosaic K5 were analyzed separately to observe the effects of including the calculated channel outflow in the water balances.

Water balances were calculated using Equation 2-13 and the assumption of zero infiltration along with rainfall, the predictive runoff models, estimated daily ET with the Penman method, and daily surface water data. The channel well data and flow equation were included in the analysis of Mosaic K5 SW-1 to account for surface water outflow. As a result of some of the sites, namely Mosaic K5 and HP-10, having intermittent outflow during the period of analysis, measured stage responses could not be used to determine runoff contributions to the balances, as stage responses may have been reduced by the outflow and would underestimate runoff amounts. Therefore, the predictive runoff models that were developed for times when there was no outflow were used to determine total runoff depths for the water balances. The predictive linear

models with non-zero y intercepts were used for all sites except for Mosaic HP-10 for which the multiple regression model was used since it performed better. While the multiple regression model also performed better for Williams Co., the results in Table 3-7 suggested the linear model may be adequate.

Water balances along with the residual totals as depth per day for all evaluated features are presented in Tables 3-8 and 3-9. Mosaic K5 SW-1's water balances are shown separately in Table 3-9 with the inclusion of the channel flow. Since Mosaic HP-10 had frequent outflow which was not instrumented, its resulting residual includes outflow. Total runoff amounts were calculated as percentages of incoming rain for each feature (Table 3-10).

Similar to the runoff analysis results, CFI SP-1 experienced the lowest runoff amounts, followed by the features at the two PCS sites, then Mosaic K5 SW-1 and H1 SW-3 (Tables 3-8, 3-9, and 3-10). The highest runoff contributions to the water balances occurred at Mosaic HP-10, Mosaic H1 SW-1, and Williams Co. (Table 3-8 and 3-10). The runoff amounts as percentages of rain are similar to the results of the slope of event response analysis (Table 3-10 and 3-4). The runoff amounts calculated in the water balance of Mosaic HP-10, however, are much lower than what was predicted with the event response slope minus one due to the multiple regression model which was used in the water balance and that predicted less runoff (Table 3-10 and 3-4). As found in the runoff analysis, the runoff to rainfall ratios demonstrate the different runoff characteristics among and within CSAs.

The residuals of the water balances for the different time periods of Mosaic K5 SW-1 suggest that the channel outflow contribution to this feature's water budget was over predicted with the channel well data and flow equation (Table 3-9). The two periods without channel flow and that include summer months resulted in daily residuals of over 2 mm, while the period of no

channel flow during fall 2007 and winter 2008 had a residual of 0.29 mm/day. The long period which included times of channel flow that was estimated with well data had a daily residual of 0.21 mm. This residual is similar but smaller than the 0.29 mm/day experienced in the winter without channel flow. Since the time period with channel flow included 2 summers and 1.5 winters, its residual should not only be higher than what was experienced in the winter but also slightly higher than the average of the summer residual and winter residuals from the time periods without channel outflow. The fact that the residual is much lower than this, may suggest that the channel flow may have been somewhat overestimated, causing a decrease in the residual. With that said, the calculated channel flow rates may still have represented what was actually outflow through the channel since it included direct rainfall to the channel itself and possible flow from other features within the CSA that are isolated from the feature evaluated here.

The differences among the daily residuals from the water balances of all sites are apparent (Table 3-8). Excluding Mosaic HP-10 and Mosaic K5 with channel flow, Williams Co and Mosaic H1 SW-1 had the highest residuals which were over 4 mm/day. The residuals for PCS SA 10 SW-1, Mosaic H1 SW-3, and CFI SP-1 were comparable and near 1 mm/day, demonstrating the differences both among sites and within one site (Mosaic H1 SW-1 and SW-3). The analysis of PCS SA 01 resulted in the only negative residual, representing an inflow that may not have been accounted for in the balance. The positive residuals found in the balances of all other sites suggest underestimation of an outflow, be it ET and/or infiltration, calling for closer examination of these flows.

Dike Seepage

The water balances suggested that some underestimation of outflow occurred at most sites. Since surface water outflow did not occur during the times analyzed, with the exception of at Mosaic HP-10 and during one of the four analyzed periods of Mosaic K5 SW-1, infiltration

and/or underestimation of ET are reasonable explanations for the residuals. Infiltration was defined as both the loss of surface water vertically to the local groundwater system and laterally across the dike as seepage (Figure 1-2). Three features which had surface water in contact with dikes, PCS SA 10 SW-1, Mosaic H-1 SW-2, and PCS SA 01, were instrumented with a well on the dike and one on the downward slope of the dike to provide data for calculation of dike seepage (Figures 2-3, 2-7, and 2-1).

Discrete water levels within the dike wells were recorded during site visits. The water levels within the dike wells and surface water data from the wells in the adjacent surface water feature were used to develop groundwater profiles. Elevations of the ground surfaces of the wells were used to determine the profiles as relative elevation differences, with zero representing the elevation at the surface water well. Groundwater profiles recorded at the dike wells on different dates are shown for PCS SA 10, Mosaic H1, and PCS SA 01 in Figures 3-41, 3-42, and 3-43. The profiles are shown along with the land elevation profiles, and the water level elevation at zero distance represents the surface water levels recorded at the wells of the adjacent features. Measurements taken at the down slope well of Mosaic H1 are not shown (Figure 3-42). This well was installed 46 m away from the surface water well but with a depth of only 4.2 m due to equipment failure and was dry during all site visits. The SW-2 well at Mosaic H1 only experienced inundated conditions on two of the four measurement periods shown, and with minimal depths (Figure 3-42).

The profiles across the dikes of the three sites indicate there were gradients to provide lateral dike seepage out of the CSAs. Lateral hydraulic gradients, however, determine the magnitude of seepage and are required to calculate seepage rates. Slug tests performed in the wells installed on top of the dikes and the Horslev method (Equation 2-14) were used to calculate

average lateral saturated hydraulic conductivities which are listed along with standard deviations in Table 3-11. Slug tests were done on three different occasions at each site. The average conductivities for the dike wells were used along with the groundwater profiles and Equation 2-15 to calculate dike seepage for each site. The steepest hydraulic gradient from the recorded profiles and the associated surface water levels were used to calculate maximum dike seepage from the record. Surface water levels used for PCS SA 10, Mosaic H1, and PCS SA 01 were 1.45, 0.22, and 1.16 m, respectively. Calculated dike seepages (cm/yr) for each site are shown in Table 3-12. The depth of water resting on the dike is represented by D, and seepage was calculated for D equal to the actual surface water in contact with the dike at the time of the steepest hydraulic gradient. Additionally, hypothetical depths of water resting on the dike equaling 1, 5, and 10 m were included in the analysis to evaluate the sensitivity of calculated dike seepage to this parameter.

Seepage rates calculated with the actual surface water levels were low for all three sites, with a maximum of 0.77 cm/yr at PCS SA 01, due to its steeper hydraulic gradients (Table 3-12 and Figure 3-43). With a hypothetical surface water depth of 10 m in contact with the dike at PCS SA 01, seepage was only estimated to be 6.63 cm/year. Despite the fairly steep hydraulic gradients, seepage was calculated to be negligible to the overall water budget as a result of the low measured hydraulic conductivities (Table 3-11). It should be noted, however, that the conductivities represent point conductivities and other portions of the dikes could have higher conductivities where more significant seepage may occur. Observation of hydrophytic vegetation along the toes of the dikes was done prior to the installation of the wells in an attempt to locate these zones to perform the dike studies. No noticeable differences in vegetation along the toes were found, however.

Local Groundwater Analysis

The residual results from the water balances indicated that outflows may have been underestimated, and the dike seepage analysis suggested that this underestimation was not from unaccounted dike seepage. Groundwater wells were installed with pressure transducers on all eight sites to further evaluate the potential for local groundwater flow to or from a surface water feature (Figures 2-1 through 2-16). The groundwater elevations relative to the surface water elevations were evaluated along with measured saturated lateral hydraulic conductivities to assess groundwater flow direction and potential.

Up to three wells were installed per site, and the names of the wells referred to here are in reference to when they were installed versus their relative position to the adjacent surface water features. Groundwater-1 wells were installed along with the original surface water wells and immediately adjacent, within 10 m, of the water feature. Groundwater-2 wells were installed during the summer of 2006 and within the upland contributing areas of the water features. The groundwater-2 wells were installed in the topographic highest point of the contributing area and at least 100 m away from the feature. The pressure transducers used in the groundwater-1 wells were removed and placed in the groundwater-2 wells and, therefore, groundwater-1 records cease at the beginning of the groundwater-2 records. Three sites, Williams Co., Mosaic K5, and Mosaic SP-1, had yet another well, groundwater-3, later installed at an elevation between the groundwater-2 and groundwater-1 wells. Therefore, groundwater-3 wells were at elevations lower than the groundwater-2 wells but at higher elevations than groundwater-1 wells. Mosaic HP-10 had only one groundwater well installed, which never recorded water despite being 7.24 m below ground.

The groundwater levels recorded in the groundwater-2 wells at seven sites are shown in Figure 3-44. These levels represent water table depths at a topographic high area within the

interior area of each CSA. Depths below ground ranged from 0.35 m to 3.7 m with the shallowest observed at PCS SA 10 and the deepest recorded at Tenoroc 4. Most sites experienced water tables ranging from 1 to 2 m below ground. Teneroc 4, Williams Co. Mosaic H1, and CFI SP-1 experienced the deepest water tables, and these sites also had the most extensive dry times in their surface water features which are associated with their deepest water table depths (Figures 3-44 and 3-17). Likewise, the sites with the most constant flooding, PCS SA 10, PCS SA 01, and Mosaic K5, experienced the shallowest water tables.

Slug tests were performed in the groundwater-2 wells and on three different occasions. The data collected during the slug tests and the Horslev Method (Equation 2-14) were used to calculate saturated lateral hydraulic conductivities of the local groundwater systems that the wells penetrated, and the averages are shown in Table 3-13 along with standard deviations, depth of installation, and the soil type encountered during installation. Also listed in Table 3-13 are the elevation differences between the ground surfaces of the surface water wells and groundwater-2 wells. The elevation differences are in reference to the SW-1 wells on all sites except for Mosaic H1. The groundwater-2 well at Mosaic H1 was installed in an upland area which surrounds the SW-3 feature, and therefore, the elevation difference between the SW-3 well and groundwater-2 well is shown. It was not possible to perform a slug test in the well at Mosaic HP-10, as the well never recorded water. The groundwater-2 well at PCS SA 01 was installed in pure sand tailings, and slug test attempts were unsuccessful since the increase in water levels after the slug was removed was almost instantaneous. The pure clay of the uplands instrumented at Mosaic K5, Williams Co., and Teneroc 4 resulted in the lowest conductivities while much higher conductivities were measured at Mosaic H1, PCS SA 10, and CFI SP-1 which had sandier conditions. The extremely quick recovery after the slug test and the pure sand at PCS SA 01

suggest that its lateral hydraulic conductivity was higher than the ones measured at the other sites.

Utilizing both surveying and LiDAR data, water levels recorded in all groundwater wells were determined relative to the ground surface of the surface water wells. Groundwater-1 and groundwater-2 levels are shown relative to the elevation of surface water levels at PCS SA 01 in Figure 3-45. The close proximity of the groundwater-1 well at PCS SA 01 to the instrumented surface water feature resulted in near equal elevations and fluctuations. Though the groundwater-1 level elevations were slightly less than the surface water level elevations, they were always within 8 cm, a magnitude that could be affected by small errors in surveying. Such a close matching of elevations and signatures demonstrates fairly good connection of the groundwater system immediately adjacent to the water feature. The groundwater-2 levels, however, were higher relative to the surface water levels and with greater response to rain events and subsequent decline. This surrounding water table measured with the groundwater-2 well was on average 0.30 m higher than the surface water elevation which suggests the potential for groundwater flow into the water feature. This flow, however, would have been controlled by the lateral hydraulic conductivity. While a conductivity was not measured at PCS SA 01 groundwater-2 well, it is estimated that it was higher than the conductivities measured at all other sites.

In contrast to what was observed at PCS SA 01, the groundwater-1 level elevations at PCS SA 10 were lower than the surface water levels and with a different signature (Figure 3-46). While the proximity of this well to the water feature is comparable to that of PCS SA 01, the well at PCS SA 10 was installed just inside of the dike. The lower elevations recorded in the groundwater-1 wells suggest a hydraulic gradient that could provide dike seepage, similar to the

results found in the dike seepage analysis (Figure 3-41). The groundwater-2 well was installed on the other side of and further from the surface water feature and in the interior of the CSA. The water elevations at this well were an average of 1.2 m above the surface water elevations. These results reveal that a hydraulic gradient existed from the interior potentially providing groundwater inflow to the water feature, but that there was also a gradient to allow lateral outflow through the dikes. Each of those flows would have been largely controlled by the conductivities of the respective paths. The measured conductivity at the groundwater-2 well was an order of magnitude higher than the one measured at the dike well (Tables 3-13 and 3-11).

The elevation of the groundwater-1 levels at Tenoroc 4 were higher but with similar signatures compared to the elevation of the levels recorded at the surface water well, which were often below ground and thus also groundwater levels (Figure 3-47). Throughout the entire record of groundwater-2, there was no inundation at the surface water system, and often the surface water well was dry which occurred around 1.5 m below ground. With that said, it is hard to conclude much from the relative elevation differences between groundwater-2 and surface water levels. It appears, though, that the groundwater system at groundwater-2 may have been lower than the system at the surface water well, but by a maximum of only 0.20 m. The elevation data used to calculate the differences at this site were strictly from LiDAR data and a difference of only 20 cm is close to the accuracy of that technology. Furthermore, nothing can be concluded for what levels would have been at groundwater-2 during the first part of the surface water data record when much higher water levels were experienced and evidence of potential groundwater flow toward the system was observed with the groundwater-1 well data.

Data from all three surface water wells and both groundwater wells are shown for Mosaic H1 in Figure 3-48, with all water elevations relative to SW-1. Similar to Tenoroc 4 and PCS SA

01, the groundwater levels (groundwater-1) just adjacent to the surface water feature were similar in elevation and signature to the surface water system. The elevations of groundwater-2 and SW-3 suggest that the hydraulic gradient created the potential for groundwater flow from groundwater-2 to SW-3. SW-3 elevations were above the water elevations of the other two surface water systems, indicating the potential direction of continued groundwater flow. Again, this flow would have been strongly regulated by the hydraulic conductivities of the system. While the conductivity measured at the groundwater-2 well was one of the highest measured (Table 3-13), it should be noted that the sandier upland where the well was installed is not characteristic of the whole site and strictly surrounds the surface water-3 system. The majority of the site is pure clay which may have conductivities similar to the ones measured at Williams Co., Tenoroc 4, and Mosaic K5 (Table 3-13) and that may limit groundwater flow from feature to feature. This limitation is supported by the fact that all three surface water systems have very different water elevations and signatures. The higher conductive soil (Table 3-13) and elevated water table that surrounded SW-3 suggests higher potential for groundwater flow into the SW-3 feature (Figure 3-49).

Three groundwater wells were installed at Williams Co., CFI SP-1, and Mosaic K5. Groundwater-2 well was installed in the most upland area surrounding the surface water feature, and groundwater-3 in an intermediate elevation between groundwater-2 and the groundwater-1 wells. As with the other sites, groundwater-1 wells were just adjacent to the water features. Similar to other sites, both Williams Co. and CFI SP-1 had groundwater-1 levels with elevations and signatures almost equal to those recorded in the surface water wells (Figures 3-50 and 3-51). Caution should be used when evaluating Figure 3-51, as both the SW-1 and groundwater-3 wells became dry after 12/8/07 and values thereafter should be disregarded.

Similar to the groundwater-1 levels, the groundwater-3 wells at Williams Co. and CFI SP-1 recorded elevations almost equivalent to the levels measured at the surface water wells (Figures 3-50 and 3-51). It should be noted that no inundation occurred at the surface water wells at either site since installation of groundwater-3 wells. As such, the similar elevations recorded at the surface water and groundwater-3 wells demonstrate that a connected local groundwater system had occurred between the wells and in the lower areas of the two sites. The groundwater-2 elevations of both sites were above the elevations recorded in the surface water and groundwater-3 wells suggesting groundwater flow towards these lower areas. The measured hydraulic conductivity at CFI SP-1 is an order magnitude higher than the one measured at Williams Co., where groundwater flow may have been more limited (Table 3-13). The average difference between the groundwater-2 and the water elevations in the lower areas was 0.97 m at CFI SP-1 compared to 0.72 m at Williams Co..

The groundwater-1 well at Mosaic K5 was installed just inside of the dike that is adjacent to surface water-1, whereas the groundwater-2 was installed on the other side of and further from the feature and in the interior of the site. This was also the case at PCS SA 10, and similar to its results, the groundwater-1 water elevations at Mosaic K5 are lower than the surface water elevations, again indicating the potential for groundwater outflow through the dike (Figures 3-46 and 3-52). Unlike the other sites, the groundwater-2 elevations at Mosaic K5 were at times equal, above, or below the surface water elevations (Figure 3-52). While the elevations were equal for an extended period after installation, the onset of summer 2007 resulted in more drying of the surface water feature compared to the groundwater-2 system. At this time, the elevations indicated the potential for groundwater inflow into the water feature. With increases of surface water levels through the later part of the summer, however, the groundwater-2 elevations became

lower than the surface water, implying that a reversal of potential groundwater flow had occurred. During most of summer 2007, the groundwater-2 elevations were also above the water elevations recorded in the groundwater-3 well which was installed between the groundwater-2 and surface water wells. However, it appears that the groundwater-2 and groundwater-3 systems became more connected near the time when the groundwater-2 elevations fell below the surface water elevations, suggesting that flow from the water feature towards the now more connected groundwater system may have occurred. Such a transient potential groundwater behavior was not observed at the other sites, but again the actual groundwater flows would be limited by the hydraulic conductivity of the groundwater systems (Table 3-13).

As previously mentioned, the one groundwater well installed at Mosaic HP-10 never recorded water despite the bottom of the well being 4.94 m below the bottom of the surface water well. Such a deep surrounding water table compared to the constantly flooded surface water system suggests that the water features on HP-10 may have been fairly disconnected from and perched above any local groundwater of the system. This site is atypical compared to the other sites and other CSAs, as it had sand tailings deposited on the entire site which were later mined.

Daily Decline Analysis

The resulting residuals from the water balance analysis suggested an underestimation of ET and/or infiltration. The dike seepage analysis gave evidence, for at least the sites evaluated, that lateral dike seepage may have been a negligible component of the possible infiltration. The results from the local groundwater analysis demonstrated that in most cases there was a potential for groundwater inflow (exfiltration) to the surface water features rather than infiltration, though these inflow rates would have been limited by the low hydraulic conductivities (Table 3-13). An

analysis of daily declines of instrumented surface water features was performed in an effort to separate and further evaluate groundwater and ET flows.

Average daily losses using the data from the less accurate pressure transducers and calculated with linear regression of surface water levels during time periods with no rain or surface outflow are shown in Tables 3-14 through 3-20. The losses calculated during particular months were averaged, along with their associated coefficients of determination (R^2), and are presented as monthly averaged daily declines. Also included in the tables are average monthly ET rates estimated with the Penman method. The estimated ET rates were subtracted from the loss slopes to calculate the differences, Δ(mm/day), which are the residual values that represent any error in ET estimation plus potential infiltration losses. The residual values for each site were averaged and are presented at the bottom of the tables. In general, the coefficients of determination suggested good fits by the linear regressions. Tenoroc 4 had the largest residual value, suggesting significant infiltration occurred (Table 3-16). It should be noted, however, that though the analyses were performed during time periods when the sites were inundated, Tenoroc 4 constantly had low surface water levels used in analysis. At such levels, the surface water declines can be strongly affected and increased by the associated decline in the surrounding soils and their much lower specific yield and, therefore, caution should be used when interpreting the results from Tenoroc 4. Mosaic K5, Williams Co., and Mosaic H1 also had large residual values but which were calculated when sufficient surface water depths occurred (Tables 3-17, 3-20, and 3-19). These results suggest infiltration occurred at these sites. Similar to the water balances, PCS SA 10, PCS SA 01, and CFI SP-1 had the lowest daily decline and thus residuals.

The monthly variability in the residual values for most sites suggests that summer ET may have been underestimated and contributed to the residuals. The daily declines from all sites

were averaged to obtain average daily declines during the growing season and the non-growing season. These average rates are listed in Table 3-21 along with associated averages for Penman-estimated ET and ET rates measured in lysimeter studies of a Florida *Typha* spp. marsh and *Cladium jamaicense* marsh (Mao *et al*., 2002). The differences between the average daily decline and various ET estimates were 6.15 to 7.94 mm during the growing season compared to differences of 3.9 to 5.2 mm during the non-growing season. And at some sites, summer residual values were substantially higher than ones calculated in the winter time indicating that ET may have been underestimated during the summer months (Tables 3-19 and 3-20). ET during the winter months also could have been underestimated, just not to the same degree as in the summer. These results suggest that infiltration could be occurring at some sites and at different rates. If it is assumed that infiltration is fairly constant throughout the year, then the seasonal variability in the residuals also suggests that not all of the residual decline can be explained with infiltration and that a portion is due to underestimation of ET.

To more accurately and quantitatively separate groundwater and ET flows, highly accurate pressure transducers were deployed in surface water features at six sites during late 2006. The new transducers replaced the less accurate ones in the original surface water wells at Mosaic H1, PCS SA 01, PCS SA 10, and Williams Co., while a new well, SW-2, was installed with the transducer at Mosaic K5. Mosaic H1 had two sites instrumented with the new transducers, SW-1 and SW-3. The accuracy of the transducers allowed the diurnal signatures of the water level declines during periods with no rain or surface water outflow to be evaluated. It was assumed that ET was negligible during the night hours, and only surface water levels above 15 cm were evaluated to avoid effects from soil specific yields. Equation 2-16, the White method, was used

to calculate daily ET and infiltration rates. Periods up to 15 consecutive days when no surface water outflow or rain events had occurred were analyzed for all six sites.

Surface water levels at Mosaic K5 SW-2 during June 2008 are shown in Figure 3-53 along with a closer view of fluctuations in a two day period. The diurnal signature is evident with declines during the day and almost flat-lined levels at night. ET rates of 1.62 cm/day and infiltration rates of -0.04 cm/day were calculated using the White method. The minimal negative infiltration, or groundwater inflow to the water feature (exfiltration), indicates that the average daily decline of 1.56 cm, shown as the slope of the linear regression line, is primarily due to ET (Figure 3-53).

Examples of the diurnal curves typically observed at PCS SA 10 and SA 01 are shown in Figures 3-54 and 3-55. The associated calculated rates for ET during this period were 1.61 and 1.77 cm/day for PCS SA 10 and SA 01, respectively. While the ET rates were similar at each site, the infiltration rates were much different causing different average daily declines as estimated with the linear regression slopes. The infiltration rate calculated for PCS SA 10 was -0.54 cm/day compared to -1.35 cm/day at PCS SA 01. Both indicated exfiltration of groundwater flow into the surface water features causing smaller daily declines than observed during a similar period at Mosaic K5 SW-2 (Figures 3-54, 3-55, and 3-53). It should be noted, however, that at higher levels when the two surface water features (SW-1 and SW-2) at Mosaic K5 became connected, higher exfiltration rates were observed.

The exfiltration rates observed with nighttime surface water levels at PCS SA 10, PCS SA 10, and Mosaic K5 were not constant rates. The surface water levels increased at a fast rate immediately following sundown but this rate decreased with time and to almost zero at PCS SA 10 (Figure 3-54). While much more pronounced at PCS SA 10, this phenomenon was still

apparent at PCS SA 01 (Figures 3-54 and 3-55). The decreasing rate of groundwater inflow at night demonstrates transient groundwater flows which are highest when the gradient is the maximum just after sundown due to daytime ET. The White method assumes that the groundwater flow rate occurring during the day is equivalent to the rate observed at the night. The method used here took the conservative estimate of nighttime exfiltration/infiltration rates by calculating it with surface water levels from 10 pm to 6 am. Therefore, this calculation did not include the faster rates observed from sundown to 10 pm.

Surface water fluctuations observed at Mosaic H1 SW-3 are shown in Figure 3-56 which resulted in a calculated ET rate of 0.6 cm/day and an infiltration rate of -0.8 cm/day. The transient groundwater rates at night were even more obvious at this site, and often surface water level diurnal signatures switched and were more similar to those seen in Figure 3-53. There were limited periods with surface water levels over 15 cm at Mosaic H1 SW-1. Winter surface water level decline is shown in Figure 3-57, where the immediate rise in levels after sundown is again apparent but then followed by declines caused by infiltration events. ET was calculated to be 0.39 cm/day and average infiltration was 0.49 cm/day. Positive infiltration was also calculated for all other inundated periods at Mosaic H1 SW-1. The instrumented features at both CFI SP-1 and Williams Co. never were sufficiently inundated since installation of the new transducers, and therefore surface water declines were not evaluated.

Rates calculated with the White method and total daily decline calculated with the slope of linear regression lines were averaged to obtain monthly averages of the various daily rates. The rates are listed for Mosaic K5 SW-2 along with the number of days sampled in each month and average daily Penman-predicted ET in Table 3-22. The monthly averages did at times include months from both 2007 and 2008. Calculated ET rates with the White method increased from

winter to summer as to be expected and were much higher than what was estimated with the Penman method. The infiltration rates were generally more negative in the winter compared to the summer when at times rates became positive indicating groundwater outflow from the water feature. The average infiltration rate for all periods analyzed was -0.82 cm/day. Similar to the ET rates, the daily declines increased in the summer and were also typically higher than Penman-predicted ET.

Of particular interest is that the daily declines significantly increased from winter to summer and much more than the calculated ET rates increased. The calculated ET rates were generally over one cm/day, even in the winter months when estimated ET rates were 0.2 to 0.4 cm/day (Table 3-22). Such differences cause suspicion in the calculated rates with the White method. While the most conservative estimate of nighttime infiltration rates were calculated by not including the immediate response after sundown, the large negative, or exfiltration, rates that still resulted may have caused overestimation in the ET calculation. Since the exfiltration rate is applied during the day, the ET rate includes the observed daytime decline plus the estimated daytime groundwater inflow. For the method to be accurate, the assumption of groundwater flow rates in the day being equal to what is observed at night must hold true. The largest calculated rates of groundwater inflow were during the winter when the calculated ET rates were substantially above estimated ET. With that said, caution should be used when evaluating the calculated rates. One explanation is that groundwater inflows are much higher during the nighttime after a gradient was established by loss of surface water via ET and that these inflow rates should not be applied during the day. The declining exfiltration rates, at times to zero, that were observed at night give support to this possible explanation (Figures 3-46 through 3-49). Assuming that the groundwater inflows observed at night do not occur during the day and that

the change in surface water levels during the daytime are solely from ET would result in more conservative ET estimates.

Considering daily ET as the total daily decline determined with the regression line is the most conservative estimate of ET using surface water fluctuations when increases are observed at night. This assumes a transient groundwater flow where the gradient established during the day causes groundwater inflow at night, but with the onset of ET, a groundwater trough develops around the water feature creating groundwater outflow during the day. If it is assumed that the inflow and outflow rates are mirrored, then net daily groundwater flow is zero. Again, this is an offered explanation for the most conservative estimates of ET, which are still higher than Penman-predicted ET but more reasonable values (Table 3-22). However, this estimate should not be used during periods when positive infiltration was calculated, such as in the case of the June and July calculations, since the infiltration rates increased the daily declines above the calculated ET rates. The daily declines from the regression slopes in the winter months are only slightly larger than the Penman-predicted estimates, while the spring and summer months, excluding June and July, had declines that average 1.8 times what the Penman method estimated.

The days sampled and the monthly averaged daily rates for PCS SA 10 and PCS SA 01 are shown in Tables 3-23 and 3-24. Average infiltration rates were always negative at both sites, with an average of -0.64 and -1.2 cm/day at SA 10 and SA 01, respectively. Similar to Mosaic K5, the calculated ET rates were near or above one cm/day even in the winter months. Also similar to Mosaic K5, the daily declines at PCS SA 10 determined with regression slopes, which are the most conservative estimates of ET, were greater than the Penman-estimated rates (Tables 3-23 and 3-22). Daily declines at PCS SA 10 were on average 1.5 times greater than Penman ET, and were almost twice as much than Penman ET during the summer months. The daily

declines at PCS SA 01, however, were typically less than Penman-predicted ET and on average 25 % less. The similar calculated ET rates of the two PCS sites but the smaller daily decline at SA 01 can be explained with the larger average exfiltration rates of SA 01. The diurnal signatures of PCS SA 01 had less transient groundwater inflows observed at night, which never approached zero as was often experienced at the other sites.

The days sampled and the monthly averaged daily rates for Mosaic H1 SW-3 and SW-1 are shown in Tables 3-25 and 3-26. As with the two PCS sites, the average daily infiltration rates calculated for SW-3 were negative suggesting exfiltration, with two exceptions (Table 3-25). The calculated exfiltration rates at Mosaic H1 SW-3, however, were less than those calculated for the PCS sites causing the daily decline values to be near the calculated ET rates (Table 3-25). The daily declines at SW-3 were often twice Penman-estimated ET during the summer months and on average 1.5 times greater than the Penman-estimated rates during the year. While only a few periods at Mosaic H1 SW-1 were appropriate for analysis, the average infiltration rates were always positive with a maximum of 0.77 cm/day groundwater outflow from the water feature (Table 3-26). These results reveal differences in hydrologic regime of separate water features within one CSA.

As previously mentioned, no sufficient inundation occurred at CFI SP-1 and Williams Co. since the time of installation of the new transducers. Without assuming a specific yield, calculation of ET and infiltration rates with below-ground water fluctuations is not possible and any such calculations would be strongly affected by an assumed specific yield. A more qualitative analysis was performed, however, to simply identify if exfiltration or infiltration occurred at these sites. Water table fluctuations for Williams Co. are shown in Figure 3-58, where the decline at night, and thus infiltration is apparent. Of the 19 periods analyzed for this

site, 11 had a signature similar to the one shown in Figure 3-58, suggesting that infiltration occurred at this site frequently. Though any calculated rates without an accurate specific yield would be erroneous, a relative comparison of the calculated infiltration rate to the calculated ET rate gives an idea of the magnitude of infiltration. The rates for 145 days were calculated with a specific yield of one and on average the infiltration was 25.2 % of calculated ET. While in previous discussions a positive infiltration was defined as loss of surface water to the local groundwater, infiltration here refers to loss of local groundwater to adjacent regions, vertically and/or laterally. The direction of this groundwater movement suggests the potential direction for surface water loss at Williams Co.

There were limited periods appropriate for analysis of CFI SP-1 as water levels were often below the well depth at CFI SP-1 since the installation of the newer transducers. Five periods totaling 28 days were evaluated for CFI SP-1 and negative infiltration was observed during all periods, with signatures similar to those of the PCS SA 10 and Mosaic H1 SW-3 (Figures 3-54 and 3-56). It should be noted, however, that the fact that positive infiltration was not observed when water levels were below ground does not fully imply that infiltration would not have occurred with inundated conditions.

Both the analysis of daily declines with the less accurate transducers and the diurnal analysis with the more accurate transducers revealed differences among sites and similar to the differences observed in the water balance analysis. The higher residuals at Williams Co. and Mosaic H1 may be explained by possible infiltration, while most sites' residuals may be more due to underestimation of ET as no evidence of infiltration was found for other sites. Furthermore, the negative residual calculated for PCS SA 01 could have resulted from constant

groundwater inflow which was suggested by the diurnal analysis since the daily declines were actually less than Penman-predicted ET.

Temporal Hydrologic Modeling

Temporal models were developed with the hydrologic flow estimates from the water budgets to further evaluate the estimates and to predict stage with rainfall and other climatic data. Temporal models were developed for seven instrumented surface water features using the simple linear runoff models, rainfall data, and ET estimated with Penman method along with actual surface water data for calibration. Only positive surface water data were used to create the models and, therefore, modeling was not performed for the surface water feature at Tenoroc 4. Furthermore, Mosaic HP-10 was excluded from modeling as a result of the limited knowledge of the surface water outflow regime. The linear runoff models with the y-axis intercept not set to zero were employed in these models due to their success in predicting event responses. Since these runoff models require only rainfall data, upland to wetland ratios and runoff coefficients were not included in the temporal models. While the diurnal curve analysis suggested some sites may have experienced groundwater inflow, zero groundwater flows were initially applied to the models. Only in situations where a model underestimated stage, were groundwater inflows (exfiltration) included. In the cases where the initial models overestimated stage, the use of both increased ET rates using seasonal coefficients and infiltration rates were explored.

The model simulation results for PCS SA 10 with no inclusion of an infiltration loss and for time periods after surface outflow had ceased are shown in Figure 3-59. The responses following rain events were similar between the actual and predicted surface water levels, with the exception of a large rain event in March 2008. The losses, however, were underestimated by the model and stage was overestimated. An infiltration term equal to the daily residual value, 1.16 mm/day, calculated in the water balance analysis was applied (Figure 3-59). Though the

final predicted stage matched the actual, declines during the summer months were underestimated while winter declines were overestimated, suggesting seasonal variability in the residuals possibly from underestimation of ET. Penman-estimated ET rates were multiplied by seasonal coefficients which were manipulated to maximize the fit of the model. Excluding infiltration and multiplying the estimated ET rates by 1.5 during the growing season by 1.1 in the non-growing season resulted in the best model (Figure 3-59). The model resulted in a non-linear coefficient of determination equal to 0.87, which increased to 0.94 when excluding the 10 cm rain event in March 2008 that was underestimated by the model. A non-growing season coefficient near one suggests that the residual value calculated in the water balances was due to underestimation of ET in the growing season, and that infiltration may be negligible at this site.

The model results with no inclusion of an infiltration loss are shown for Williams Company in Figure 3-60. The responses following rain events were similar between the actual and predicted surface water levels, but the losses were substantially underestimated by the model. An infiltration term equal to the daily residual value, 4.87 mm/day, calculated in the water balance analysis was included (Figure 3-60). The ending predicted and actual stages matched, but as a result of underestimating summer decline and overestimating winter decline. The seasonal variation in declines for this site was greater than it was for PCS SA-10 (Tables 3-20 and 3-14). A seasonal coefficient for the non-growing season of 1.0 and an infiltration term was calculated to allow the predicted non-growing season decline to match the actual decline. An infiltration of 1.5 mm/day resulted which was used to calculate a seasonal coefficient for the growing season to match predicted growing season decline with actual. A growing season coefficient of 2.5 resulted which is well out of the range for reported values of crop coefficients, though crop coefficients are typically applied to the FAO adjusted Penman-Monteith method

(Drexler et al., 2004). A non-growing season coefficient of 0.6 was then used, which is within the range for crop coefficients of a Typha sp. dominated marsh during the winter (Drexler *et al.*, 2004), to again solve for infiltration and a growing season coefficient. An infiltration of 2.54 mm/day and a growing season coefficient of 2.1 were found to produce the best predictive model (Figure 3-60). The model fit the data well, with a coefficient of determination equal to 0.95. These results suggest that infiltration is significant at this site and that ET had a more pronounced seasonal variation than what was predicted or experienced at PCS SA 10.

Similar to the modeling results of PCS SA 10 and Williams Co., solely applying Penman-predicted ET and the linear runoff models while excluding infiltration overestimated stage at Mosaic H1 SW-3 and CFI SP-1. Including the water balance residuals resulted in end stage matching but by underestimating growing season and overestimating non-growing season declines. The best models for both features were developed by excluding infiltration and applying seasonal coefficients. A non-growing coefficient equal to 1.0 and a growing season equal to 1.4 were applied to the Mosaic H1 surface water-3 model, which resulted in a coefficient of determination equal to 0.93 (Figure 3-61). Growing and non-growing season coefficients were 1.3 and 1.1, respectively, for the CFI SP-1 model which had a coefficient of determination equal to 0.94 (Figure 3-62).

Three different time periods with no channel flow were used in model development of Mosaic K5 SW-1. Again, similar to the other modeling results, models initially overestimated stage. One non-growing season period was modeled which required no seasonal coefficient or infiltration term to accurately predict stage with a coefficient of determination of 0.99 (Figure 3-63). Two different growing season time periods were modeled which had water balance residual values slightly over 2 mm/day. Since the non-growing season model required no infiltration,

only seasonal coefficients were included in the growing season models. A seasonal coefficient of 1.4 resulted in the best fits for both periods with coefficients of determination equaling 0.93 and 0.99 (Figures 3-63). Both growing season models underestimated declines and responses to rain events at stages below 10 cm, likely due to the specific yield of surrounding soils.

A model for Mosaic K5 to include channel flow was developed by applying the seasonal coefficients that were used in the three models without channel flow and including daily outflow (m/day) that was calculated in the surface water outflow analysis. The time period with the channel well data available, May 2006 to January 2008, was used. Predicted and actual stage are shown in Figure 3-64 which resulted in a coefficient of determination of 0.91. Again, declines and responses to rain events were underestimated when stage was near zero. While the predicted response to the large rain event late in August 2006 is in agreement with the actual response, the subsequent decline is overestimated, causing the actual stage to be above the predicted for the most of the remaining period. At such high stage, the channel flow may not have solely originated from the modeled feature but could have also included flow from other isolated features, as well as from direct rainfall from such a large event. These results and the offered explanation are similar to that presented in the water balance results concerning channel flow. Other declines are better predicted, however, including during times of channel flow, demonstrating utility of the seasonal coefficients and the channel flow estimations.

The model results with no inclusion of an infiltration loss are shown for Mosaic H-1 SW-1 in Figure 3-65. The model was applied to two separate time periods and not during times where surface water levels were below zero. As with the other sites, the model substantially underestimated losses and over predicted stage. An infiltration term equal to the residual value of 4.30 mm/day was included in the model which resulted in marked improvement (Figure 3-65).

Some declines, however, were still underestimated, especially during the period following the dry period. Seasonal coefficients were manipulated with infiltration equal to 3.00 mm/day, to best fit stage prior to the dry period (Figure 3-66). The lower infiltration rate required a growing season coefficient of 1.7 and non-growing season one of 1.2 to produce the best fit during the first period (Figure 3-66). While the model with infiltration equal to 3.00 mm/day sufficiently predicted the declines that were experienced prior to the dry period, it still underestimated the declines after the dry period. Increasing the infiltration rate to 4.00 mm/day and applying the same seasonal coefficients caused somewhat better prediction of decline during the second period but resulted in the first period's decline to be overestimated (Figure 3-66). While the predicted stage better matches the end stage of the second period, it still underestimated decline and the end matching was a result of the model underestimating response to rainfall in February 2007.

An analysis of the surface water data collected at Mosaic H1 SW-1 suggested that the rate of losses were different during the two periods which occurred at similar times in the year and at similar water depths. Different infiltration terms for the two periods were manipulated but with the same seasonal coefficients for ET to produce the best overall fit. Infiltration was adjusted to 2.79 mm/day for the period prior to the dry times and to 5.08 mm/day for the period after inundation occurred again (Figure 3-66). Though the predicted stage was less than actual stage at the end of the period, the slopes of the declines are better predicted with an overall coefficient of determination equal to 0.83. Again, underestimating stage responses was responsible for the lower predicted stages rather than the rates of loss. These results suggest that not only is ET higher than what the Penman method predicted, but that also significant infiltration occurred which seemed to increase after a dry period. The latter observation could have possibly been a

result of cracks developing in the feature with drying of the clay soils during the prolonged dry period.

A negative residual resulted from the water balance analysis of PCS SA 01, suggesting groundwater inflow may have occurred. A model was developed using the linear models for runoff and Penman-predicted ET while excluding exfiltration (Figure 3-67). Unlike the initial models for the other sites, the model overestimated declines during the entire period and under predicted stage. An exfiltration term, 1.2 mm/day, equal to the negative residual from the water balance was included resulting in a considerable improvement and a coefficient of determination of 0.92 (Figure 3-67). If it is assumed that this site could have also experienced elevated ET rates, then the exfiltration term would increase as seasonal coefficients were not applied to the Penman estimates in this model.

The seasonal coefficients and infiltration rates included in the models of the seven surface water features are listed in Table 3-27 along with the non-linear coefficients of determination. The infiltration rates of Williams Co. and Mosaic H1 SW-1, the negative infiltration rate of PCS SA-01, and the need for seasonal coefficients support the results from the water balance and drawdown analyses.

Ecohydrology

An ecohydrologic study was performed to develop moisture release curves, document soil moisture regimes, and measure root biomass allocation of Salix caroliniana. The moisture curves were developed to relate soil moisture values to water potential, a measure of soil water availability, and identify critical soil moisture values. Soil moisture regimes were measured continuously with depth and along a hydraulic gradient. Soil moisture values were evaluated in reference to associated water potentials and to the groundwater regimes. Root biomass and

transpiration rates were measured and related to soil water availability, and transpiration rates were scaled-up using total biomass to estimate stand level transpiration.

Moisture Release Curves

Moisture release curves were developed in the laboratory using soils sampled at Mosaic K5, CFI SP-1, and Williams Co to relate volumetric water content (VWC) to water potential in terms of negative cm of water pressure. The moisture release curves were necessary to relate the soil moisture regimes that were measured in situ to their associated water potential and identify critical values such as saturation levels, permanent wilting points (PWP), and capillary fringe heights. Soil was sampled at the three different ecohydrology stations (upland, transitional, and saturated) of each site to construct a curve per station. Drier subsamples prevented a measurement of VWC, and only GWC was measured to represent soil moisture values for these subsamples. The GWCs measured for the subsamples which allowed measurement of VWC with the soil moisture probe were used along with Equation 2-19 to relate calculated and measured VWC and to adjust the air-filled porosity to result in a one to one fit between the two. Using samples from all three stations at Mosaic K5 resulted in a coefficient of determination equal to 0.81 using an air-filled porosity of 0.23 (Figure 3-68). An air-filled porosity equal to 0.23, the measured GWCs, and Equation 2-19 were used to calculate VWCs for drier subsamples which prohibited a VWC to be measured with the soil moisture probe.

The measured water potentials and the measured and/or calculated VWCs resulted in moisture release curves for the three different stations at Mosaic K5 which were in good agreement and allowed a composite curve using all data to be evaluated (Figure 3-69). With that said, the driest samples of all three stations required Equation 2-19 and the one value for air-filled porosity to determine their VWC, but these VWC values only represented a relatively small number of data points and ones on the tail end of the curve (Figure 3-69). The curve

demonstrates that saturation for soils at Mosaic K5 occurred at a VWC near 0.60 m^3/m^3. The inflection point of the curve with decreasing VWC was near -200 cm H_2O, indicating an approximate capillary fringe of 2 m. Assuming a permanent wilting point (PWP) of -1.5E^4 cmH_2O (Dingman 2002), soils at Mosaic K5 may have experienced PWP pressures at a VWC near 0.42 m^3/m^3.

A one to one relationship between measured and calculated VWCs on samples from all three stations at Williams Co. resulted in a coefficient of determination equal to 0.80 using an air-filled porosity equal to 0.25 (Figure 3-70). Similar to the curves developed for Mosaic K5, the three curves for Williams Co. were in good agreement and allowed a composite curve to analyzed (Figure 3-71). The curve illustrates that saturation occurred when VWC was approximately 0.60 m^3/m^3. The inflection point occurred near -100 cm H_20, corresponding to a capillary fringe approximately 1 m for the soils at Williams Co.. PWP may have been induced at VWC's near 0.42 m^3/m^3.

The moisture release curves of the stations at CFI SP-1 were much different comparing the transitional and saturated zones to the upland zones. The upland soils were dominated by sand with very little clay as a result of this site receiving sand-clay mix causing spatial soil heterogeneity. The curve for the transitional zone was developed using soil sampled 40 cm below the ground surface which was more dominated by clay. The top 30 cm in this zone was similar to the sandy soil sampled in the upland. The entire soil profile at the saturated zone was similar to the sampled soil from the transitional zone. A one to one relationship between measured and calculated VWCs from samples of the transitional and saturated zones resulted in a coefficient of determination equal to 0.70 using an air-filled porosity of 0.14 (Figure 3-72). The curves developed for the transitional and saturated zones were comparable allowing a composite

curve to be evaluated (Figure 3-73). Soils at the saturated zone and 30 cm below ground at the transitional zone experienced saturation at VWC's approximately 0.57 m^3/m^3. The curves suggest a capillary fringe of these soils near 1 m and that PWP may have been induced at VWC's near 0.37 m^3/m^3.

The sandier soils of the upland at CFI SP-1 allowed one bulk density, 1.7 g/cm^3, to be measured and applied to the GWCs to calculate VWCs, thereby negating the need for an empirical relationship to be determined as was done with clayey soils. The sand-dominated upland at CFI SP-1 resulted in a dissimilar curve compared to the curves developed for the other stations and to the composite curves for Mosaic K5 and Williams Co. (Figures 3-69, 3-71, 3-73, and 3-74). Saturation for the sandy soils occurred near 0.33 m^3/m^3 (Figure 3-74). The inflection point occurred at -20 cm H_20, suggesting a much lower capillary fringe compared to the clayey soils. PWP pressures may have been induced when the soils reached VWCs approximately 0.1 m^3/m^3.

Soil Moisture Analysis

Soil moisture regimes were measured with depth, along a hydraulic gradient, and in conjunction with the moisture release curves and groundwater regimes to identify at what depths and frequency saturation and PWP make occur and to evaluate the interactions between the water table and soil moisture regimes. Logging soil moisture probes were installed at various depths at the three ecohydrology stations of Mosaic K5, Williams Co., and CFI SP-1. Groundwater levels at the upland station of Mosaic K5 recorded in the groundwater-2 well from 5/15/07 to 9/27/07 are shown Figure 3-75 and the corresponding soil moisture levels are shown in Figure 3-76. The soil moisture probes were installed within 1 m of the groundwater-2 well with an elevation change of less than 5 cm. The logger for the soil moisture probes experienced equipment failure on 9/27/07 and the 25 cm probe stopped recording on 9/14/07. Responses to increases in

groundwater levels were pronounced at the 10 cm probe and to a lesser extent in the deeper probes. The 70 and 100 cm probes recorded levels with minimal variation from 0.62 and 0.59 m^3/m^3, respectively. The 25 cm probe recorded soil moisture levels consistently over 0.5 m^3/m^3, as did the 40 cm probe with the exception during the end of the record. Also shown in Figure 3-76 is a dashed line representing the PWP determined for Mosaic K5 with the moisture release curves. The 10 cm probe frequently recorded soil moisture levels below PWP, with a minimum of 0.27 m^3/m^3 that corresponded to the deepest recorded water table.

Groundwater levels recorded at groundwater-3 at Mosaic K5, which was installed immediately adjacent to the soil moisture probes at the transitional station, are shown in Figure 3-77. The corresponding soil moisture levels recorded at the transitional zone are shown in Figure 3-78. Both the 25 and 70 cm probes experienced failure and stopped recording on 9/7/07. The 100 cm probe only worked briefly before it stopped recording on 6/25/07. The probes at 10, 25, and 40 cm probe all responded to the decreasing water table during June 2007 and recorded soil moisture levels below 0.3 m^3/m^3. The 70 and 100 cm probes did not experience lower levels during this decline period. Though the water table at this station was consistently closer to the ground surface compared to the water table at the upland station, lower soil moisture levels were recorded (Figures 3-75 through 3-78). While all probes except for the 10 cm probe recorded near or above 0.5 m^3/m^3 at the upland station, the 10, 25, and 40 cm probes at the transitional zone often fell below this VWC, and often below PWP, and experienced much more fluctuations (Figures 3-76 and 3-78). Similar to the groundwater levels, the 10 and 40 cm probes recorded more constant and elevated levels at the beginning of October and end of the growing season (Figures 3-77 and 3-78).

Soil moisture levels recorded at the saturated zone of Mosaic K5 from 5/16/07 to 11/14/07 are shown in Figure 3-79. A well was not installed near this station but the ground surface at this location was 20 cm lower than the well at the transition zone. The 20 and 50 cm probes experienced equipment failure during the record. All probes recorded values over 0.52 m^3/m^3 and with exception of two time periods, always over 0.55 m^3/m^3 including at the shallower probes. The 20 cm difference in elevation between the two stations apparently caused different soil moisture regimes, possibly a result of differences in water table depths (Figures 3-78 and 3-79). Similar to the transitional zone, the two working probes recorded more constant levels at the onset of the non-growing season.

The soil moisture probes at the upland station of Williams Co. were installed immediately adjacent to the groundwater-2 well. Groundwater levels from 6/9/2007 to 9/25/07 and the associated soil moisture levels at the upland station are shown in Figures 3-80 and 3-81, respectively. The upland station experienced deeper water table depths than observed at the upland station of Mosaic K5 (Figures 3-80 and 3-75). The water table was approximately and consistently 2 m below ground at Williams Co. and slight declines corresponded with decreasing soil moisture levels at the 10 and 25 cm probes (Figures 3-80 and 3-81). The 40 and 70 cm probes constantly recorded VWCs between 0.55 and 0.60 m^3/m^3, and only the 10 cm probe recorded values that approached PWP but only for a short period during August 2007. Of particular interest are the recordings from the 100 cm probe which recorded similar levels as the shallower 40 and 70 cm probes, except during the month of July. The levels recorded at the 100 cm probe during July were less than those recorded at the shallowest probes. Other than this period, the 100 cm probe always recorded values higher than the 10 and 25 cm probes and ones near saturation even at times when the 10 and 25 cm probes recorded the minimum values of the

entire record. This observation suggests that a possible crack had intermittently developed around the 100 cm probe during July.

Soil moisture levels and the groundwater levels recorded at the adjacent well, groundwater-3, for the transition station at Williams Co. are shown in Figures 3-82 and 3-83. The groundwater-3 well was installed after the installation of the soil moisture probes, and the immediate increase in groundwater levels are due to equilibration of the well. The 100 cm probe, data not shown, only recorded for 9 days after installation before equipment failure and recorded values similar to those recorded at the 40 cm probe. The 40 cm probe stopped recording on 8/13/07. The groundwater levels at the transitional station also reached 2 m below, similar to the levels at the upland station, but were much more variable and often shallower (Figures 3-82 and 3-80). The soil moisture levels recorded at the 10 cm probe fluctuated between 0.40 and 0.50 m^3/m^3, briefly recorded values near PWP, and corresponded to changes in water table depth (Figure 3-83). The 25 and 40 cm probes were less affected by changes in groundwater levels, consistently recording over 0.55 m^3/m^3. The deepest working probe, however, recorded net drying over the entire period, with values approaching 0.45 m^3/m^3. The differences between the recordings of the 70 cm probe and the shallower probes (25 and 40 cm) may be a result of a developed crack or localized soil moisture regimes. The latter could be caused by heterogeneity in soil with depth.

Soil moisture probes were installed adjacent to the surface water well at Williams Co.. This region, referred to here as the saturated zone, is one of the lowest elevation areas on the site but had not experienced inundation since fall 2006 (Figure 3-5). The water levels during the soil moisture data collection period ranged between 0.5 and 1.35 m below the ground surface (Figure 3-84). The fact this area had been historically inundated and soil moisture levels were collected

during an extended dry period allowed an evaluation of soil moisture regimes of a surface water feature during a dry period. The 50 cm probe experienced failure soon after installation and was repaired on 8/4/07 when the 35 cm probe, which stopped logging on 7/9/07, was also repaired. The 10, 20, and 50 cm probes recorded values above 0.55 m^3/m^3, except during a drier period in late July (Figure 3-85). Higher values, however, were recorded at these probes during the end of the summer when lower groundwater levels were observed. The 35 cm probe also recorded near 0.60 m^3/m^3 before it stopped logging, but began recording much lower values shortly after repair. Values recorded by the 35 cm probe were slightly above 0.55 m^3/m^3 for 10 days after installation, but substantially decreased with the water table decline (Figures 3-84 and 3-85). The other probes, both shallower and deeper, did not record decreasing soil moisture levels during this time. Furthermore, the 35 cm probe recorded immediate increases up to 0.5 m^3/m^3 after rain events with subsequent declines back to values below 0.3 m^3/m^3. The extreme drying observed at this probe and the fact that it recorded such drastic responses to rain and drying following rain events strongly suggests a crack had developed around the probe.

The groundwater and soil moisture levels recorded at the upland station of CFI SP-1 are shown in Figures 3-86 and 3-87. The 10 cm probe stopped recording in early October 2007. All probes recorded fluctuating soil moisture levels that ranged from 0.08 to 0.2 m^3/m^3 and that corresponded to increases and decreases in groundwater levels (Figure 3-87). The sandier soils at this station resulted in the deeper probes recording more dynamic regimes and all probes recording much lower VWCs compared to the other upland systems evaluated (Figures 3-76, 3-81, and 3-87). Furthermore, the 10, 25, and 40 cm probes all recorded values near the PWP that was determined with the moisture release curve for soils of this station.

Groundwater and soil moisture levels recorded at the transitional station of CFI SP-1 are shown in Figures 3-88 and 3-89. Groundwater-3 was installed immediately adjacent to the probes and at a later date. The immediate increases in water levels after installation are due to well equilibration. The 10 and 25 cm probes recorded values consistently under 0.30 m^3/m^3 and that were more variable compared to the 40 and 100 cm probes which recorded values between 0.45 and 0.60 m^3/m^3. The top 30 cm of soil at this region was similar to the sandy soils at the upland station, whereas below 30 cm was typically more clay dominated. The different soil types resulted in markedly different soil moisture regimes with depth. The PWP determined with the clayey soils from the transitional and saturated stations and the PWP for the sandy soils at the upland station are both shown in Figure 3-89. Interestingly, the 70 cm probe's recordings were below recordings from both the shallower 40 cm probe and the deeper 100 cm probe, were more fluctuating, and recorded values near PWP for clay. Soil heterogeneity with depth and some interlacing sand near the 70 cm probe may have caused the lower and more fluctuating VWCs.

Similar to Williams Co., soil moisture probes were installed adjacent to the surface water well at CFI SP-1 and referred to here as the saturated station. The surface water feature at CFI SP-1 had not experienced inundation since fall 2006 (Figure 3-11). The groundwater levels recorded at the surface water well and the soil moisture levels are shown in Figures 3-90 and 3-91. The 35 cm probe stopped recording in early August. All probes recorded values over 0.45 m^3/m^3 with the deepest probe consistently recording near 0.6 m^3/m^3. The 60 cm change in groundwater levels did not cause much variation in the soil moisture levels (Figures 3-90 and 3-91). The shallowest probe actually recorded values higher than those recorded at the 20 and 35 cm probes and often near 0.55 m^3/m^3, again suggesting possible soil heterogeneity with depth.

Root Biomass Analysis

Root biomass with depth was measured of a dominant CSA species to relate root allocation with soil moisture regimes and groundwater depths. *Salix caroliniana* roots were sampled at three trees surrounding the soil moisture stations of Mosaic K5 and CFI SP-1 using the coring method and up to 1.5 below the ground surface. Additionally, three trees in an inundated region at Mosaic K5 were sampled. Mean dry root biomass per depth at each station of Mosaic K5 are shown in Figure 3-92. Roots were only successfully sampled up to 1.05 m below ground at the inundated zone as a result of the water pressure limiting sufficient removal of the samples when sampling the deeper cores. The deepest peak of biomass allocation occurred at the upland zone and a depth of 105 cm (Figure 3-92). The upland zone also had the highest total root biomass. There was a slight trend of shallower biomass allocation with wetter conditions, but with biomass equal to or greater than 3 kg/m^3 at a depth of 90 cm even in the wettest locations.

Mean dry root biomass per depth for the upland, transitional, and saturated stations at CFI SP-1 are shown in Figure 3-93. Root biomass allocation appeared to be different at CFI SP-1 than Mosaic K5 with peaks being more restricted to shallower depths (Figures 3-93 and 3-92). Furthermore, the total allocation was lower at CFI SP-1 compared to the upland, transitional, and saturated stations at Mosaic K5. It should be noted that the trees sampled at the transitional and saturated zones of CFI SP-1 had adventitious rooting whereas the trees sampled at these zones of Mosaic K5 did not. Only the inundated trees at Mosaic K5 had adventitious rooting. The adventitious rooting on the sampled trees at CFI SP-1 demonstrates historical flooding had occurred at both the saturated and transitional zones. Flooded conditions in these zones could have resulted in root biomass allocation to be similar to that observed at the inundated conditions of Mosaic K5. The upland trees sampled at CFI SP-1 had shallower and less total biomass than

the upland trees at Mosaic K5. Anecdotally speaking, it appeared that the sampled roots of the upland trees at Mosaic K5 tended to vertically spread, whereas the roots at the upland of CFI SP-1 had a more lateral spread.

Transpiration Analysis

Transpiration data was collected over 14 days at each ecohydrology station of Mosaic K5 and CFI SP-1 to evaluate how transpiration rates respond to soil water availability and to provide stem flow rates to estimate stand level transpiration. Four stems of separate *Salix caroliniana* trees were instrumented at each station and hourly flow rates were collected for each stem. An example of the raw data collected is shown in Figure 3-94. The hourly flow rates were converted to daily flow rates for each stem and were divided by the stem cross-sectional area to obtain daily stem flow rates per stem area as g $H_20/cm^2/day$. The daily stem flow rates per stem area were indexed with the associated daily Penman-estimated ET (cm), and the flow rates for the four stems were averaged to obtain mean daily stem flow/Penman ET for each station. Indexing with the daily Penman-predicted ET allowed comparison among stations and sites while excluding climatic effects. Mean indexed daily stem flow rates per stem area at the four stations of the Mosaic K5 are shown in Figure 3-95 along with standard deviations. The upland stems had the highest average flow rates per stem area followed by the transitional stems. The flow rates for the wetter regions, saturated and inundated zones, were comparable and lower than the upland and transitional zones. The higher stem flow rates per stem area measured at the upland zone suggest that stress was not induced at the drier regions of Mosaic K5.

Stem flow rates measured at Mosaic K5 by the two different size gauges (25 and 50 mm diameters) were compared to observe if stem flow per stem area changed with increase in stem area (Figure 3-96). Both the upland and transitional stations experienced higher flow rates per

stem area in smaller stems whereas the reverse was observed at the saturated and inundated stations.

Basal areas at breast height from the 20 x 6 m^2 belted transects that surrounded each station were used to scale up daily stem flow rates per stem area to estimate daily stand level transpiration (cm/day). The size class distribution, as measured dbh, of the trees within all four belted transects used to scale up stem flows to stand level transpiration at Mosaic K5 is shown in Figure 3-97. The size of trees instrumented were in three out of the 9 size classes, representing 89 trees out of the total 192 trees on all four belted transects. The frequency of trees declined with increase in size and 52 trees were in size classes greater than the ones of instrumented trees. There only four trees on the four belted transects with a dbh over 14 cm.

Size class distributions were also developed separately for each belted transect of the four ecohydrologic stations at Mosaic K5 to compare the distributions among transects and identify at which transect more large trees were present (Figures 3-98). The fewest trees were present at the upland station which had only one tree larger than those that were instrumented. Trees at the transitional station in size classes larger than those of the instrumented trees accounted for 60 % of all the trees present. There over twice as many trees at the saturated station compared to the upland and transitional stations, and approximately 50 % of trees at the saturated station were in size classes larger than those of instrumented trees. The inundated transect had twice as many trees as the saturated station, but only 32 % of the trees at the inundated station were in larger size classes than those of instrumented trees.

Scaling up stem flows with total basal area to calculate stand level transpiration assumes that all *Salix caroliniana* trees within a stand experience equivalent stem flow per stem cross sectional area as the instrumented trees in that transect. Sapwood depth analysis was performed

to evaluate reduced stem conductivity per cross sectional area, and thus reduced potential flow, with tree size. Individual trees (n=18) at Mosaic K5 that spanned the range of tree sizes present on the transects (Figures 3-97 and 3-99) were cored at breast height to determine sapwood depths.

Visual inspection was first performed to observe the sapwood to heartwood transition. No transition from more translucent to darker wood was evident, however. As a result, cores were segmented into 5 mm samples and moisture content and dry wood density per core depth were determined to evaluate changes in wood properties with core depth. Moisture contents and densities of all 18 sampled trees were averaged along core depth and are shown in Figures 3-100 along with standard deviations. No significant and rapid decline in water content with depth, as expected in a transition from sapwood and heartwood, was observed for all 18 sampled trees. On the contrary, some of the larger trees had lower moisture contents at shallower core depths while other large trees had consistent high moisture content throughout depth. Furthermore, the smaller trees had moisture contents similar to the lower values in the shallower depths of the large trees with variable moisture content. Therefore, the average moisture contents shown in Figure 3-100 are lower in the shallower depths and with more variability. The larger variability in the shallower depths was also due to a larger sample size since the shallower depths included all trees whereas the deeper depths only included trees with such radii. The dry wood densities showed less variability with an average density of 0.43 g/cm^3 (Figure 3-100). Despite the variability in the shallower depths, the higher moisture contents in the deeper portions of the larger trees suggest little presence of heartwood in the trees of the size classes sampled. The constant densities throughout core depth of all trees sampled further and possibly more definitively support this conclusion.

Following the results from the tree core analysis, it was assumed that all trees on the transects of Mosaic K5 were predominantly sapwood and thus have similar potential flow per stem cross sectional area as the instrumented trees in their respective ecohydrologic station. One method of scaling up stem flow rates to stand level transpiration using total stand basal area, referred to here as regression biometric scaling, requires developing a regression equation of measured stem flow versus instrumented stem area. Plotting all the measured stem flow rates (indexed with Penman ET) versus stem area and forcing the y-intercept to zero resulted in a good fit and a coefficient of determination of 0.93 (Figure 3-101). The fit, however, was strongly affected by the large difference in stem areas that were measured with the two gauge sizes. Using the resulting regression equation, density of water (0.998 g/cm^3), total basal area at the inundated station, the area of the belted transect, and Equation 2-25 resulted in a ratio of stand transpiration to Penman predicted ET (cm/cm) of 2.77 for the time period sampled. Applying such an equation, which was essentially a product of two clusters of points (Figure 3-101), may not be the best method as variability in measured stem flow per stem area rates was documented (Figure 3-96) and this variability cannot be evaluated with this method, which provides one average daily transpiration rate per sampling period.

Applying the discrete biometric method using Equation 2-27 and total basal area allowed a daily stand level transpiration to be calculated for each daily stem flow rate, four rates per day, each of which was indexed with Penman-predicted ET. The daily stand transpiration rates indexed with Penman rates were averaged to calculate mean daily stand transpiration/Penman ET (cm/cm) for each station over the time period sampled (Figure 3-102). Utilizing this method allows direct evaluation of the variability over the sampling period and in the stem flow rates that

were measured by the four gauges by observing standard deviations from the averages of stand transpiration/Penman ET.

Scaling up to stand level transpiration at Mosaic K5 resulted in an opposite trend compared to the measured stem flow rates (Figures 3-102 and 3-95). Stand level transpiration from *Salix caroliniana* at the inundated conditions was on average 2.17 times greater than the total ET rate as estimated with the Penman method, compared to the ratio of 2.77 that resulted when employing the regression equation approach. The averages of the indexed rates at both the transition and saturated zone were over one, also indicating stand transpiration rates were greater than Penman-predicted total ET. While there was more variability in the rates calculated for the inundated station compared to the other three stations, subtracting one standard deviation still results in stand transpiration of *Salix caroliniana* approximately 50% higher than Penman ET. Though stem flow rates were lower in the wetter regions, scaling up to stand level suggests that stress was also not induced in flooded conditions since transpiration rates were higher than typical ET rates (Figure 3-102).

Total basal area measured at each transect surrounding each station and average leaf area per stem area of the instrumented stems are shown for Mosaic K5 on Figure 3-103. Tent caterpillars caused significant damage to the canopies of the instrumented stems at the transitional area before measurements were made, and thus no leaf area data is shown. Total basal area increased with wetter conditions resulting in higher stand transpiration rates in those areas (Figure 3-103 and 3-102). With more basal area, however, there were more trees and less space for canopies to spread causing less total leaf area per stem area in the wetter regions compared to the upland zone (Figure 3-103). With more leaf area per stem area, higher stem flow rates were possible in the upland zone (Figure 3-95).

One other biometric method of scaling stem flow rates to stand level transpiration, referred to here as simple biometric scaling, uses Equation 2-26 and total stand basal area. Similar to the discrete biometric scaling method, this method allows calculation of stand transpiration for each day of the sampling period, from which an average daily rate can be determined. However, unlike the discrete biometric scaling method, the simple method aggregates the four measured stem flows per day, thus not directly demonstrating daily variability in measured flow rates. The simple biometric method was applied to the measured flow rates at the inundated station of Mosaic K5 to compare to the daily stand transpiration/Penman ET results from the discrete biometric method (Figure 3-104). Equipment failure did not allow calculation of rates on 8/2/07. Ratios of stand transpiration to Penman ET from both methods are near or over 2.0 over the entire time period sampled. The daily ratios resulting from the simple method are consistently higher than those calculated with the discrete method, with an average difference of 0.41 cm/cm between values from the two methods. The variability of the ratios from the discrete method resulting from the variability in the measured flow rates on each day are shown as standard deviations. Applying one negative standard deviation to the results for the discrete method maintains transpiration rates of *Salix caroliniana* at least equal to Penman estimated total ET and which often approach rates 50 % higher than Penman ET.

Similar to the results from Mosaic K5, stem flow rates were higher in the drier zones at CFI SP-1 (Figures 3-105). Collection of data in an inundated zone was not possible at CFI SP-1 since the entire site was dry during summer 2007. The size of trees instrumented at CFI SP-1 represented three out of seven size classes which accounted for 69 trees out of 219 trees along all three belted transects (Figure 3-106). Similar to Mosaic K5, the frequency of trees on the three

transects at CFI SP-1 declined with size but to a greater extent than at Mosaic K5. Only 10 trees were in a size class greater than the ones of the instrumented trees (Figure 3-106).

The discrete biometric scaling method resulted in more conservative results for the inundated station at Mosaic K5 and allowed observation of the effects from the variability in the stem flow measurements. As a result, only this method was applied with measured stem flow rates at CFI SP-1 and resulted in average stand transpiration of *Salix caroliniana* that was 1.22 times greater than Penman-estimated total ET at the saturated zone and 1.07 times greater at the transition zone (Figure 3-107). The upland zone had stand transpiration rates much lower which were on average 85 % lower than total ET predicted by the Penman method. A similar comparison to the stand transpiration and stem flow rates as performed with the rates at Mosaic K5, suggests little stress in either the driest or wettest regions of CFI SP-1 studied (Figures 3-105 and 3-107).

Total basal area increased with wetter conditions at CFI SP-1, explaining the higher stand transpiration rates in the wetter regions (Figures 3-108 and 3-107). The low basal area at the upland zone resulted in much lower stand transpiration rates (Figures 3-108 and 3-107). There was higher leaf area per stem area in the upland regions than the wetter regions, but leaf area was much more variable among the instrumented stems at the upland region (Figure 3-108). While the stem flow rates were higher at the transitional zone compared to the saturated zone, average leaf area per stem area of instrumented stems was lower.

As calculated with the discrete biometric method, Mosaic K5 experienced higher stand transpiration rates in the upland, transitional, and saturated zones but with more variability compared to the rates measured at these zones of CFI SP-1 (Figure 3-109). Higher basal area at the stations of Mosaic K5 resulted in higher stand transpiration rates compared to the stations at

CFI SP-1 (Figure 3-110). The results from the transitional and saturated zones of both sites and the inundated zone of Mosaic K5 demonstrated that transpiration from *Salix caroliniana* alone was over typical total ET as estimated with the Penman method. It should be noted, however, that *Salix caroliniana* was by far the dominant species in the transitional, saturated, and inundated conditions and likely contributed the most to total ET of the stands.

Figure 3-1. Water depths at PCS SA 01

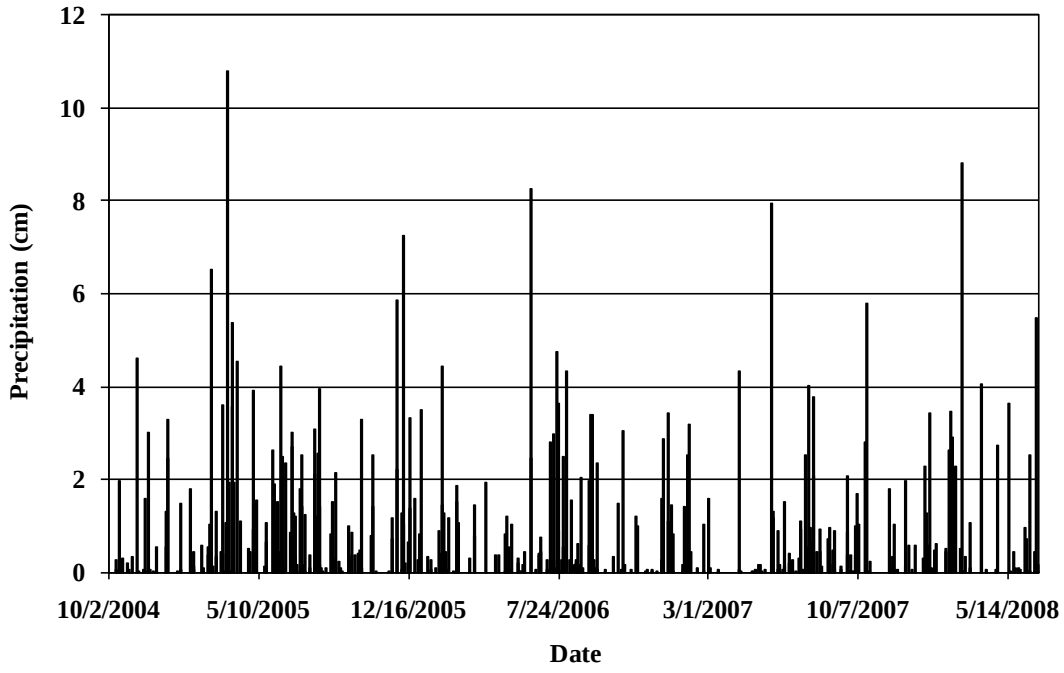

Figure 3-2. Precipitation for PCS SA 01

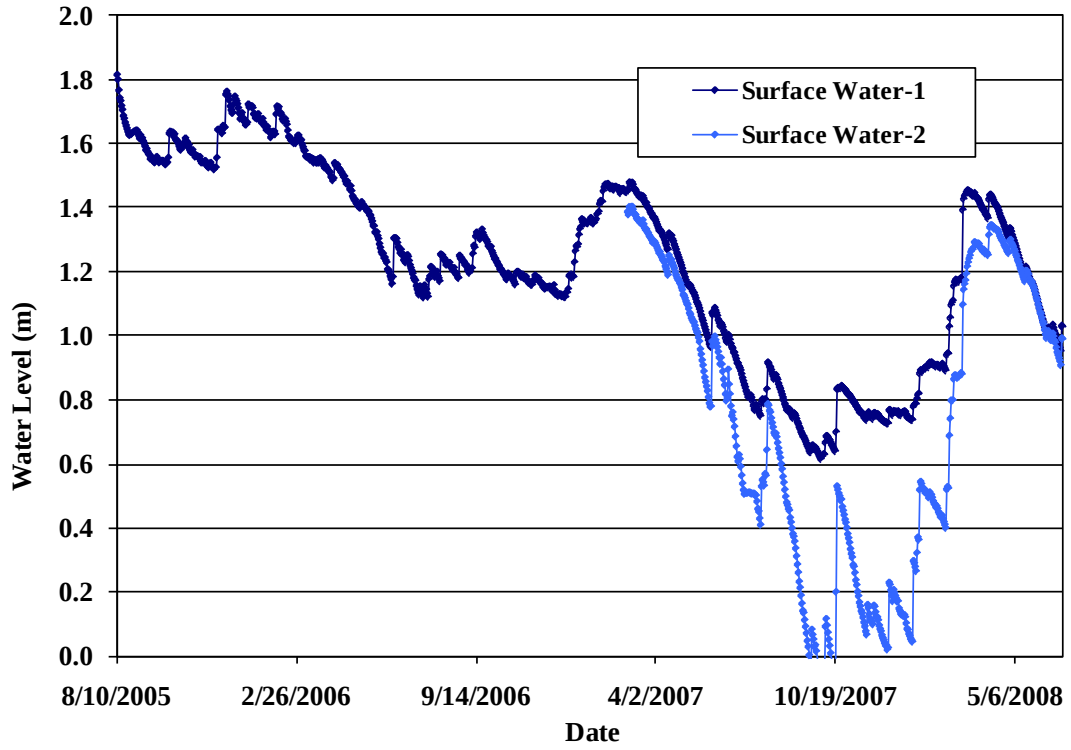

Figure 3-3. Water depths at PCS SA 10

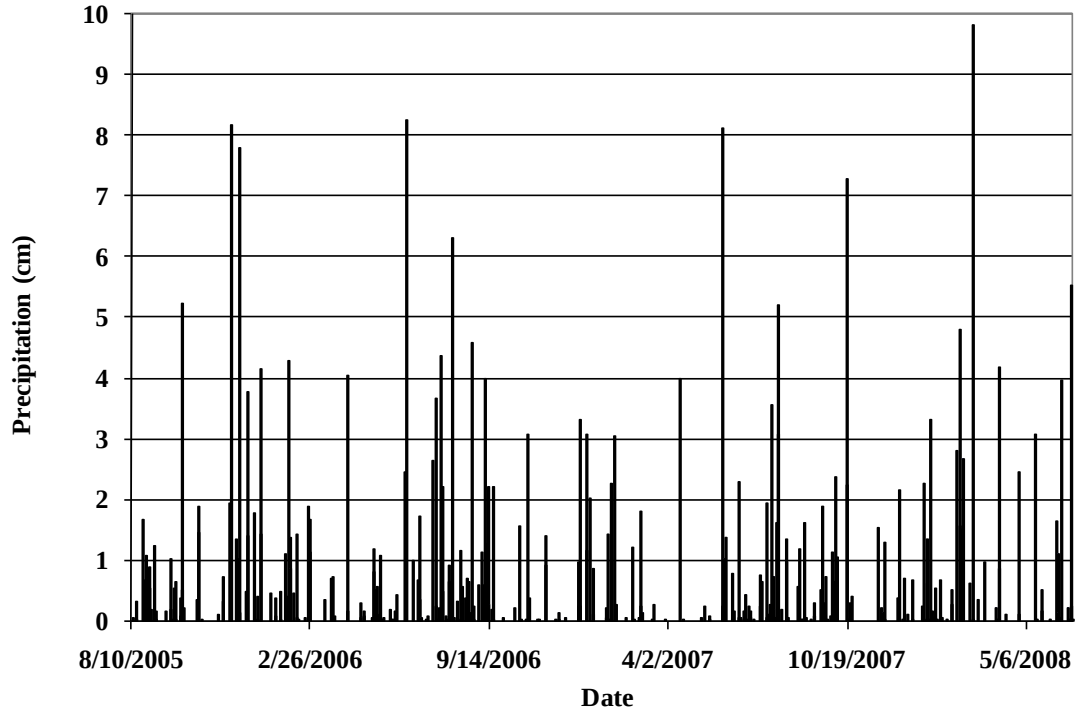

Figure 3-4. Precipitation for PCS SA 10

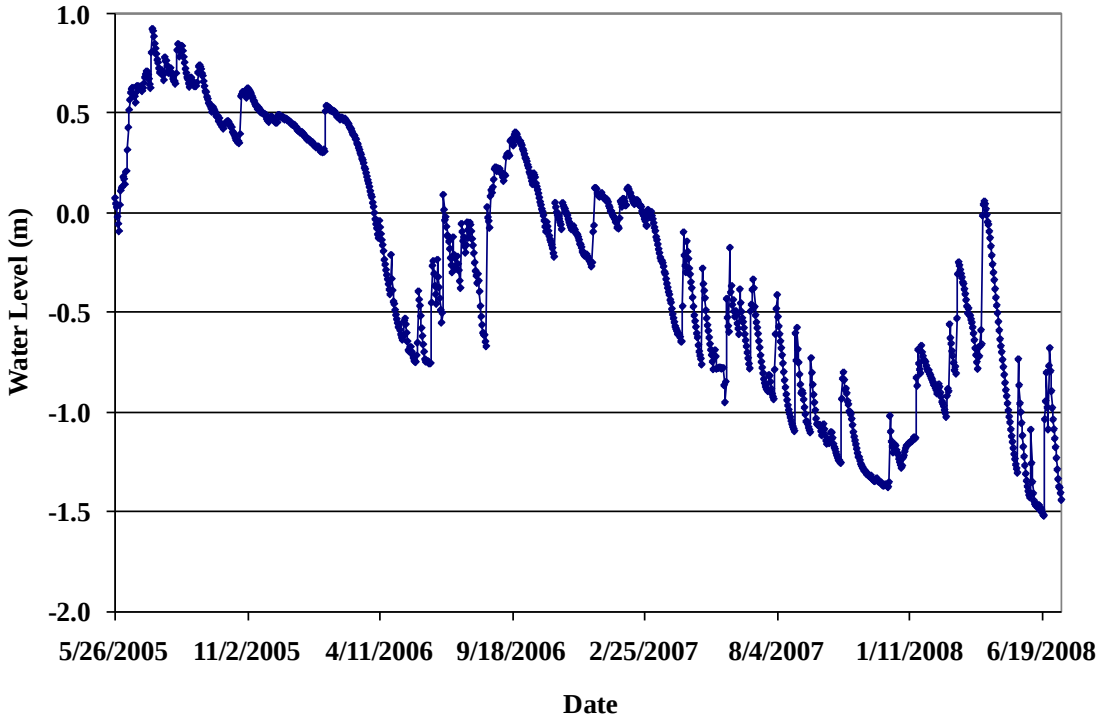

Figure 3-5. Water depths at Williams Co.

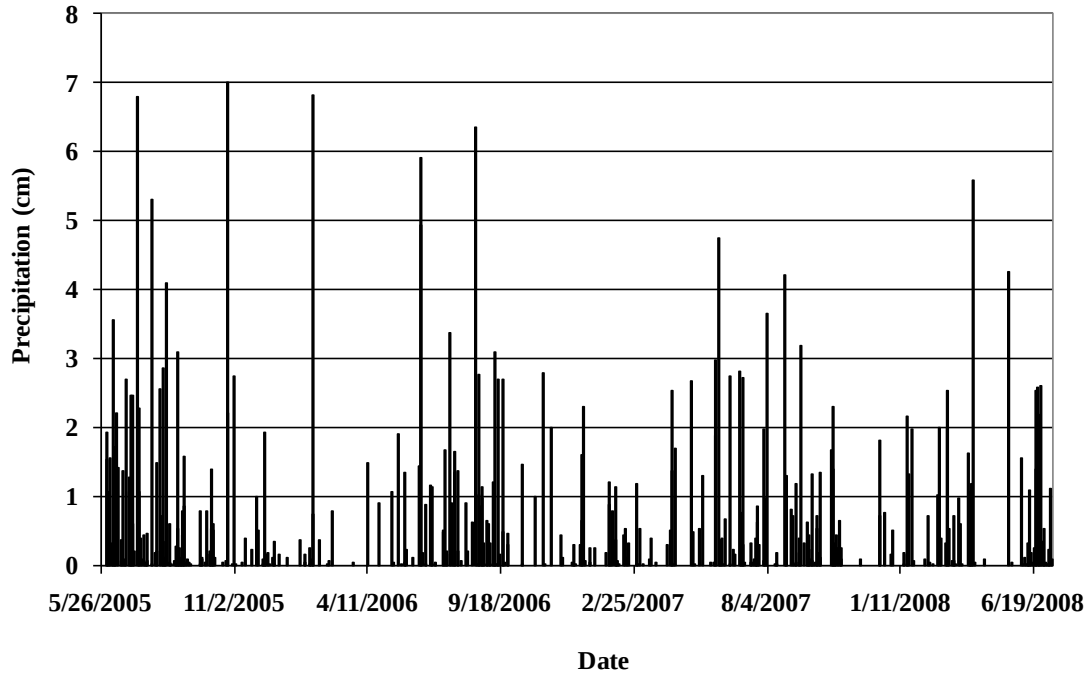

Figure 3-6. Precipitation for Williams Co.

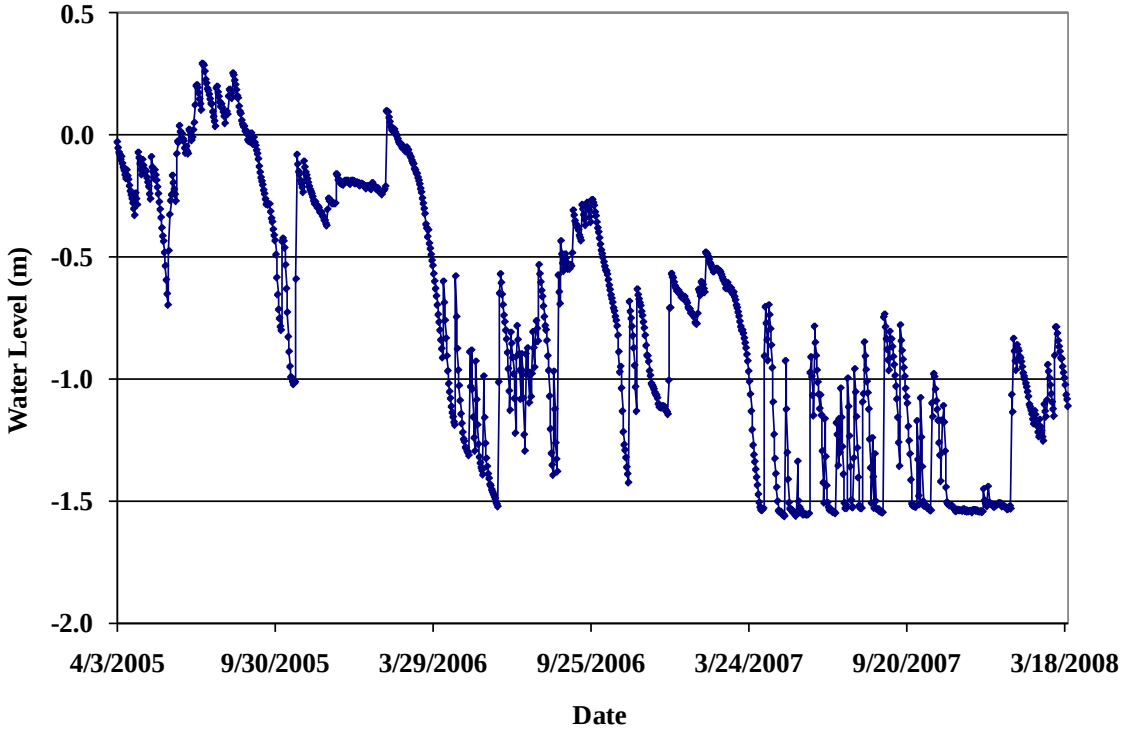

Figure 3-7. Water depths at Tenoroc 4

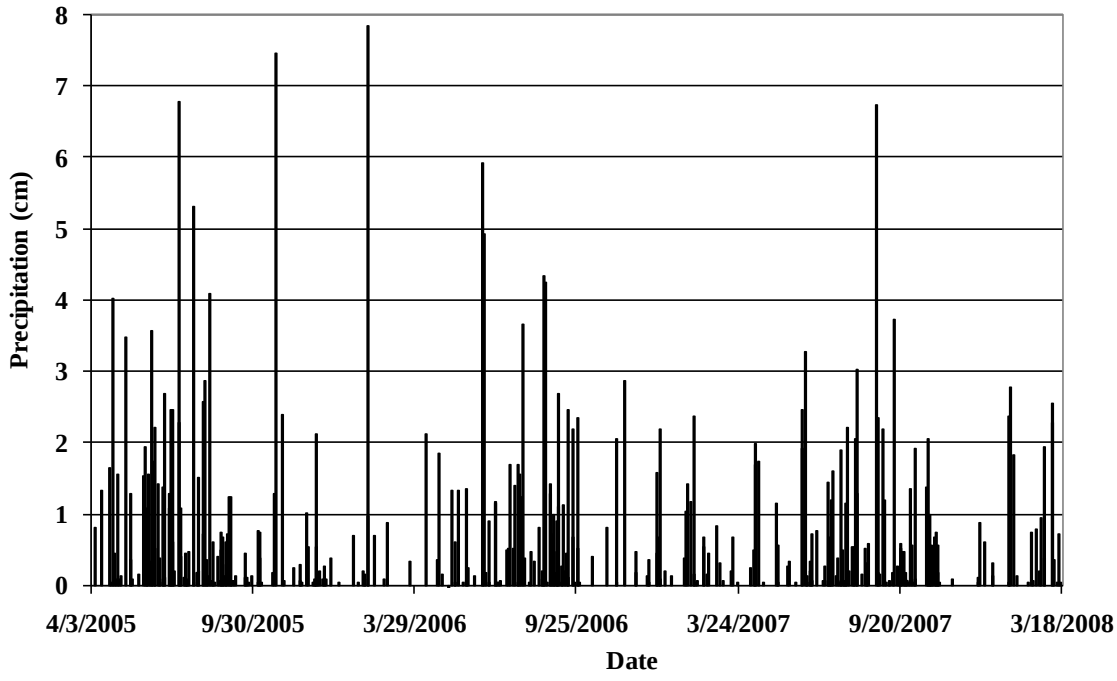

Figure 3-8. Precipitation for Tenoroc 4

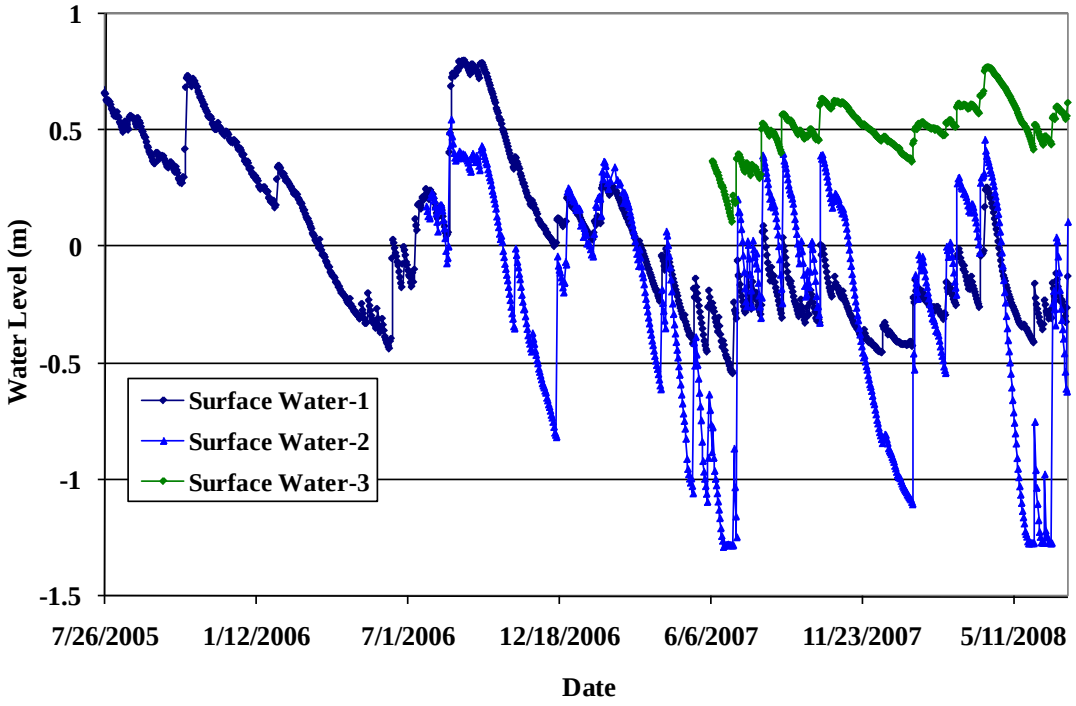

Figure 3-9. Water depths at Mosaic H1

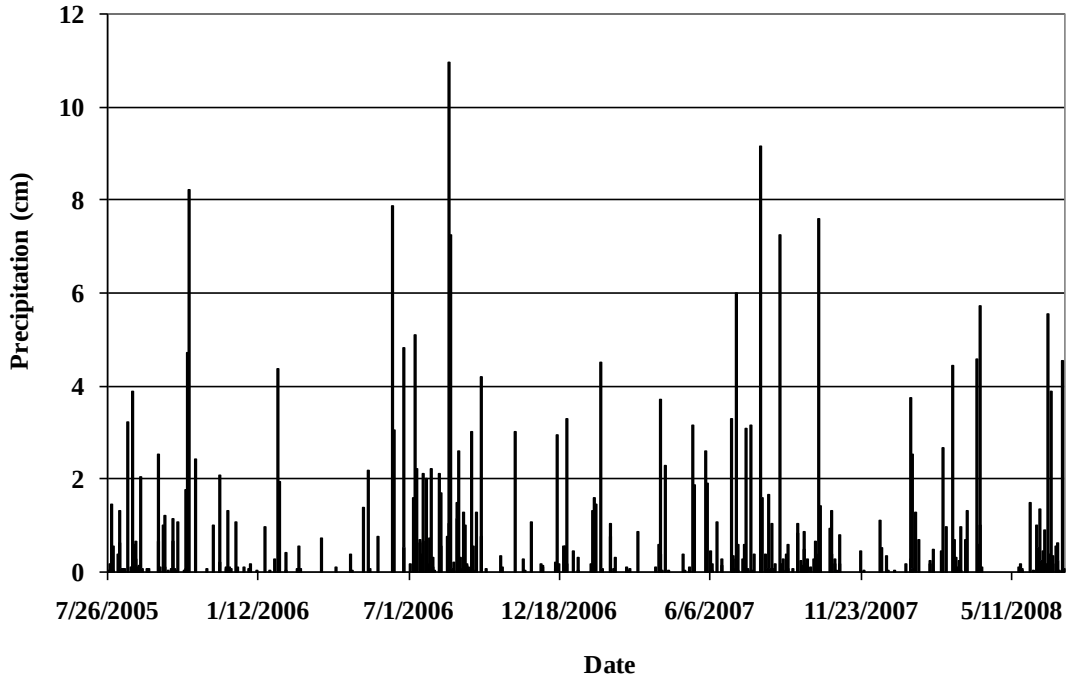

Figure 3-10. Precipitation for Mosaic H1

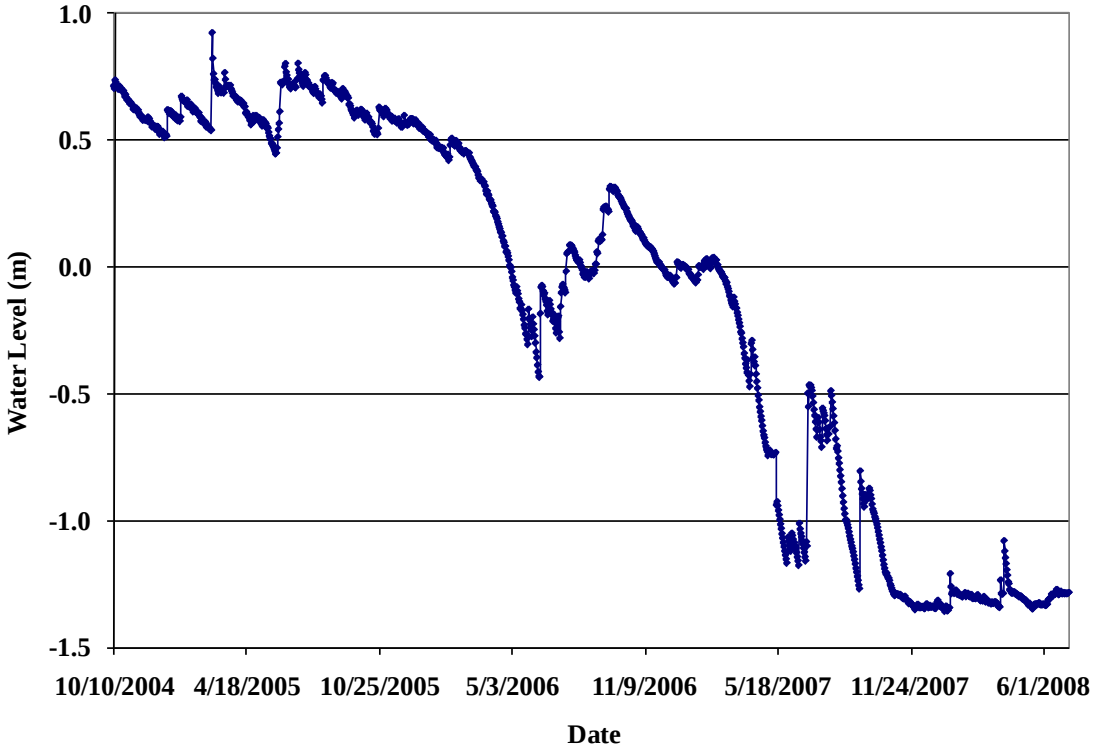

Figure 3-11. Water depths at CFI SP-1

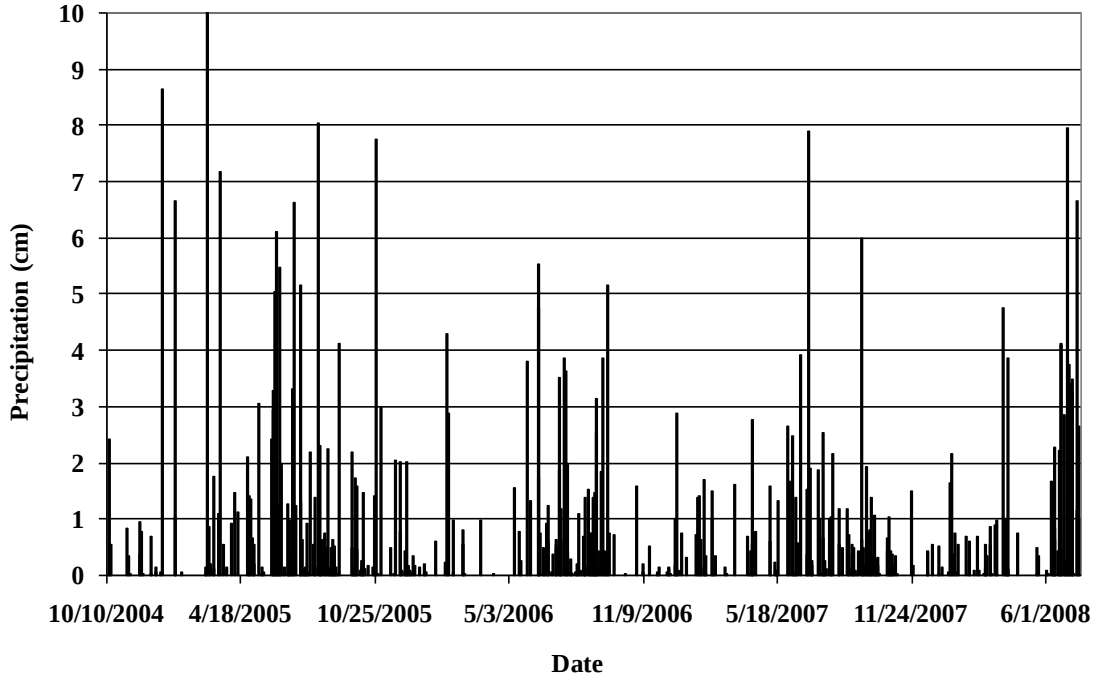

Figure 3-12. Precipitation for CFI SP-1

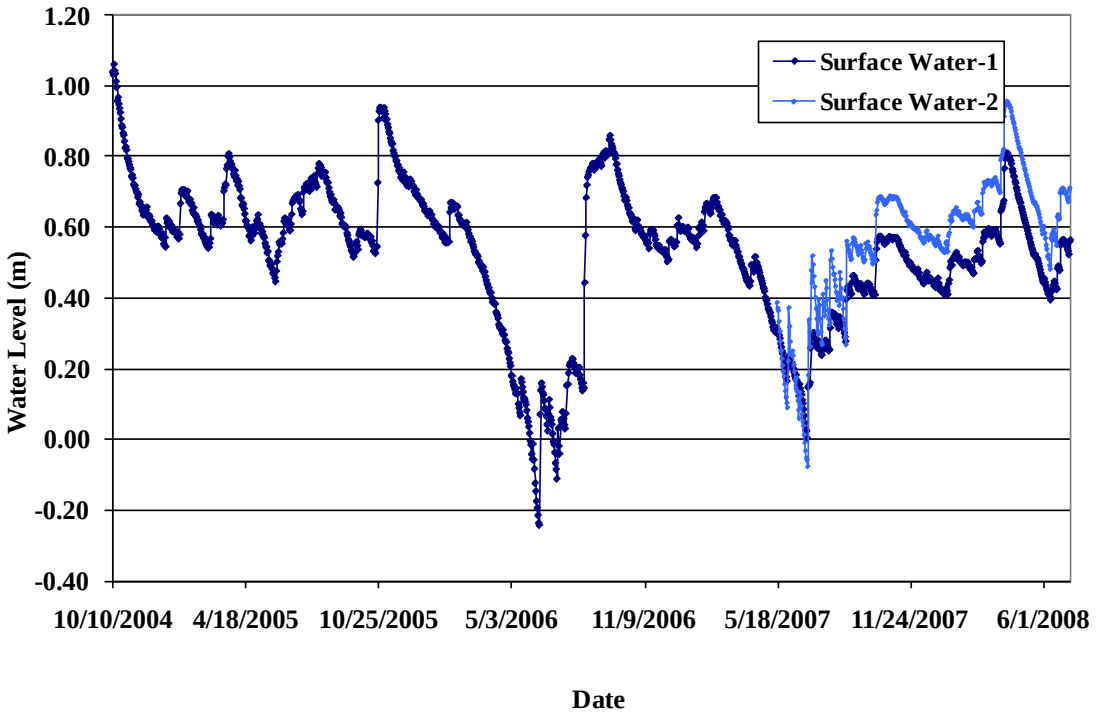

Figure 3-13. Water depths at Mosaic K5

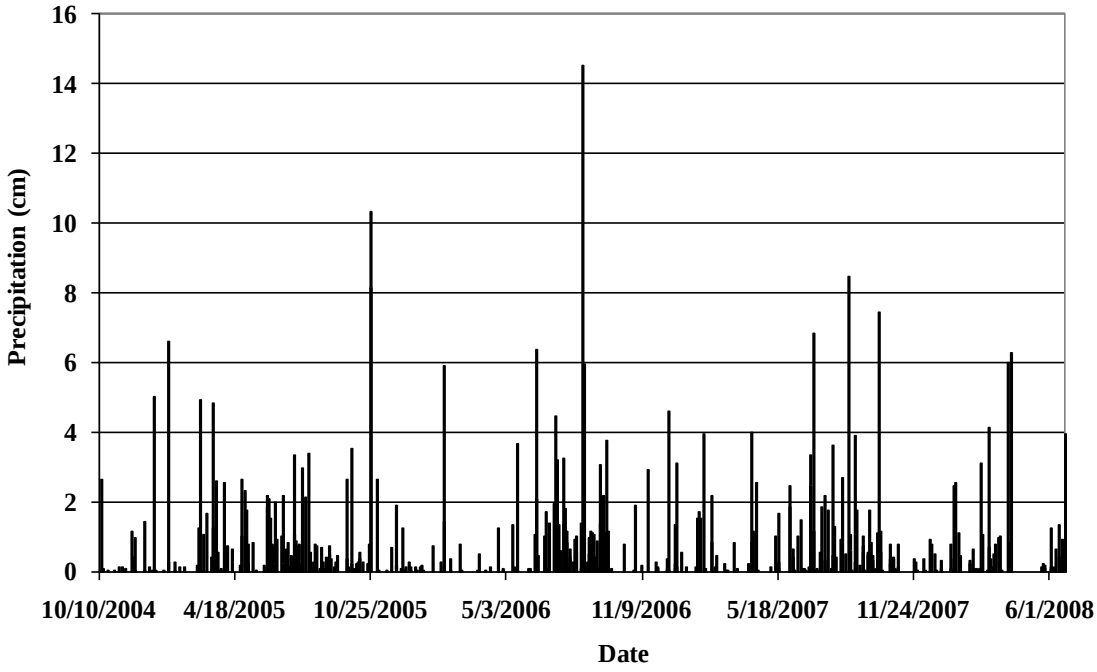

Figure 3-14. Precipitation for Mosaic K5

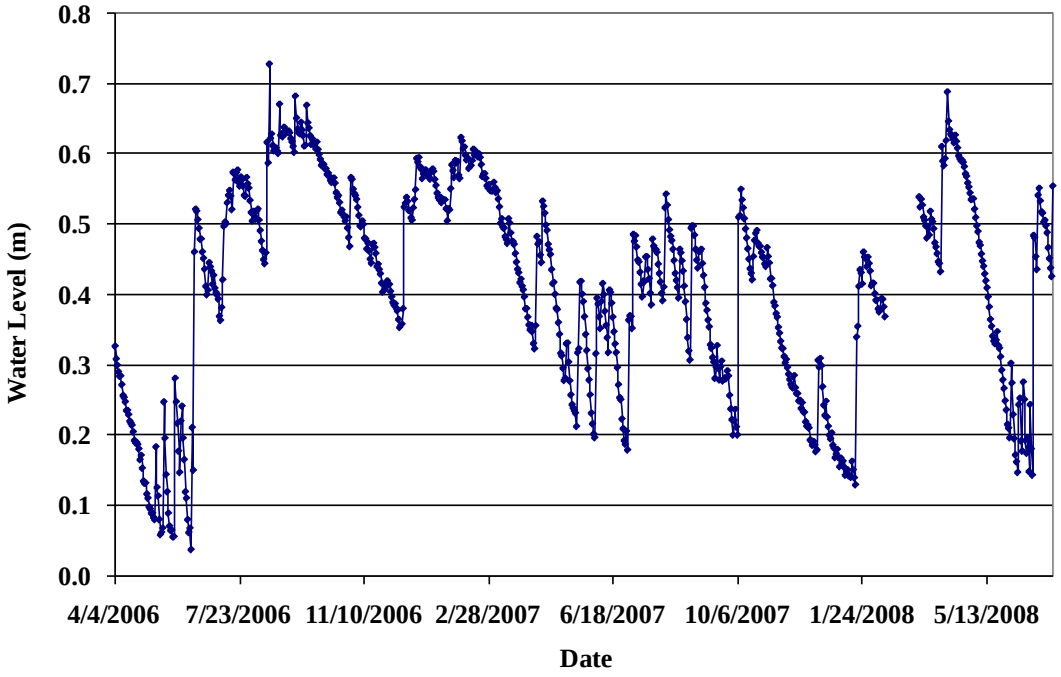

Figure 3-15. Water depths at Mosaic HP-10

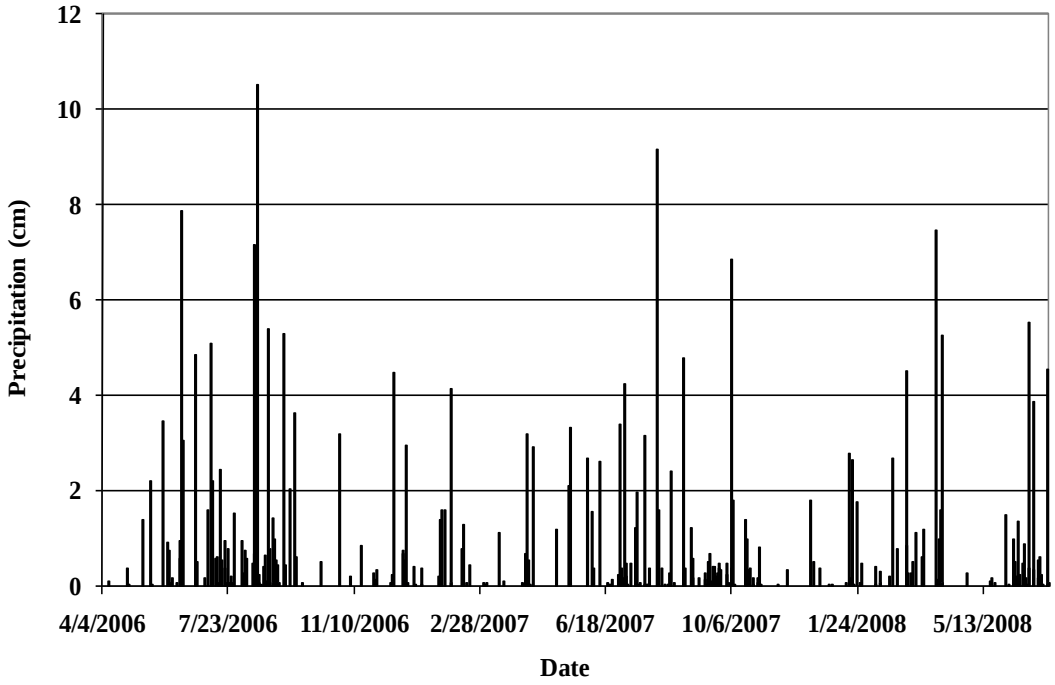

Figure 3-16. Precipitation for Mosaic HP-10

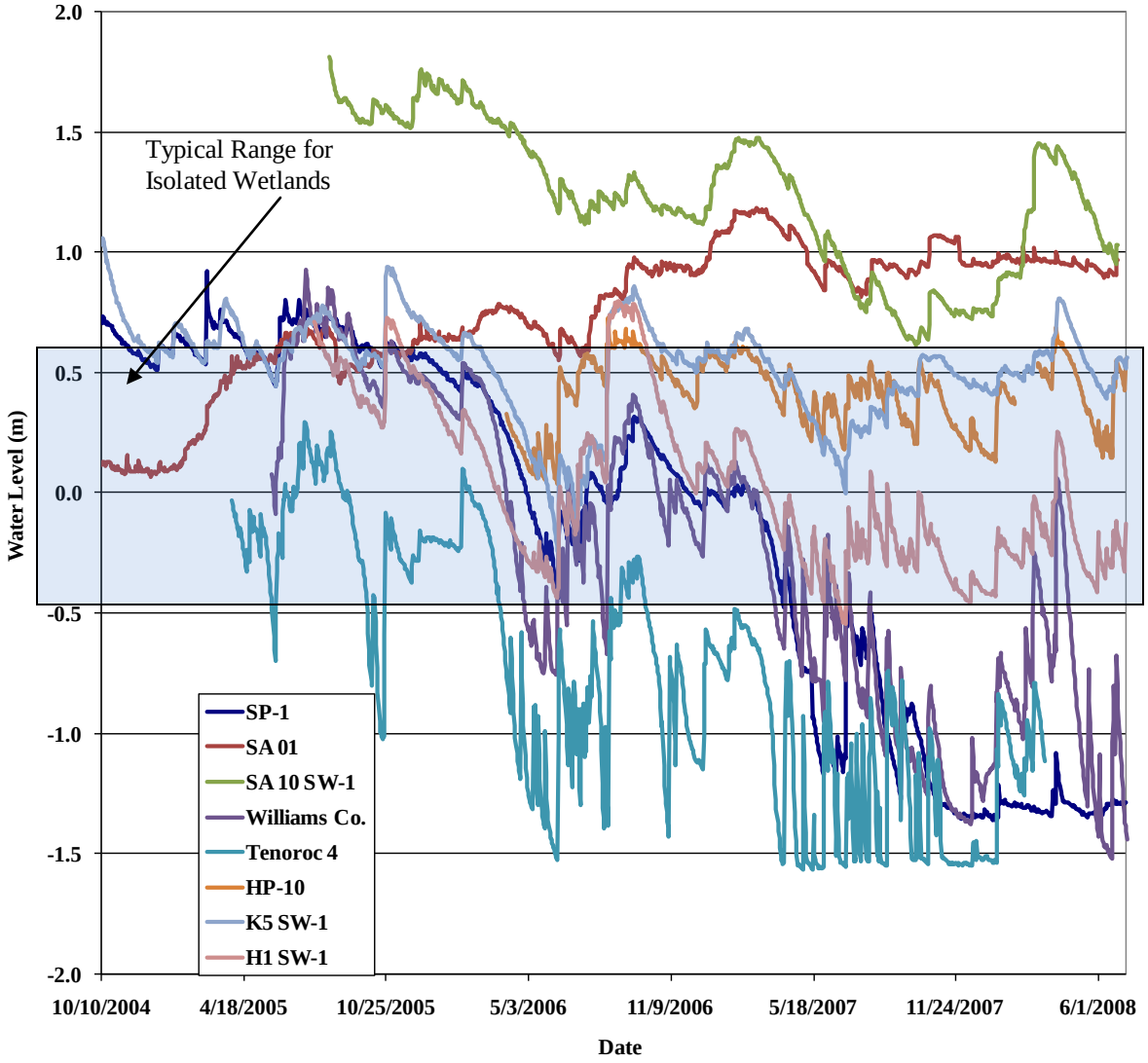

Figure 3-17. Water depths at all eight sites

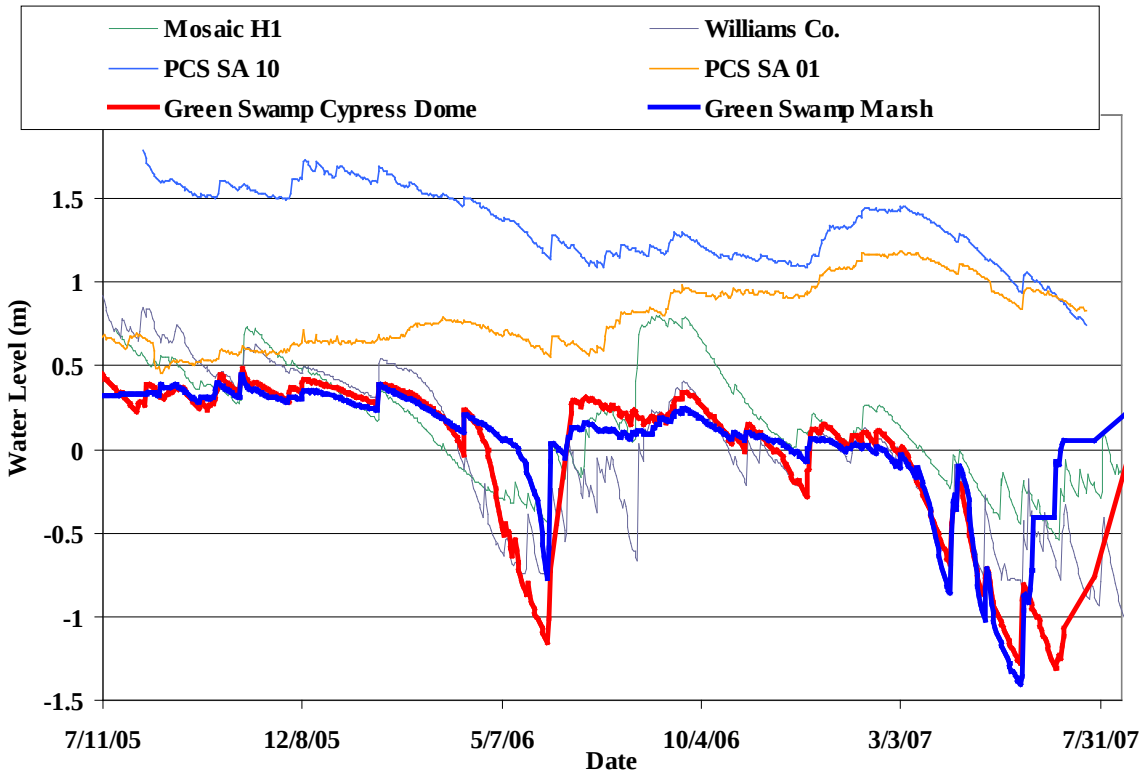

Figure 3-18. Comparison of water depths from PCS SA 10 SW-1, Mosaic H1 SW-1, Williams Co., PCS SA 01, Green Swamp cypress dome and Green Swamp marsh system

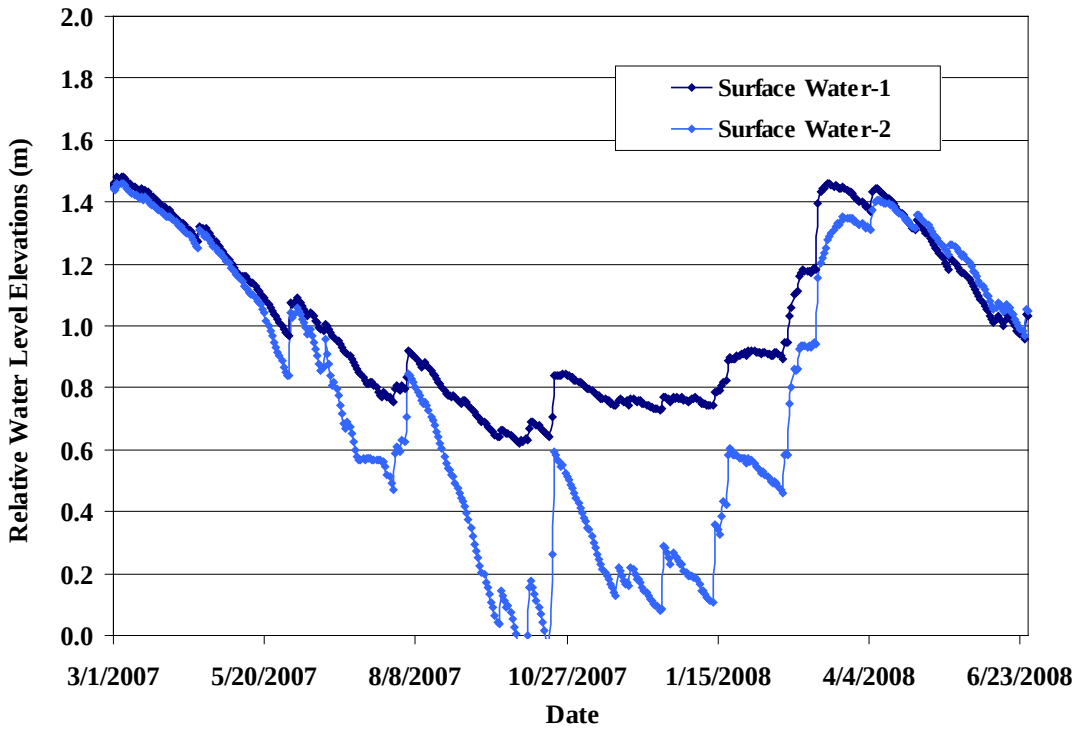

Figure 3-19. Surface water elevations relative to SW-1 for PCS SA-10

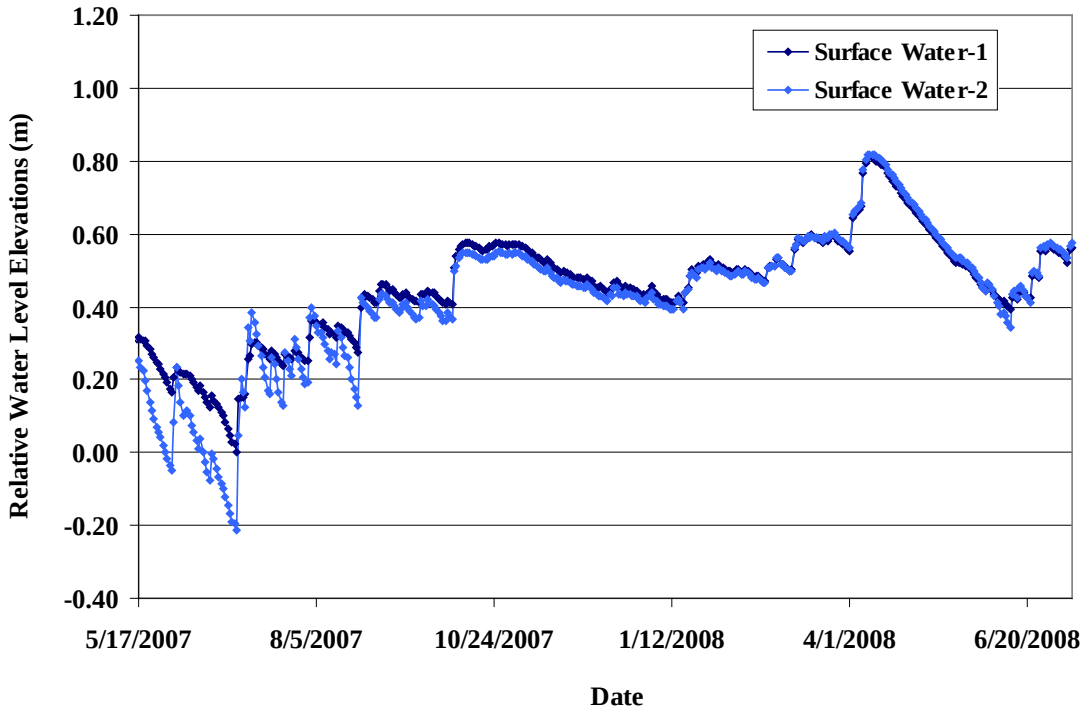

Figure 3-20. Surface water elevations relative to SW-1 for Mosaic K-5

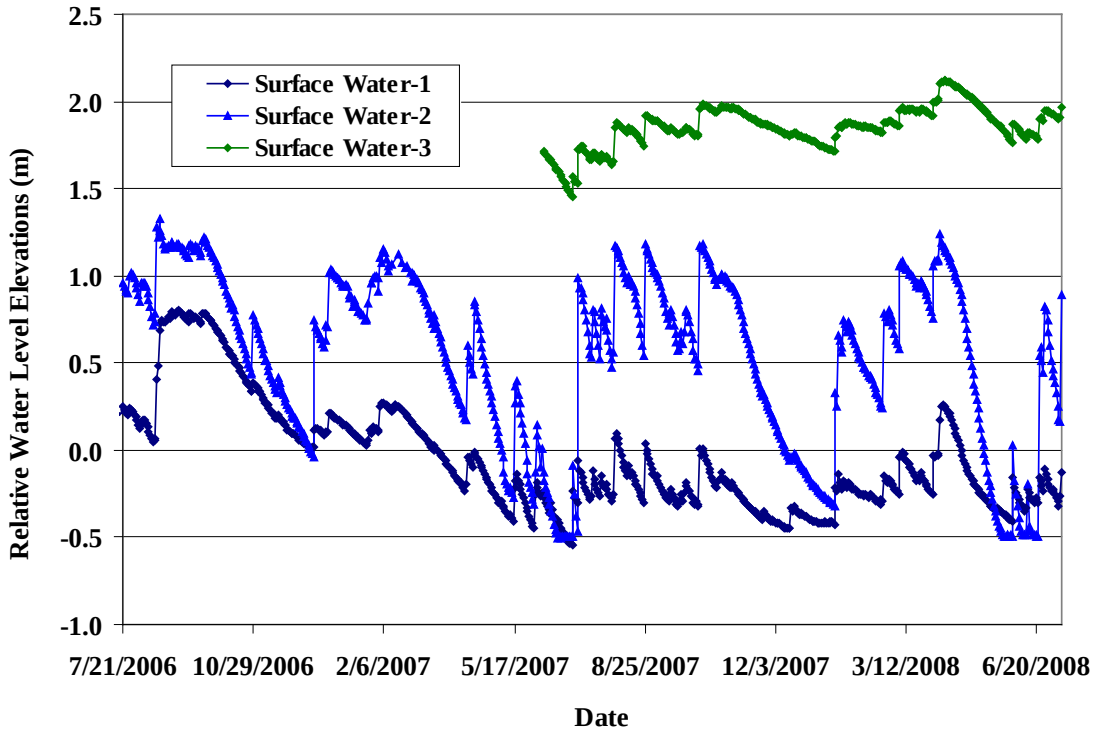

Figure 3-21. Surface water elevations relative to SW-1 for Mosaic H-1

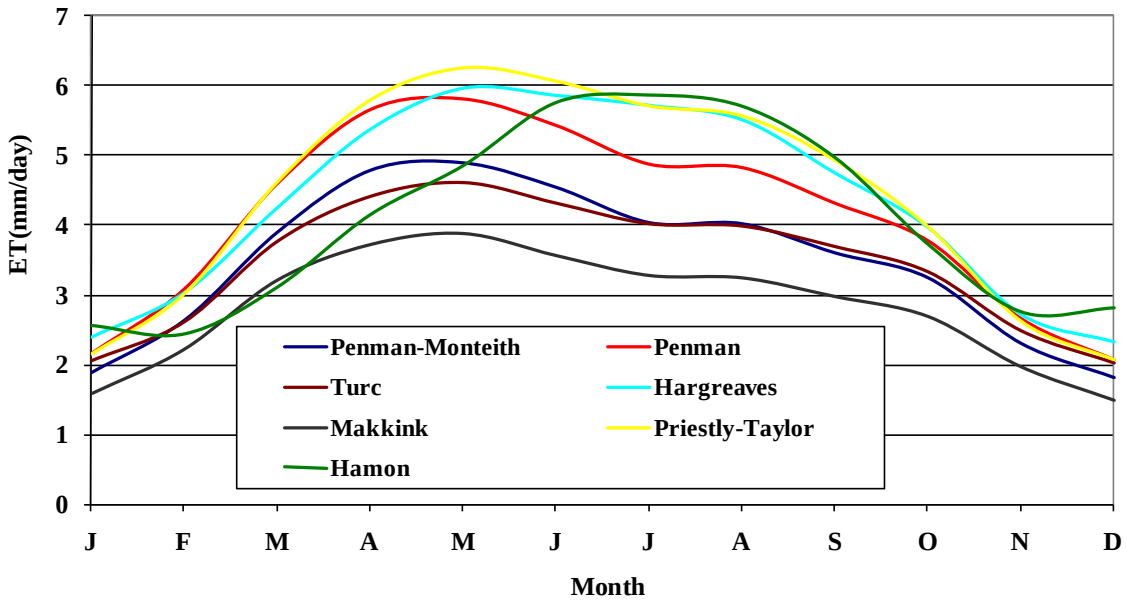

Figure 3-22. Monthly averages of daily ET estimated with different methods

Table 3-1. Total ET 2/1/06 through 1/31/07 at Williams Co

Method	Total ET(m)
Penman-Monteith	1.28
Penman	1.55
Turc	1.26
Hargreaves	1.58
Makkink	1.03
Priestly-Taylor	1.60
Hamon	1.49

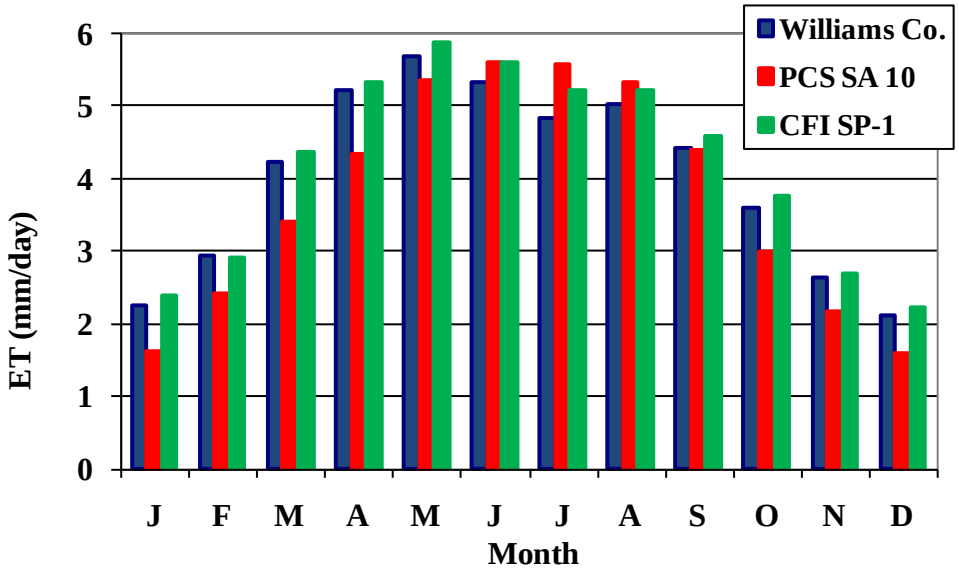

Figure 3-23. Monthly Averages of Daily ET with Penman method for Williams Co., PCS SA 10, and CFI SP-1

Table 3-2. Total ET (m) estimated with Penman method

Site	2006	2007
Williams Co.	1.49	1.47
CFI SP-1	1.55	1.52
PCS SA 10	1.39	1.40

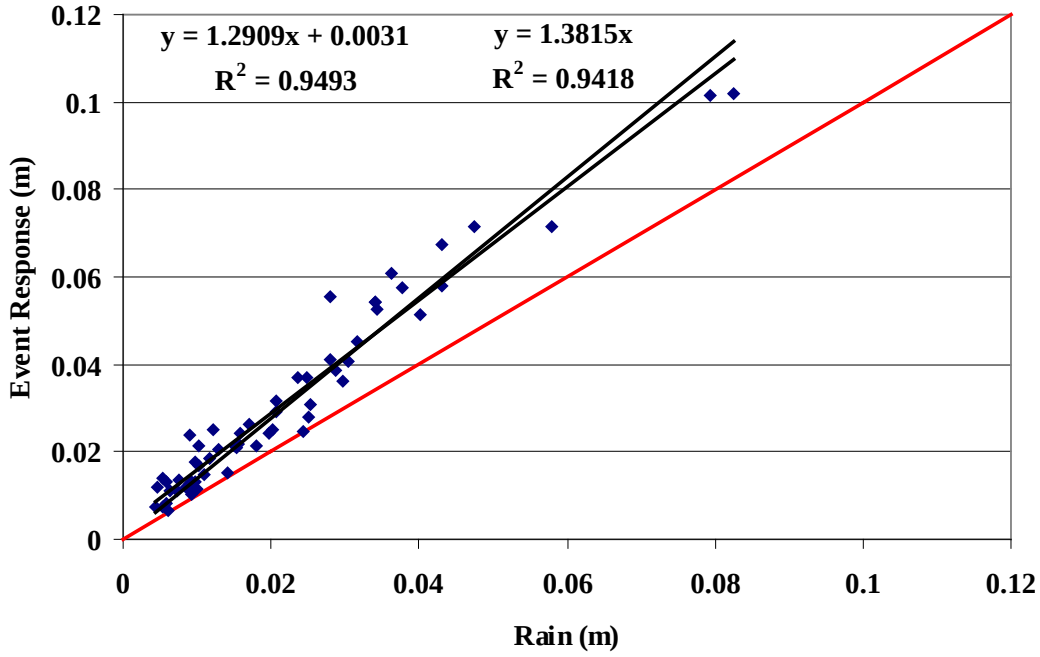

Figure 3-24. Event response versus rain for PCS SA 01

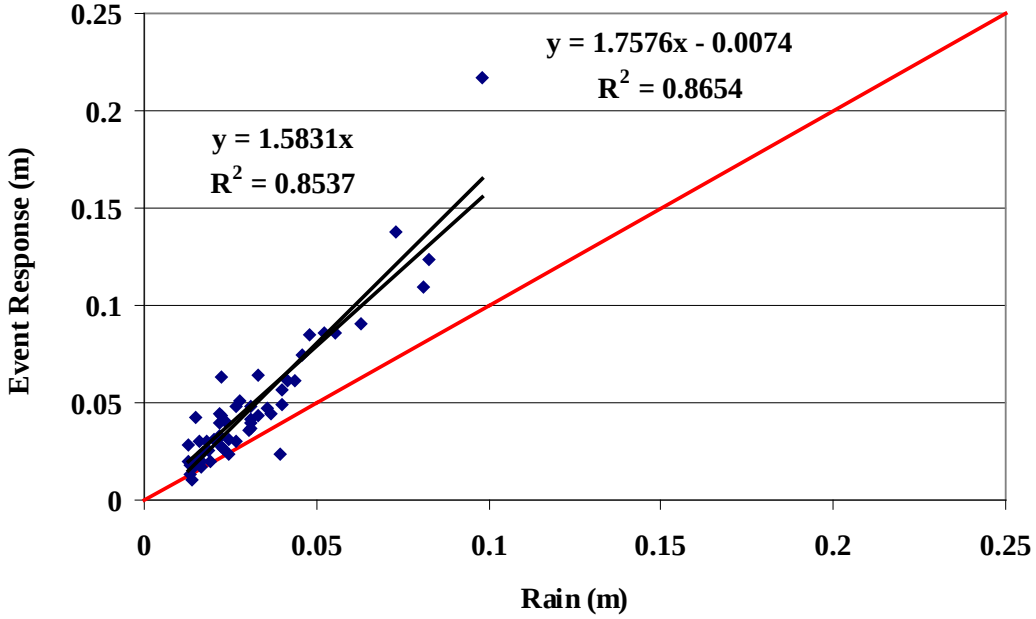

Figure 3-25. Event response versus rain for PCS SA 10

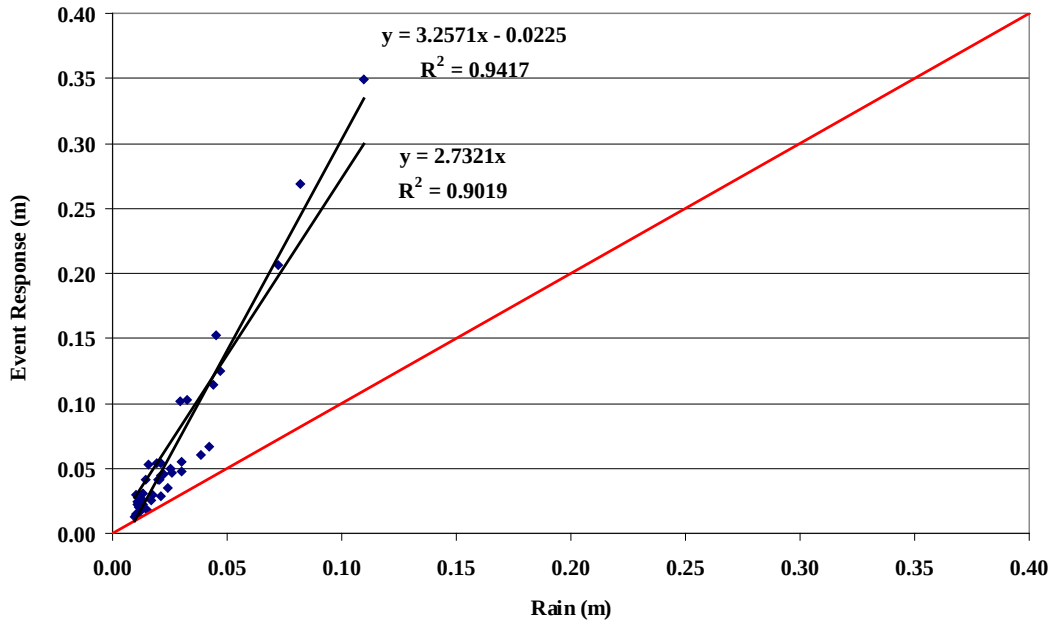

Figure 3-26. Event response versus rain for Mosaic H1 SW-1

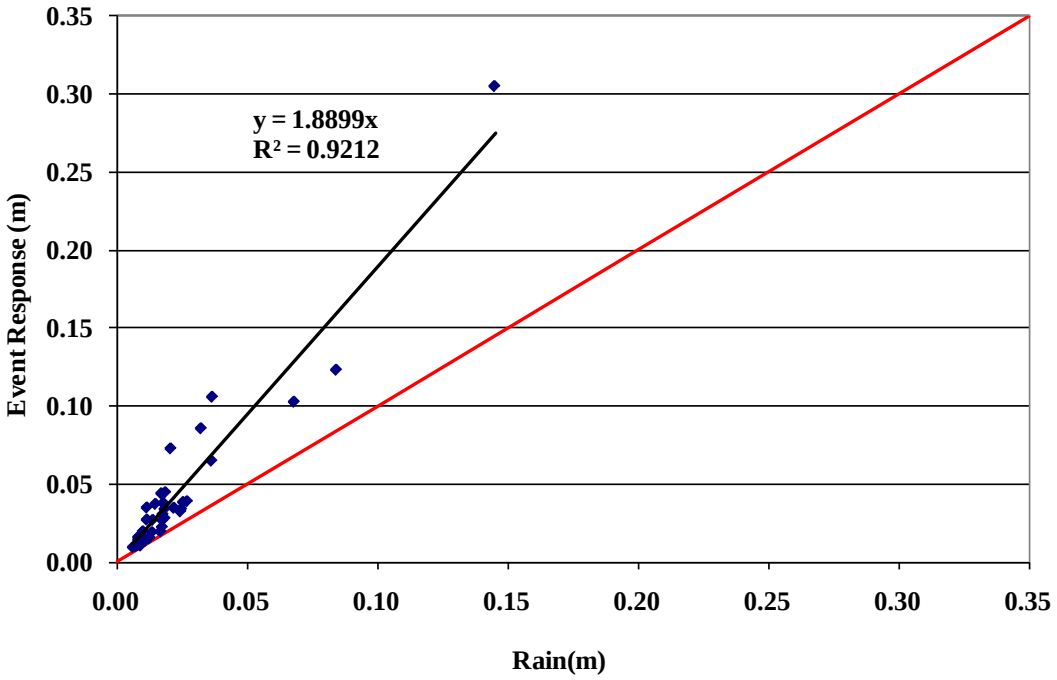

Figure 3-27. Event response versus rain for Mosaic H1 K5

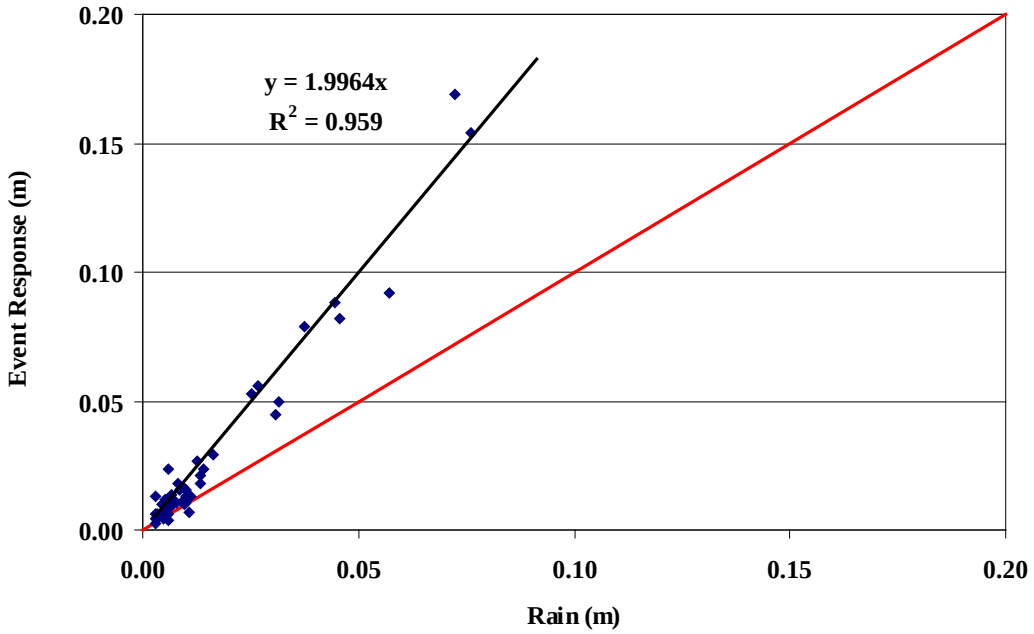

Figure 3-28. Event response versus rain for Mosaic H1 SW-3

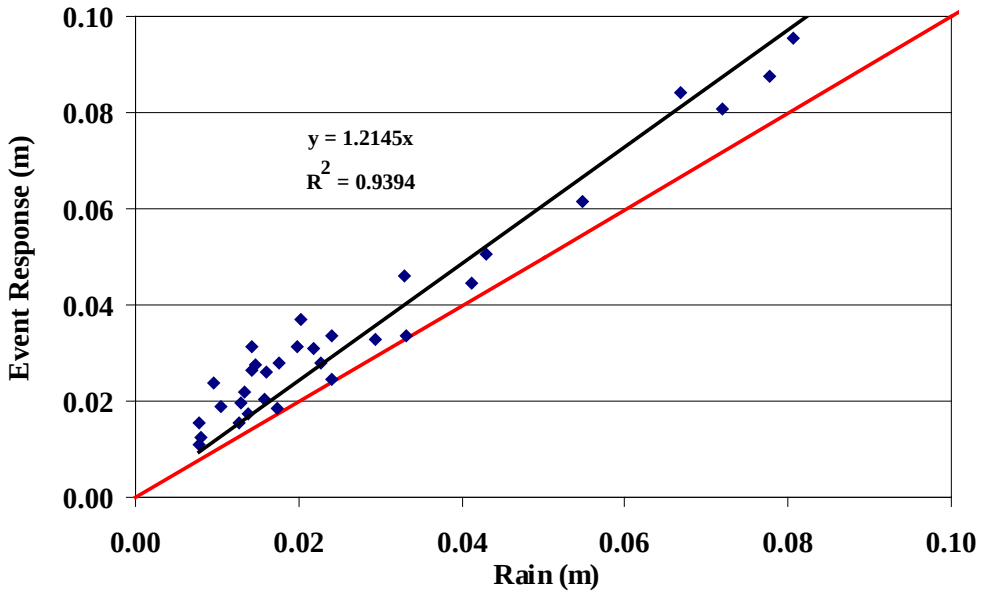

Figure 3-29. Event response versus rain for CFI SP-1

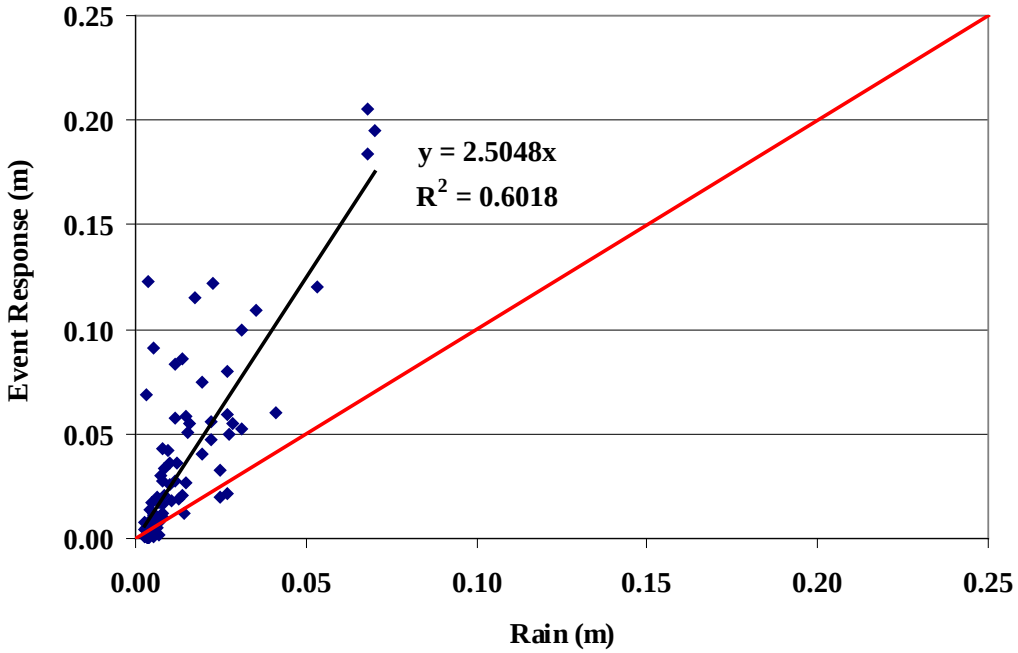

Figure 3-30. Event response versus rain for Williams Co.

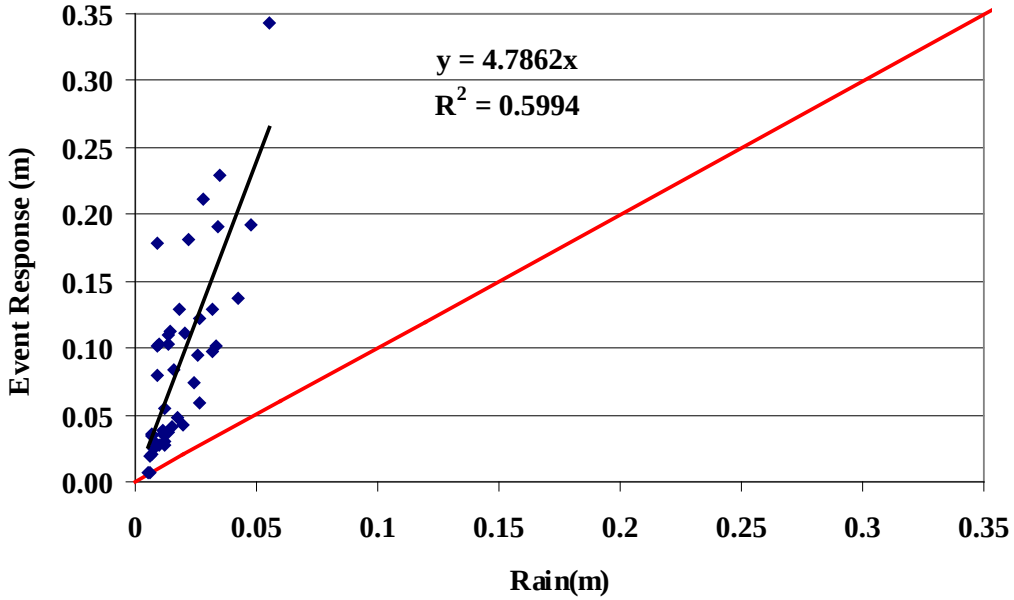

Figure 3-31. Event response versus rain for Mosaic HP-10

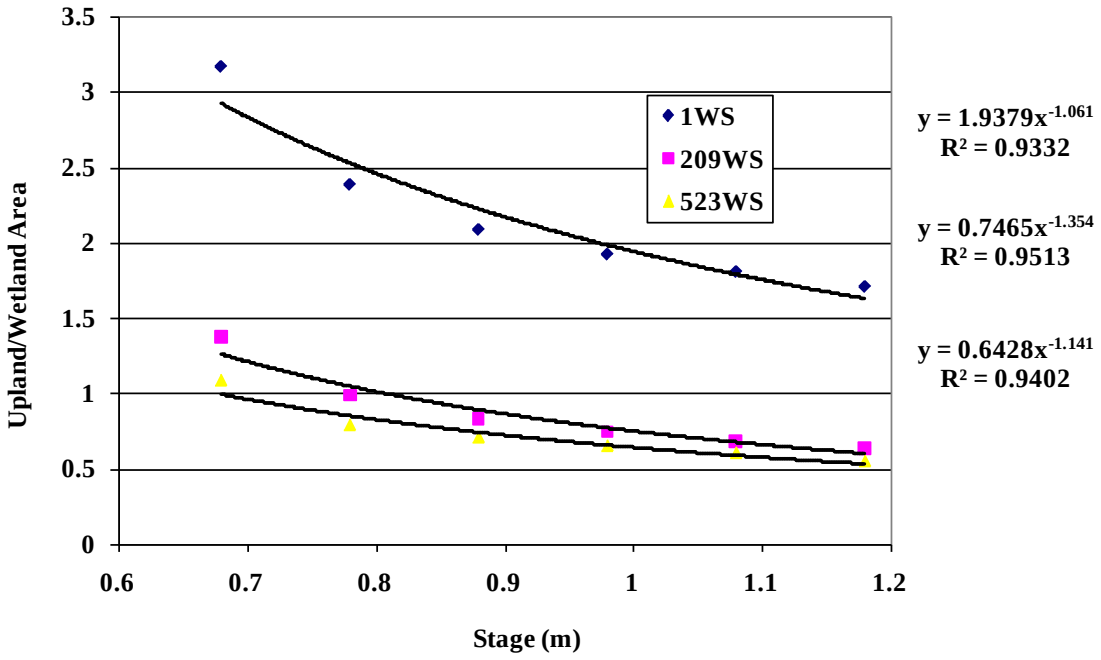

Figure 3-32. Upland/wetland area as a function of stage for different scales of watersheds at PCS SA 10

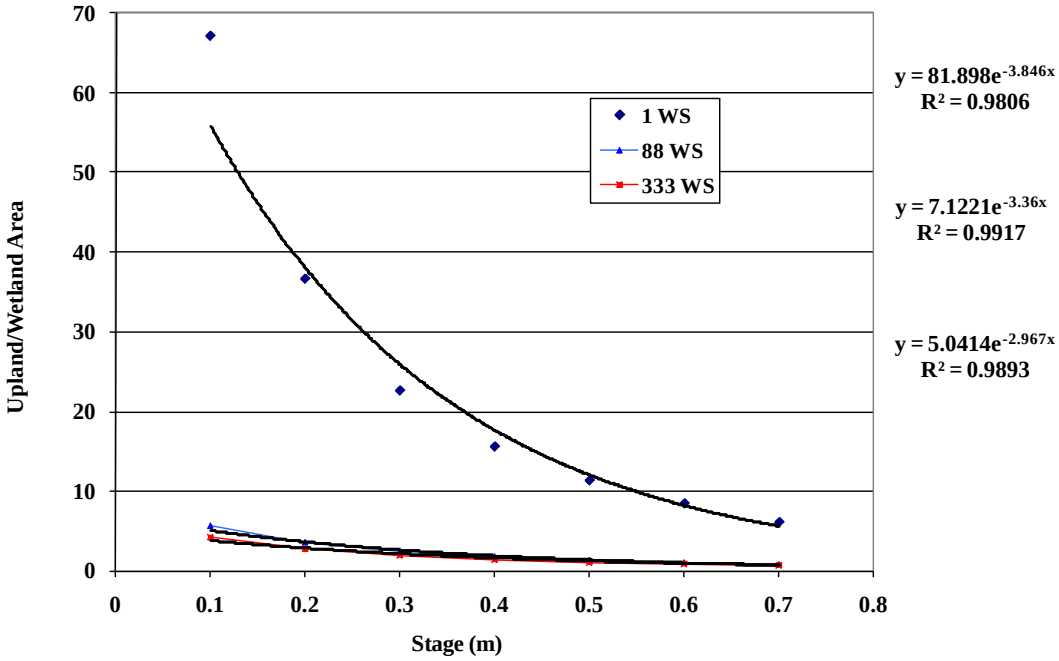

Figure 3-33. Upland/wetland area as a function of stage for different scales of watersheds at Mosaic H1

Table 3-3. Average runoff coefficients for different scales of watershed analysis

Scale of Watersheds	PCS SA-10	Mosaic H-1
Large	0.06	0.06
Medium	0.12	0.57
Small	0.20	0.66

Table 3-4. Runoff analysis summary

Site	Event Response Slope	Average C	Average Up/Wet
Mosaic H1 SW-1	3.26	0.66 ± 0.39	2.41 ± 1.7
Mosaic H1 SW-3	2.12	0.26 ± 0.14	2.93 ± 1.1
PCS SA 10	1.41	0.20 ± 0.09	2.94 ± 1.4
PCS SA 01	1.29	0.22 ± 0.10	1.81 ± 0.3
CFI SP-1	1.08	0.15 ± 0.09	3.02 ± 1.2
Mosaic HP-10	4.58	0.21 ± 0.14	31.70 ± 16.4
Mosaic K5	1.95	0.22 ± 0.13	3.64 ± 2.6
Williams Co.	2.56	0.32 ± 0.15	5.40 ± 2.3

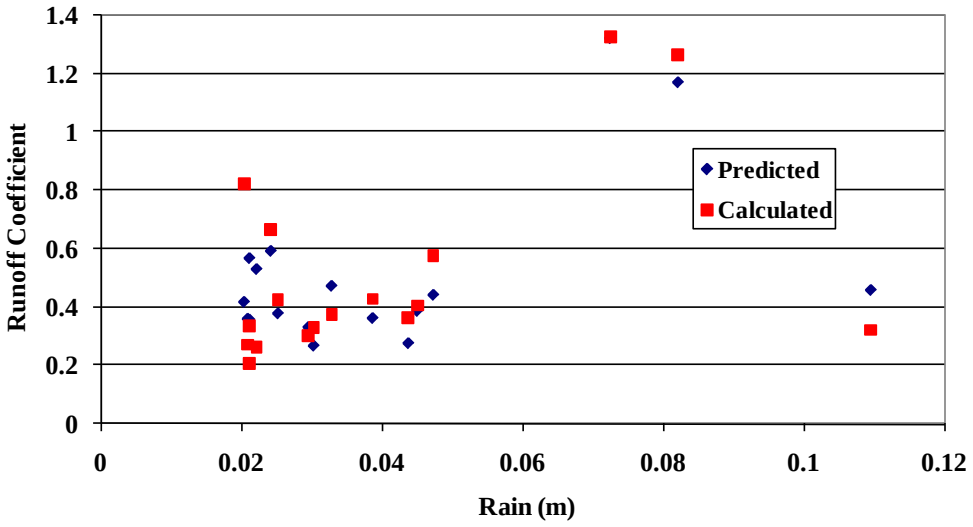

Figure 3-34. Calculated and predicted runoff coefficients versus rainfall for Mosaic H1 SW-1

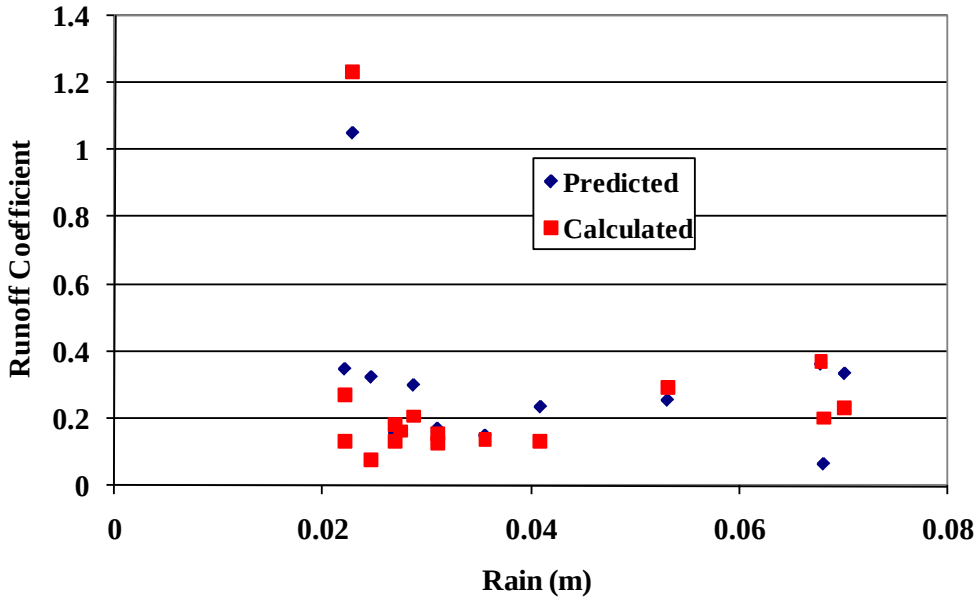

Figure 3-35. Calculated and predicted runoff coefficients versus rainfall for Williams Co.

Table 3-5. Runoff analysis and modeling results

Site	Event Response R^2	Multiple Regression R^2
Mosaic H1 SW-1	0.94	0.76
Mosaic H1 SW-3	0.97	0.46
PCS SA 10	0.87	0.94
PCS SA 01	0.95	0.30
CFI SP-1	0.96	0.23
Mosaic HP-10	0.60	0.82
Mosaic K5	0.92	0.37
Williams Co.	0.60	0.81

Table 3-6. Measured and predicted rainfall plus runoff totals with linear and multiple regression models

Site	Measured (m)	Simple Linear (m)	Multiple Regression (m)
PCS SA 10	1.02	1.01	0.91
Mosaic H1 SW-1	2.87	2.82	2.63
Williams Company	1.85	1.87	1.46

Table 3-7. Measured and predicted rainfall plus runoff totals with linear models

Site	Rain+Predicted Runoff (m)	Measured (m)
PCS SA 01	2.13	2.10
Mosaic K5	2.73	2.70
CFI SP-1	2.28	2.32
Mosaic H1 SW-3	2.02	2.17

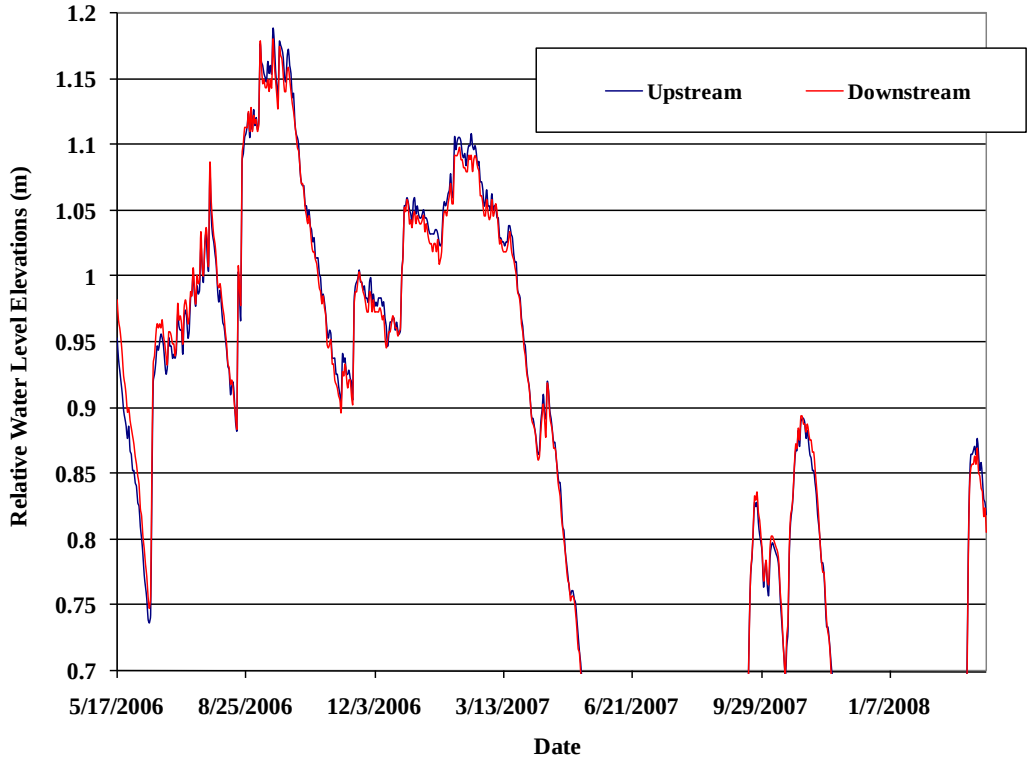

Figure 3-36. Relative water elevations at upstream and downstream channel wells at Tenoroc 4

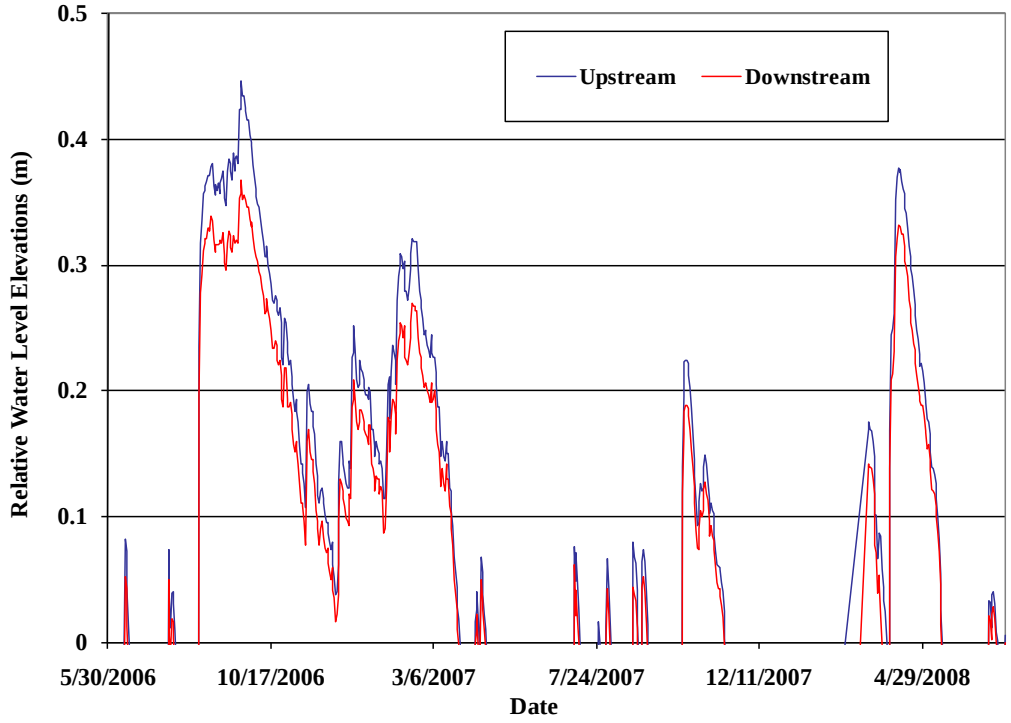

Figure 3-37. Relative water elevations at upstream and downstream channel wells at Mosaic K5

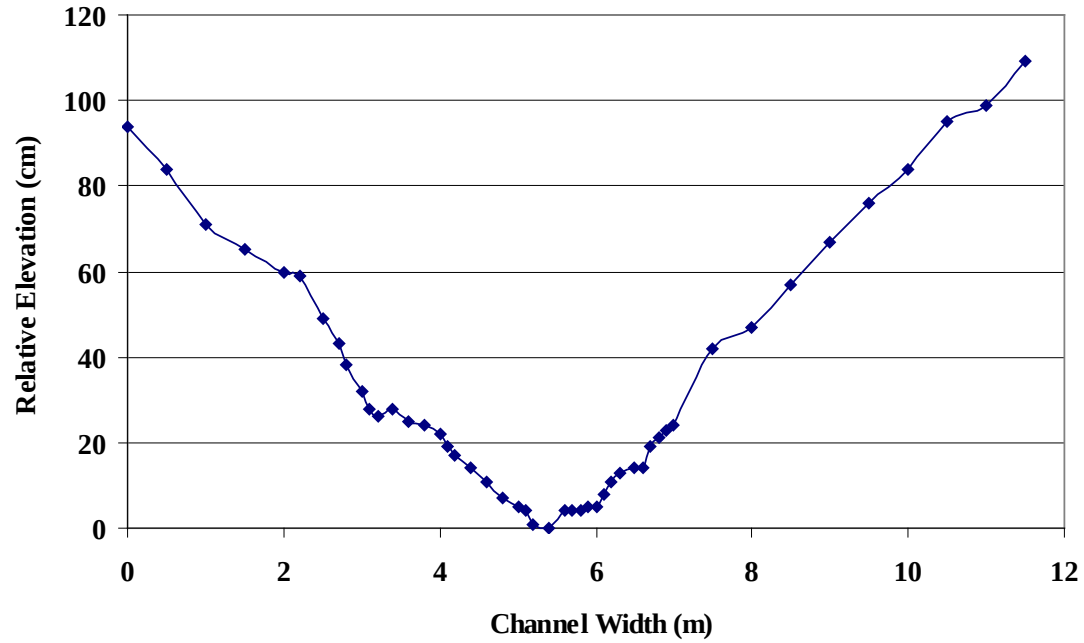

Figure 3-38. Channel cross sectional profile at the upstream well at Mosaic K5

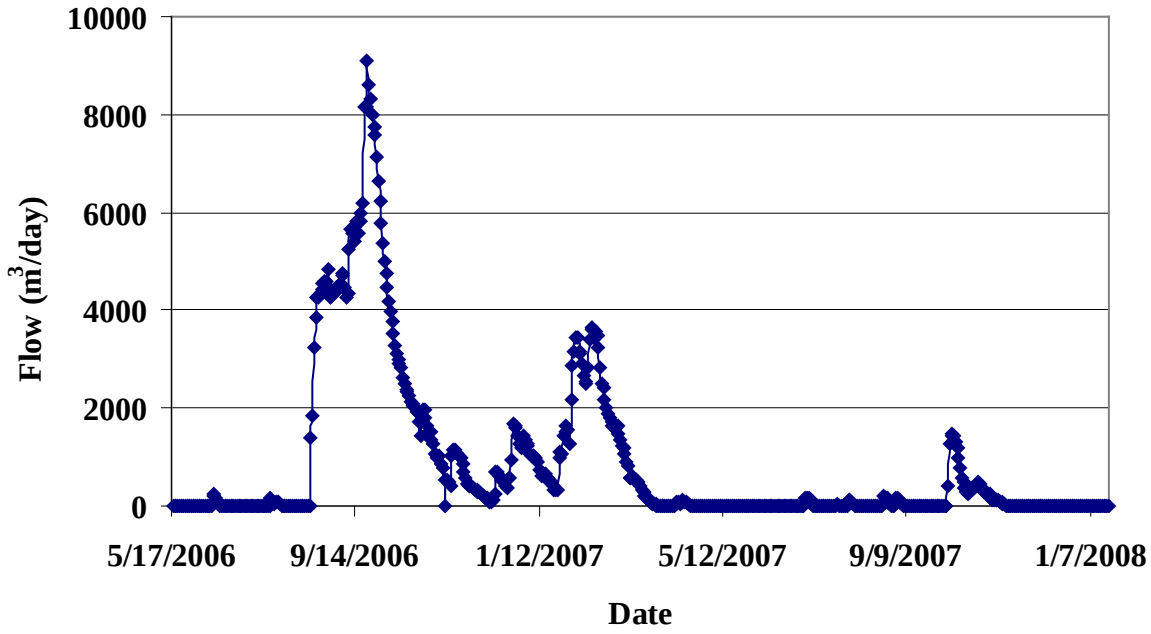

Figure 3-39. Channel flow at Mosaic K5

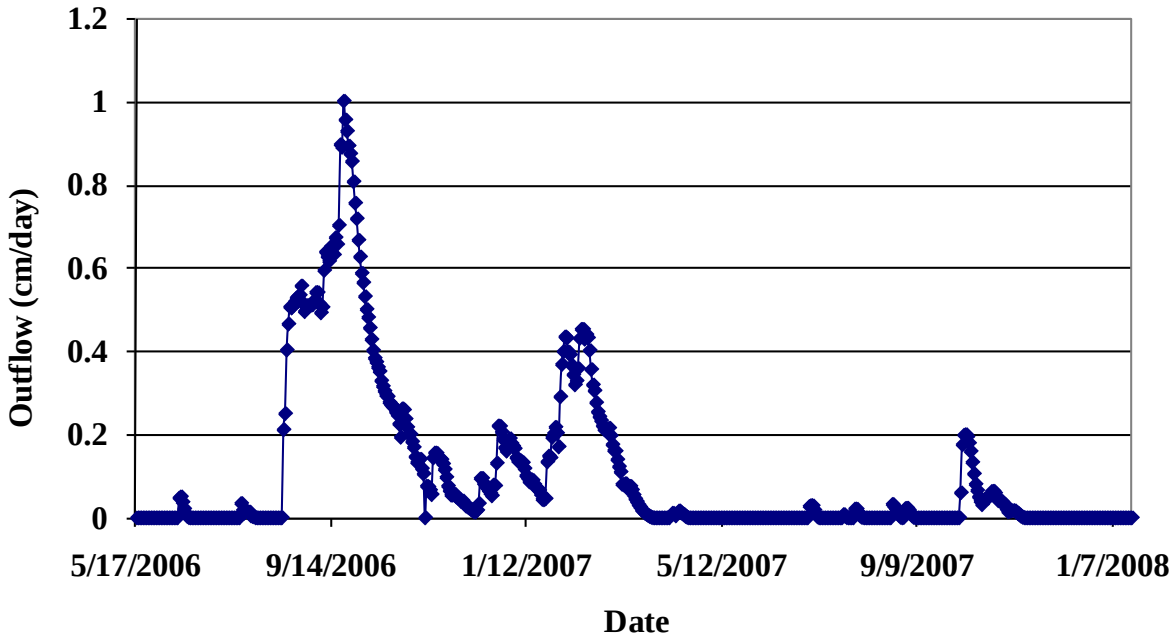

Figure 3-40. Channel flow as depth at Mosaic K5

Table 3-8. Water balance results

Site	Time Period	Rain (m)	Runoff (m)	ET (m)	ΔStorage (m)	residual (m)	residual/day (mm)
Mosiac H1 SW-3	7/7/07 - 7-9-08	1.13	1.04	1.63	0.22	0.32	0.88
Mosaic HP-10	4/4/06 - 2/12/08	2.00	2.80	2.46	-0.09	2.43	3.98
PCS SA 01	6/1/06 - 11/27/07	1.48	0.65	2.33	0.45	-0.65	-1.19
CFI SP-1	10/10/04 - 4/10/06	1.94	0.38	2.23	-0.51	0.60	1.11
Mosaic H-1 SW-1	7/26/05 - 3/22/06	0.57	0.69	0.87	-0.64	1.03	4.32
Mosaic H-1 SW-1	7/12/06 - 3/6/07	0.79	0.98	0.83	-0.08	1.02	4.29
Williams Co.	6/14/05 - 4/4/06	0.87	1.00	1.04	-0.61	1.44	4.87
PCS SA 10	4/26/06 - 6/27/08	2.25	1.30	3.06	-0.43	0.92	1.16

Table 3-9. Water balance results for Mosaic K5

Time Period	Rain (m)	Runoff (m)	ET (m)	Channel outflow (m)	ΔStorage (m)	residual (m)	residual/day (mm)
5/18/06 - 1/18/08	2.06	1.54	2.54	0.65	0.28	0.13	0.21
3/13/06 - 8/15/06	0.62	0.49	0.85	0.00	-0.08	0.34	2.17
3/27/07 - 10/4/07	0.76	0.57	1.03	0.00	-0.09	0.39	2.02
11/10/07 - 3/5/08	0.17	0.10	0.29	0.00	-0.05	0.03	0.29

Table 3-10. Runoff depth as percentages of rain depth

Site	Time Period	Runoff/Rain (%)
Mosiac H1 SW-3	7/7/07 - 7-9-08	92.12
Mosaic HP-10	4/4/06 - 2/12/08	139.68
PCS SA 01	6/1/06 - 11/27/07	44.14
CFI SP-1	10/10/04 - 4/10/06	19.54
Mosaic H-1 SW-1	7/26/05 - 3/22/06	119.79
Mosaic H-1 SW-1	7/12/06 - 3/6/07	123.35
Williams Co.	6/14/05 - 4/4/06	115.19
PCS SA 10	4/26/06 - 6/27/08	57.68
Mosaic K5	5/18/06 - 1/18/08	74.90

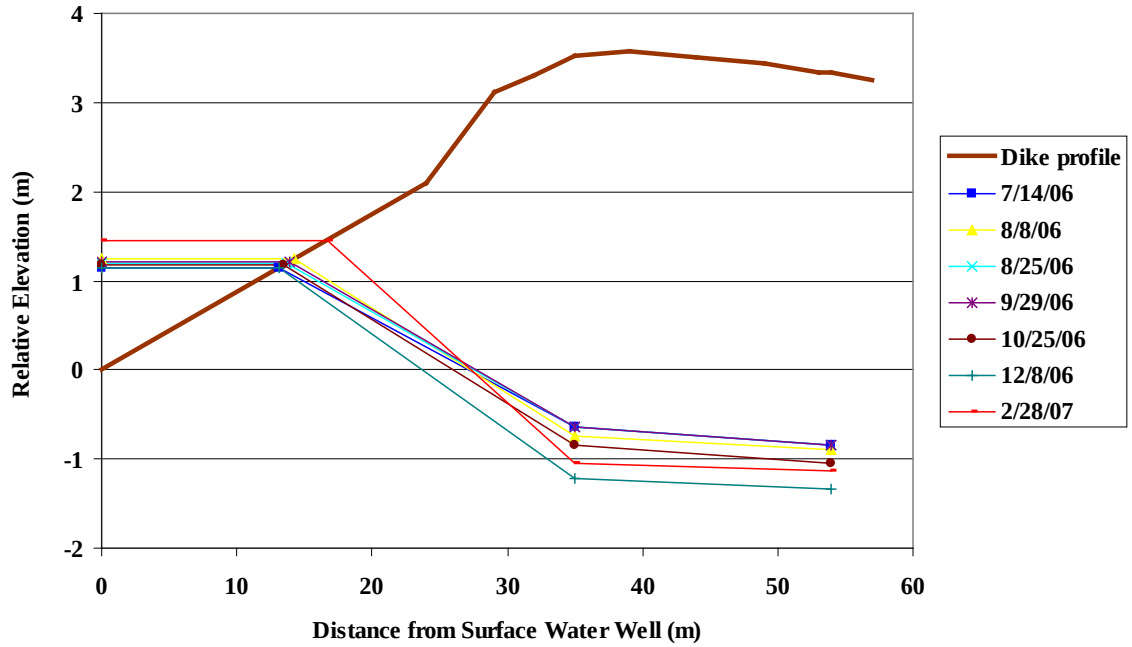

Figure 3-41. Groundwater profiles across the east dike of PCS SA-10

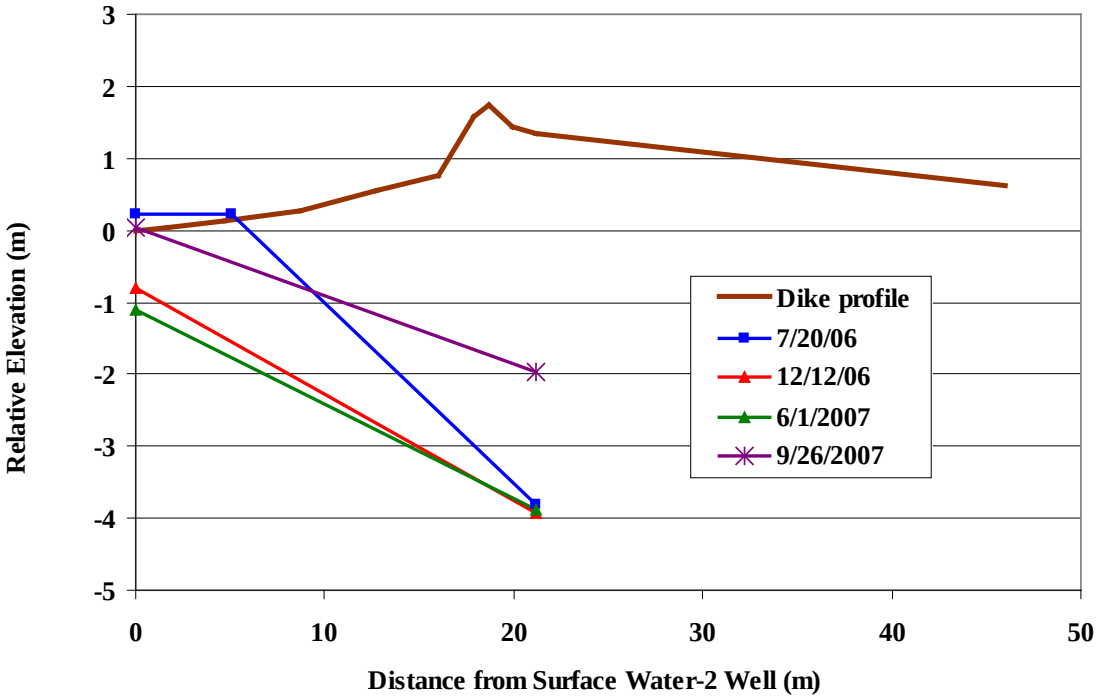

Figure 3-42. Groundwater profiles across the west dike of Mosaic H-1

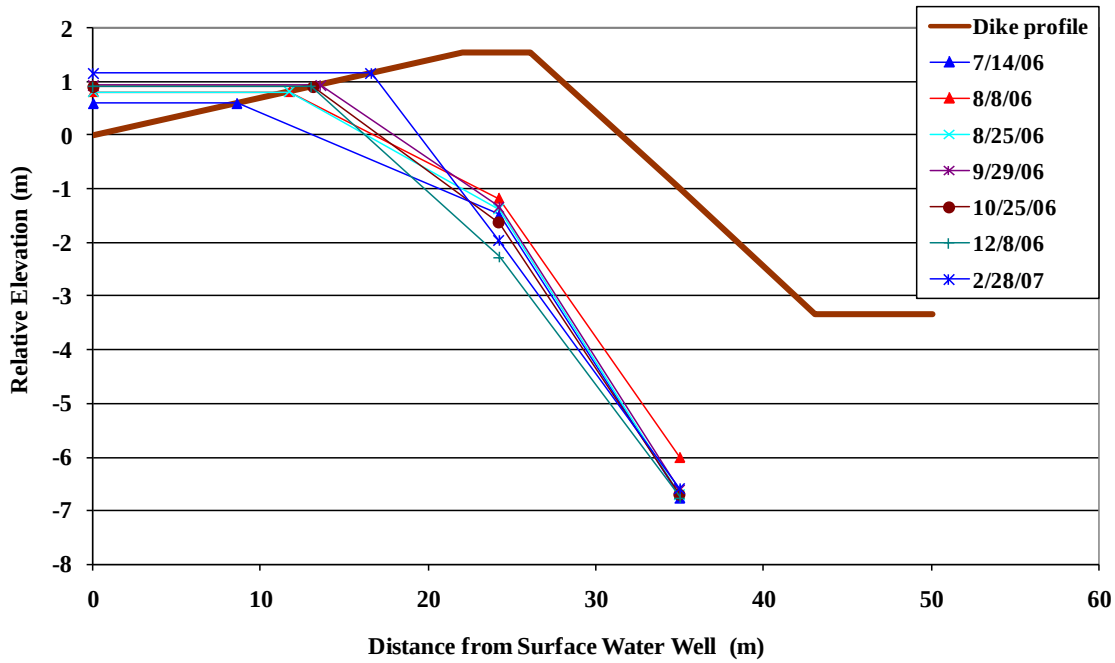

Figure 3-43. Groundwater profiles across the south dike of PCS SA-01

Table 3-11. Average lateral hydraulic conductivities at dike wells

Site	K_{sat} (cm/sec)	Std Dev
PCS SA 10	2.66E-05	1.60E-05
PCS SA 01	3.83E-06	1.48E-06
Mosaic H1	1.54E-06	5.49E-07

Table 3-12. Calculated dike seepage (cm/yr)

D(m)	PCS SA 10	PCS SA 01	Mosiac H1
Surface water	0.69	0.77	0.05
1	0.48	1.99	0.23
5	2.39	3.32	1.13
10	4.79	6.63	2.25

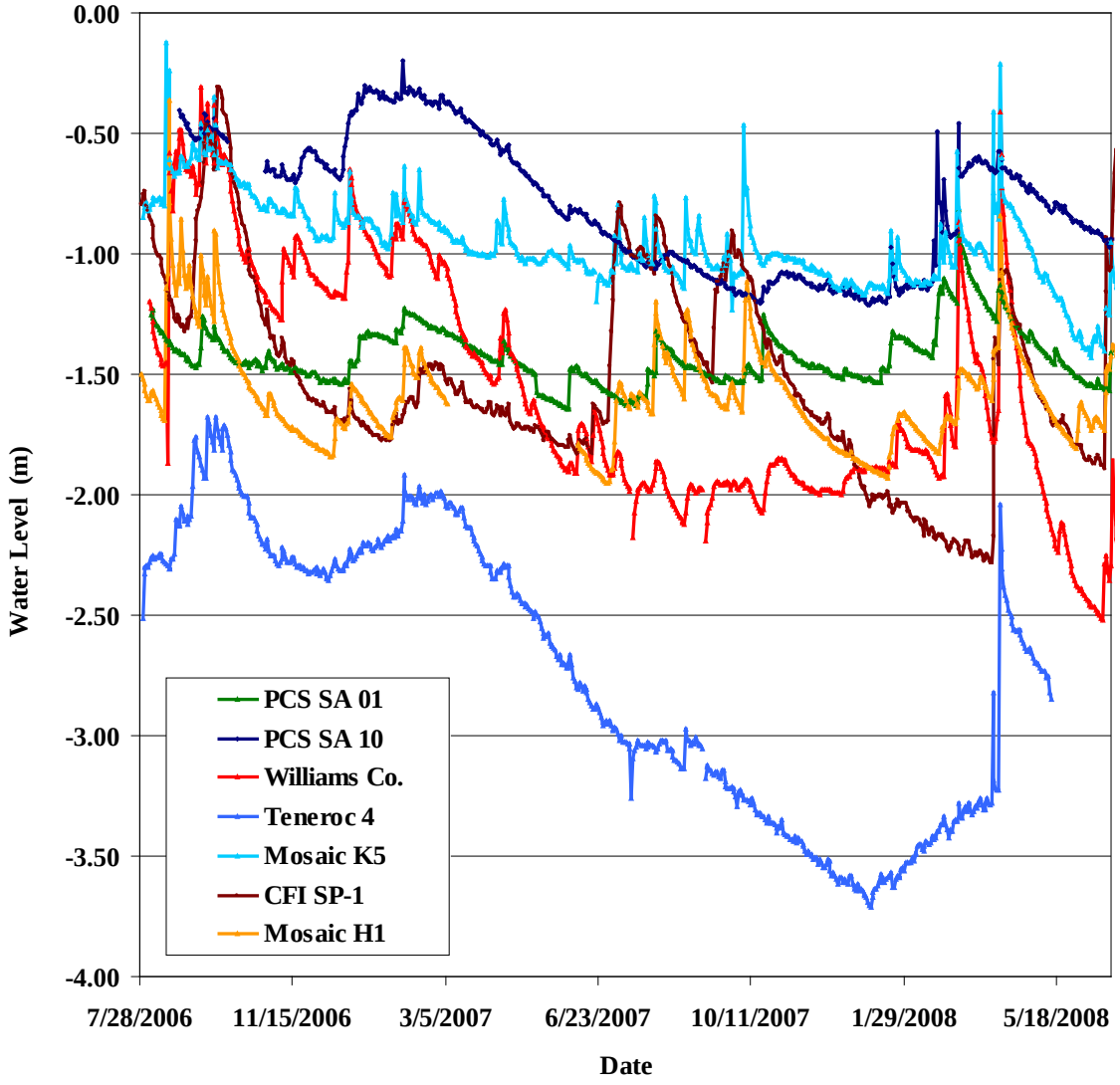

Figure 3-44. Groundwater levels at topographical high interior areas

Table 3-13. Average lateral hydraulic conductivities at groundwater-2 wells

Site	K_{sat} (cm/sec)	Std Dev	Elev. Difference (m)	Well depth (m)	Soil type
Williams Co.	1.42E-06	2.06E-07	1.64	4.34	unconsolidated clay
Mosaic H1	1.34E-04	6.94E-05	2.45	3.66	sandy clay to pure clay
Teneroc 4	4.55E-06	1.09E-06	1.20	5.23	unconsolidated clay
Mosaic K5	3.01E-06	1.26E-06	1.44	3.95	unconsolidated clay
CFI SP-1	1.20E-05	1.69E-06	1.82	4.07	sandy clay
PCSA SA 10	3.77E-04	1.47E-04	3.06	3.16	sandy clay
PCS SA 01	-	-	2.70	3.68	sand
Mosaic HP-10	-	-	2.27	7.24	sand to sandy clay

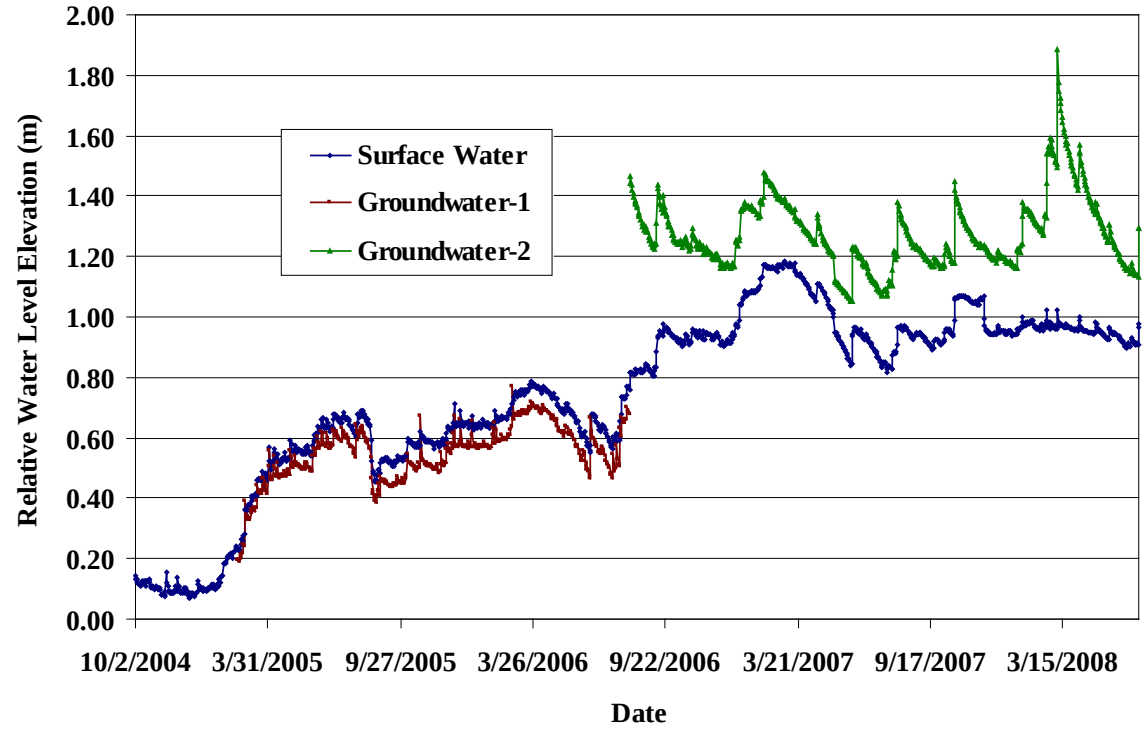

Figure 3-45. Groundwater levels relative to surface water at PCS SA 01

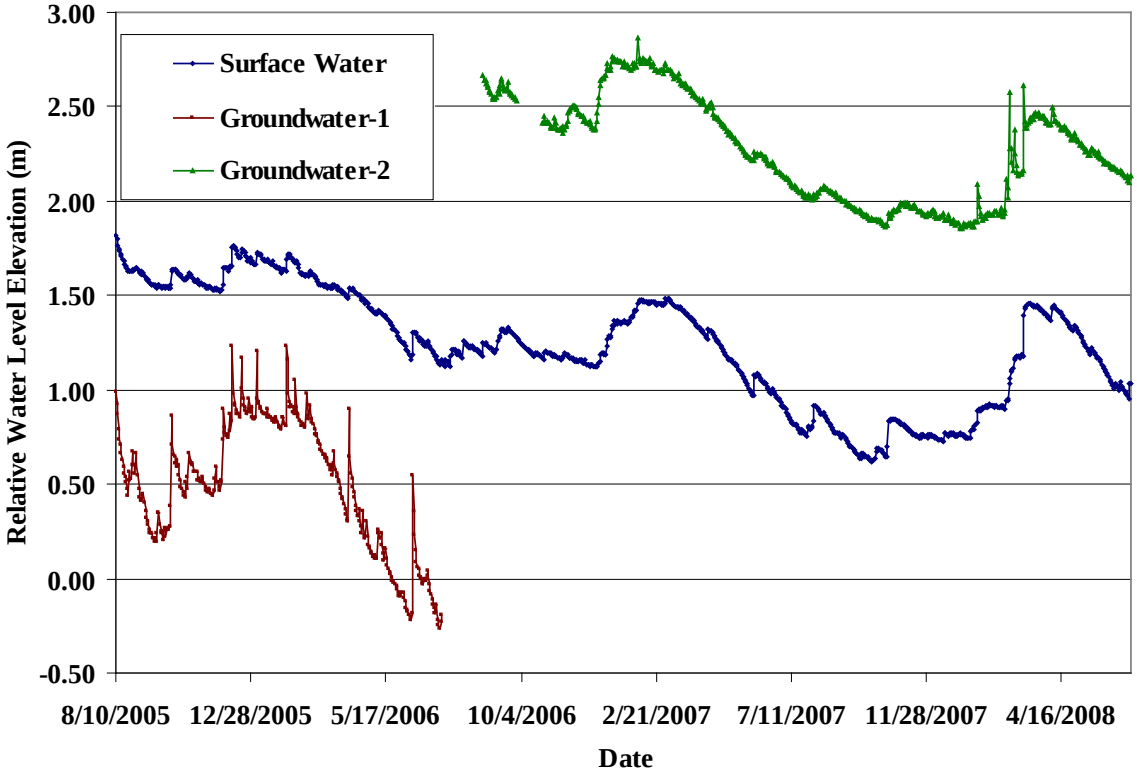

Figure 3-46. Groundwater levels relative to surface water at PCS SA 10

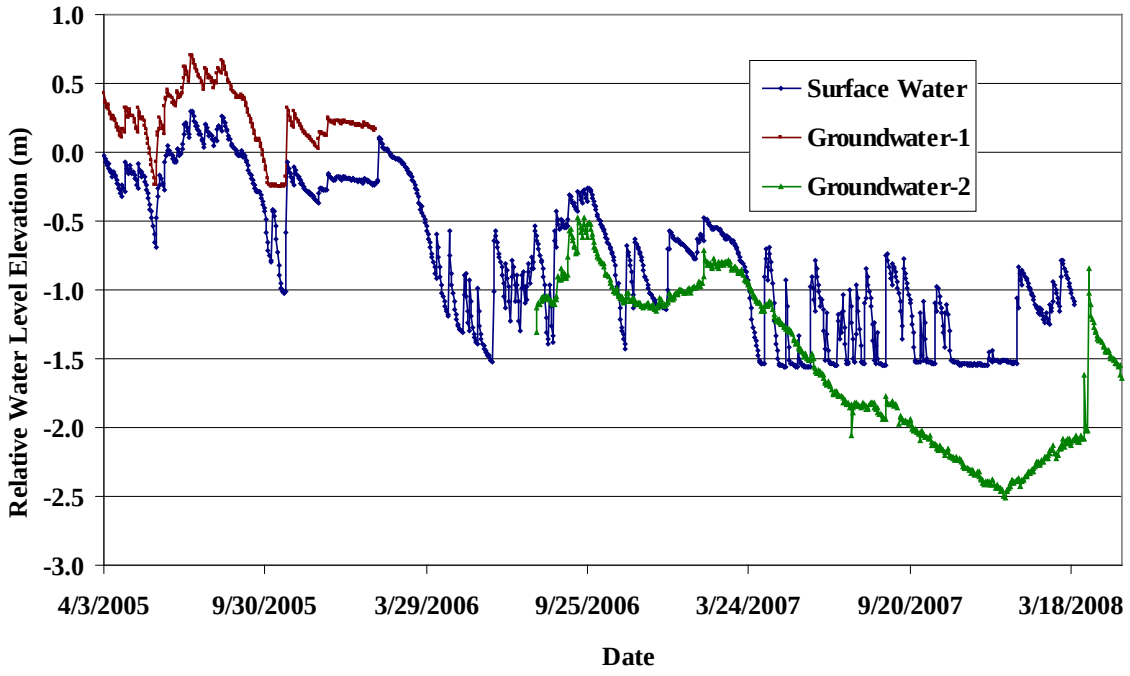

Figure 3-47. Groundwater levels relative to surface water at Tenoroc 4

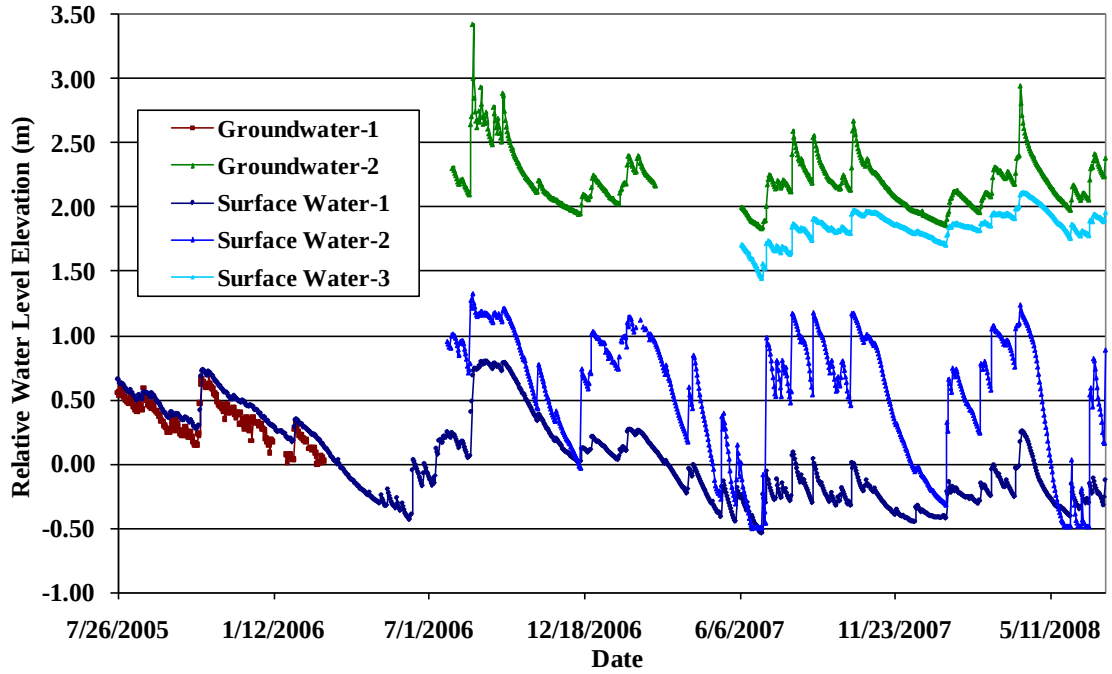

Figure 3-48. Groundwater levels relative to SW-1 at Mosaic H1

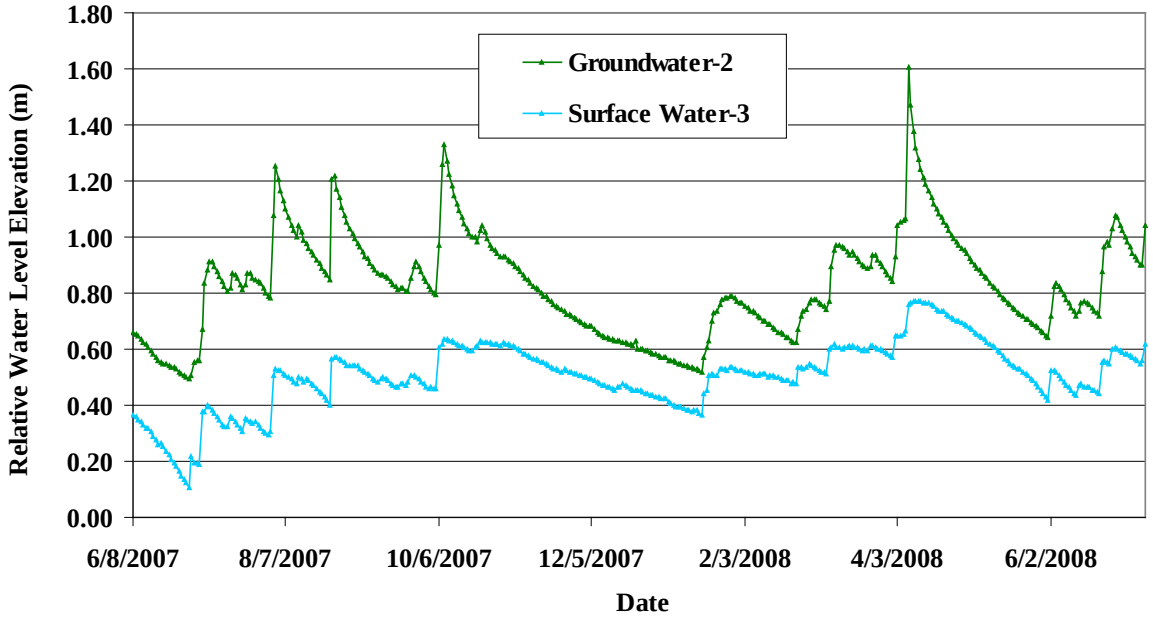

Figure 3-49. Groundwater levels relative to SW-3 at Mosaic H1

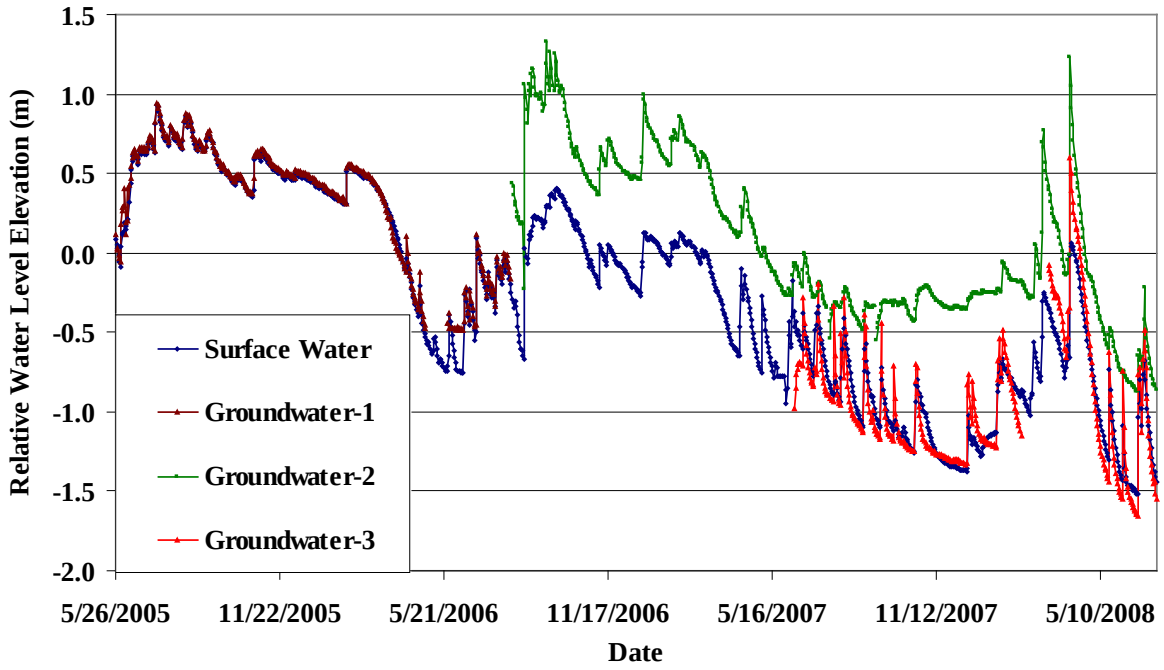

Figure 3-50. Groundwater levels relative to surface water at Williams Co.

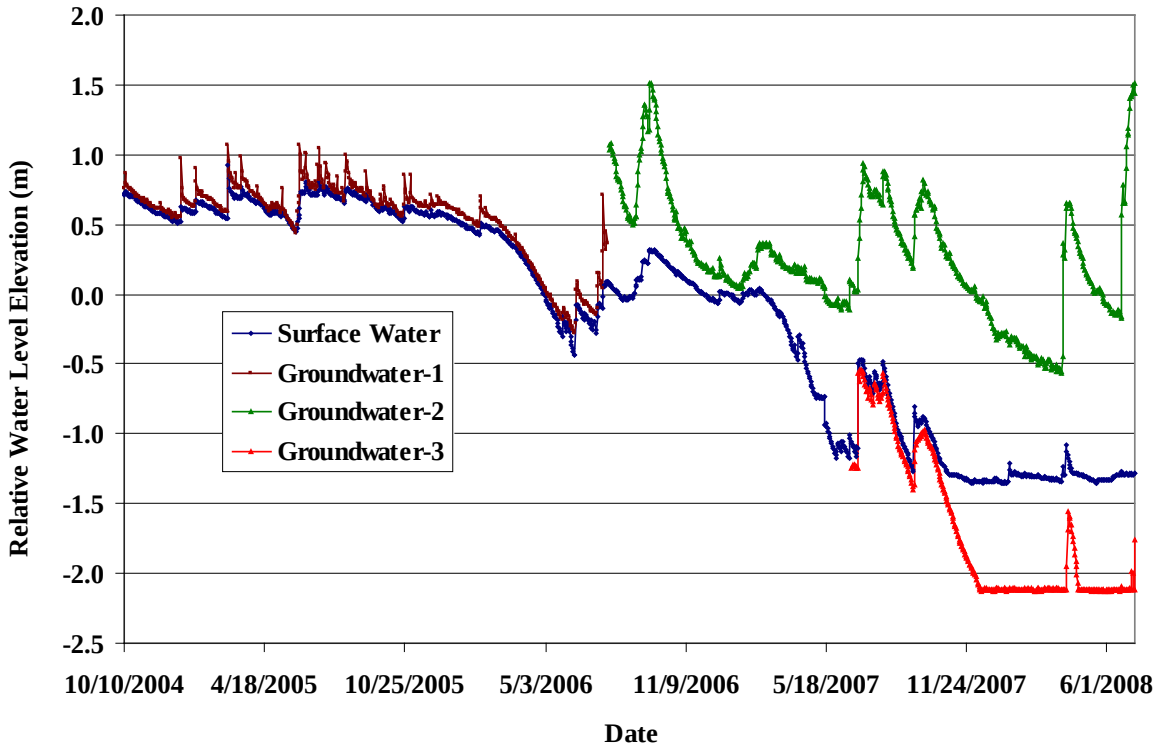

Figure 3-51. Groundwater levels relative to surface water at CFI SP-1

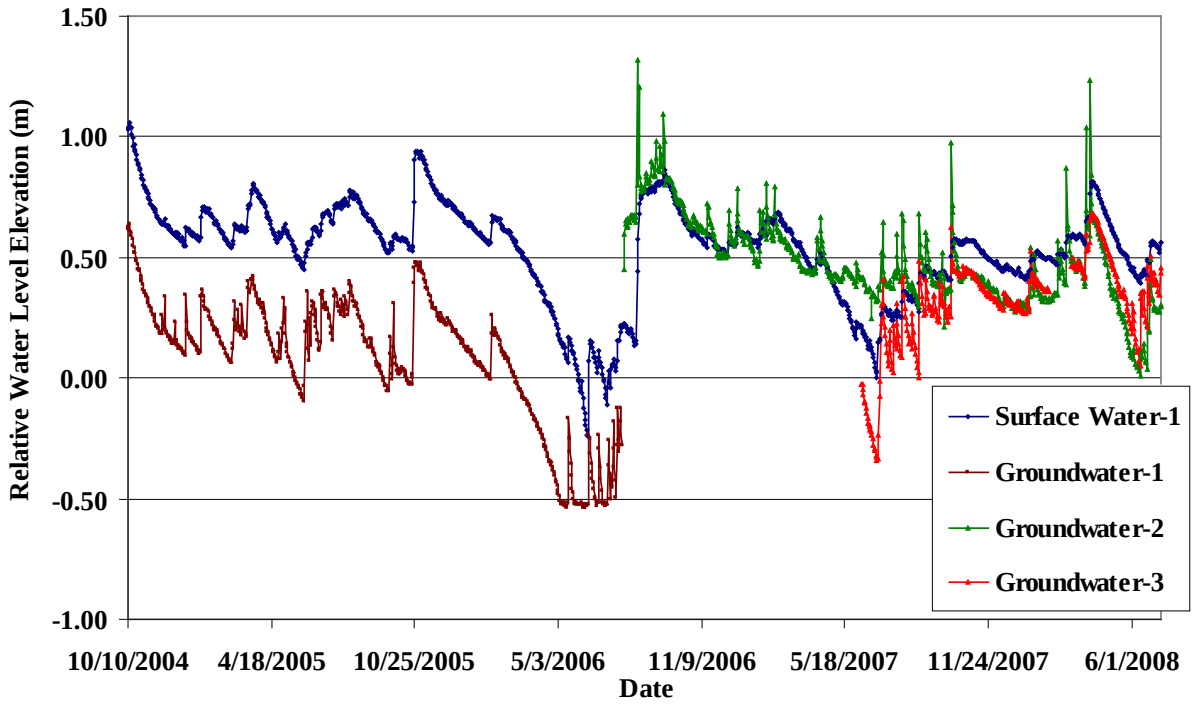

Figure 3-52. Groundwater levels relative to SW-1 at Mosaic K5

Table 3-14. Daily decline summary for PCS SA 10 SW-1

Month	Slope (mm/day)	R^2	ET (mm/day)	Δ(mm/day)
May	-7.48	0.91	4.88	-2.60
June	-10.03	0.88	5.51	-4.52
July	-10.67	0.92	6.24	-4.43
August	-7.03	0.74	5.92	-1.11
Sept	-7.01	0.84	5.04	-1.97
			average=	-2.92

Table 3-15. Daily decline summary for PCS SA 01

Month	Slope (mm/day)	R^2	ET (mm/day)	Δ(mm/day)
May	-9.14	0.85	4.88	-4.26
June	-6.22	0.78	5.51	-0.71
July	-6.60	0.80	6.24	-0.36
			average=	-1.78

Table 3-16. Daily decline summary for Tenoroc 4.

Month	Slope (mm/day)	R^2	ET (mm/day)	Δ(mm/day)
June	-17.53	0.92	5.51	-12.01
July	-22.27	0.97	6.24	-16.03
August	-21.72	0.97	5.92	-15.80
Feb	-11.30	0.87	2.67	-8.63
			average=	-13.12

Table 3-17. Daily decline summary for Mosaic K 5 SW-1

Month	Slope (mm/day)	R^2	ET (mm/day)	Δ(mm/day)
May	-12.62	0.91	4.88	-7.73
June	-15.24	0.96	5.51	-9.73
August	-11.18	0.84	5.92	-5.26
			average=	-7.57

Table 3-18. Daily decline summary for CFI SP-1

Month	Slope (mm/day)	R^2	ET (mm/day)	Δ(mm/day)
Nov	-3.47	0.63	3.06	-0.41
Dec	-2.37	0.52	2.15	-0.22
Feb	-3.81	0.88	2.67	-1.14
March	-5.59	0.98	3.08	-2.51
April	-7.70	0.93	3.73	-3.98
May	-8.13	0.97	4.88	-3.25
July	-8.13	0.85	6.24	-1.89
Aug	-7.37	0.92	5.92	-1.45
Sept	-6.60	0.79	5.04	-1.57
Oct	-6.10	0.93	3.93	-2.17
			average=	-1.86

Table 3-19. Daily decline summary for Mosaic H1 SW-1

Month	Slope (mm/day)	R^2	ET (mm/day)	Δ(mm/day)
Aug	-17.72	0.90	5.92	-11.80
Sept	-10.92	0.96	5.04	-5.88
Oct	-9.31	0.91	3.93	-5.39
Nov	-9.40	0.99	3.06	-6.34
Dec	-7.49	0.89	2.15	-5.34
Feb	-6.86	0.96	2.67	-4.19
March	-8.64	0.92	3.08	-5.55
			average=	-6.36

Table 3-20. Daily decline summary for Williams Co.

Month	Slope (mm/day)	R^2	ET (mm/day)	Δ(mm/day)
July	-23.37	0.93	6.24	-17.13
Aug	-25.15	0.95	5.92	-19.23
Sept	-14.48	0.90	5.04	-9.44
Oct	-9.40	0.94	3.93	-5.47
Nov	-9.40	0.86	3.06	-6.34
Dec	-4.32	0.90	2.15	-2.17
Jan	-4.57	0.83	2.46	-2.11
Feb	-5.33	0.83	2.67	-2.66
March	-13.21	0.99	3.08	-10.13
			average=	-8.30

Table 3-21. Average daily decline and ET estimates (mm/day)

	Growing Season	Non-Growing Season
Average of 8 sites	12.08	7.27
Penman ET	4.84	3.37
Fl *Typha* Marsh ET [1]	4.14	2.17
Fl *Cladium* Marsh ET[1]	5.93	2.06

[1]Mao *et al.* (2002).

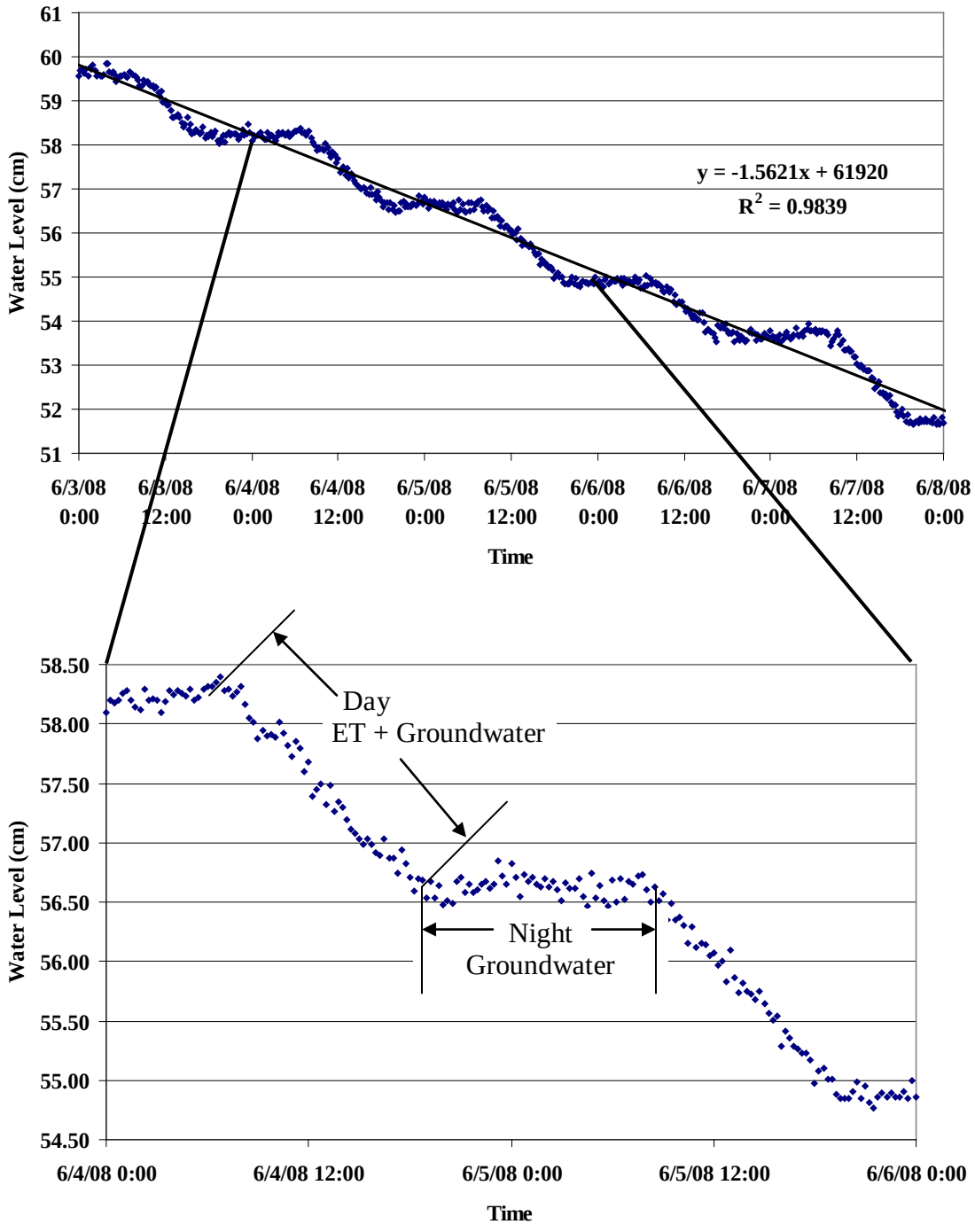

Figure 3-53. Surface water level decline and example of White method at Mosaic K5 SW-2

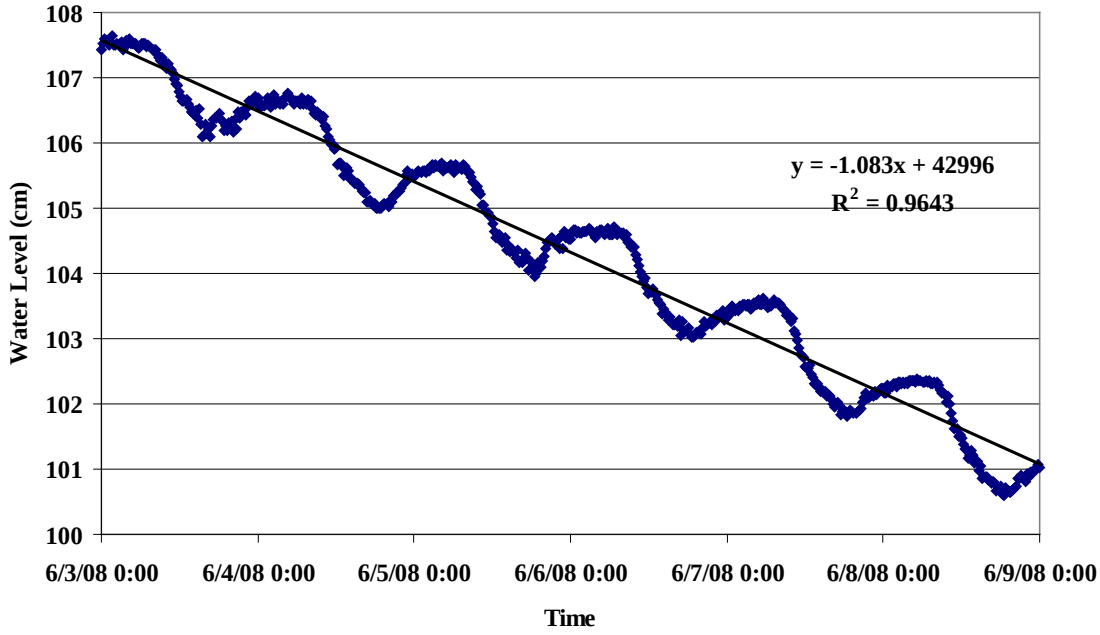

Figure 3-54. Surface water level decline at PCS SA 10

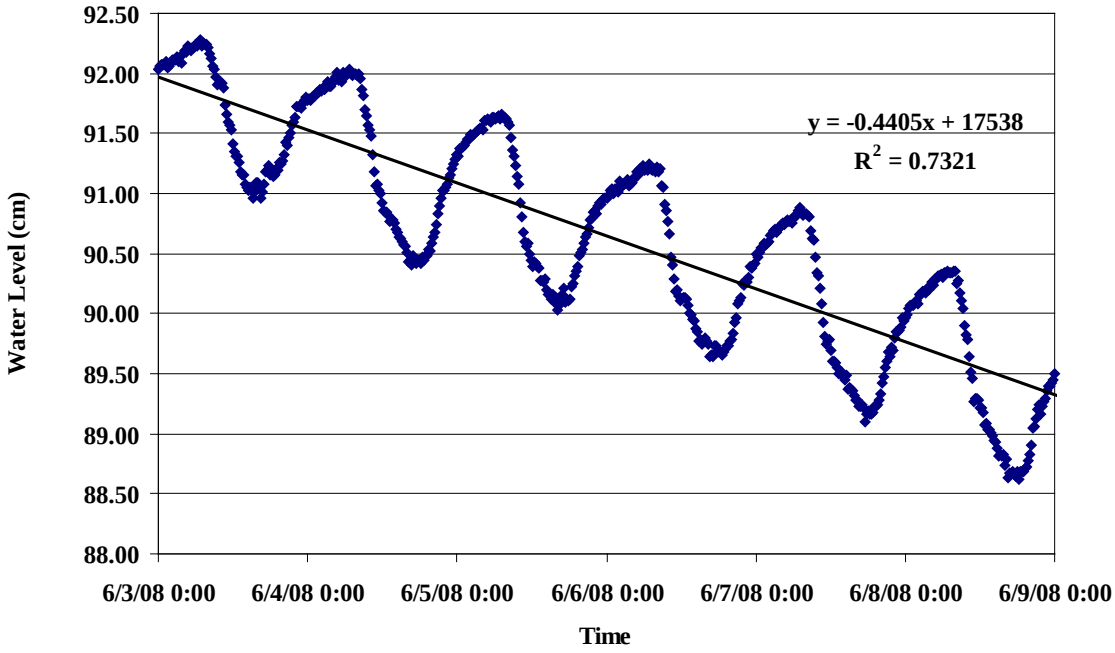

Figure 3-55. Surface water level decline at PCS SA 01

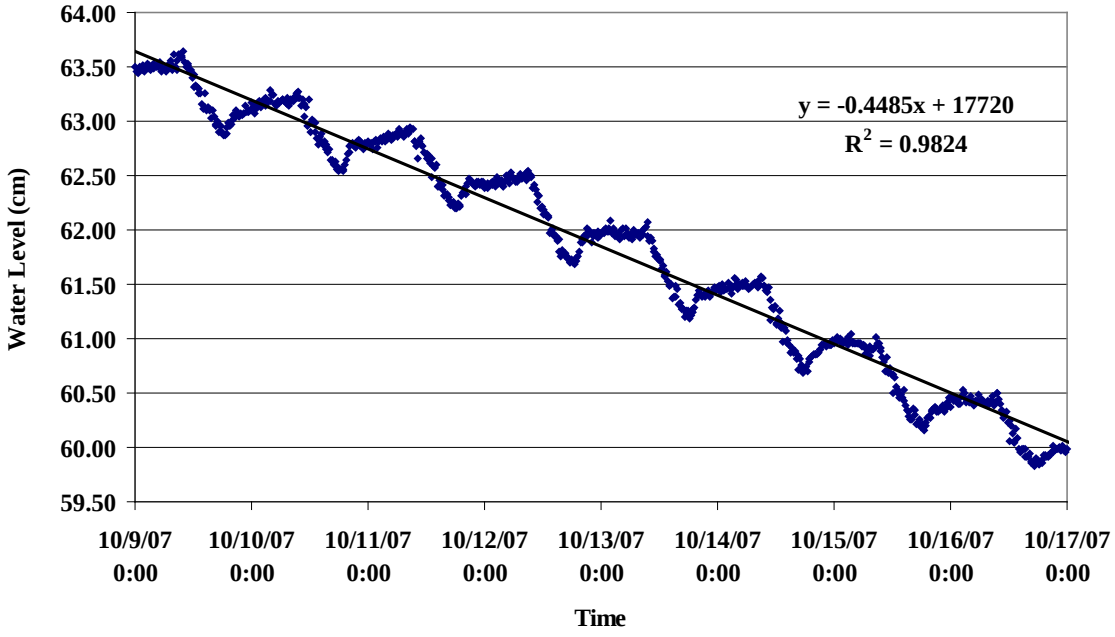

Figure 3-56. Surface water level decline at Mosaic H1 SW-3

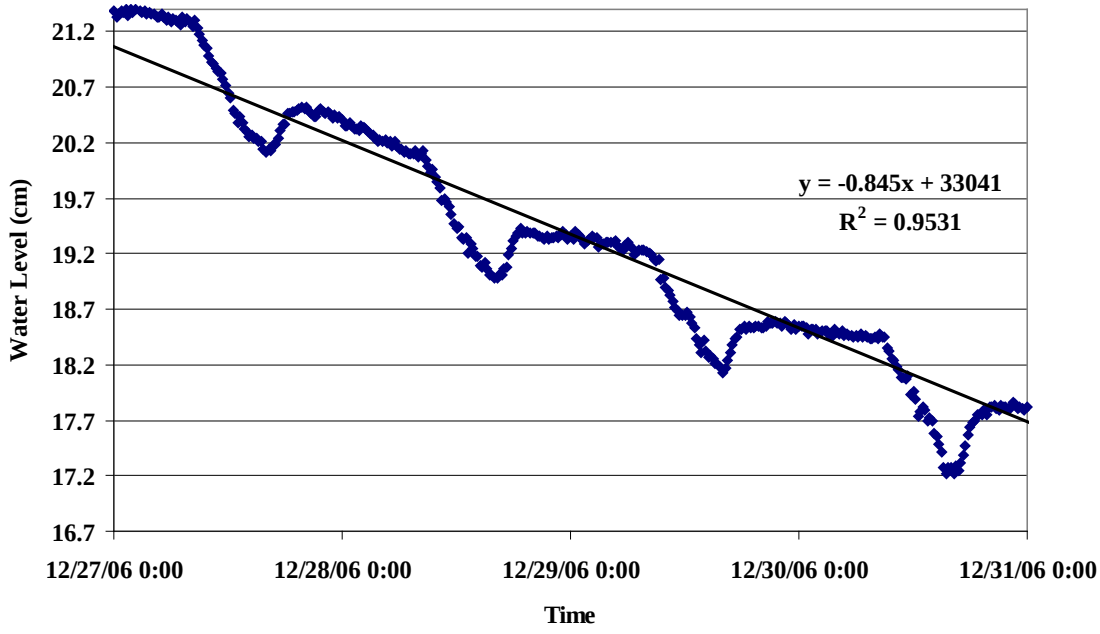

Figure 3-57. Surface water level decline at Mosaic H1 SW-1

Table 3-22. Calculated rates, daily decline, and Penman ET (cm/day) at Mosaic K5

Month	Sampled Days	White ET	White Infiltration	Daily Decline	Penman ET
January	10	1.42	-1.07	0.40	0.23
February	15	1.26	-0.91	0.29	0.29
March	12	1.51	-1.00	0.49	0.43
April	20	1.07	-0.56	0.60	0.52
May	23	1.56	-0.70	0.85	0.57
June	12	1.74	0.10	1.84	0.53
July	13	2.72	0.29	3.06	0.48
August	8	2.62	-0.75	1.84	0.50
September	9	1.62	-0.70	0.87	0.44
October	9	0.82	-0.68	0.22	0.36
November	20	1.05	-0.68	0.41	0.26
December	12	1.34	-0.98	0.26	0.21

Table 3-23. Calculated rates, daily decline, and Penman ET (cm/day) at PCS SA 10

Month	Sampled Days	White ET	White Infiltration	Daily Decline	Penman ET
January	9	0.92	-0.68	0.32	0.16
February	4	1.24	-0.96	0.24	0.24
March	13	1.69	-1.28	0.40	0.34
April	17	1.44	-0.85	0.66	0.44
May	31	1.45	-0.63	0.91	0.54
June	13	1.44	-0.43	1.03	0.56
July	0	-	-	-	0.56
August	14	1.02	-0.11	0.89	0.53
September	21	0.92	-0.22	0.70	0.44
October	10	1.00	-0.48	0.54	0.30
November	21	0.99	-0.61	0.41	0.22
December	12	1.01	-0.78	0.25	0.16

Table 3-24. Calculated rates, daily decline, and Penman ET (cm/day) at PCS SA 01

Month	Sampled Days	White ET	White Infiltration	Daily Decline	Penman ET
January	10	1.10	-1.00	0.17	0.16
February	11	1.22	-0.96	0.27	0.24
March	17	1.77	-1.53	0.25	0.34
April	16	1.72	-1.50	0.31	0.44
May	16	1.70	-1.41	0.29	0.54
June	30	1.65	-1.22	0.46	0.56
July	13	1.43	-0.78	0.69	0.56
August	12	1.23	-0.88	0.35	0.53
September	18	1.11	-0.78	0.35	0.44
October	10	1.13	-0.89	0.27	0.30
November	21	1.00	-0.91	0.14	0.22
December	10	1.30	-1.23	0.06	0.16

Table 3-25. Calculated rates, daily decline, and Penman ET (cm/day) at Mosaic H1 SW-3

Month	Sampled Days	White ET	White Infiltration	Daily Decline	Penman ET
January	10	0.49	-0.07	0.39	0.23
February	13	0.48	-0.15	0.32	0.29
March	12	0.76	-0.32	0.46	0.43
April	12	0.50	-0.23	0.35	0.52
May	20	1.05	-0.20	0.85	0.57
June	25	1.06	-0.06	1.04	0.53
July	15	1.01	-0.05	1.03	0.48
August	10	0.84	0.01	0.87	0.50
September	12	0.68	0.05	0.74	0.44
October	9	0.60	-0.18	0.45	0.36
November	22	0.60	-0.15	0.46	0.26
December	12	0.61	-0.22	0.40	0.21

Table 3-26. Calculated rates, daily decline, and Penman ET (cm/day) at Mosaic H1 SW-1

Month	Sampled Days	White ET	White Infiltration	Daily Decline	Penman ET
January	17	0.54	0.19	0.73	0.23
February	11	0.71	0.23	0.96	0.29
March	-	-	-	-	0.43
April	6	1.08	0.77	1.84	0.52
May	-	-	-	-	0.57
June	-	-	-	-	0.53
July	-	-	-	-	0.48
August	-	-	-	-	0.50
September	-	-	-	-	0.44
October	-	-	-	-	0.36
November	-	-	-	-	0.26
December	4	0.39	0.45	0.85	0.21

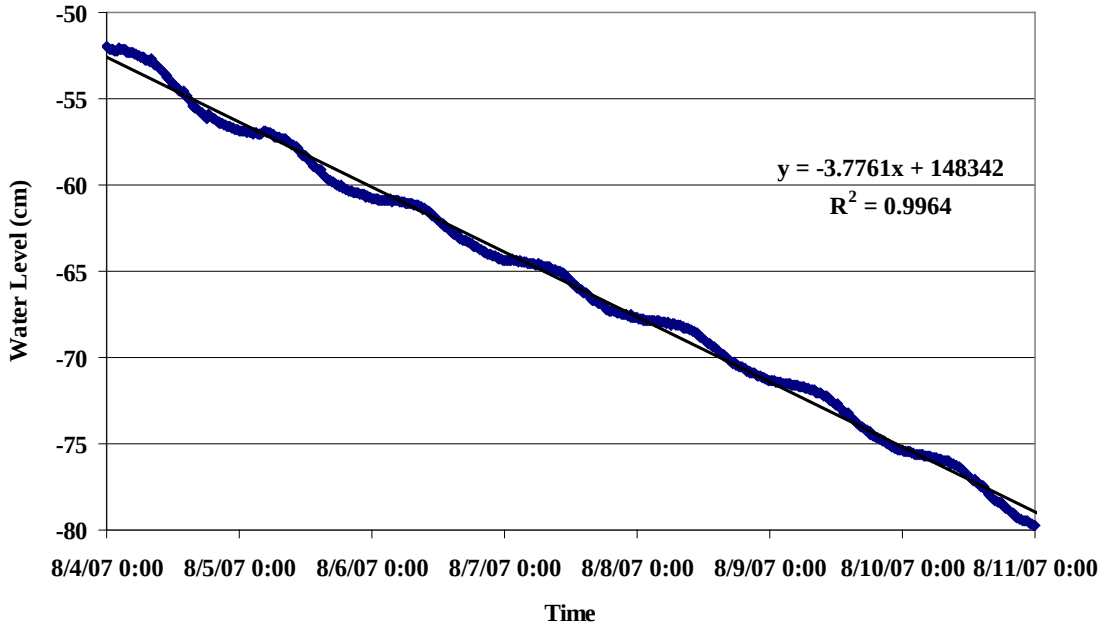

Figure 3-58. Water table decline at Williams Co.

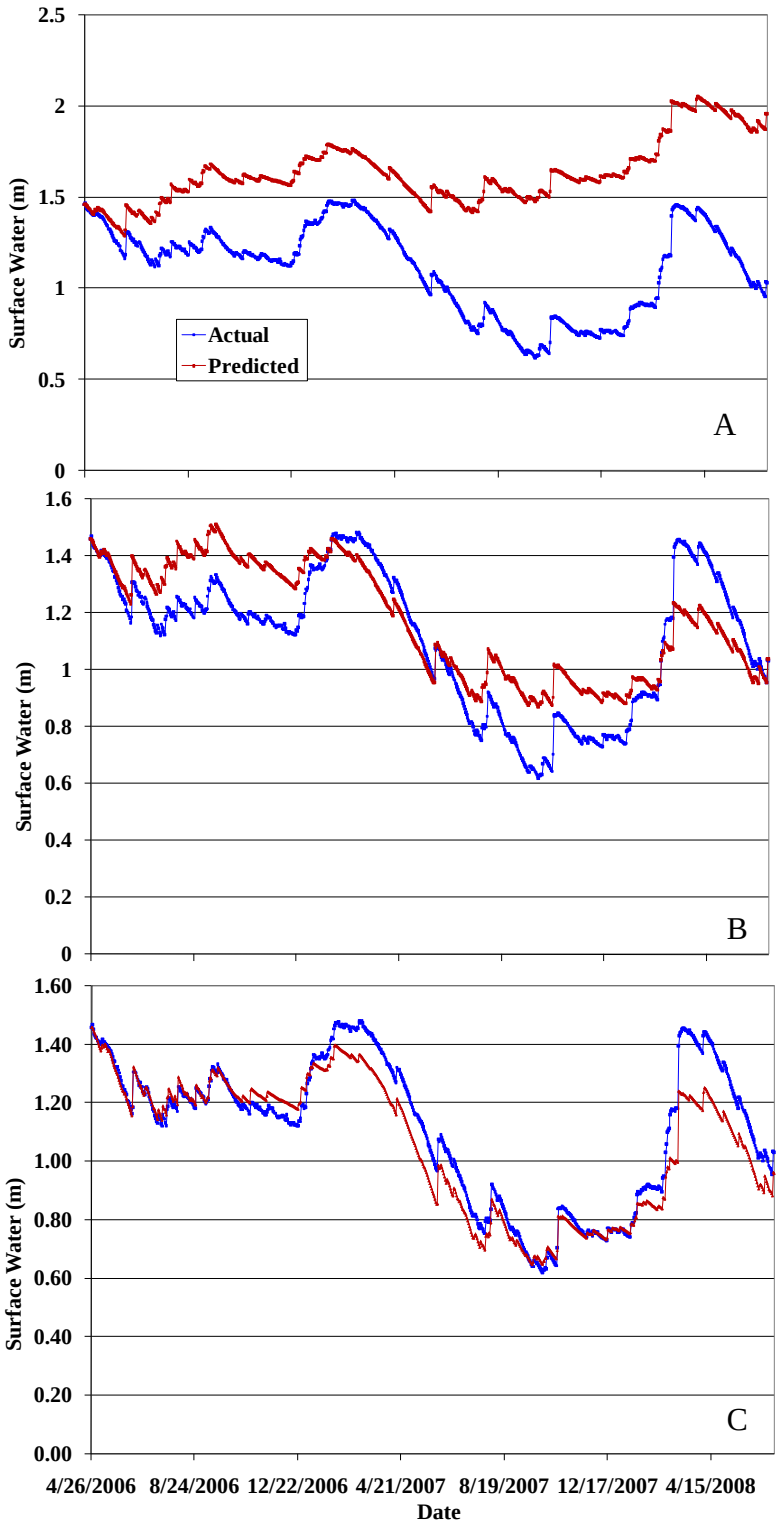

Figure 3-59. Simulation results for PCS SA 10 compared to measured stage. A) Simulation results with zero infiltration. B) Simulation results with I=1.16 mm/day. C) Simulation results with growing season Penman ET increased by 50%, non-growing season Penman ET increased by 10%, and no infiltration.

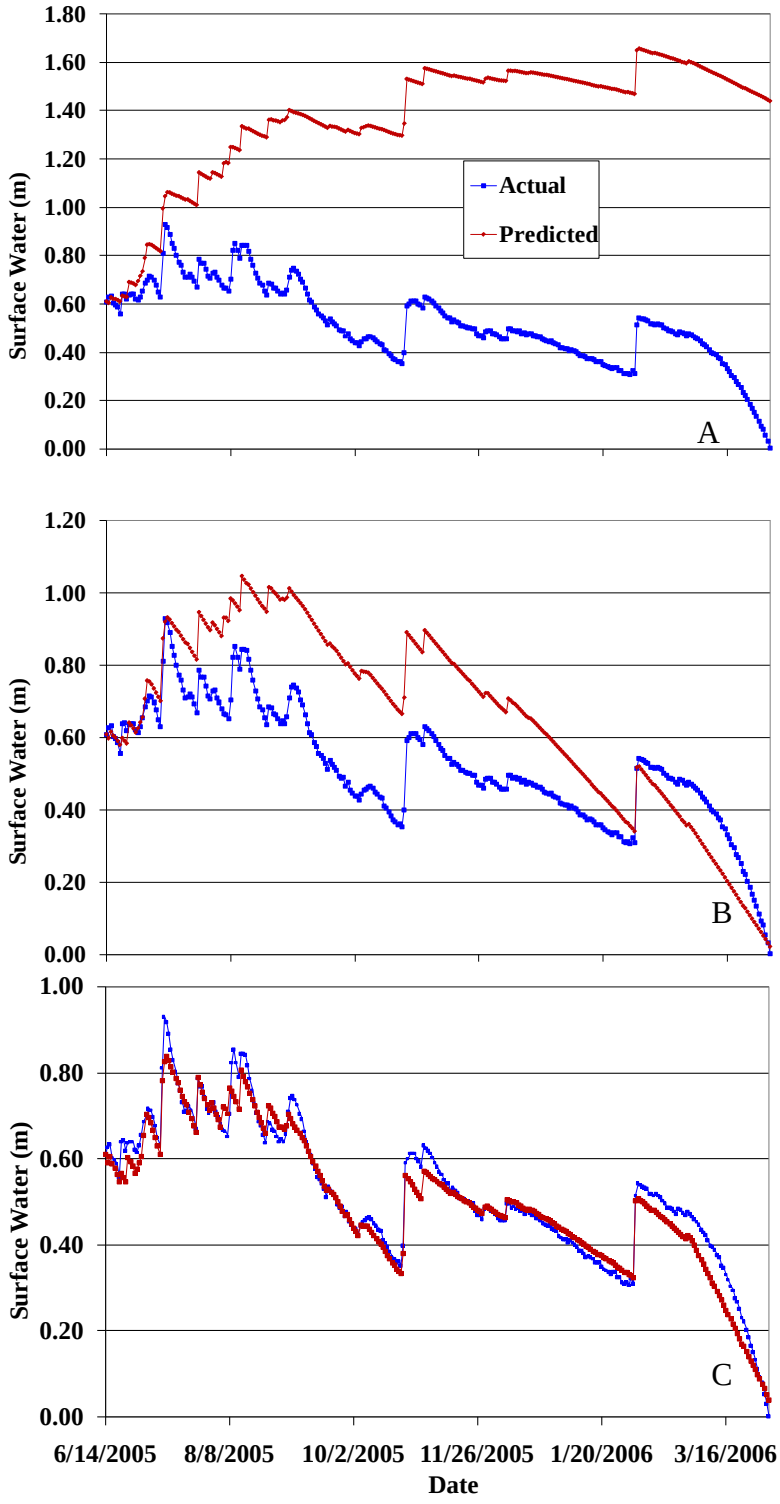

Figure 3-60. Simulation results for Williams Co. compared to measured stage. A) Simulation results with zero infiltration. B) Simulation results with I=4.87 mm/day. C) Simulation results with growing season Penman ET increased by 110%, non-growing season Penman ET decreased by 40%, and I=2.54 mm/day.

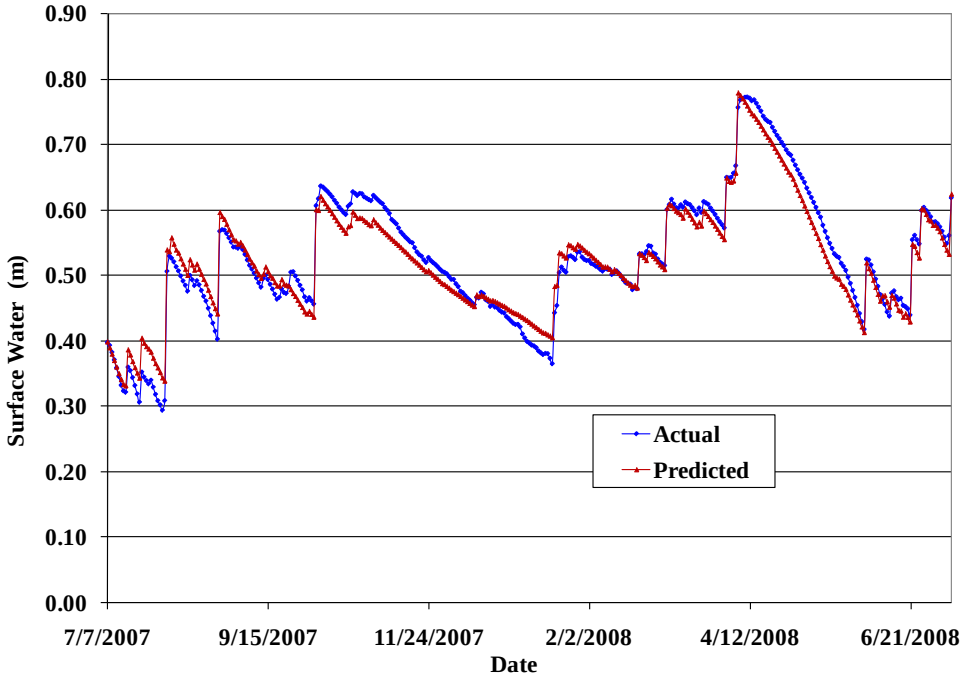

Figure 3-61. Simulation results for Mosaic H1 SW-3 compared to measured stage with growing season Penman ET increased by 40% and no infiltration.

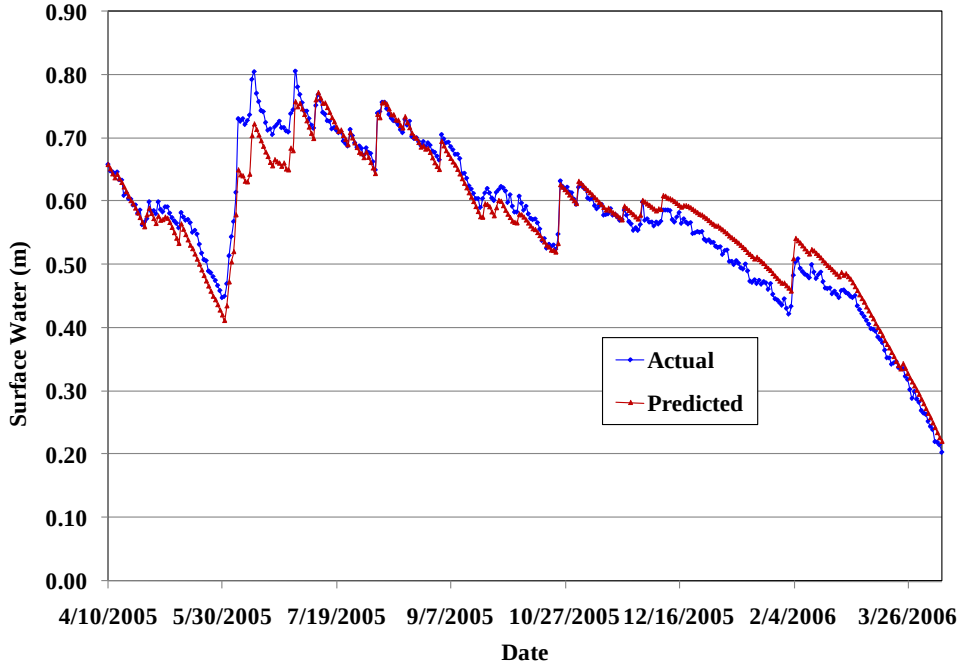

Figure 3-62. Simulation results for CFI SP-1 compared to measured stage with growing season Penman ET increased by 30%, non-growing Penman ET increased by 10%, and no infiltration.

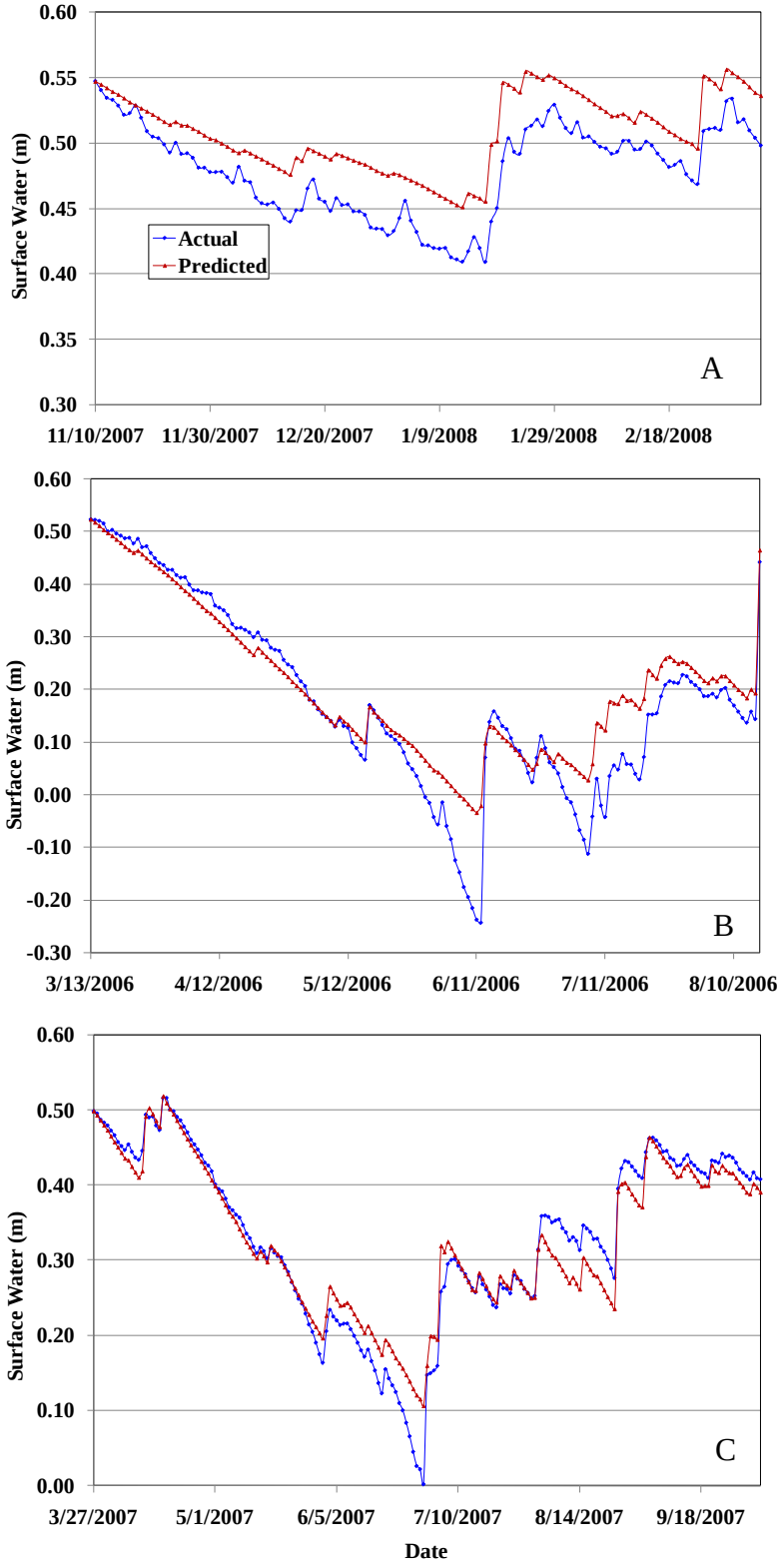

Figure 3-63. Simulation results for Mosaic K5 compared to measured stage with growing season Penman ET increased by 40% and no infiltration. A) Results for 11/10/07 to 3/5/08. B) Results for 3/13/06 to 8/15/06. C) Results for 3/27/07 to 10/4/07

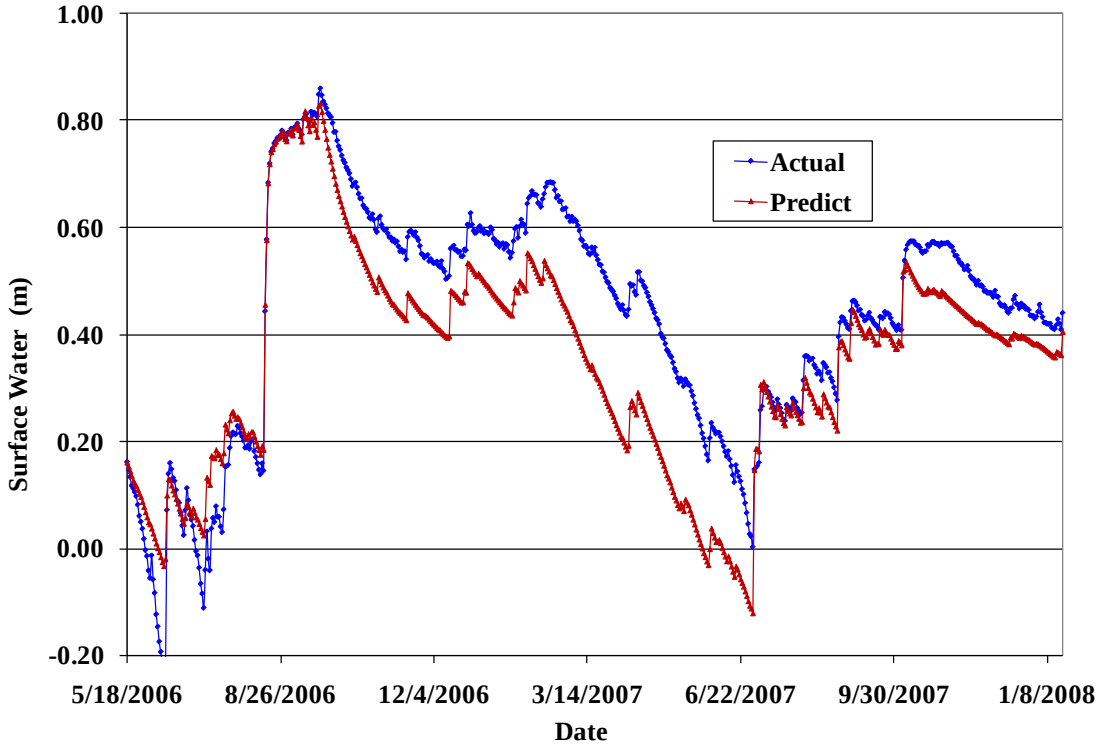

Figure 3-64. Simulation results for Mosaic K5 compared to measured stage with growing season Penman ET increased by 40%, channel flow, and no infiltration.

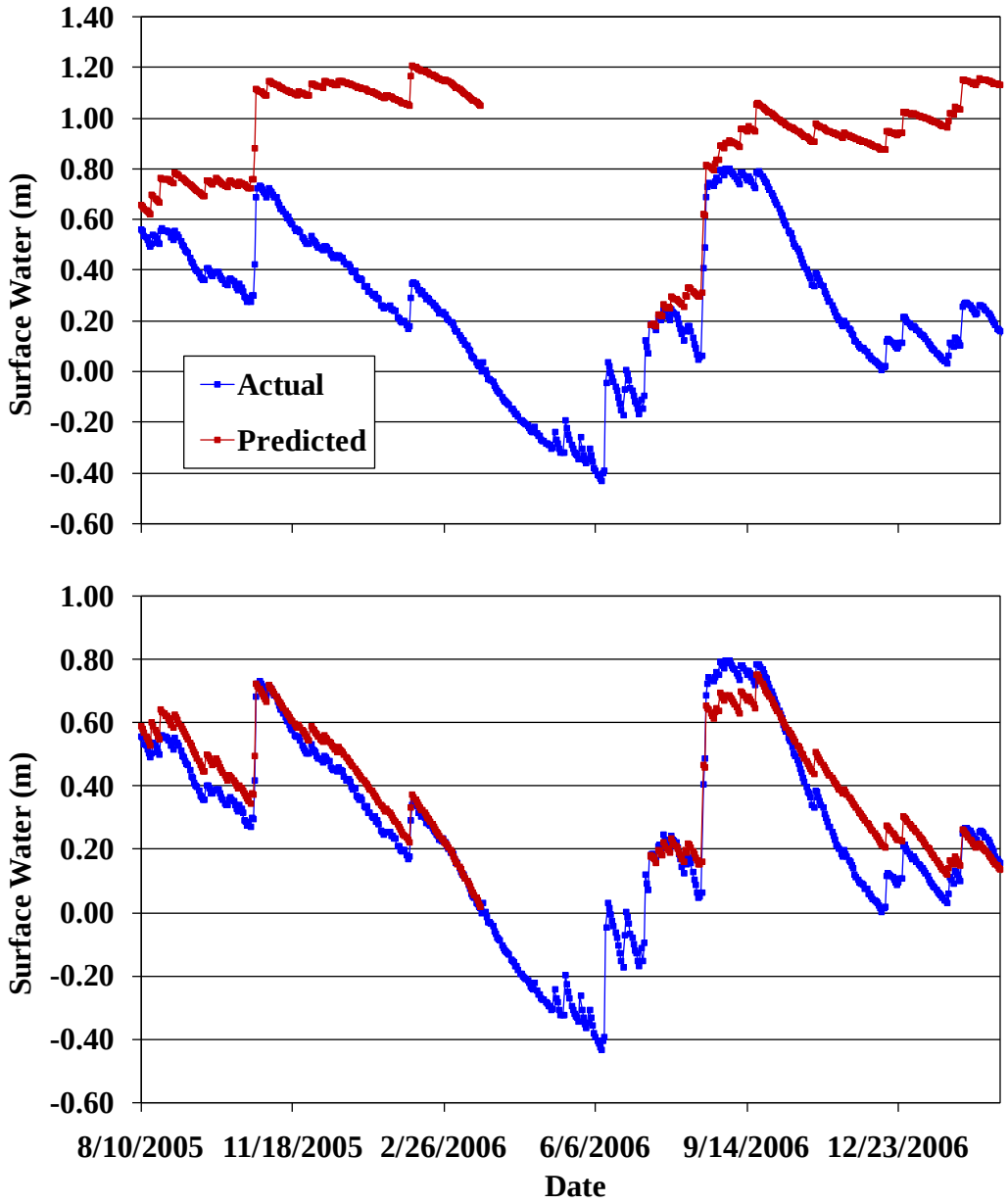

Figure 3-65. Simulation results for Mosaic H1 SW-1 compared to measured stage. A) Simulation results with no infiltration. B) Simulation results with I=4.30 mm/day.

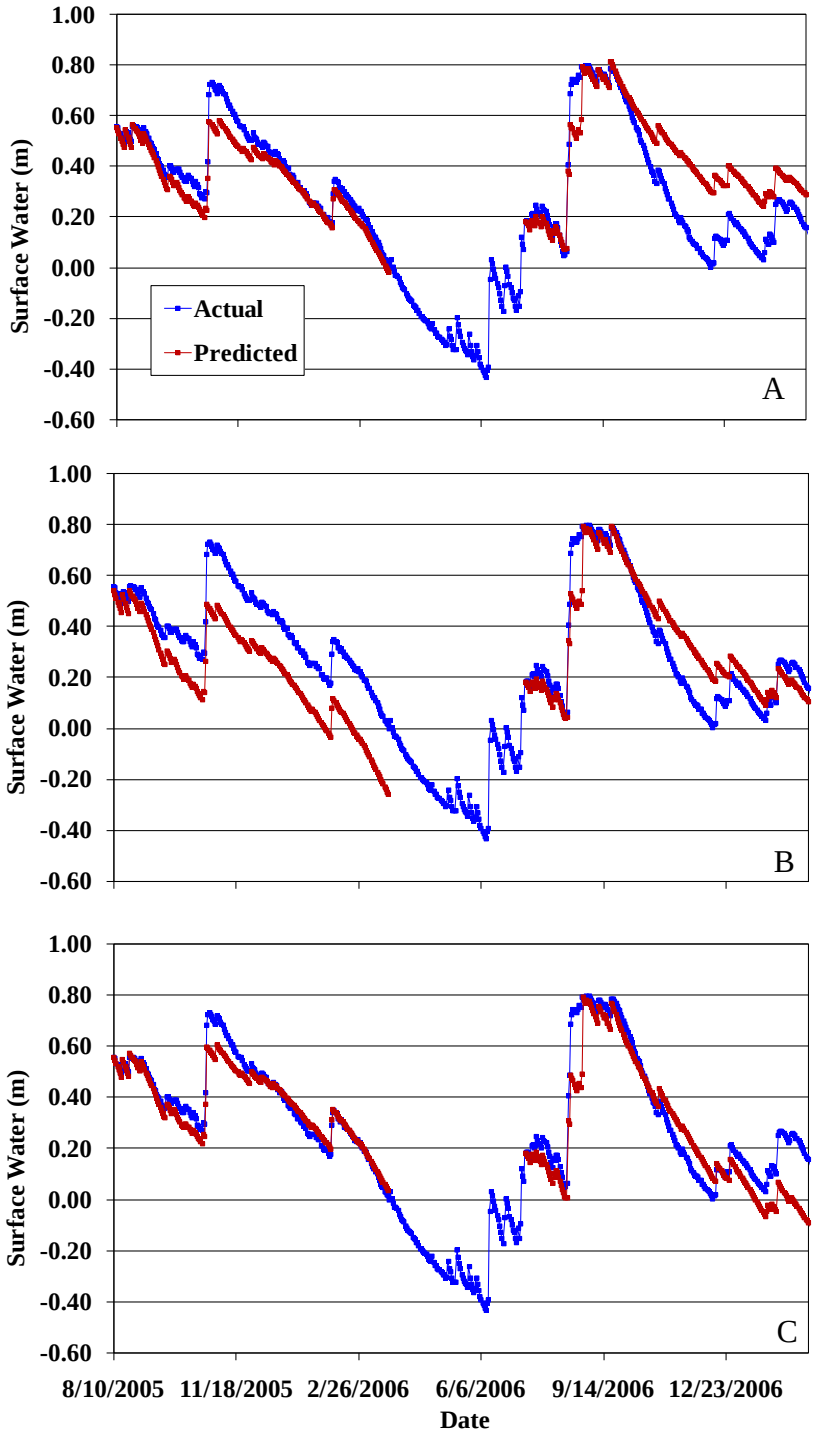

Figure 3-66. Simulation results for Mosaic H1 SW-1 compared to measured stage with growing season Penman ET increased by 70% and non-growing season Penman ET increased by 20%. A) Simulation results with I=3.00 mm/day. B) Simulation results with I=4.00 mm/day. C) Simulation results with I_1=2.79 mm/day and I_2=5.08 mm/day.

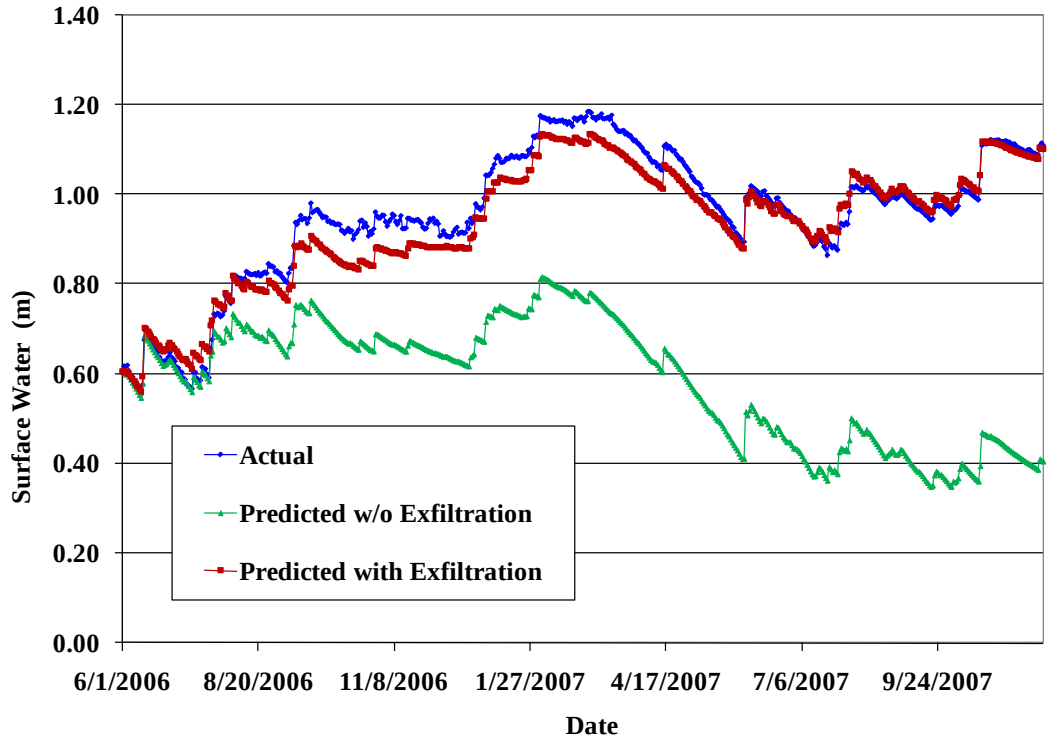

Figure 3-67. Simulation results for PCS SA 01 compared to measured stage without exfiltration and with exfiltration=1.2mm/day.

Table 3-27. Modeling results summary

	Seasonal ET Coefficients		Infiltration	
Site	Growing	Non-Growing	(mm/day)	R^2
PCS SA 10	1.5	1.0	0	0.87
Williams Co.	2.1	0.6	2.54	0.95
Mosaic H1 SW-3	1.4	1.0	0	0.93
CFI SP-1	1.3	1.1	0	0.94
Mosaic K5	1.4	1.0	0	0.91
Mosaic H1 SW-1	1.7	1.2	2.79; 5.08	0.83
PCS SA 01	1.0	1.0	-1.20	0.92

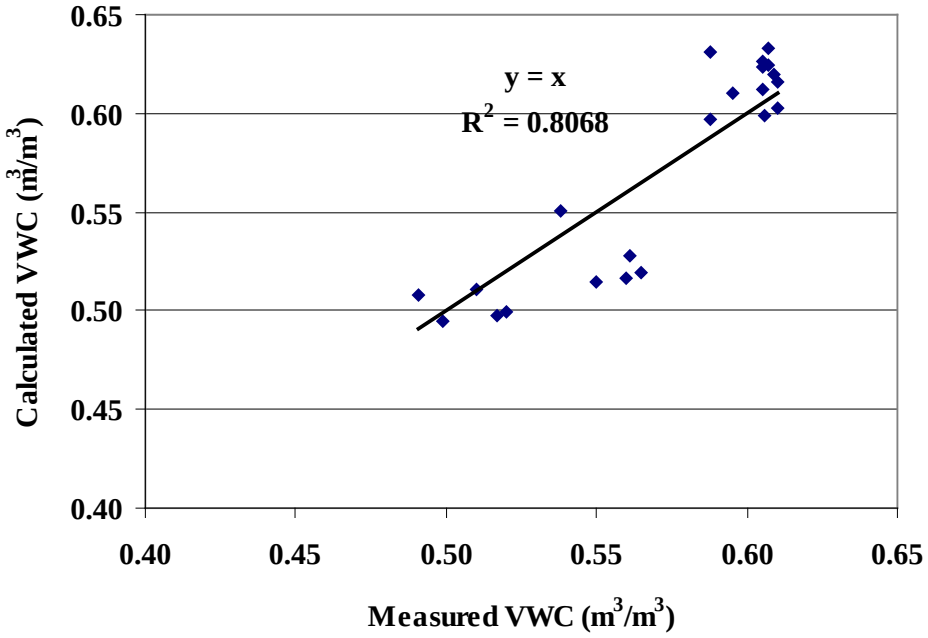

Figure 3-68. Calculated VWC using GWC versus measured VWC with EC-5 probes for Mosaic K5

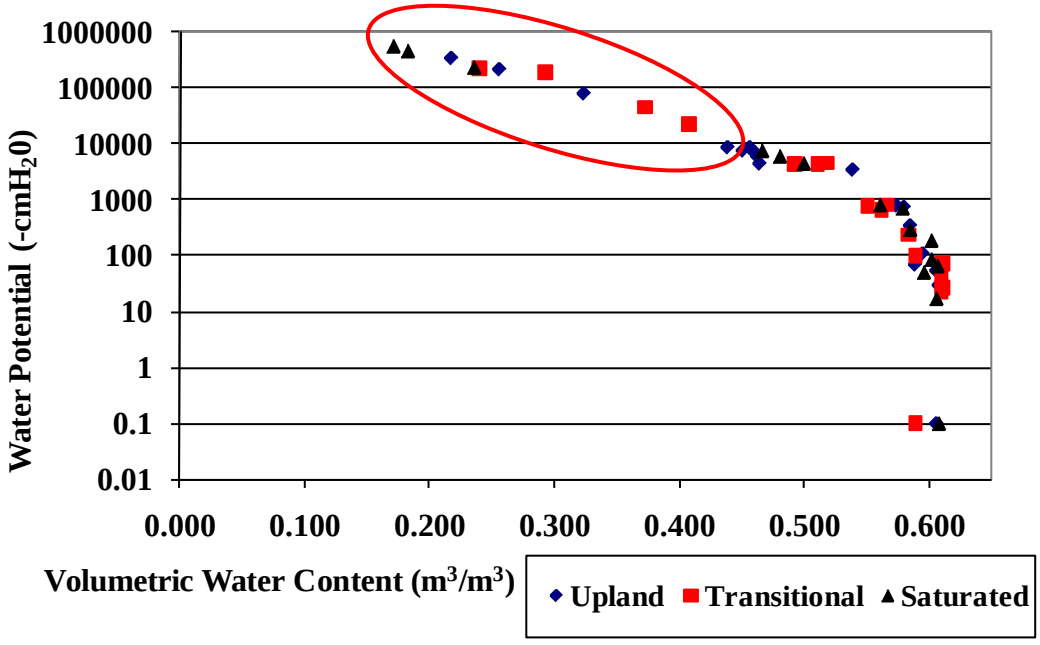

Figure 3-69. Moisture release curves for Mosaic K5. The red circle denotes VWCs calculated using GWCs.

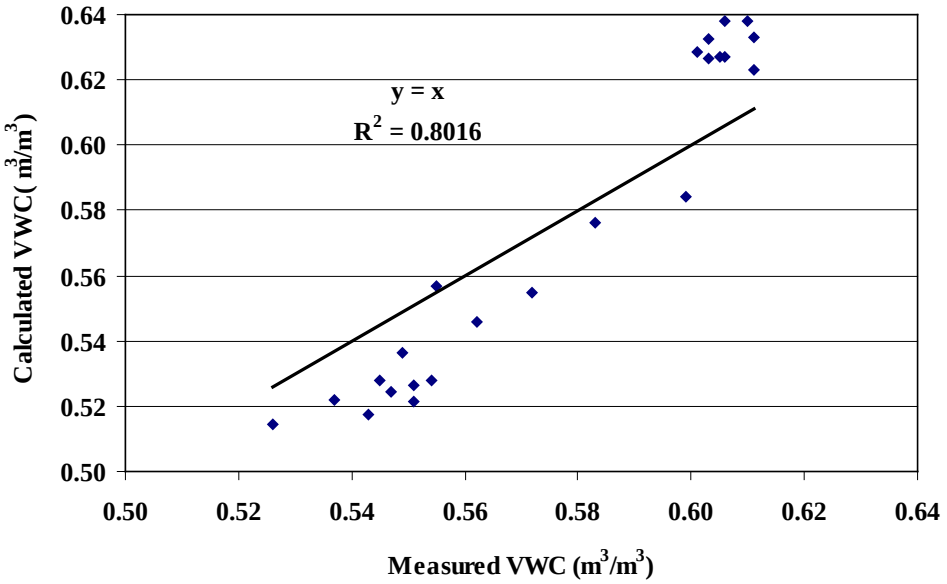

Figure 3-70. Calculated VWC using GWC versus measured VWC with EC-5 probes for Williams Co.

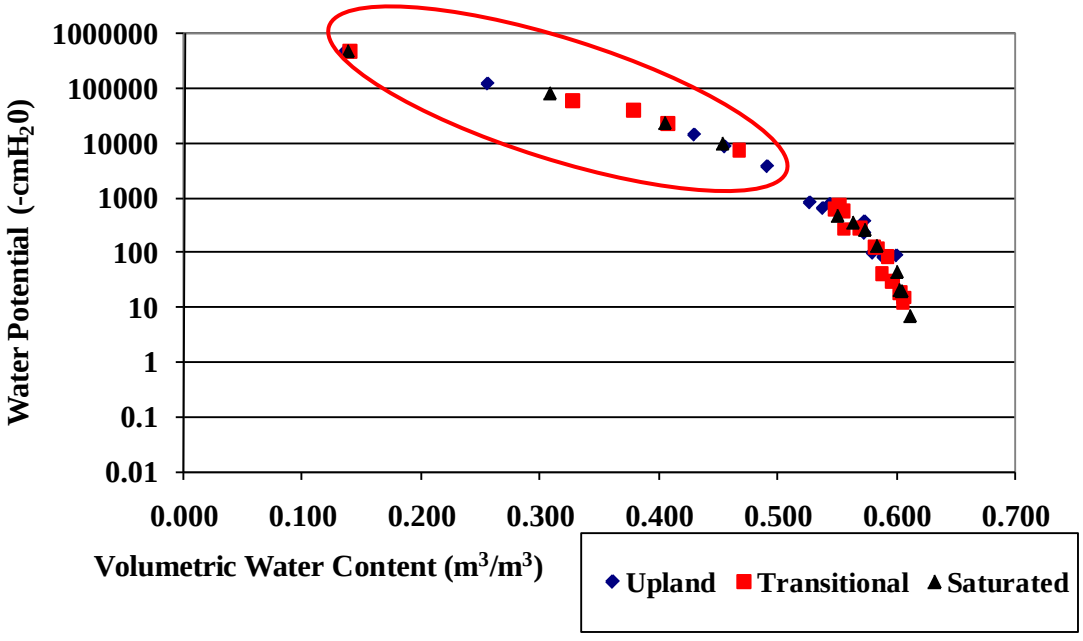

Figure 3-71. Moisture release curves for Williams Co. The red circle denotes VWCs calculated using GWCs.

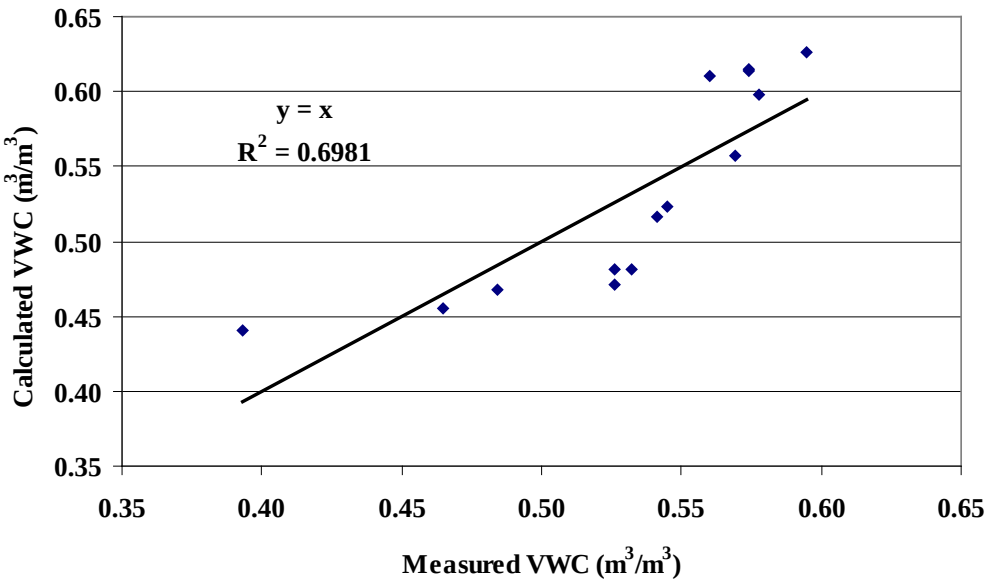

Figure 3-72. Calculated VWC using GWC versus measured VWC with EC-5 probes for CFI SP-1

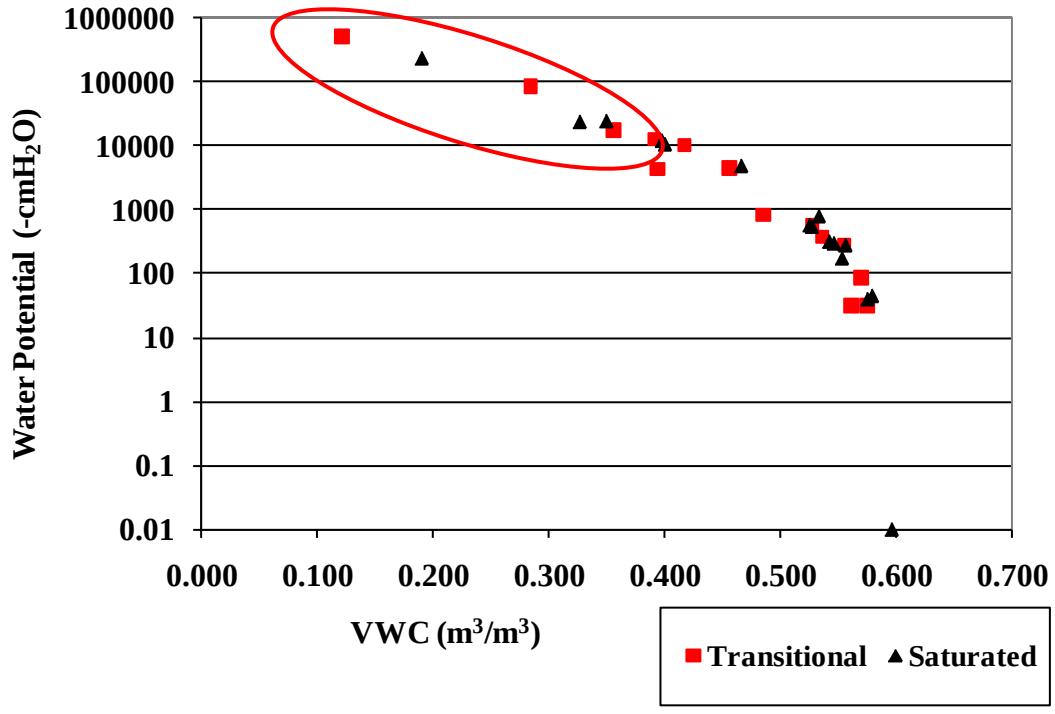

Figure 3-73. Moisture release curves for transitional and saturated at CFI SP-1. The red circle denotes VWCs calculated using GWCs.

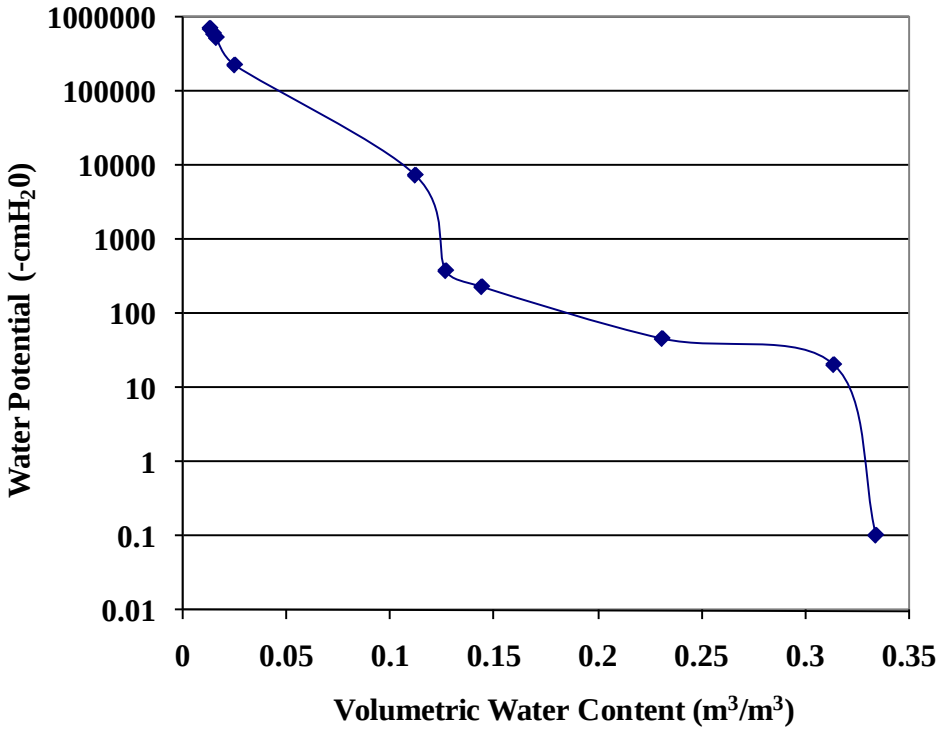

Figure 3-74. Moisture release curves for upland at CFI SP-1

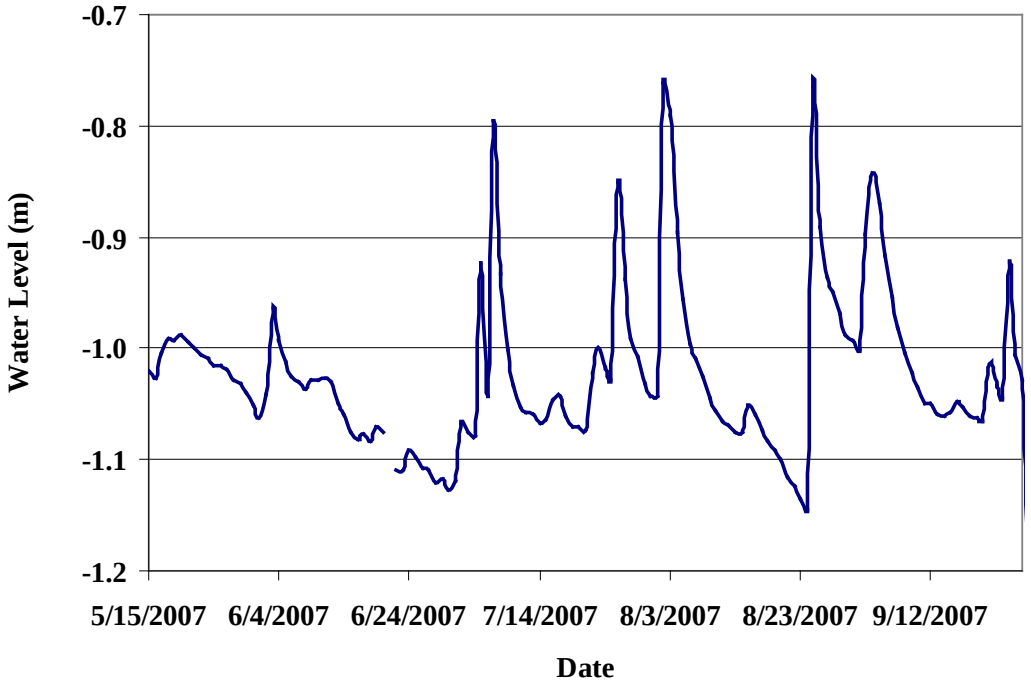

Figure 3-75. Groundwater-2 levels at Mosaic K5

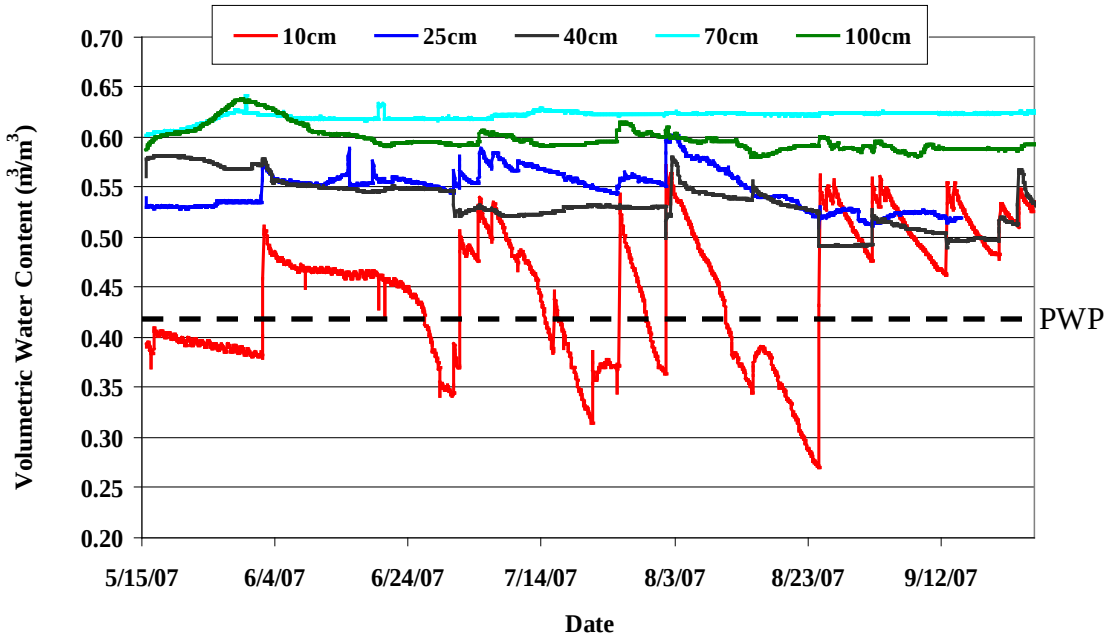

Figure 3-76. Upland zone soil moisture levels at Mosaic K5 with a dashed line denoting PWP

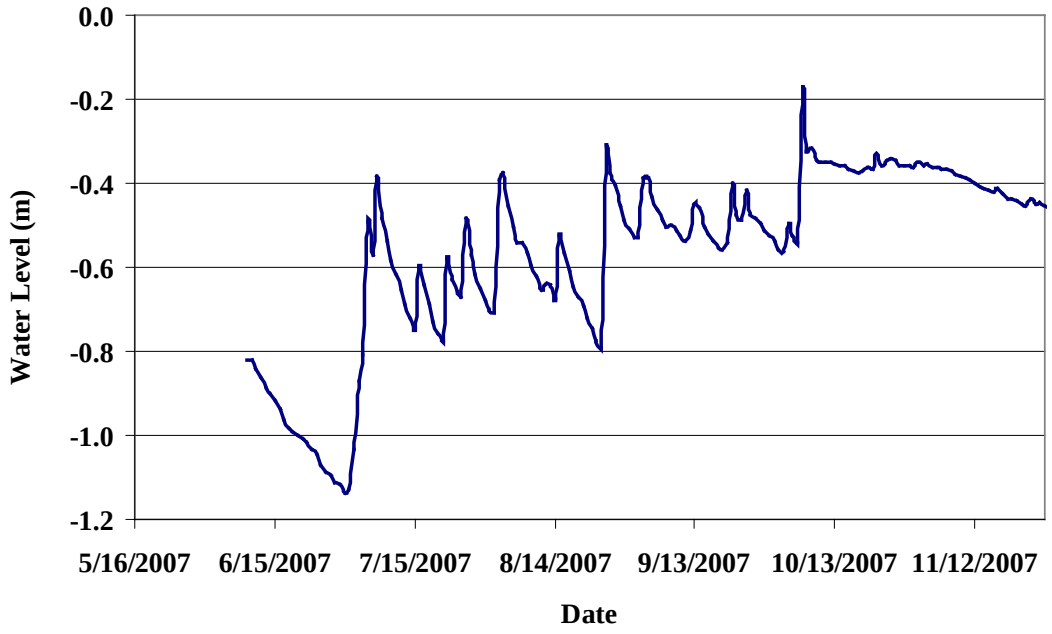

Figure 3-77. Groundwater-3 levels at Mosaic K5

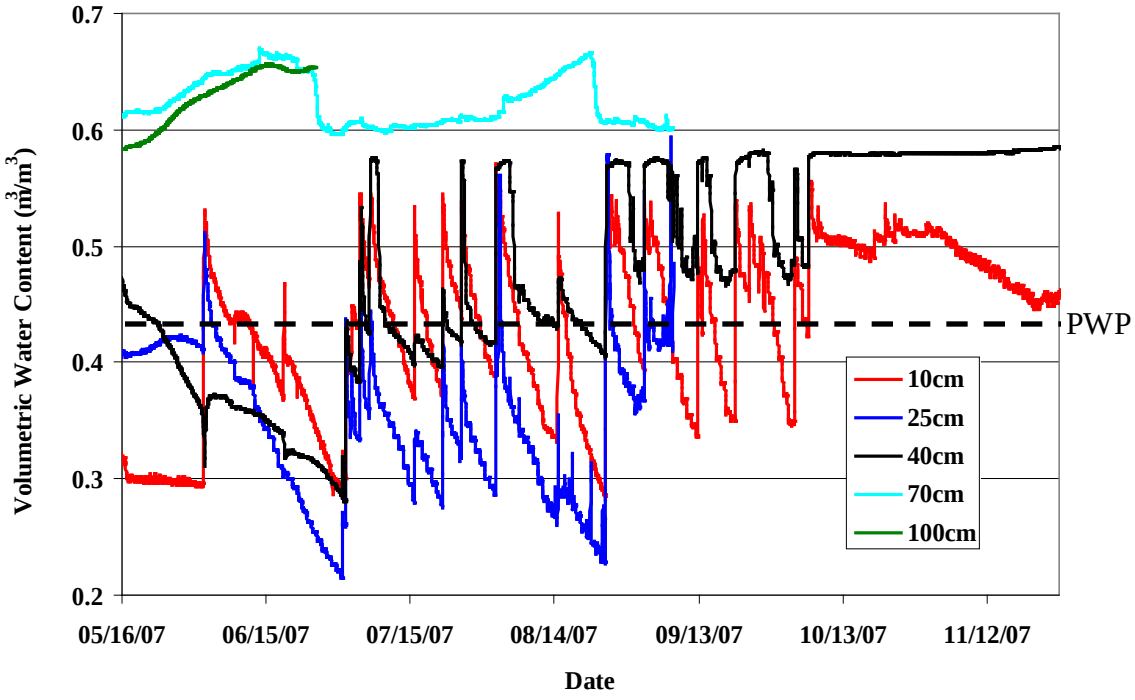

Figure 3-78. Transitional zone soil moisture levels at Mosaic K5 with a dashed line denoting PWP

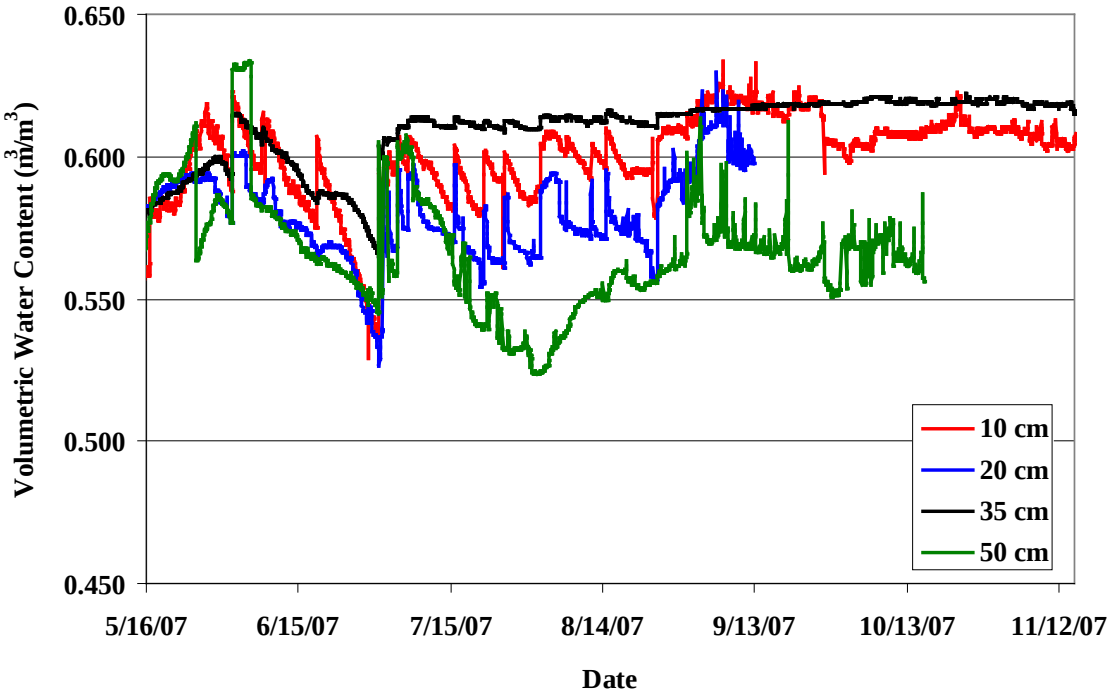

Figure 3-79. Saturated zone soil moisture levels at Mosaic K5

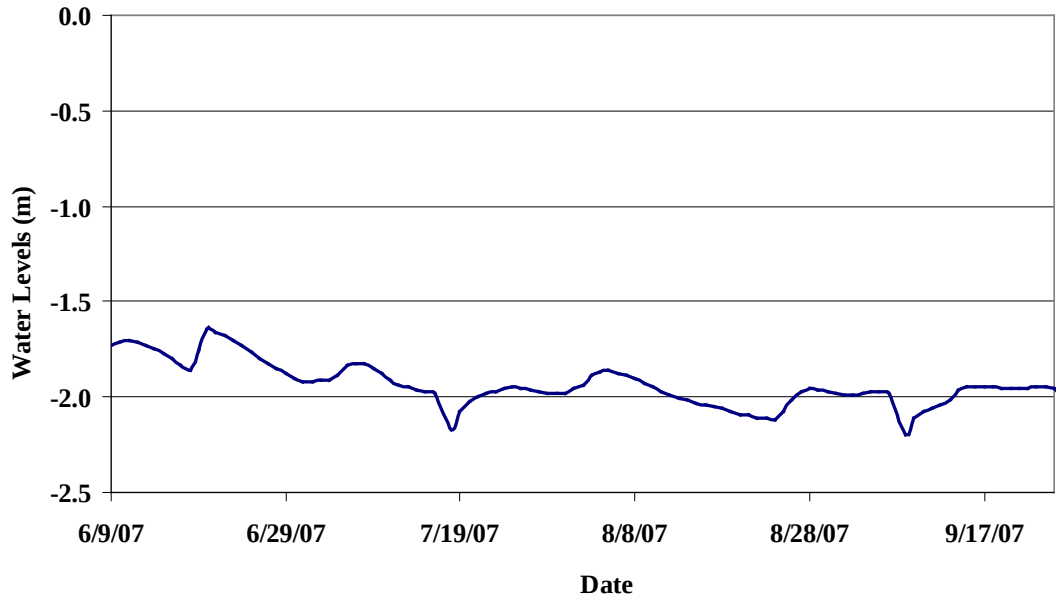

Figure 3-80. Groundwater-2 levels at Williams Co.

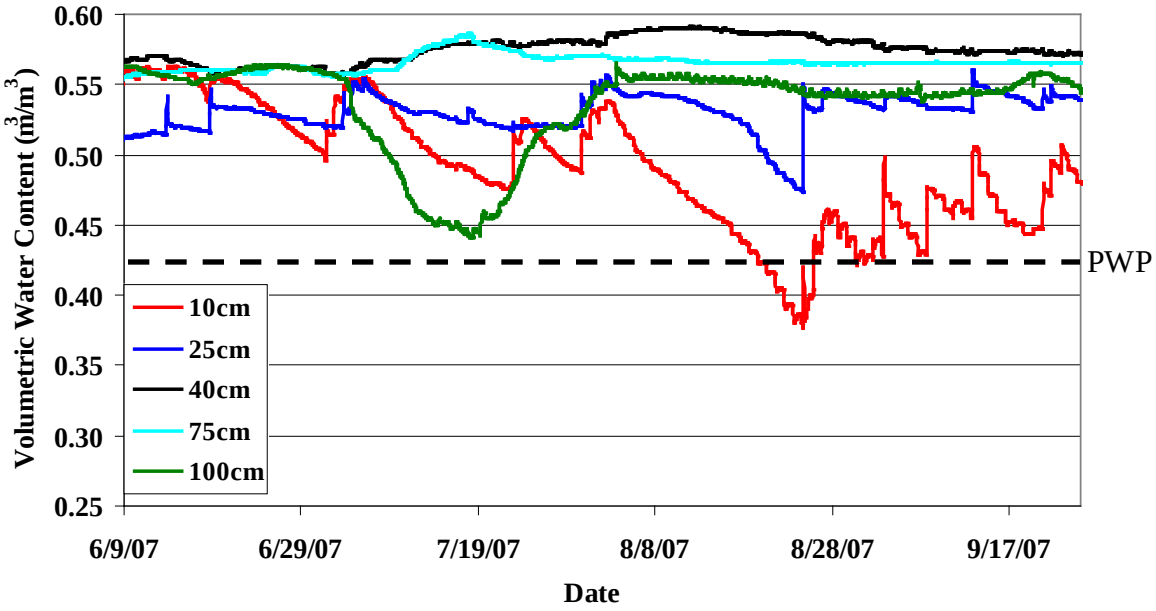

Figure 3-81. Upland zone soil moisture levels at Williams Co. with a dashed line denoting PWP

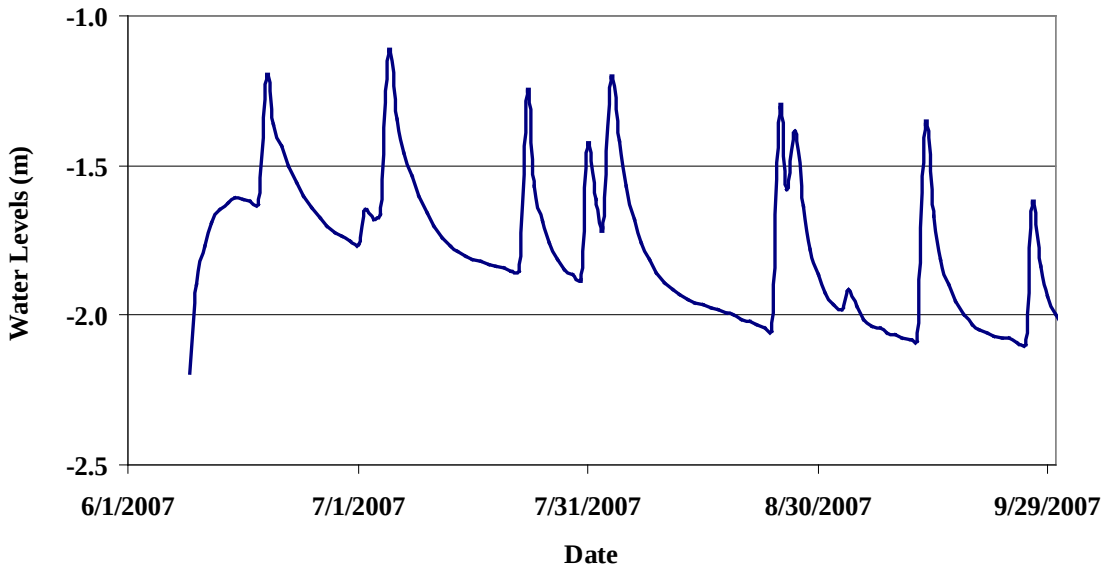

Figure 3-82. Groundwater-3 levels at Williams Co.

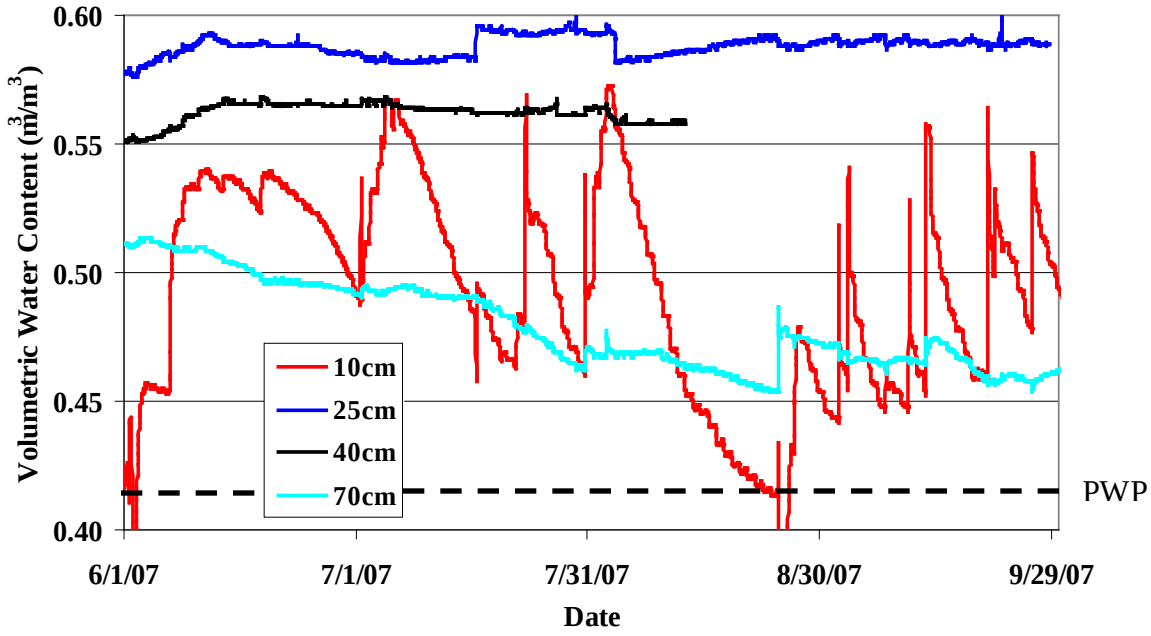

Figure 3-83. Transitional zone soil moisture levels at Williams Co. with a dashed line denoting PWP

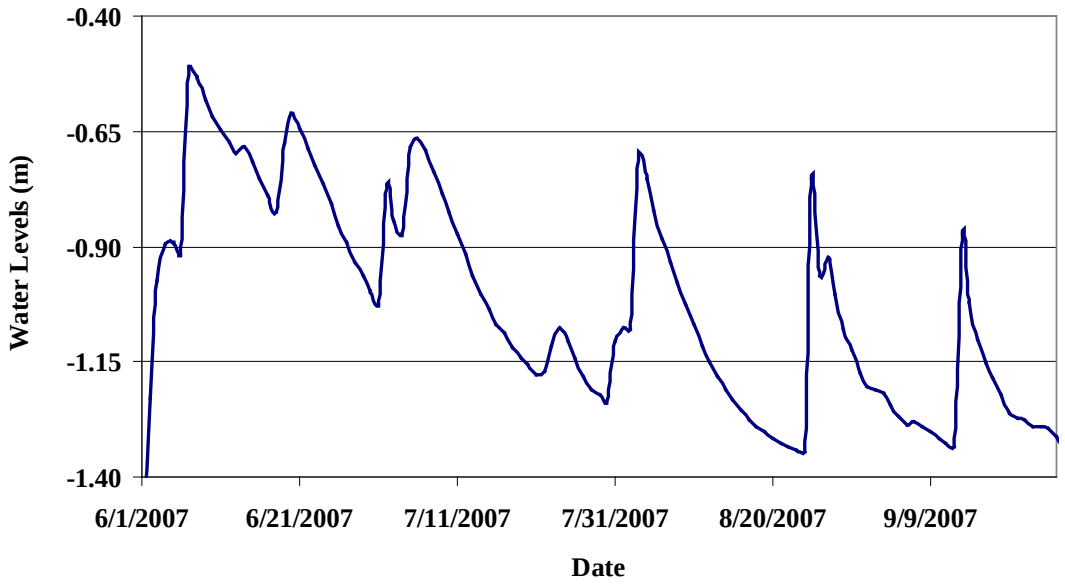

Figure 3-84. Groundwater levels at saturated zone of Williams Co.

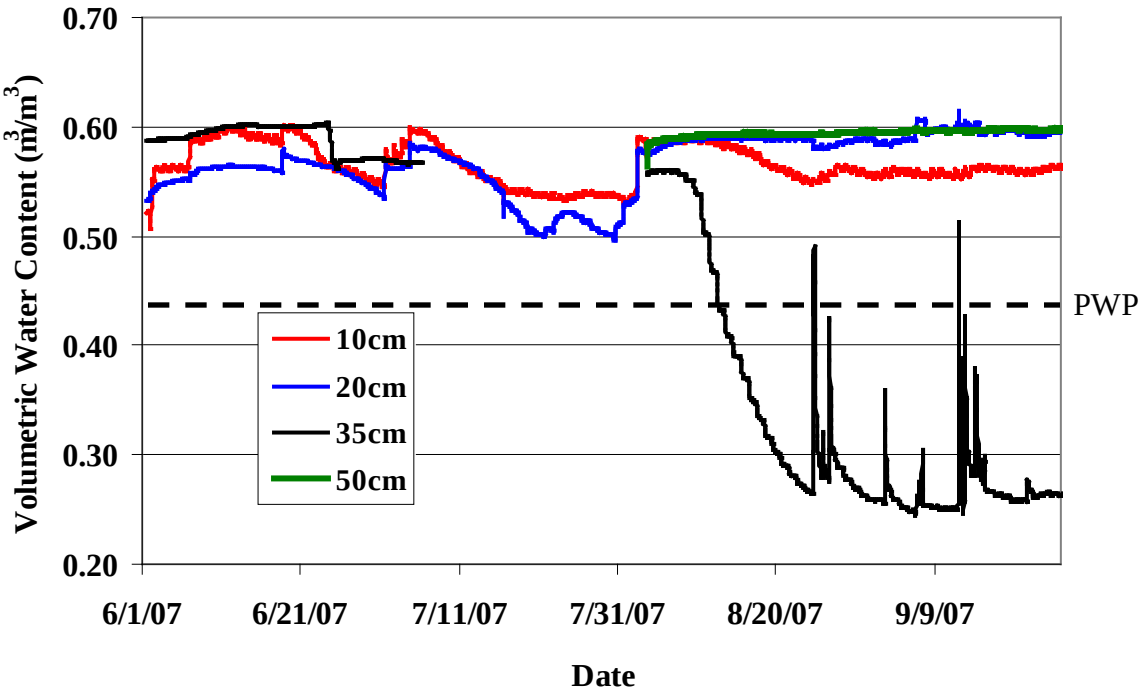

Figure 3-85. Saturated zone soil moisture levels at Williams Co. with a dashed line denoting PWP

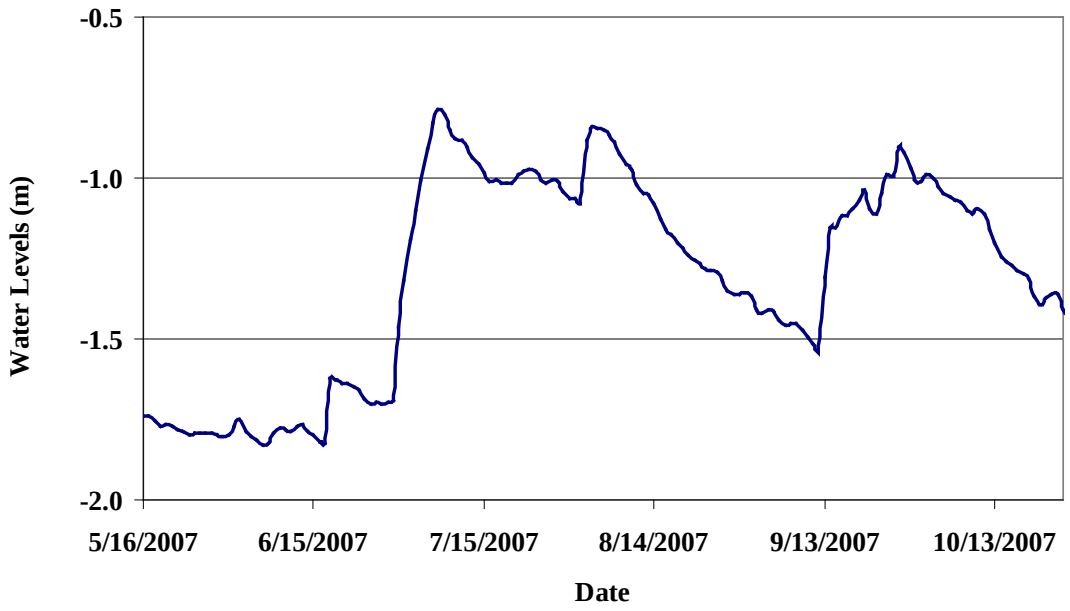

Figure 3-86. Groundwater-2 levels at CFI SP-1

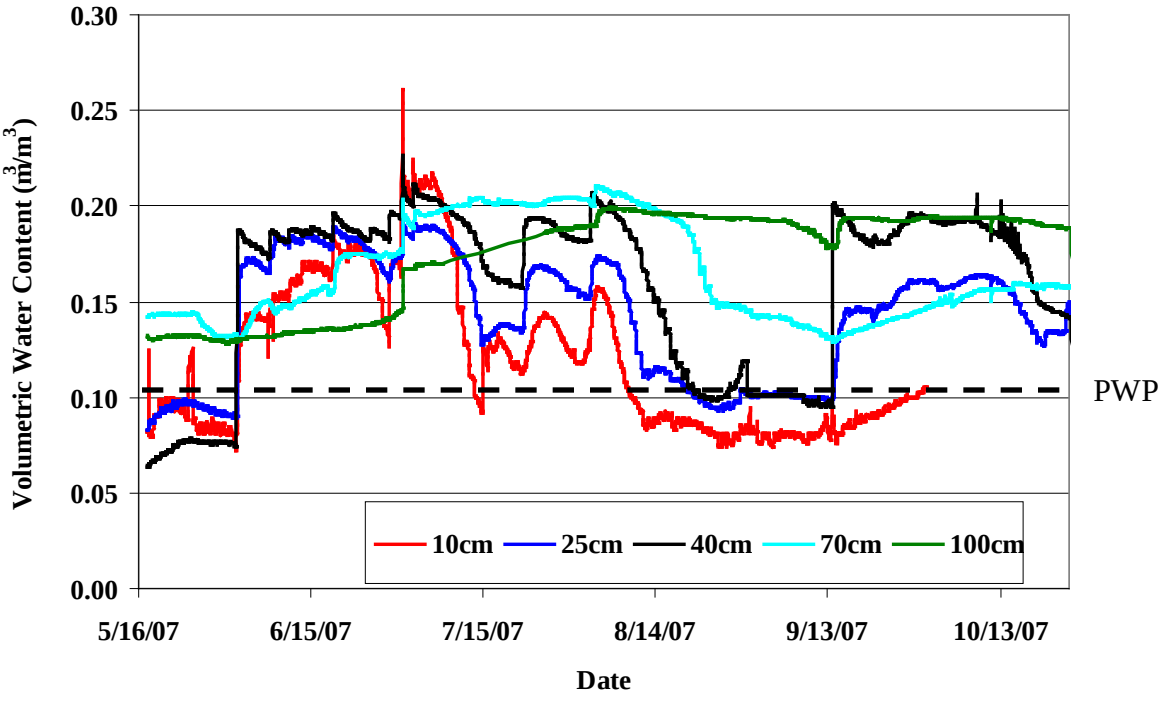

Figure 3-87. Upland zone soil moisture levels at CFI SP-1 with a dashed line denoting PWP

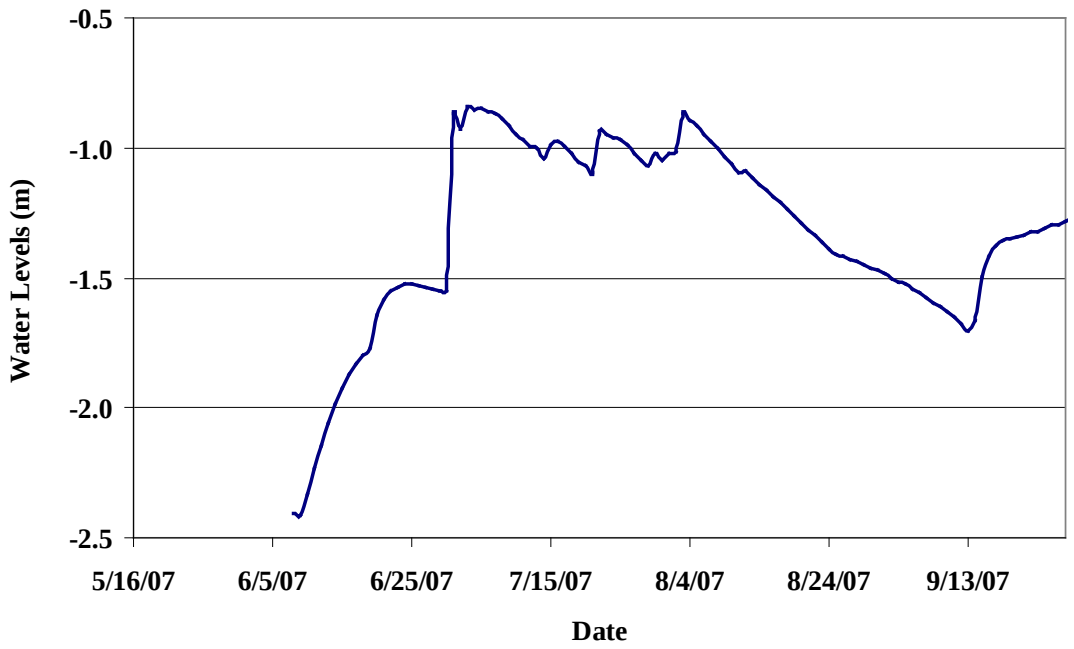

Figure 3-88. Groundwater-3 levels at CFI SP-1

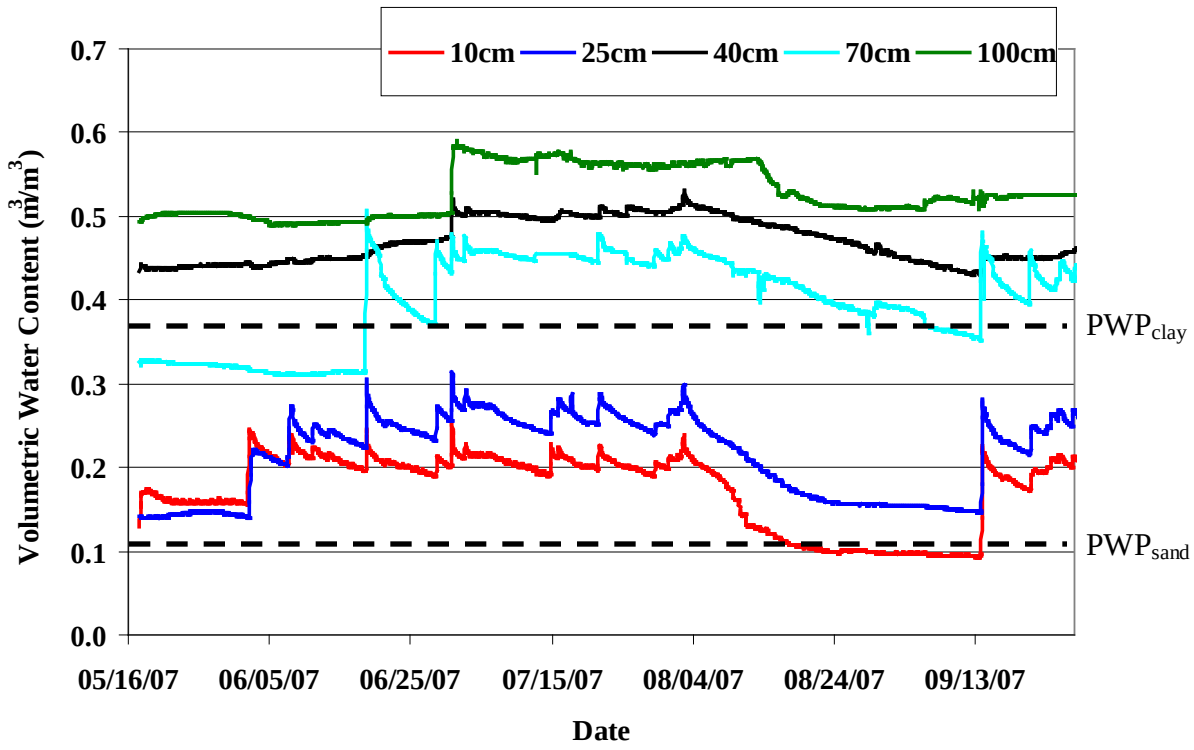

Figure 3-89. Transitional zone soil moisture levels at CFI SP-1 with dashed lines denoting PWPs

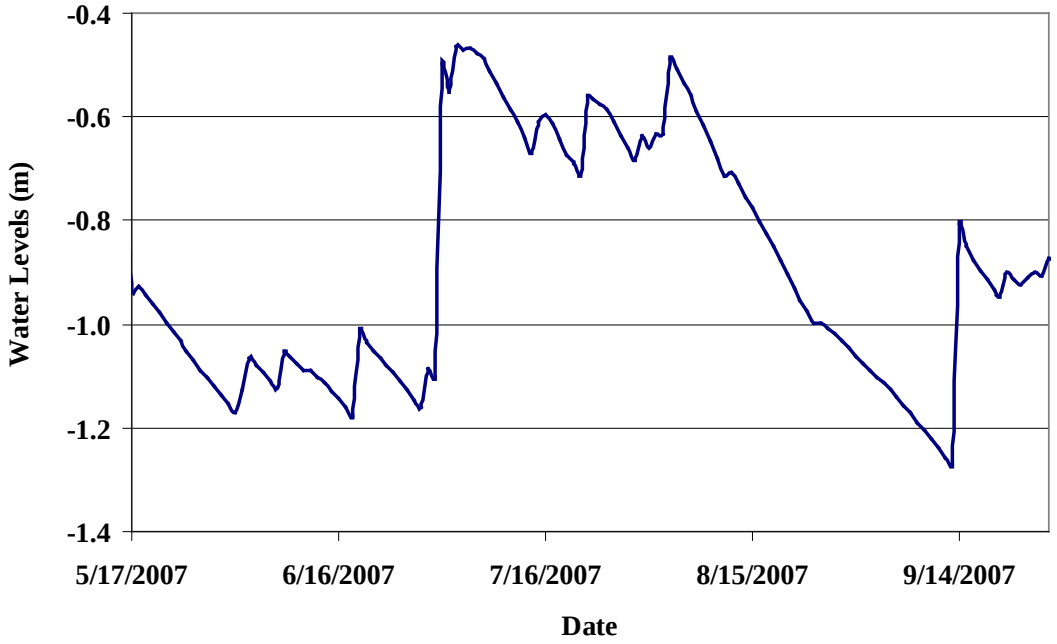

Figure 3-90. Groundwater levels at saturated zone of CFI SP-1

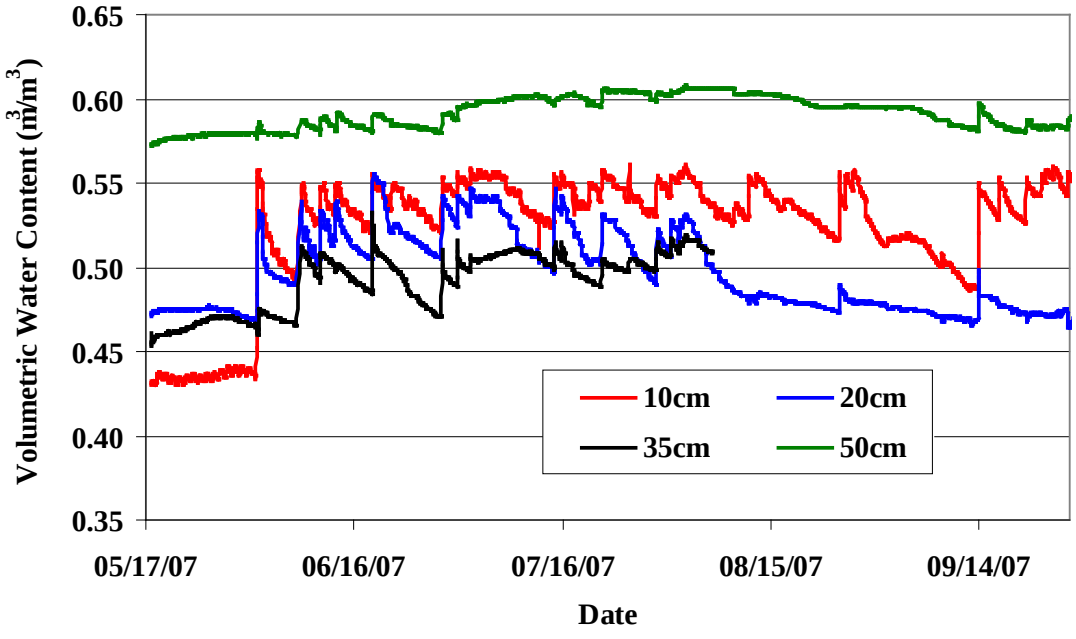

Figure 3-91. Saturated zone soil moisture levels at CFI SP-1

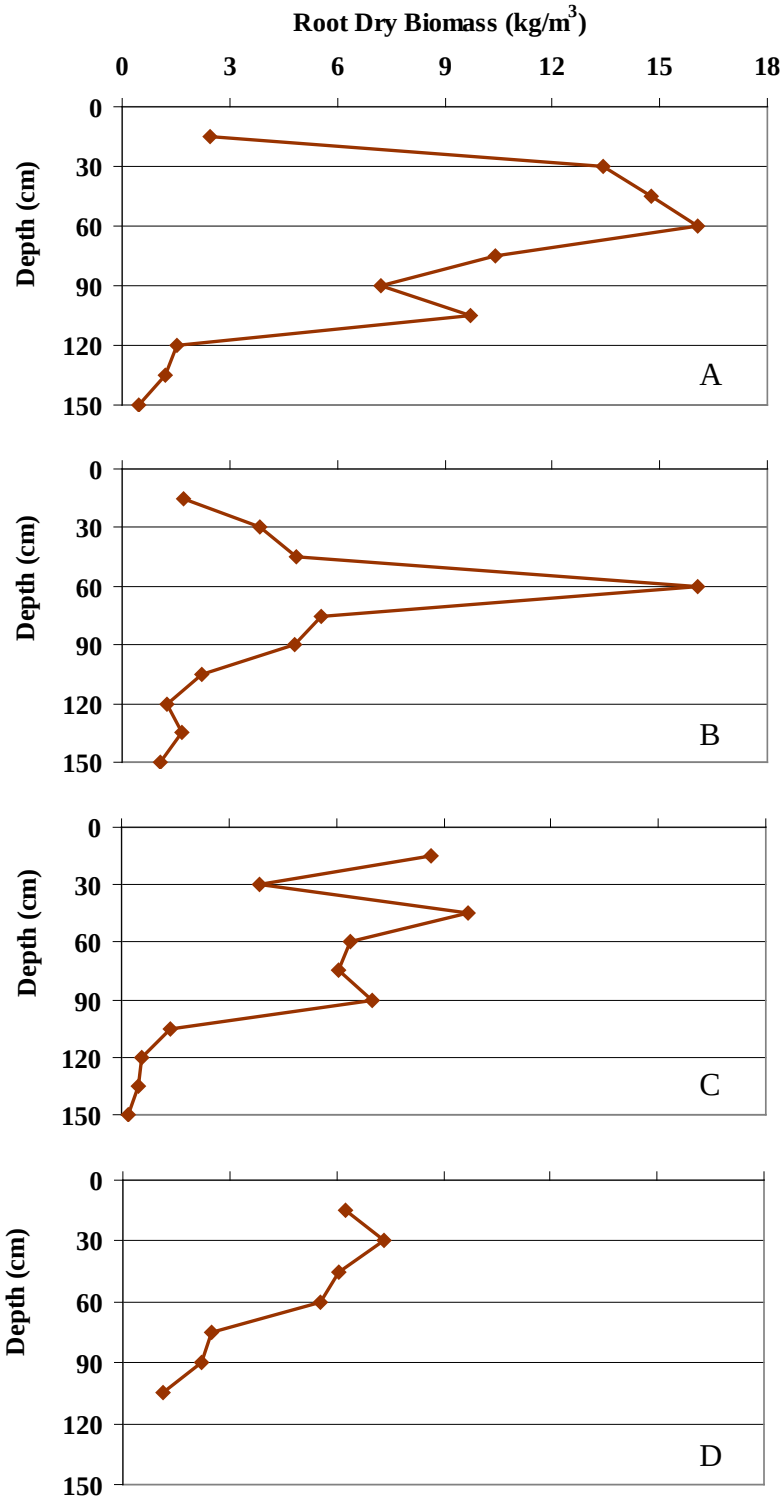

Figure 3-92. Root biomass at Mosaic K5. A) Upland zone. B) Transitional zone. C) Saturated zone. D) Inundated zone.

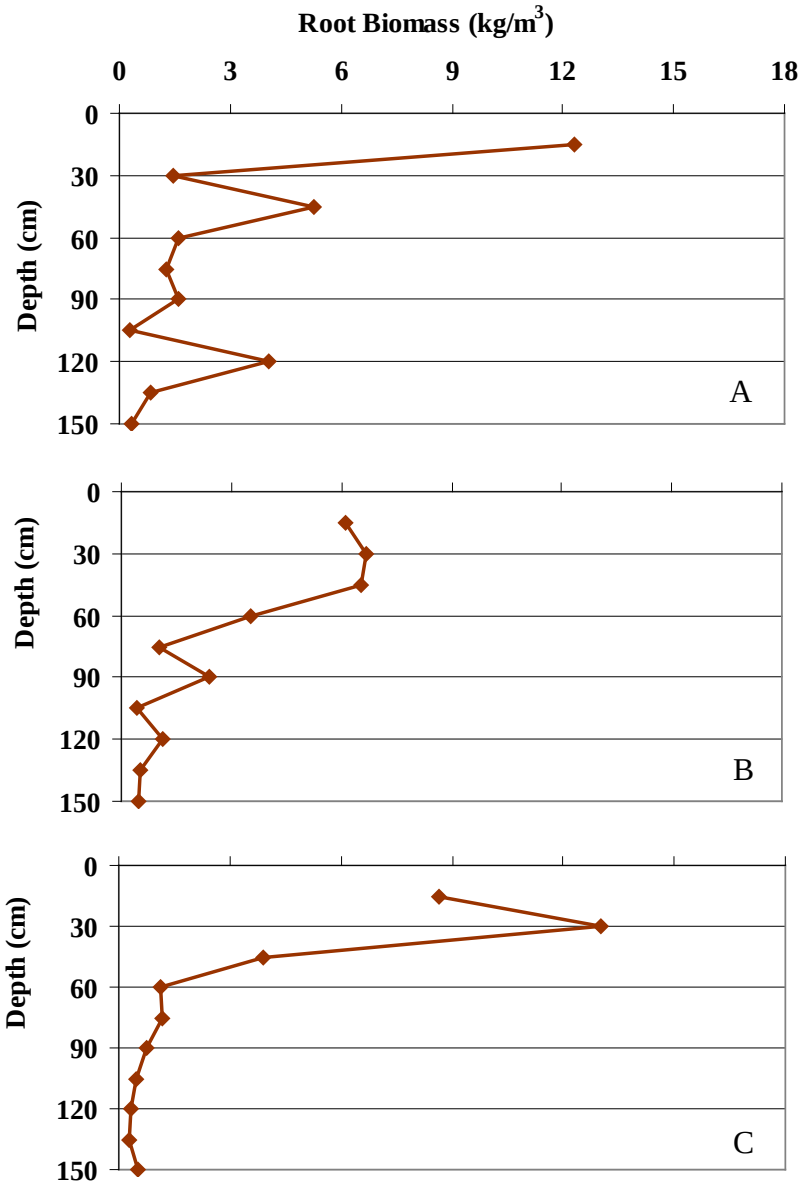

Figure 3-93. Root biomass at CFI SP-1. A) Upland zone. B) Transitional zone. C) Saturated zone.

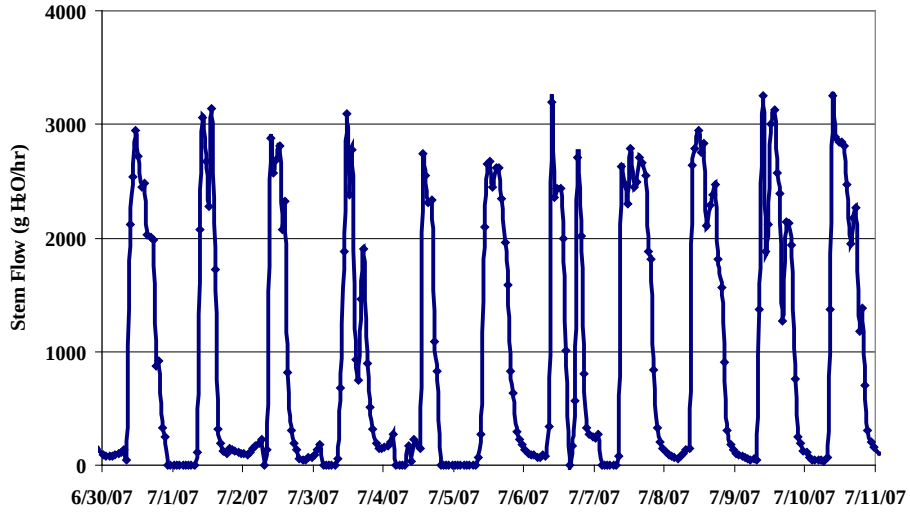

Figure 3-94. Transpiration data for stem flow at upland zone at Mosaic K5

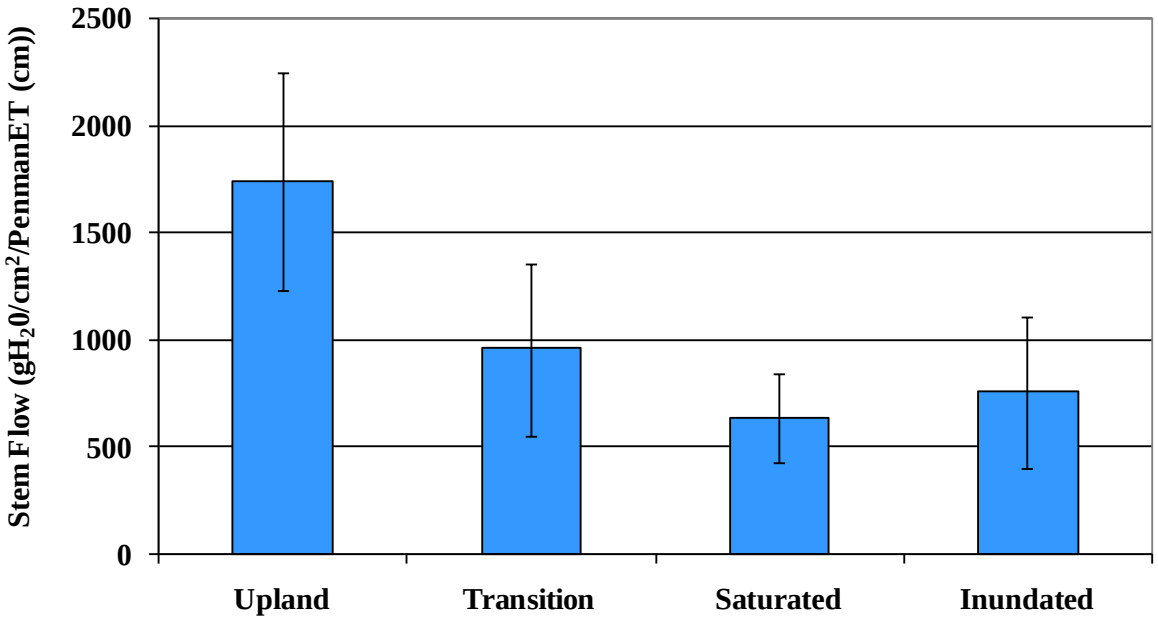

Figure 3-95. Stem flow at Mosaic K5

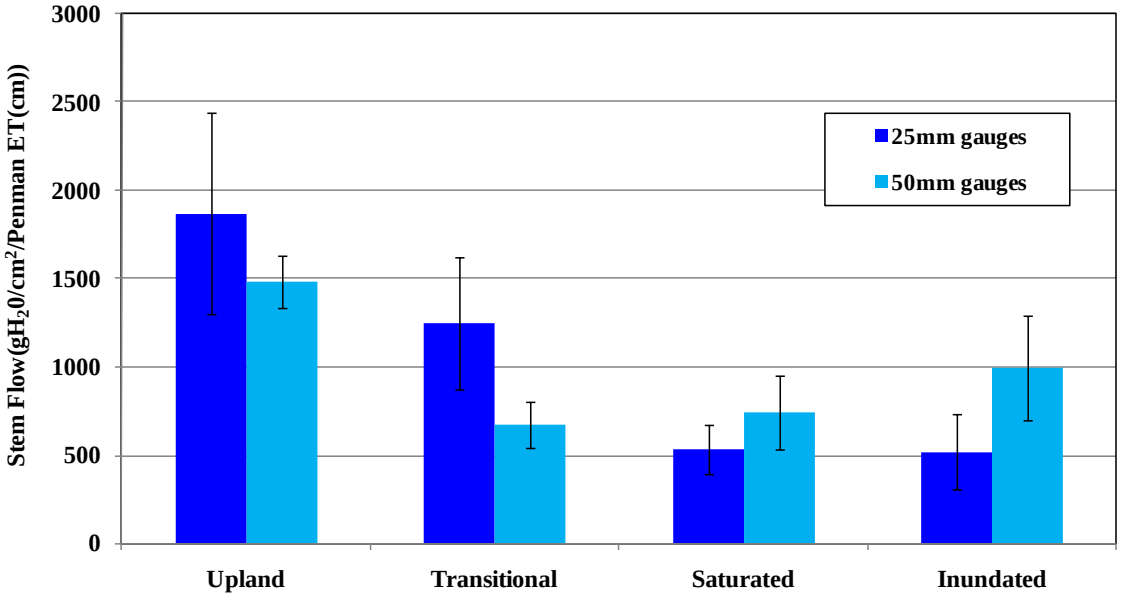

Figure 3-96. Stem flow separated by gauge size at Mosaic K5

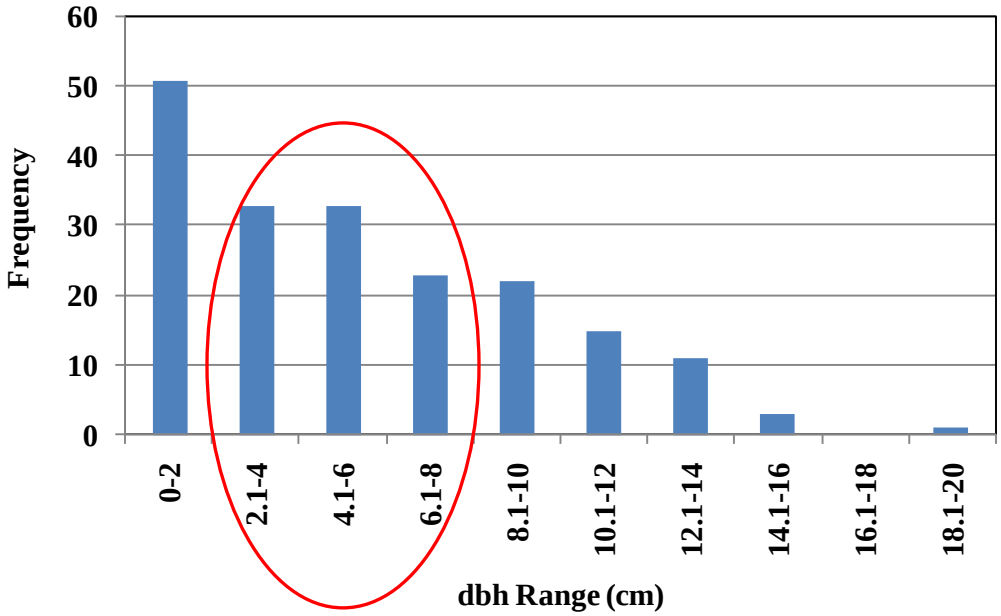

Figure 3-97. Size class histogram of *Salix Caroliniana* on belted transects at Mosaic K5. Red circle denotes size classes of instrumented trees.

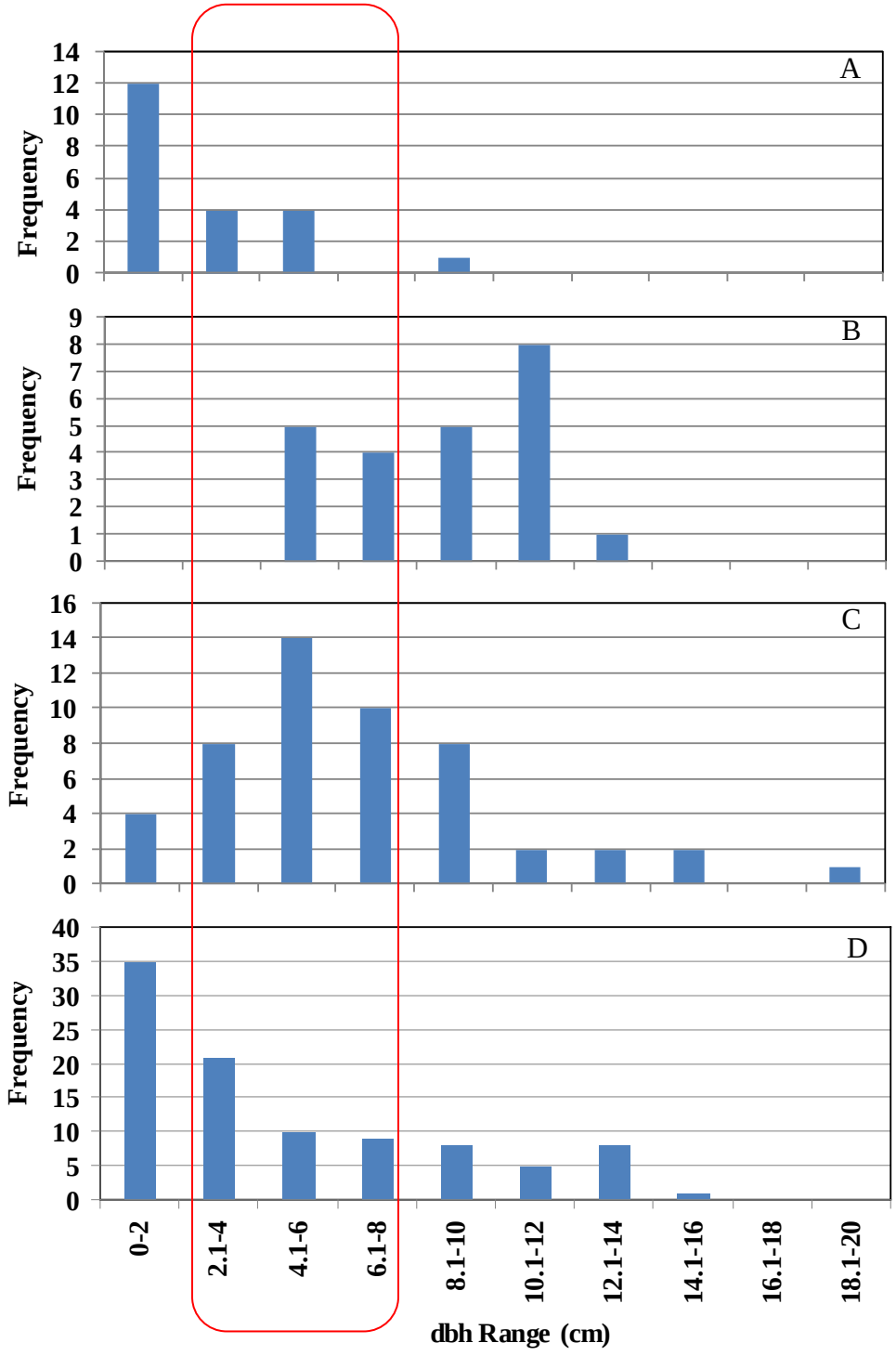

Figure 3-98. Size class histograms of *Salix Caroliniana* on belted transects at Mosaic K5. Red box denotes size classes of instrumented trees. A) Transect surrounding upland station. B) Transect surrounding transitional station. C) Transect surrounding saturated station. D) Transect surrounding inundated station

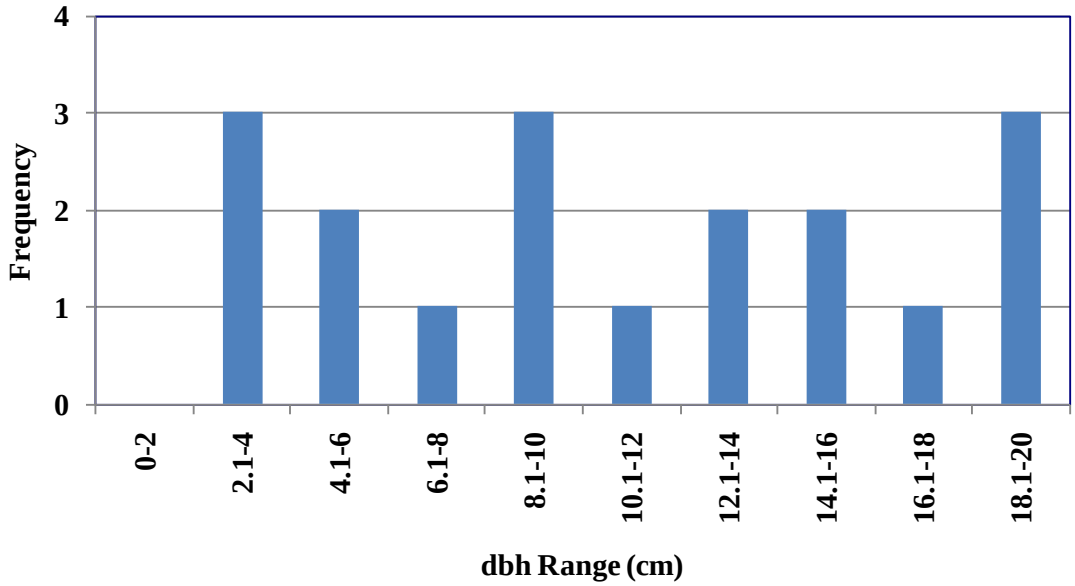

Figure 3-99. Size class histogram of cored *Salix Caroliniana* individuals

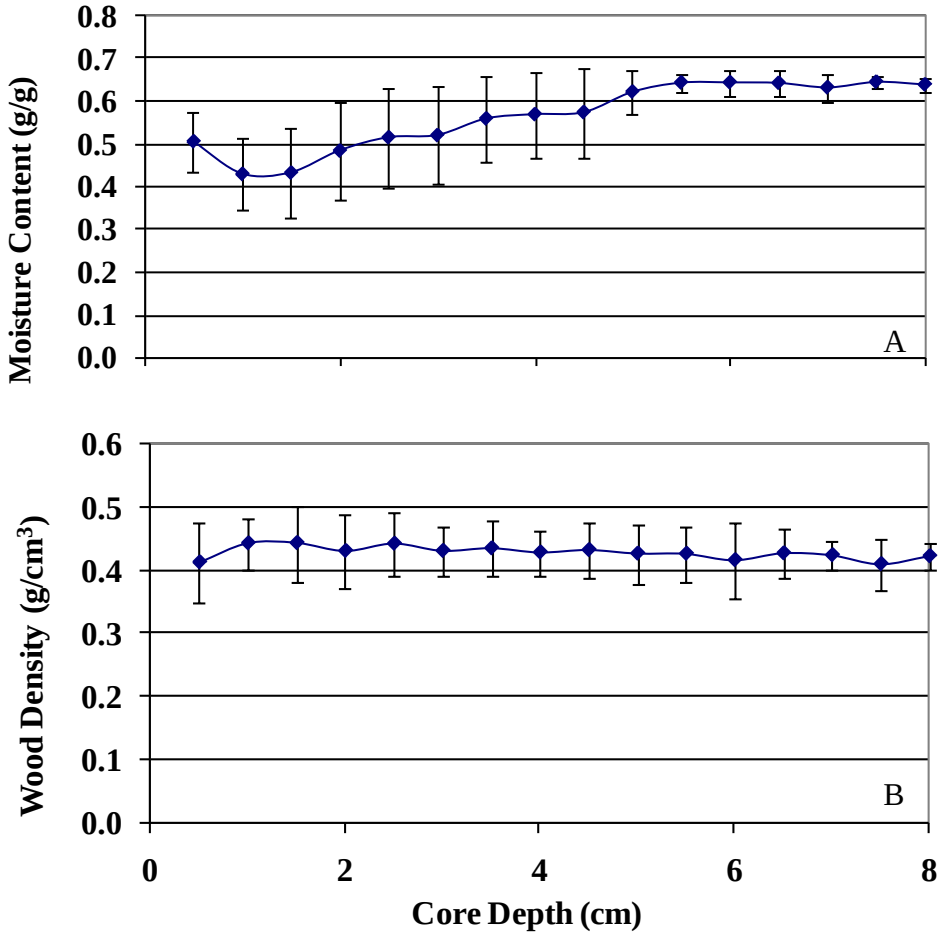

Figure 3-100. Tree core analysis results. A) Average moisture content along core depth. B) Average dry wood density along core depth.

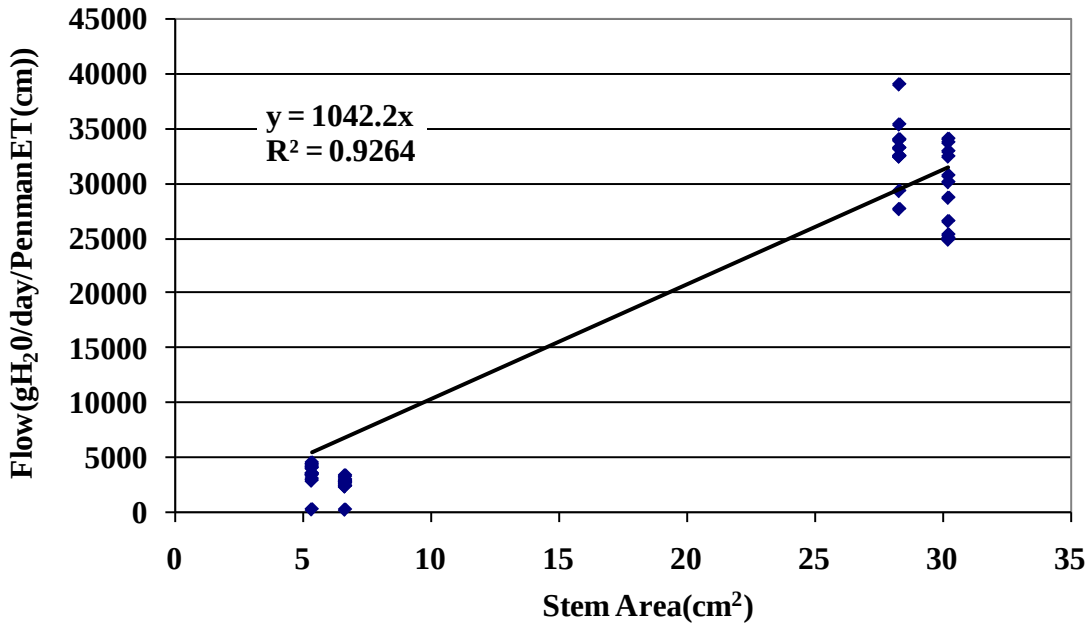

Figure 3-101. Stem flow versus stem area at the inundated station of Mosaic K5

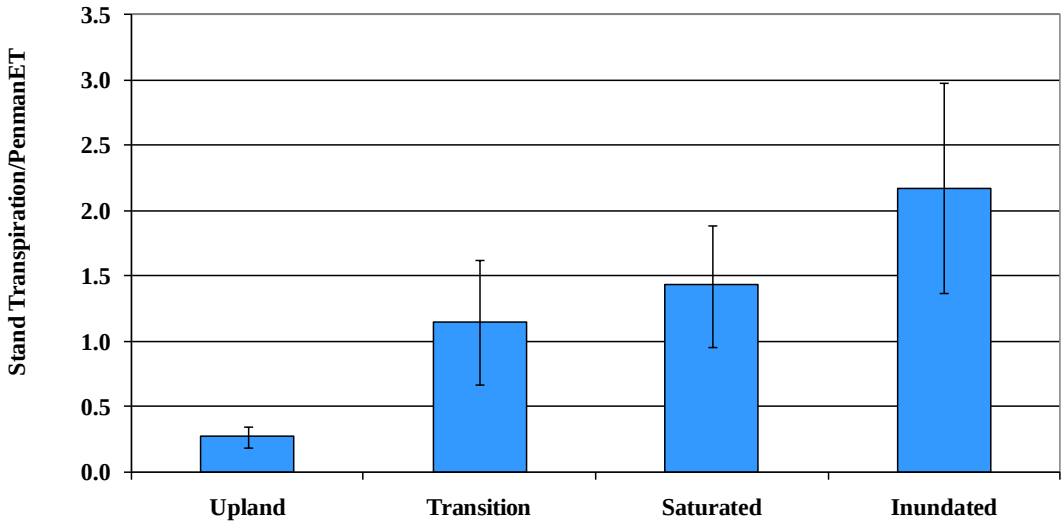

Figure 3-102. Stand level transpiration at Mosaic K5

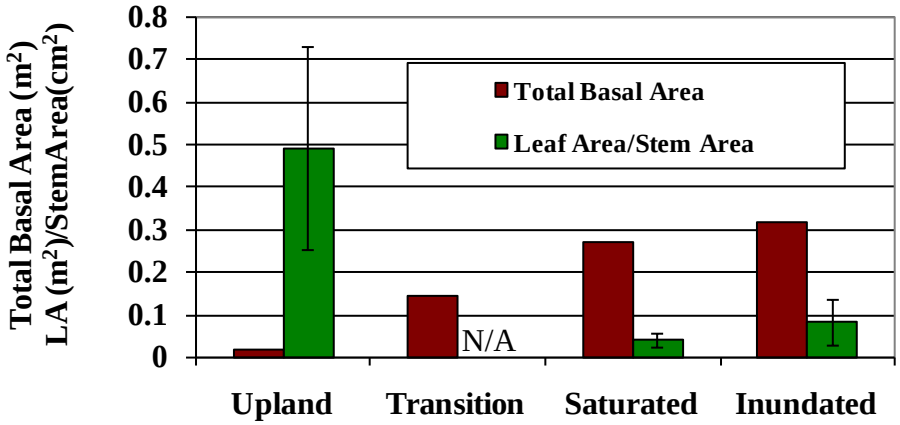

Figure 3-103. Total basal area on transects and leaf area per stem area of instrumented stems at Mosaic K5

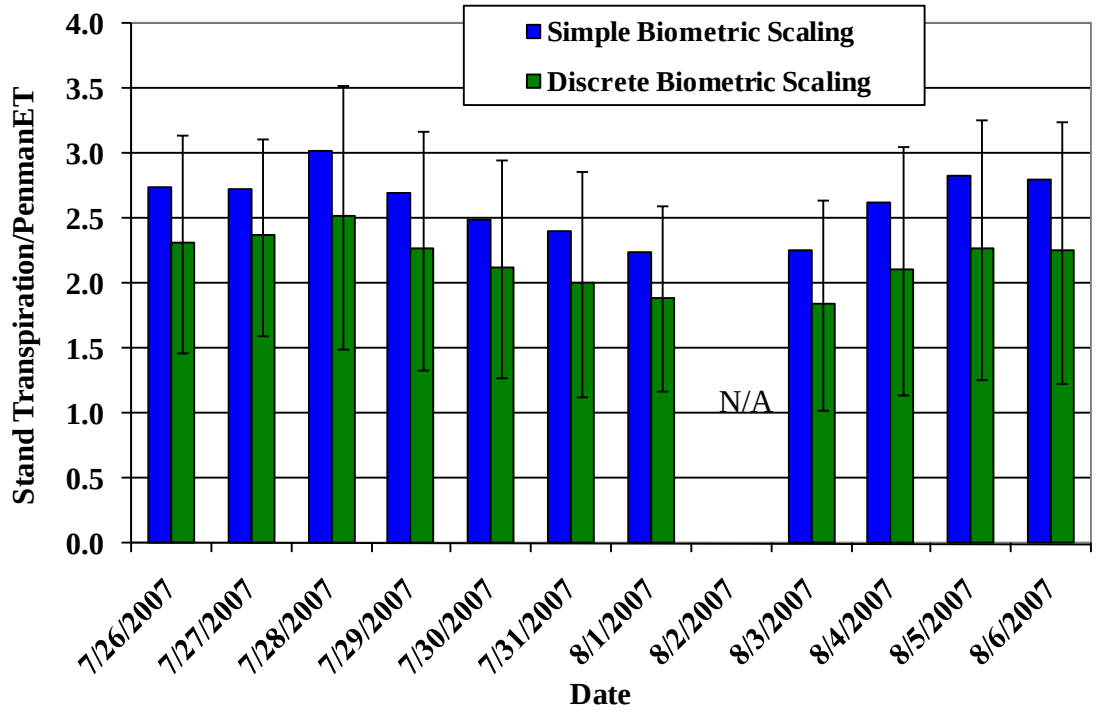

Figure 3-104. Daily comparison of stand transpiration/Penman ET at inundated station of Mosaic K5 using two different biometric methods for scaling

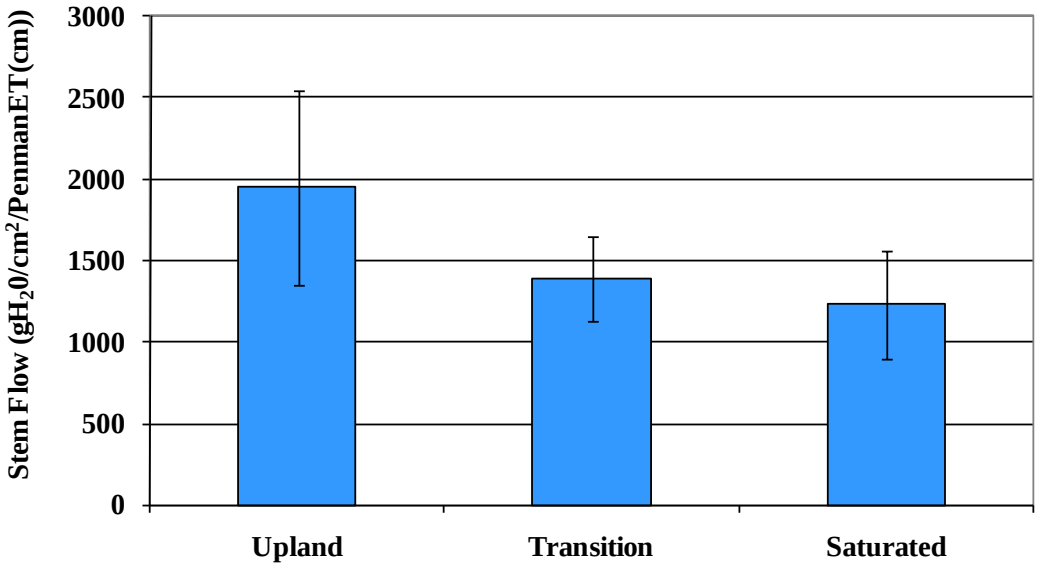

Figure 3-105. Stem flow at CFI SP-1

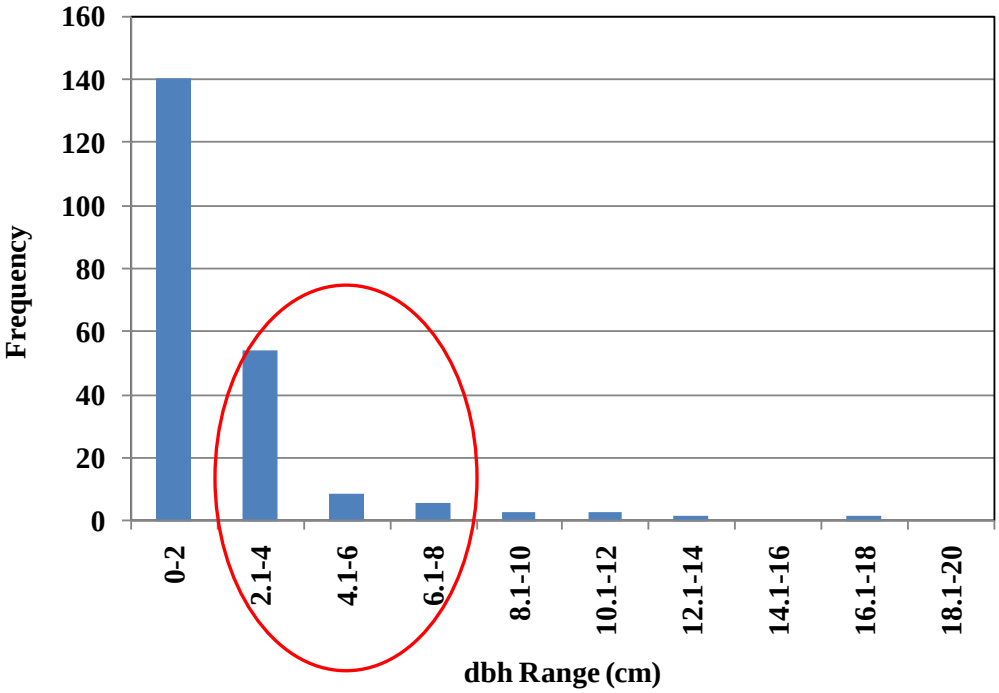

Figure 3-106. Size class histogram of *Salix Caroliniana* on belted transects at CFI SP-1. Red circle denotes size classes of instrumented trees.

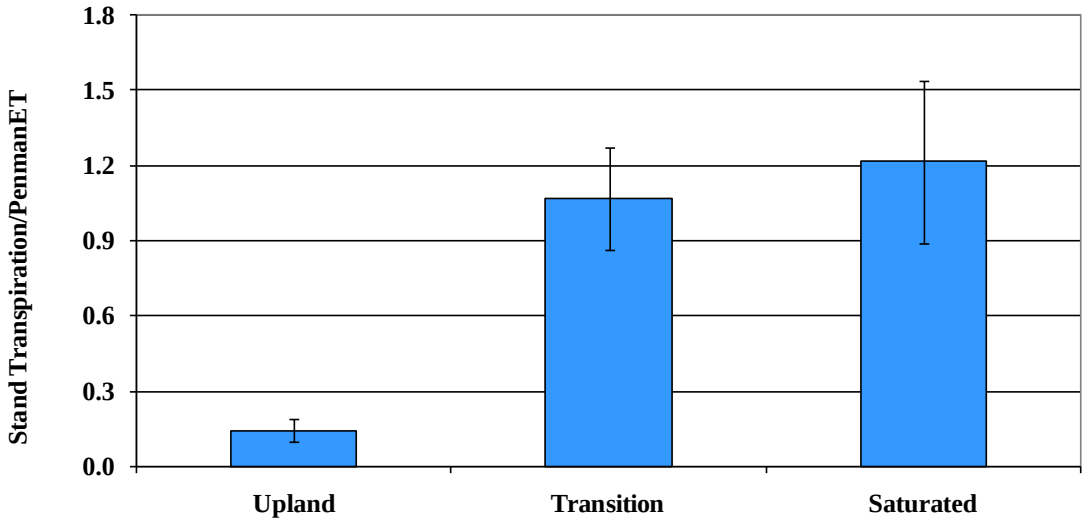

Figure 3-107. Stand level transpiration at CFI SP-1

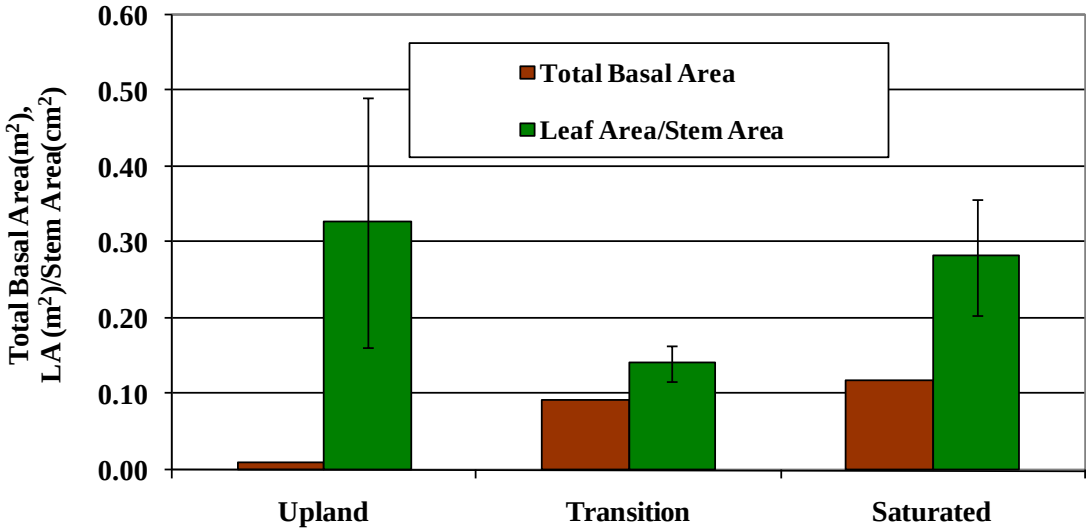

Figure 3-108. Total basal area on transects and leaf area per stem area of instrumented stems at CFI SP-1

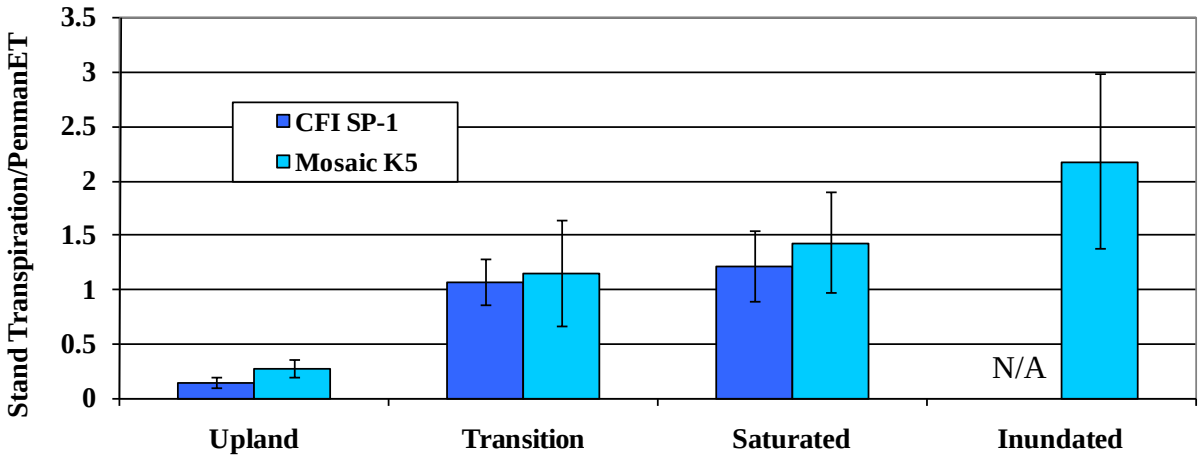

Figure 3-109. Stand transpiration at CFI SP-1 and Mosaic K5

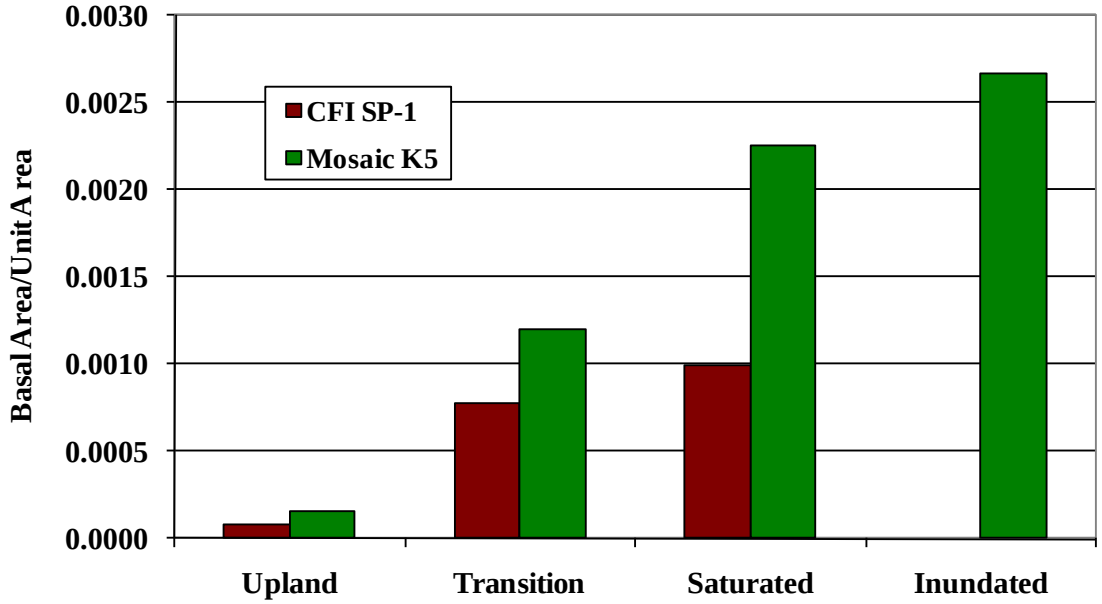

Figure 3-110. Total basal area per unit area at CFI SP-1 and Mosaic K5

CHAPTER 4
DISCUSSION

Conclusions

When attempting to enhance or create wetland ecosystems, an understanding of the hydrology and its major determinants are of primary concern. This study monitored the internal hydrology of eight CSAs to calculate water budgets, observe surface and groundwater interactions, analyze ET in detail, and develop temporal hydrologic models. Additionally, an ecohydrologic component was included in the study to document interactions between a dominant CSA species and CSA soils and hydrology. Major conclusions from this research include:

- Surface water features demonstrate substantial differences in hydrologic regime among and within CSAs, highlighting the need for site-specific analysis when developing restoration plans. Some features consistently experience extreme water depths that may inhibit wetland development, while other features exhibit water depths and seasonal flooding and drying more typical of wetland systems and that may be conducive to wetland restoration.
- Surrounding uplands which have more conductive soils reduce runoff amounts, potentially facilitate groundwater flow, and maintain higher surface water levels, while limiting the extent of saturated zones beyond inundated features. Pure clay substrate extends the transitional zone from the wetland where there is adequate soil water for planting wetland tree species, while increasing the runoff volume and reducing surface to groundwater interactions. Restoration activities should acknowledge and utilize the differences of clay-dominated versus mixed soil uplands.
- The high ET and limited infiltration that was observed at the eight monitored CSAs suggest that CSAs may negatively affect regional hydrology by reducing groundwater flow and providing limited surface water contribution to downstream water bodies.

Flooding Regimes

Observed hydrologic regimes for surface water features of the eight sites demonstrated differences between sites (Figure 3-17). Some sites experienced water depths and seasonal flooding similar to the Green Swamp systems and typical Florida isolated wetland systems but with quicker and larger responses to rain events and faster rates of decline (Figures 3-18 and 3-

17). Other sites, however, had surface water features that were more buffered from rain events, had lower rates of decline, and experienced more ponded conditions compared to other monitored sites and to natural wetland systems. Different hydrologic regimes were also observed at multiple surface water features within one CSA (Figure 3-9). An understanding of what factors create differences both among and within CSAs and when compared to natural systems is imperative when trying to predict future hydrologic regimes and planning a restoration design.

Water Budgets

Water budgets were performed for the instrumented surface water features of the eight CSAs to account for all hydrologic flows which included runoff from rain events, ET, surface water outflow, dike seepage, and groundwater inflow and outflow.

Runoff

In past studies, CSA runoff analysis has primarily focused on runoff events measured at a gauged outflow of the CSA and thus treated the CSA as one watershed (Lewelling and Wylie, 1993; Reigner and Winkler, 2001; Riekerk *et al*., 1990). As a result, these studies often resulted in runoff amounts lower than what its expected for clayey soils. The focus of this study, however, was on individual surface water features within a CSA and their response to rainfall, requiring a multiple watershed approach (Figures 2-20 through 2-26). The runoff analysis revealed differences in runoff characteristics, in terms of runoff to rain depth ratios, between water features and resulted in runoff responses at some sites more typical of clays compared to findings from past studies of CSA hydrology (Figures 3-24 through 3-31). Runoff coefficients for small watersheds in the eastern U.S. as calculated with the method employed in this study typically range from 0.04 to 0.18 (Lee, 1980), whereas values calculated here for CSA watersheds ranged from 0.15 to 0.66 (Table 3-4). It should be noted that these reported values

are for soils ranging from silty loam to sandy clay, and no values for pure clay soils were provided.

The runoff analysis suggested that on most sites rainfall depth was a better predictor of runoff depth than were runoff coefficients with multiple regression models (Table 3-5). Runoff depth was a constant percentage of rain depth despite varying contributing areas at six of the eight features evaluated. The fact that the multiple regression models, which included upland to wetland areas, were less successful suggests that runoff may have been primarily from a constant contributing area such as the edges of the feature. Furthermore, because the inclusion of antecedent conditions did not typically result in better models, it appears that the runoff coefficients of these constant contributing areas may be largely determined by magnitude of rain. The results from the modeling of Williams Co. and Mosaic HP-10 were exceptions, and these are sites where both contributing areas and antecedent conditions may play a more important role. Nevertheless, the differences in characteristic runoff responses to rain events among CSAs and even within a single CSA were clear. In their study of three CSAs, Lewelling and Wylie (1993) also observed variability between the CSAs regarding runoff responses.

The most pronounced buffering conditions were observed at the surface water features of PCS SA 10 and SA 01, which may be partially explained by the higher conductive soils in portions of their surrounding uplands limiting runoff amounts (Table 3-13). PCS SA10 had the highest saturated hydraulic conductivity measured and one of lowest runoff contributions to its water balance (Tables 3-4, 3-10, 3-13). A hydraulic conductivity at PCS SA 01 was not reported as a result of the sand tailings at this site inhibiting a measurement with Hvorslev method due to the almost instantaneous recovery following slug removal, suggesting a higher conductivity than measured at the other sites. PCS SA 01 experienced the second lowest runoff contributions.

While CFI SP-1 did not experience constant flooding through the entirety of the study period, the inundated period that occurred from fall 2004 to spring 2006 also experienced a more buffered hydrologic regime compared to other systems (Figure 3-11). CFI SP-1 had the third highest conductivity measured as a result of its sand-clay mix, and experienced the lowest runoff contributions, with 80 % of observed event response at CFI SP-1 being explained by direct rainfall (Table 3-4).

The runoff contributions to the surface features at Williams Co. and Mosaic H1 SW-1, which were surrounded by pure clay uplands, were the highest, with the exception of Mosaic HP-10, and explain their flashy nature with rapid response to rain events (Table 3-4). While Mosaic HP-10 had the largest contribution to its water budget from runoff, it was frequently connected to an outfall system, which minimized flooding depths (Figure 3-15). In addition to low conductive soils limiting infiltration and increasing runoff simply from low permeabilities (Figure 1-3), they also reduce percolation as a result of the strong capillary forces from the clays limiting infiltration and storage capacity (Levine and Salvucci, 1999). The latter results from higher initial soil moisture content and minimal depths to the saturated zone that occur with soils with low conductivities and high capillary fringe heights. These effects on infiltration and overland flow of rain may explain the differences between the runoff contributions of features that were surrounded by uplands with different conductivities.

Surface Water Outflow

Surface water outflow was limited from the monitored CSAs during the study period with only Mosaic K5 and HP-10 experiencing frequent outflow events. While there were outfall systems at all but one CSA, most were inactive during the monitoring period due to drought conditions and/or consolidation. Reigner and Winkler (2001) observed that water storage on CSAs was greater than anticipated due to underestimation of clay consolidation. Of the four

CSAs studied by Riekerk *et al.* (1990), only one experienced regular surface water outflow during the four and half year study. Lewelling and Wylie (1993) also observed outflow from only one of the three monitored CSAs during a two year study. Outflow was observed at PCS SA 10 in the early part of this study, but this occurred when surface water levels were above 1.5 m. The extreme depths at PCS SA 10 were much higher than isolated wetland systems typically experience (Figure 3-17), and such depths would have been avoided with a lower outfall invert elevation. PCS SA 01 had an outfall that when active successfully limited water depths, but the effects from adding inserts within the outfall structure were obvious (Figure 3-1). The insertion of inserts essentially mimicked continued consolidation negating connection between surface waters and outfall structures. As recommended by Reigner and Winkler (2001), flexible outfall designs may help minimize extreme water depths from continued consolidation as well as provide baseflow to downstream systems.

Water Balances

Water balances were performed using rain, ET estimated with the Penman method, and the results from the runoff and surface water outflow analysis, while assuming zero groundwater flow, to balance inflows and outflows with change in stage. The water balances required residuals which represented underestimation of losses to the systems, and these residuals varied among surface water features (Table 3-8). Similar to the runoff analysis results, the differences in the residuals between features corresponded to the different observed hydrologic regimes. Water balances resulted in the lowest residuals at the more buffered systems of Mosaic H1 SW-3, PCS SA 10, and CFI SP-1 (Figure 3-17 and Table 3-8). While the flasher systems with quick declines, such as Williams Co. and Mosaic H1 SW-1, experienced residuals that were four times greater. The positive residuals represented underestimation of surface water losses, and the variability in the residuals demonstrate how these losses vary among sites. The water balance of

PCS SA 01 resulted in a negative residual suggesting that the sand tailings in the upland of this site may have provided groundwater inflow.

Dike Seepage

The water balance residuals of all water features but PCS SA 01 suggested underestimation of an outflow, particularly ET and/or infiltration. Infiltration was defined as surface water loss vertically and as lateral dike seepage. The potential for dike seepage demonstrated by the hydraulic gradients across the dikes was limited by the low lateral hydraulic conductivities, and negligible dike seepage rates were calculated (Tables 3-11 and 3-12). Dike seepage was calculated to be less than 1 cm/yr at all three sites analyzed compared to the measured rates of 10-20 cm/yr by Riekerk *et al.* (1990). Though the sensitivity of depth of surface water in contact with the dike to the calculated rates was minimal (Tables 3-12), higher water depths may create different flow paths across the dikes and potentially affect hydraulic conductivities and seepage rates. The significant increase in dike seepage through saturated overburden versus clay was demonstrated by Reigner and Winkler (2001), highlighting the effect of flow paths on seepage rates.

Local Groundwater

The groundwater analysis demonstrated that, in most cases, water tables in the surrounding uplands were elevated above the surface water elevations suggesting the potential for groundwater inflow to the water features (Figures 3-45 through 3-51). Groundwater inflow to the water features, however, was not demonstrated with the water balances, and in fact, the opposite was suggested with the residuals (Table 3-8). Again, PCS SA 01 was the exception. Though the potential for groundwater inflow was observed, the low hydraulic conductivities (Table 3-13), especially at Mosaic K5, Williams Co., and Tenoroc 4 which ranged from1.4 E^{-6} to

4.6 E^{-6} cm/s , may have limited groundwater flow. Dingman (2002) gives typical saturated hydraulic conductivities for clayey soils ranging from 1.03 E^{-4} to 2.45 E^{-4} cm/s.

As discussed in Levine and Salvucci (1999), lower conductive soils that limit vertical and lateral distribution of water typically result in a water table with elevations that strongly reflect the surface relief. Dingman (2002) points out that the higher the conductivities, the more subdued the reflection. The clayey soils of the sites in this study often resulted in water table gradients that mimicked surface elevation gradients as observed with the elevated upland groundwater elevations compared to surface water elevations. The reflection occurs as a result of a feedback mechanism provided by the strong coupling that occurs between the vadose zone and water table. This coupling is strongest with shallow water tables and soils with high capillary fringe heights (Levine and Salvucci, 1999). Higher water tables and capillary forces tend to increase groundwater loss to the vadose zone through ET while increasing runoff and decreasing infiltration. As water tables rise and shallow soil profiles become tension-saturated due to capillary forces, infiltration is decreased and runoff increases as discussed above and ET is increased, thereby decreasing the water table elevation (Levine and Salvucci, 1999). However, as the water table decreases, percolation of rain increases as a result of lower soil moisture and increased storage capacity (Dingman, 2002) and ET becomes more limited. These mechanisms create feedbacks that tend to direct the water table to some depth, where there is a balance between groundwater losses to capillary rise and gains from intermittent percolation (Levine and Salvucci, 1999). With low lateral conductivities and minimal lateral movement of groundwater, this feedback mechanism dominants groundwater movement and creates water table relief similar to surface relief.

Levine and Salvucci (1999) further discuss the relationship between the capillary forces and groundwater movements. Water tables which are fairly shallow and experience large capillary fringes cause groundwater discharge to be primarily via ET versus discharge to lower surface water features. This further explains why elevated surrounding water tables were observed in this study while groundwater inflow to the water features was often not. This phenomenon, however, may also develop groundwater troughs that create gradients that affect flow between surface water systems and extremely local and adjacent groundwater. Elevated transpiration from phreatophytic vegetation surrounding a water feature may intercept groundwater flow towards a surface water system while creating a cone of depression (Sophocleous 2002), and such a cone of depression surrounding a water feature develops a gradient that may provide outflow from the surface water system towards the trough.

Rosenberry and Winter (1997) performed a detail study of groundwater connection between two nearby wetlands, one elevated relative to the other. The authors measured hydraulic conductivities using slug tests within groundwater wells that ranged from 2 E^{-4} to 6 E^{-4} cm/s and observed significant capillary fringe heights. The conspicuous gradient from the elevated wetland to the other often did not result in net groundwater movement with the gradient. Observations from twelve groundwater wells instrumented within the 150 m that separated the two systems revealed the formation of groundwater mounds and troughs which limited groundwater flow between the systems. Rosenberry and Winter (1997) found groundwater troughs, as discussed in Sophocleous (2002), surrounding the wetlands that interrupted groundwater inflow to the wetland and created outflow from the wetland to the trough. In summary, the strong capillary forces determined with the moisture release curves (Figures 3-69 through 3-73) and low conductivities of the clay uplands (Table 3-13) support mechanisms to:

1) create strong coupling between water table and vadose zone; 2) limit discharge to downstream water features; 3) increase ET flux, limit infiltration, and increase runoff; 4) create mounds and troughs; and 5) limit groundwater circulation.

Daily Decline Analysis

While the residuals from the water balance and the above discussion suggest zero groundwater inflow to most water features studied, an analysis of the diurnal surface water fluctuations with the White (1932) method often indicated otherwise. The analysis calculated positive exfiltration into most sites and often with rates over one cm/day (Tables 3-22 through 3-25). Applying the White method also resulted in extremely high ET rates, with over one cm/day frequently calculated for the winter months. A closer examination of surface water increases at night, which were experienced by most sites, revealed that declining rates of groundwater inflow occurred over the nighttime hours (Figures 3-54 and 3-56). The White method assumes constant groundwater flow during the entire day and this assumption was not met. Hill and Neary (2007) also observed changing groundwater inflows at night, which resulted in high calculated ET rates. Though the groundwater rates here were conservatively calculated by not including the initial increases immediately after sundown, ET was still likely overestimated. The calculated ET rates for winter were well over typical values and ET calculated with various climatic-based methods (Jacobs *et al*., 2002; Mao *et al*., 2002). The same held true for the calculated summer rates, just not to the same degree.

The most conservative ET estimate was calculated with the average decline over 24 hours assuming zero net groundwater flow to the surface water system. This assumes a transient groundwater flow where groundwater inflow to the surface water feature at night is balanced by groundwater outflow during the day, and a hypothesis is offered referring back to the discussion of groundwater troughs. As ET is diurnal, so may be the trough that develops around the water

feature. The low specific yields of clay soils (Dingman, 2002) and the strong capillary forces may significantly increase the cone of depression surrounding the surface water feature during the day and create gradients for groundwater outflow. As ET ceases at night, the forces to create the trough would be relaxed allowing recovery of both the trough and surface water system. Dingman (2002) suggests the majority of groundwater to surface water connections occur through the littoral zone. The good connection between the surface water and immediately adjacent local groundwater was observed with the groundwater-1 wells (Figures 3-45, 3-48, 3-50, and 3-51), and such a connection may have provided diurnal and transient exchange between the surface water system and extremely local groundwater. An increased number of wells around and from a water feature would provide more information to test this hypothesis. Nevertheless, the most conservative ET rates during the summer were often 1.5 to 2 times greater than typical rates for the region, while winter rates were more comparable (Tables 3-22 through 3-26) (Jacobs *et al.*, 2002; Mao *et al.*, 2002, Lu *et al.*, 2005). Again, this is the most conservative estimate of ET and was calculated without including the observed groundwater inflow at night as done in the White method, which significantly increased ET estimates.

The water balances and the diurnal curve analysis of surface water levels at PCS SA 01 demonstrated that exfiltration to the surface water feature occurred. The higher conductive soils that surround the water feature at PCS SA 01 may have limited the extent of trough development due to lower capillary forces (shown for sandy soils with the moisture release curve for the SP-1 upland in Figure 3-74). Also, the lower capillary forces likely decreased water table and vadose coupling resulting in better groundwater connection, which along with a minimal trough, resulted in net groundwater inflow to the water feature. Murphy *et al.* (2008) also observed lateral

transport of groundwater on a CSA with sand tailings with significant inflows to an isolated surface water feature on the site.

While assuming the most conservative estimate of ET negates net groundwater inflow to the other monitored features, zero groundwater inflow should not be a definitive conclusion of all conditions. The diurnal analysis was performed using surface water levels from 2007 which was a fairly dry year. Rosenberry and Winter (1997) suggest that trough development is much more significant during drier years when water levels are low. The buffered regime at PCS SA 10 and its higher conductivity relative to the other sites suggests that it too could experience intermittent groundwater inflow.

The water balance residuals for Williams Co. and Mosaic H1 SW-1 were much higher compared to other sites and to another feature on Mosaic H1 (SW-3), demonstrating differences both among and within sites (Table 3-8). The analysis of diurnal fluctuations of these two features indicated that net infiltration had occurred from their systems (Figures 3-57 and 3-58). The pathway of the groundwater outflow was unknown, but speculated to be vertical as these features are low areas in their respective watersheds. Reigner and Winkler (2001) calculated negligible infiltration rates using measured permeabilities, whereas Lewelling and Wylie (1993) witnessed the possibility of higher infiltration rates through underlying overburden piles. Murphy *et al.*, (2008) concluded that vertical infiltration was significant on one CSA using a bromide tracer but only within the upper and unsaturated CSA soils with transport negligible past a depth of 1 m. Preferential flows through cracks were identified as pathways for the vertical transport in the upper CSA soils (Murphy *et al.*, 2008).

The water budget analysis demonstrated differences among and within CSAs in regards to runoff and groundwater interactions, both of which can be likely explained by the upland soil

conditions. The observed runoff and infiltration/exfiltration rates also were consistent with and explain the different hydrologic regimes of the surface water features. The analysis also suggested that ET from CSAs may be elevated compared to other wetland systems and a major contributor to the water budget of surface water features within CSAs.

Temporal Hydrologic Modeling

Temporal models were developed for the instrumented surface water features to predict stage with climatic data and to further evaluate the hydrologic flows estimated in the water budgets. The temporal modeling with Penman-estimated ET, the runoff models, and the omission of infiltration overestimated stage and supported the water balance results. PCS SA 01 was an exception as stage was underestimated. Inclusion of infiltration terms for all other sites resulted in end stage matching between predicted and actual stage but caused summer decline to be underestimated and winter decline to be overestimated. The application of seasonal coefficients improved the models' predictions (Table 3-27). Without inclusion of infiltration, seasonal coefficients during the non-growing season for PCS SA 10, Mosaic H1 SW-3, CFI SP-1, and Mosaic K5 were near one indicating that winter decline could be explained by Penman-estimated ET and without infiltration rates. The growing season coefficients that were required to accurately predict decline without infiltration for these sites ranged from 1.3 to 1.5. The need for seasonal coefficients to adjust ET rates and since the inclusion of infiltration rates alone did not create accurate models, again support the underestimation of ET for these systems using empirically derived, climatic-based methods. To keep seasonal coefficients for Williams Co. and Mosaic H1 SW-1 within the range used for the other sites, inclusion of significant infiltration rates to the models was required, supporting the results from the diurnal curve analysis (Table 3-27). The temporal model for Mosaic H1 SW-1 required an increased infiltration rate following a prolonged dry period, which may be due to development of cracks within the feature that did not

recover upon re-flooding (Reigner and Winkler (2001). The model for PCS SA 01 required an exfiltration rate of 1.2 mm/day to avoid under predicting stage, which agrees with the results from the water balance and daily decline analyses (Table 3-27). This rate was determined when seasonal coefficients to apply to Penman-estimated ET were 1.0 and would increase if similar growing season coefficients required for other models were applied.

The FAO adjusted Penman-Monteith method, also referred to as the Canopy Cover Coefficient method, estimates ET with climatic data and the Penman-Monteith method for a uniform, well-watered and expansive stand of grass. Reported values for non-growing and growing season coefficients applied with the FAO adjusted method for wetland environments in central Florida are 0.73 and 1.09 for a *Cladium jamaicense* marsh and 0.64 and 1.00 for a *Typha latifolia* marsh (Drexler *et al*., 2004). Growing season values of 1.4 to 1.8, however, have been reported for wetland systems in other regions (Drexler *et al*., 2004). Growing season coefficients over one are also commonly reported for fertilized and irrigated crops with the maximum, 1.25, measured for sugar cane (FAO, 1998). Again, these coefficients are applied to the FAO adjusted Penman-Monteith method which when used with on-site climatic data resulted in ET rates lower than those estimated with the Penman method (Figure 3-22 and Table 3-1). The growing season coefficients used here were applied to the Penman-estimated ET, however, and ranged from 1.3 to 1.5 for all sites except PCS SA 01. These values would be larger if used with the lower ET rates estimated with the FAO adjusted method, demonstrating the elevated ET from wetland systems on CSAs compared to other wetland systems and fertilized crops.

The temporal models' predictive abilities were demonstrated, and high non-linear coefficients of determination were obtained (Table 3-27). Sites, however, required different infiltration rates, either positive, negative, or zero, supporting the observation of differing

hydrologic regimes among and within CSAs. Different upland soil types control the runoff characteristics and surface and groundwater interactions, significantly affecting hydrologic regimes and demanding site specific analysis when predicting hydrology. Furthermore, the full hydrologic analysis highlights the utility of upland sand/overburden-capping as a design tool in CSA restoration attempts to buffer otherwise flashy hydrologic regimes.

Ecohydrology

Wetland boundaries are not limited to areas of flooding and include areas of permanent and temporary soil saturation. Therefore, an understanding of groundwater dynamics and its effects on soil moisture levels and plant behavior is also important when wetland restoration includes, as it should, transitional zones between upland and inundated conditions. To address these interactions, a study of the ecohydrologic relationships between *Salix caroliniana* and CSA soils was performed which included development of moisture release curves, measurement of soil moisture regimes with depth, and measurement of root biomass allocation and transpiration of *Salix caroliniana*.

Moisture Release Curves

The strong capillary forces of the clayey soils, which increase the coupling between the water table and vadose zone as discussed above, were calculated with the moisture release curves (Figures 3-69, 3-71, and 3-73). Fringe heights over a meter resulted and were greater than typical heights of clayey soils, which range from 50 to 65 cm (Dingman, 2002). The moisture release curves also indicated saturation levels of 57 to 60 % VWC which are slightly higher than typical clays (Dingman, 2002). Saturation of typical clays occurs at approximately 50 % VWC, and the higher saturation levels found here demonstrate the higher porosity of CSA soils compared to typical clayey soils. Permanent wilting may be induced when soil moisture in the clay decreases to approximately 40 % VWC (Figures 3-69, 3-71, and 3-73). The sand-

dominated upland at CFI SP-1, however, resulted in a much different moisture release curve and one typical of sandy soils (Figure 3-74) (Dingman, 2002). Saturation levels occurred at 33 % VWC, capillary fringe heights were near 20 cm, and PWP corresponded to a VWC of 10 %.

Soil Moisture Analysis

Coupling the moisture release curves with the recorded soil moisture and groundwater regimes further demonstrated the role of the capillary forces from the clays. Though not observed in all cases, groundwater levels as deep as one to two meters maintained constant soil moisture near saturation levels well above the water table (Figures 3-75 and 3-91). It was also observed, however, that the top 10 to 25 cm of the soil profiles in upland areas had fluctuating soil moisture levels and ones frequently below soil VWCs that may induce PWP. The soil moisture levels collected at the saturated stations of Williams Co. and CFI SP-1 revealed that high soil moisture levels can be maintained up to ground surface in intermittently inundated areas during an extended dry period (Figures 3-85 and 3-91). These results support the inverse texture effect hypothesis (Laio *et al.*, 2001a) and exhibit the ability of the clayey soils to extend saturation zones beyond inundated areas and to maintain suitable saturation for wetland species in a historically flooded area during a dry period.

The upland and transitional stations at CFI SP-1 demonstrated the effect of a sand-clay mix fill compared to a pure clay fill (Figures 3-87 and 3-89). Saturation levels, as indicated by the moisture release curves, were never reached throughout the entire soil profile that was monitored at the upland. Furthermore, recorded soil moisture levels frequently reached values which may induce PWP, despite the VWC for PWP in sands being substantially lower than that for clay (Figures 3-87 and 3-74). The differences of soil moisture regime in the top 30 cm of the soil profile at the transitional station compared to regimes at greater depths were apparent, exhibiting the soil heterogeneity with depth that is created by sand-clay fill (Figures 3-89). So

while a higher conductive upland such as a sand cap may buffer hydrologic regime of water features, it reduces the saturated zone that extends from the feature.

Root Biomass

An analysis of the root biomass allocation revealed *Salix caroliniana*'s ability to penetrate the clays without preclusion and to depths of saturation and into the water table (Figures 3-92 and 3-93). *Salix* spp. are often thought of as obligate phreatophytes which extract water from the groundwater and the saturated zone versus the unsaturated zone (Busch *et al*., 1992), and the deep rooting measured here supports this for *Salix caroliniana* on CSAs. The rather deep rooting that was measured is consistent with other studies which found rooting depths greater in humid climates (Schenk and Jackson, 2002; Porporato *et al*., 2000), while differing from some studies which found decreased rooting depths in clays compared to coarser soils (Schenk and Jackson, 2002; Laio *et al*., 2001). The latter, however, was found to occur in drier climates with deep water tables. Deep rooting in humid climates creates a constant source of available water from the shallow water table and capillary forces that can be relied on rather than periodic rain events and a shallow rooting system (Snyder and Williams 2000).

The combination of fairly extensive rooting depths and the strong capillary forces of the clays help explain the success of *Salix caroliniana* across large, including never flooded, areas on CSAs. These results demonstrate the potential for including large transitional zones at distance from surface water features in wetland restoration plans. The results also point out that caution should be used during planting attempts, however, as initial rooting depths of seedlings should be sufficiently deep enough to reach wetter zones upon establishment unless they receive supplemental irrigation. So while the clay may increase the flashy nature of water features, it may also act to increase the wetland environment beyond the typically flooded areas.

Transpiration

Transpiration studies on *Salix caroliniana* supported the conclusions from coupling rooting depths with soil moisture profiles, which demonstrated that trees are able to root deeply and thus reach available soil water. In terms of stem flow, trees did not experience stress conditions in the upland locations, where higher rates of stem flow per stem area occurred compared to more saturated conditions (Figures 3-95 and 3-105). The stem flow rates were measured using the SHB method which has been found to be accurate when comparing to gravimetric methods (Akilan *et al.*,1994; Baker and Bavel, 1997; Weibel and Boersma, 1995; Steinberg *et al.*, 1989, Guitierrez *et al.*, 1993; Heilman and Ham, 1990); and is often preferred to the THB when measuring flow rates in smaller stem diameters of angiosperms(< 120 mm) (Hall *et al.*, 1998; Herzog *et al.*, 1996).

Total basal area per transect was used to scale up stem flow rates to stand level transpiration by *Salix caroliniana* while assuming that all individuals within a transect experienced similar stem flow rates per stem area as the instrumented stems in that transect. Sapwood depths of tree cores were evaluated to observe if trees larger than the ones instrumented possibly had reduced stem flow per stem area due to heartwood development. While visual inspection offered no conclusive evidence of sapwood to heartwood transition, analysis of moisture content and dry wood density per core depth suggested little heartwood development in tree sizes used in scaling up to stand transpiration (Figure 3-100). Lower moisture contents were measured in the small trees sampled and in the shallower depths of some larger trees. Cavitation of the initially contacted wood during coring or after sampling could have likely affected measured values. It has been shown that younger, and thus shallower, wood tends to be more susceptible to cavitation which may help explain the results found here (Kavanagh *et al.*, 1999). The higher moisture contents with increased depth in the large trees,

however, suggested sapwood depths equaled the tree radii (Barbour and Whitehead, 2003; Holbrook and Zwieniecki, 2005). The dry wood densities were more consistent both among and within trees further supporting this conclusion (Holbrook and Zwieniecki, 2005).

It has been demonstrated that there is inverse relationship between wood hydraulic conductivity, and thus stem flow, and wood density both within an individual tree and among species (Roderick and Berry, 2001; Barbour and Whitehead, 2003; Pockman and Sperry, 2000; Holbrook and Zwieniecki, 2005). Gymnosperms experience larger differences of densities between non-conductive heartwood and conductive sapwood than angiosperms (Roderick and Berry, 2001; Barbour and Whitehead, 2003). However, other studies have also shown significant and measurable differences within angiosperms (Lamb and Marden, 1970; Wikburg, 2006). Wickburg (2006), in particular and explicitly related to this study, found stem hydraulic conductivity and wood density varied among different *Salix* species, and that there was a strong and inverse correlation between conductivity and density across all individuals sampled. Wickberg and Ogren (2004) found wood densities of four *Salix* spp. that ranged from 0.5 to 1.5 g/cm^3 compared to the average of 0.43 g/cm^3 found here. In a survey of 48 tree and shrub species native to the U.S., which included 16 families, Hacke *et al.* (2001) documented densities ranging from 0.4 to 0.85 g/cm^3 but with only two species having densities less than the average found here and only 12 % of species with densities lower than 0.50 g/cm^3. Following the theory of inverse correlation between wood density and stem hydraulic conductivity, the comparatively low densities measured for *Salix caroliniana* on CSAs demonstrates the potential for high water use by the species.

The low variability in the densities measured among and within all sampled cores of *Salix caroliniana* suggests that all individuals within the belted transects had similar potential

maximum hydraulic conductivities, validating scaling up with total basal area in a transect with homogenous soil water availability (Figure 3-100). The latter was assumed since the belted transects were established in a low-relief area that surrounded each ecohydrologic station. It should be noted that some trees that were not cored but which were used in scaling up may have had less conductive area. With that said, the station at Mosaic K5 with the highest stand transpiration rates, the inundated station, had the second lowest percentage of trees larger than instrumented trees (Figures 3-102 and 3-98). Furthermore, stem flow rates per stem area measured on larger stems at both the saturated and inundated stations of Mosaic K5 were actually higher than measured rates from smaller instrumented stems and not lower as heartwood development would likely have caused (Figure 3-96).

While the sapwood analysis did not provide evidence of heartwood development, the possibility for variable sap velocity in sapwood among different tree sizes of the same species and with equivalent water availability is possible, often with increased velocities observed in larger trees (Barbour and Whitehead, 2003). As just mentioned, this was observed here when comparing measured flow rates per stem area from the different sized gauges per station at Mosaic K5 (Figures 3-96). Schaeffer *et al*. (2000) also found variable sap velocities within different sized individuals of *Salix goodingii* with similar water availability. It follows that velocities within sapwood can potentially change resulting in either increased or decreased total sap flow per stem area with age even in the absence of heartwood development. The wood density results suggested equivalent hydraulic conductivities while assuming a tight correlation between conductivity and density. The variability in the stem flow rates per stem area, however, indicates that either maximum conductivities were not always reached or slight variability in conductivities may not be necessarily demonstrated with measurable differences in wood

densities, particularly in angiosperms. A more detailed analysis of the relationship between sap velocities, maximum wood hydraulic conductivities, and wood densities within and among different sized *Salix caroliniana* individuals may help to resolve this uncertainty.

Three different biometric-based methods were explored to scale up measured stem flows with total basal to determine stand level *Salix caroliniana* transpiration. The discrete biometric method resulted in the most conservative estimate while also allowing the variability over time and among measured stem flow rates to be directly evaluated (Figure 3-104). Again, scaling up with total basal area, regardless of the scaling method, assumed similar stem flow rates per stem area across all individuals on a transect which was supported by the tree core analysis but not necessarily found when comparing measured rates (Figure 3-96). The stem flow gauges used only allowed two diameter ranges to be instrumented prohibiting sap flow measurements on larger and a wider range of tree sizes. A modified experimental design to allow all size classes on a transect to be represented with sap flow measurements would provide a sufficient data set necessary for a more robust scaling method. A scaling up method based on sap flow distribution in dbh classes as described in Cermak *et al.* (2004) addresses the phenomenon of varying sap velocity with size and requires all of the pre-determined size classes to be instrumented. The measured sap flow rates then allow different biometric scaling ratios to be determined and applied to the different size classes.

When stem flow rates were scaled and expressed as stand level transpiration, the higher biomass of *Salix caroliniana* in the wetter regions of both sites resulted in higher stand rates in those regions compared to the upland stations, suggesting that stress conditions were also not caused by saturated or inundated conditions (Figures 3-102 and 3-107). The latter condition was most likely tolerated and exploited via extensive adventitious rooting typical of *Salix* spp.

(Kuzovkina *et al.*, 2003). Mean (± 1 S.D.) stand level transpiration solely from *Salix caroliniana* at the inundated station of Mosaic K5 was calculated with the discrete method to be 2.17 (±0.80) times greater than Penman-estimated total ET using on-site climatic data. The other two biometric approaches, the regression and simple methods, resulted in ratios of 2.77 and 2.43, respectively, for the inundated station of Mosaic K5. While sap flow measurements at an inundated region at CFI SP-1 was not possible, mean stand transpiration at the saturated station was determined with the discrete method to be 1.22 (±0.33) times greater than Penman-estimated total ET.

With the uncertainty in sap flow rates of larger stems and the lack of sufficient data set for a more robust scaling method acknowledged, the stand transpiration rates from the transition, saturated, and inundated stations of the two sites equaled or exceeded total estimated ET; supporting the results from the water balance, daily decline, and modeling analyses as well as further supporting the possibility of trough development around water features. High photosynthetic rates and stomatal conductivities have been reported for a variety of *Salix* spp. (Cienciala and Lindroth, 1995b; Cleverly *et al*.,1997; Wickburg, 2006) demonstrating the potential for high transpiration rates. Other studies using various methods to calculate *Salix* spp. transpiration also found rates exceeding open water evaporation and ET rates of typical regional systems. Conger (2003) also used SHB technology and Dynagage® stem gauges on a *Salix* sp. (*Salix nigra*) dominated stand in South Louisiana and utilized a scaling method similar to the discrete biometric method. Two plots were each instrumented with 16 different stems for 10 days at a time during the entirety of two growing seasons which resulted in mean transpiration rates of 1.1 cm H_2O/day compared to an average Penman-estimated ET with on-site climatic data of 0.55 cm H_2O/day.

Hall *et al.* (1998) performed a study to evaluate growing season water use in the U.K. from coppiced *Salix burjatica* on a clay loam soil using SHB methodology and equipment. Scaling up measured flows with leaf area resulted in transpiration rates that exceeded any reported values for other agriculture or tree crops in the region and which were 1 to 2.5 times total ET as predicted by the FAO adjusted Penman-Monteith method. The authors also employed the same experimental design and SHB technology on *Populas trichocarpa* but in conjunction with THB experiments and found good agreement with rates determined with the two methods.

Gripp *et al*. (1989) performed lysimeter studies with irrigated *Salix viminalis* plots to determine parameters, particularly stomatal functioning and water use, to develop an ET simulation model for the studied system. The model was used to simulate total ET for two types of *Salix viminalis* stands, one irrigated and fertilized and one with no treatment. Model simulations demonstrated that stand ET was 36% and 11% higher than Penman-estimated ET at the treated and non-treated stands, respectively. Persson and Lindroth (1994) estimated total ET from a fertilized and irrigated short rotation *Salix viminalis* stand on clay soil in Sweden using data from energy balance/Bowen ratio measurements. The authors determined rates that exceeded Penman-estimated ET by 31% in three out of four years and that were considerably greater than reported ET from a mature coniferous forest, barley crop, or grass stand in the region. Similar to the seasonal coefficients applied here in the temporal models, Persson and Lindroth (1994) found seasonal coefficients applied to Penman-estimated ET that ranged from 1.0 in the non-growing season to 2.0 by the end of the growing-season.

Munroe (1991) used chamber enclosure methods to monitor changes in water vapor due to transpiration on a suite of species ubiquitous to CSAs which included *Salix caroliniana*, *Typha latifolia*, and *Ludwigia peruviana*. Transpiration rates were measured during October and as

daily mass flux of water per dry mass of vegetation. When rates were coupled with estimates of dry standing biomass, the transpiration rates of all species were found to be above open water evaporation or cumulative ET of the region as estimated with a temperature-based empirical method. In a study of the spectral reflectance of wetland vegetation common to CSAs and other species common to the region, McClanahan and Odum (1991) partitioned species' reflectance values into either water-using or water-conserving modes largely dependent on the availability of nutrients. The water-using mode is typical of fast-growing species that have low reflectances and are in nutrient-rich settings where high productivity is possible. Species common to more nutrient-limited conditions, on the other hand, typically have lower photosynthetic rates and depend more on reflectance versus transpiration to limit heating of leaves and potential wilting. Through measuring reflectance of CSA vegetation, McClanahan and Odum (1991) concluded that the water-using mode is dominant on CSAs.

The analyses of ET with surface water levels and measurements of transpiration resulted in high, yet consistent rates, and some explanation is offered. CSAs are eutrophic systems, where water availability is sufficient through capillary forces and *Salix caroliniana* occurs in pure stands or in mixed communities (Rushton, 1988) with other species with water-using characteristics (McClanahan and Odum, 1991). *Salix* spp. are phreatophytes which are pioneer and typically occur in nutrient-rich conditions and often in small, disturbed areas (Kuzovkina and Quigley, 2005). Most CSAs are in arrested succession because of limited seed source (Rushton, 1983) and have high nutrient availability (Brown *et al.*, 2008), allowing *Salix caroliniana* and other fast-growing species to establish at higher densities and across larger areas than would be typically found. The combination of pioneer-dominated systems with high water and nutrient availability and the landscape that surrounds them may help to create ET hot spots. The oasis

effect, advection from surrounding areas with lower water availability, and the clothesline effect, increased ET from isolated or taller vegetation, have been attributed to elevated ET rates of other wetland systems (Drexler *et al*., 2004). The former could result from expansive *Imperata cylindrica* stands on sandy soils, gypsum stacks, and recently cleared areas from mining that surround CSAs, though surrounding wetter areas such as newer CSAs and water-filled mine cuts may also limit this effect. The clothesline effect could be stimulated by the elevation and canopy structure of CSAs compared to the surrounding landscape.

Transpiration is proportional to primary productivity and the extremely high rates observed in this study provide evidence of the potential for high ecosystem productivity on CSAs. The temporal modeling and daily decline analyses suggested annual ET could approach over 2 m/yr compared to the 1.4 m of annual rain that is typical of the region (Erwin *et al*., 1997). It should be noted, however, that the ET rates determined in the modeling and daily decline analyses were only for the surface water features, and since the transpiration analysis exclusively considered *Salix caroliniana*, no rates for total ET from the upland areas were reported. Therefore, caution should be used when using these results for entire CSA ET, as rates determined from the wetter regions should not be applied system-wide.

Future Work

This research has identified a set of hypotheses that should be tested during future work. A transient groundwater trough was given as a potential explanation for the ET and infiltration results using the White method. A more intensive monitoring scheme where a series of well transects surrounding and extending away from surface water features would provide data to observe if such a diurnal cone of depression existed. Furthermore, results here suggested that the connection between the local groundwater and surface water systems of CSAs was limited beyond the areas immediately surrounding surface water features and that the majority of local

groundwater movement within a CSA was to the atmosphere as ET. Such behavior is likely due to the low conductivities and strong capillary forces of the clay soils, following Levine and Salvucci (1999). Again, a more intensive groundwater monitoring scheme would provide more information to evaluate such behavior.

Anecdotal (Figures 3-81 and 3-85) and visual evidence demonstrated the development of cracks during drying of the clays, and these cracks were both surficial and below ground. The modeling results from Mosaic H1 SW-1 suggested that cracks which developed during a prolonged dry period may increase surface water infiltration following re-wetting (Table 3-27). It seems that the development of cracks and drying of surface water features on CSAs may be an autocatalytic relationship, as drying of the clays creates cracks and the developed cracks stimulate further drying by increased infiltration and storage. Such a phenomenon would cause systems which periodically become non-inundated to become so more frequently with a perpetual decrease in flooding potential. On the other hand, crack development would be limited in ponded systems that are potentially buffered by upland soil types. Employment of a technology such as ground penetrating radar (Peters *et al.*, 1994) before and after dry periods along with a longer term monitoring and comparison of surface water levels of ponded and flashy surface water features may help evaluate this hypothesis.

The value of sand and/or overburden fill to CSAs was identified, and the effect of these soils to buffer hydrologic regime is likely due to increased groundwater and surface water connection. The buffering may also be stimulated by the higher conductive soils allowing rains to infiltrate to depths in uplands where ET loss is reduced and the water is available for flow to the surface water features. A monitoring and modeling attempt to observe if similar CSAs with the same precipitation inputs and watershed areas but with different upland soils would differ in

flooding regimes, where the sandier uplands would create more water storage as surface water by minimizing the footprint of ET. With that said, ET was found to be extremely high, with the elevated transpiration rates of eutrophic species such as *Salix caroliniana* as a major contributor. With restoration and revegetion with more desirable and later-successional species, total CSA ET may decrease and largely affect hydrologic regimes of CSAs. The ecohydrologic approach used here but applied to species in CSAs which are more typical of climax conditions would help shed light on this hypothesis.

LIST OF REFERENCES

Akilan K, Considine J, Marshell J. 1994. Water use by Geraldton wax (*Chamelaucium uncinatum* Schauer) as measured by heat balance stem flow gauges. *New Zealand Journal of Crop and Horticultural Science* **22:** 285-294.

Baker JM, Bavel CH. 1987. Measurement of mass flow of water in the stems of herbaceous plants. *Plant, Cell and Environment* **10:** 777-782.

Barbour MM, Whitehead D. 2003. A demonstration of the theoretical prediction that sap velocity is related to wood density in the conifer *Dacrydium cupressinum*. *New Phytologist* **158:** 477-488.

Beriswill JA, Bloomquist D, Townsend FC. 1989. Reclamation of phosphate clay waste ponds. Bartow, FL: Florida Institute of Phosphate Research: Report nr 02-030-075.

Boyd MC. 2008. Revegetation of wetland ecosystems on clay settling areas. M.S. Thesis, University of Florida, Gainesville, Fl

Brown MT, Boyd MC, Ingwersen WW, King SA, McLaughlin DL. 2008. Wetlands on clay settling areas: Final Report. Bartow, FL: Florida Institute of Phosphate Research: In press.

Brown MT, Tighe RE. 1991. Techniques and guidelines for reclamation of phosphate mined lands. Bartow, FL: Florida Institute of Phosphate Research: Report nr 03-044-095.

Busch DE, Ingram NL, Smith SD. 1992. Water uptake in woody riparian phreatophytes of the Southwestern United States: A stable isotope study. *Ecological Applications* **2:** 450-459.

Carrier WD, Bromwell L, Somogoyi F. 1983. Design capacity of slurried mineral waste ponds. *Journal of Geotechnical Engineering* **109:** 699-716.

Cermak J, Kucera J, Nadezhdina N. 2004. Sap flow measurements with some thermodynamic methods, flow integration within trees and scaling up from sample trees to entire forest stands. *Trees* **18:** 529-546.

Chen JM, Rich PM, Gower ST, Norman JM, Plummer S. 1997. Leaf area index of boreal forests: Theory, techniques, and measurements. *Journal of Geophysical Research* **102:** 429-443.

Cienciala E, Lindroth A. 1995a. Gas exchange and sap flow measurements of *Salix viminalis* trees in short-rotation forest. *Trees* **9:** 289-294.

Cienciala E, Lindroth A. 1995b. Gas exchange and sap flow measurements of *Salix viminalis* trees in short-rotation forest. II. Diurnal and seasonal variations of stomatal response and water use efficiency. *Trees* **9:** 295-301.

Cleverly JR, Smith SD, Sala A, Devitt DA. 1997. Invasive capacity of *Tamarix ramosissima* in a Mojave Desert floodplain: the role of drought. *Oecologia* **111:** 12-18.

Conger RM. 2003. Black willow (*Salix nigra*) use in phytoremediation techniques to remove the herbicide bentazon from shallow groundwater. Ph.D. Dissertation, Louisiana State University, Baton Rouge, Louisiana, USA.

Department of Environmental Regulation (DEP). 1994. Delineation of the Landward Extent of Wetlands and Surface Waters. Chapter 62-340, Florida Administrative Code.

Dingman, L. 2002. *Physical hydrology. 2nd Edition*. Upper Saddle River, New Jersey: Prentice-Hall, Inc.

Drexler JZ, Snyder RL, Spano D, Tha Paw K. 2004. A review of models and micrometeorological methods used to estimate wetland evapotranpiration. *Hydrological Processes* **18:** 2071-2101.

Dynamax, Inc. 2005. Dynagauge™ installation and operation manual. 107p.

Erwin KL, Doherty SJ, Brown MT, Best GR. 1997. Evaluation of constructed wetlands on phosphate mined lands in Florida. Bartow, FL: Florida Institute of Phosphate Research: Report nr 03-103-139.

FAO. 1998. Crop evapotranspiration-Guidelines for computing crop water requirements In: FAO Irrigation and Drainage Papers. #56.

FIPR. Phosphate Primer. [updated January 2008; cited January 2008]. Available from http://www1.fipr.state.fl.us/PhosphatePrimer.

Garlanger JE. 1982. Field evaluation of sand-clay mix reclamation. Bartow, FL: Florida Institute of Phosphate Research: Report nr 03-06-007.

Garlanger JE, Kennedy PA, Cheung FK. 2005. Potential technologies to reduce or replace groundwater consumption in the Southwest Florida Management District. Bartow, FL: Florida Institute of Phosphate Research: Report nr 03-01-179.

Gripp H, Halldin S, Lindroth A. 1989. Water use by intensively cultivated willow using estimated stomatal parameter values. *Hydrological Processes* **3:** 51-63.

Guitierrez MV, Harrington RA, Meinzer FC, Fownes JH. 1994. The effect of environmentally induced stem temperature gradients on transpiration estimates from the heat balance method in two tropical woody species. *Tree Physiology* **14:** 179-190.

Guswa AJ, Celia MA, Rodriquez-Iturbe I. 2002. Models of soil moisture dynamics in ecohydrology: A comparative study. *Water Resources Research* **38:** 1166-1181.

Hacke UG, Sperry JS, Pockman WT, Davis SD, McCulloh KA. 2001. Trends in wood density and structure are linked to prevention of xylem implosion by negative pressure. *Oecologia* **126:** 457-461.

Hall RL, Allen SJ, Rosier PT, Hopkins R. 1998. Transpiration from coppiced poplar and willow measured using sap-flow methods. *Agricultural and Forest Meteorology* **90:** 275-290.

Herzog KM, Thum R, Zweifel R, Hasler R. 1997. Heat balance measurements—to quantify sap flow in thin stems only? *Agricultural and Forest Meteorology* **83:** 75-94.

Hill AJ, Neary VS. 2007. Estimating evapotranspiration and seepage for a sinkhole wetland from diurnal surface-water cycles. *Journal of the American Water Resources Association* **43:** 1373-1382.

Hochman Z, Dalgliesh NP, Bell KL. 2001. Contributions of soil and crop factors to plant available soil water capacity of annual crops on black and grey vertosols. *Australian Journal of Agricultural Research* **52:** 955-961.

Holbrook NM, Zwieniecki MA. 2005. *Vascular transport in plants*. Amsterdam, Netherlands: Elsvier, Academic Press.

Horslev, MJ. 1951. Time lag and soil permeability in ground water observations. Army Corps of Engineers: Bulletin, No. 36. U.S.

Heilman JL, Ham JM. 1990. Measurement of mass flow rate of sap in *Ligustrum japonicum*. *Horticulture Science* **25:** 465-467.

Ingwersen WW. 2006. Viability of wetland trees after twenty years on phosphatic clay settling areas and their role in ecosystem development. M.S. Thesis, University of Florida, Gainesville, Fl

Jacobs JM, Mergelsberg SL, Lopera AF, Myers DA. 2002. Evapotranspiration from a wet prairie wetland under drought conditions: Paynes Prairie, Florida, USA. *Wetlands* **22:** 374-385.

Kavanagh KL, Bond BJ, Aitken SN, Gartner BL, Knowe S. 1999. Shoot and root vulnerability to xylem cavitation in four populations of Douglas-fir seedlings. *Tree Physiology* **19:** 31-37.

Kuzovkina YA, Knee M, Quigley MF. 2004. Effects of soil compaction and flooding on the growth of 12 willow (*Salix* L.) species. *Journal of Environmental Horticulture*. **22:** 155-160.

Kuzovkina YA, Quigley MF. 2005. Willows Beyond Wetlands: Uses of *Salix* L. Species for Environmental Projects. *Water, Air, and Soil Pollution* **162:** 183-204.

Lamb FM, Marden RM. 1970. Variation in density of sugar maple sapwood and heartwood. USDA Forest Service. North Central Forest Experiment Station, ST. Paul, MN: Research Note NC-90.

Lamont WE, McClendon JT, Clements LW, Field IL. 1975. Characterization studies of Florida phosphate slimes. USDI, Burea of Mines, Washington, D.C.: Report Investigation 8089.

Laio F, Porporato A, Ferdandez-Illescas CP, Rodriquez-Iturbe I. 2001a. Plants in water-controlled ecosystems: active role in hydrologic processes and response to water stress IV. Discussion of real cases. *Advances in Water Resources* **24:** 745-762.

Laio F, Porporato A, Ridolfi L, Rodriquez-Iturbe I. 2001b. Plants in water-controlled ecosystems: active role in hydrologic processes and response to water stress II. Probabilistic soil moisture dynamics. *Advances in Water Resources* **24:** 707-723.

Lee R. 1980. *Forest hydrology*. New York, NY: Columbia University Press.

Levine JB, Salvucci, GD. 1999. Equilibrium analysis of groundwater-vadose zone interactions and the resulting spatial distribution of hydrologic fluxes across a Canadian prairie. *Water Resources Research* **35:** 1369-1383.

Lewelling BR, Wylie RW. 1993. Hydrology and water quality of unmined and reclaimed basins in phosphate-mining areas, West-Central Florida. Prepared in cooperation with the Florida Institute of Phosphate Research. Water Resources Investigation Report: 93-4002.

Lu J, Sun G, McNulty SG, Amatya DM. 2005. A comparison of six potential evapotranspiration methods for regional use in the Southeastern United States. *Journal of AWRA* **39:** 621-633.

Mao LM, Bergman MJ, Tai CC. 2002. Evapotranspiration measurement and estimation of three wetland environments in the Upper St. Johns River Basin, Florida. *Journal of AWRA* **38:** 1271-1285.

Martin TA, Brown KJ, Kucera J, Meinzer FC, Sprugel DG, Hinkley TM. 2001. Control of transpiration in a 220-year-old *Abies amabilis* forest. *Forest Ecology and Management* **152:** 211-224.

McClanahan TR, Odum HT. 1991. Infrared reflectance and water budgets of vegetation in reclamation after phosphate mining. In: Odum HT editor. Evaluation of alternatives for restoration of soil and vegetation on phosphate clay settling ponds. Bartow, FL: Florida Institute of Phosphate Research: Report nr 03-076-094.

Meeks DW, Hatfield JC, Howell TA, Idso SB, Reginato RJ. 1984. A generalized relationship between photosynthetically active radiation and solar radiation. *Agronomy* **76:** 939-945.

Mitsch WJ, Gosselink JG. 1993. *Wetlands*. New York, NY: Van Norstrand Reinhold.

Munroe M. 1991. Transpiration in clay settling ponds. In: Odum HT editor. Evaluation of alternatives for restoration of soil and vegetation on phosphate clay settling ponds. Bartow, FL: Florida Institute of Phosphate Research: Report nr 03-076-094.

Murphy KE, Rains MC, Kittridge MG, Stewart MT, Ross MA. 2008. Hydrology of clay settling areas and surrounding landscapes in the phosphate mining district, peninsular Florida. *JAWRA* **44:** 980-995.

Nagler PL, Glenn EP, Thompson TL. 2003. Comparison of transpiration rates among saltcedar, cottonwood, and willow trees by sap flow and canopy temperature methods. *Agricultural and Forest Meteorology* **116:** 73-89.

Odum HT. 1994. *Ecological and general systems*. Niwot, CO: University Press of Colorado.

Odum HT, Miller MA, Rushton BT, McClanahan TR, Best GR. 1983. Interaction of wetlands with the phosphate industry. Bartow, FL: Florida Institute of Phosphate Research: Report nr 03-007-025.

Odum HT, Best GR, Miller MA, Rushton BT, Wolfe RW, Bersok C, Feiertag J. 1990. Accelerating natural processes for wetland restoration after phosphate mining. Bartow, FL: Florida Institute of Phosphate Research: Report nr 03-041-086.

Odum HT, Rushton BT, Paulic M, Everett S, McClanahan T, Munroe M, Wolfe RW. 1991. Evaluation of alternatives for restoration of soil and vegetation on phosphate clay settling ponds. Bartow, FL: Florida Institute of Phosphate Research: Report nr 03-076-094.

Persson G, Lindroth A. 1994. Simulating evaporation from short-rotation forest: variations within and between seasons. *Journal of Hydrology* **156:** 21-45.

Peters L, Daniels JJ, Young JD. 1994. Ground penetrating radar as a subsurface environmental sensing tool. *Proceedings of the IEEE* **82:** 1802-1822.

Pockman WT, Sperry JS. 2000. Vulnerability to xylem cavitation and the distribution of Sonoran desert vegetation. *American Journal of Botany* **87:** 1287-1299.

Porporato A, Laio F, Ridolfi L, Rodriquez-Iturbe I. 2000. Plants in water-controlled ecosystems: active role in hydrologic processes and response to water stress III: Vegetation water stress. *Advances in Water Resources* **24:** 725-744

Reigner WR, Winkler W. 2001. Reclaimed phosphate clay settling area investigation: hydrologic model calibration and ultimate clay elevation prediction: Final Report. Bartow, FL: Florida Institute of Phosphate Research: Report nr 03-109-176.

Riekerk H, Korhnak LV, Brown MT. 1990. The hydrology of reclaimed phosphate-mined wetlands. Bartow, FL: Florida Institute of Phosphate Research: Report nr 83-03-044T.

Roderick ML, Berry SL. 2001. Linking wood density with tree growth and environment: a theoretical analysis based on the motion of water. *New Phytologist* **149:** 473-485.

Rodriquez-Iturbe I. 2000. Ecohydrology: A hydrologic perspective of climate-soil-vegetation dynamics. *Water Resources Research* **36:** 3-9.

Rodriquez-Iturbe I. 2001. Plants in water-controlled ecosystems: Active role in hydrologic processes and response to water stress I. Scope and general outline. *Advances in Water Resources* **24:** 695-705.

Rosenberry DO, Winter TC. 1997. Dynamics of water-table fluctuations in an upland between two prairie-pothole wetlands in North Dakota. *Journal of Hydrology* **191:** 266-289.

Rushton BT. 1983. Ecosystem organization in phosphate clay-settling ponds. M.S. Thesis, University of Florida, Gainesville, Fl.

Rushton B. 1988. Wetland reclamation by accelerating succession. Ph.D. Dissertation, University of Florida, Gainesville, Fl.

Scanlon BR, Andraski BJ, Bilskie JM. 2002. 3.2.4 Miscellaneous methods for measuring matric or water potential. In: Dane JH, Topp GC, editors. *Methods of Soil Analysis, Part 4, Physical Methods*. Madison, WI: Soil Science Society of America.

Schaeffer SM, Williams DG, Goodrich DC. 2000. Transpiration of cottonwood/willow forest estimated from sap flux. *Agriculture and Forest Meteorology* **105:** 257-270.

Schenk HJ, Jackson RB. 2002. Rooting depths, lateral root spreads and below-ground/above-ground allometries of plants in water-limited ecosystems. *Journal of Ecology* **90:** 480-494.

Schnoes RS, Humphrey SR. 1980. Terrestrial plant and wildlife communities on phosphate mined lands in central Florida. Florida State Museum, Gainesville, Fl: Special Scientific Report No. 3.

Shigo AL, Hillis WE. 1973. Heartwood, discolored wood, and microorganisms in living trees. *Annual Review of Phytopathology* **11:** 197-22.

Smith DM, Allen SJ. 1996. Measurement of sap flow in plant stems. *Journal of Experimental Botany* **47:** 1833-1844.

Snowdon P, Raison J, Keith H, Ritson P, Grierson P, Adams M, Montagu K, Bi H, Burrows W, Eamus D. 2002. Protocol for sampling tree and stand biomass. National Carbon Accounting System, Australian Greenhouse Office: Technical Report #31.

Snyder KA, Williams DG. 2000. Water sources used by riparian trees varies among stream types on the San Pedro River, Arizona. *Agricultural and Forest Meteorology*. **105:** 227-240.

Sophocleous M. 2002. Interactions between groundwater and surface water: the state of the science. *Hydrogeology Journal* **10:** 52-67.

Steinberg SL, Bavel CH, McFarland MJ. 1990. Improved sap flow gauge for woody and herbaceous plants. *Agronomy Journal* **82:** 851-854.

Stewart CM. 1966. Excretion and heartwood formation in living trees. *Science, New Series* **153:** 1068-1074.

Weibel FP, Boersma K. 1995. An improved stem heat balance method using analog heat control. *Agricultural and Forest Meteorology* **75:** 191-208.

White WN. 1932. A method of estimating ground-water supplies based on discharge by plants and evaporation from soil: Results of investigation in Escalante Valley, Utah. *Water Supply Paper*: 659-A.

Wickberg J. 2006. Water relations in *Salix* with focus on drought responses. Ph.D. Dissertation, Swedish University of Agricultural Sciences, Umea, Sweden.

Wickberg J, Ogren E. 2004. Interrelationships between water use and growth traits in biomass-producing willows. *Trees* **18:** 70-76.

Wilcox BP, Thurow TL. 2006. Emerging issues in rangeland ecohydrology: vegetation change and the water cycle. *Rangeland Ecology Management* **59:** 220-224.

Woods R, Rowe L. 1996. The changing variability of subsurface flow across a hillslope. *Journal of Hydrology* **35:** 51-86.

Zalewski M. 2000. Ecohydrology-the scientific background to use ecosystem properties as management tools toward sustainability of water resources. *Ecological Engineering* **16:** 1-8.

BIOGRAPHICAL SKETCH

Daniel L. McLaughlin was born in 1979 in Anderson, SC and grew up in Pendleton, SC. He attended Lander University and Clemson University during his undergraduate career in a dual-degree program in mathematics and civil engineering and received a Bachelors of Science in both fields. He graduated summa cum laude in civil engineering at Clemson University. He then continued his education at Clemson University as a graduate student in environmental engineering and received a Masters of Science. Though he enjoyed his research on bioremediation of chlorinated pollutants during graduate work at Clemson University, he still yearned to do research within natural systems and on larger scales. At the University of Florida and under the advisement of Dr. Mark T. Brown, he was introduced to systems ecology and ecological engineering, filling his desire for holistic thinking and to be immersed in ecosystems, mentally and physically.